

# Increasing the efficiency of anaerobic waste digesters by optimising flow patterns to enhance biogas production

---

Rebecca Clare Sindall

A thesis submitted to

The University of Birmingham

for the degree of

DOCTOR OF PHILOSOPHY

School of Civil Engineering

College of Engineering and Physical Sciences

The University of Birmingham

August 2014

UNIVERSITY OF  
BIRMINGHAM

**University of Birmingham Research Archive**

**e-theses repository**

This unpublished thesis/dissertation is copyright of the author and/or third parties. The intellectual property rights of the author or third parties in respect of this work are as defined by The Copyright Designs and Patents Act 1988 or as modified by any successor legislation.

Any use made of information contained in this thesis/dissertation must be in accordance with that legislation and must be properly acknowledged. Further distribution or reproduction in any format is prohibited without the permission of the copyright holder.

## Abstract

The wastewater treatment industry makes extensive use of anaerobic digestion to stabilise sewage sludge and produce biogas. Whilst the need to mix digesters, to bring biomass and micro-organisms into contact, is well-recognised, the level of mixing required and its effects on biogas production are not clear. Here, the effects of mixing speed in mechanically-mixed lab-scale digesters on flow patterns, digester stability, microbiological community and biogas production are considered.

For the first time, positron emission particle tracking was used to visualise flow patterns in lab-scale digesters at different mixing speeds. Computational fluid dynamics models of the digester were then built to identify the turbulence characteristics present. Four lab-scale digesters were run for a period of four months at different mixing speeds and key indicators of digester stability were recorded alongside gas production. Samples were taken at the end of each retention time in order to analyse the microbiological communities, particularly the methanogens, present in the digester.

It has been shown that increased mixing speed leads to higher levels of turbulence. Experimental work has shown that in these digesters, increasing the mixing speed reduces the stability of the methane generation process and accordingly has a detrimental effect on the gas production. Similarly, the abundance of methanogenic communities, dominated by the acetoclastic *Methanosaeta*, was adversely affected by increased VFA concentrations brought about by increasing mixing speeds. However, the unmixed digester produced less biogas than the digester mixed at a low speed, due to the formation of pockets of different environments in the digester which leads to uncontrolled digestion. As such, in the case of these digesters, minimal mixing represents the ideal scenario.

By considering the velocity gradient in the digester as a surrogate for turbulence, a threshold of  $6-8 \text{ s}^{-1}$  was identified. Below this threshold, increased mixing was seen to be beneficial but increasing mixing above the threshold was detrimental to both digester stability and gas production.

## Acknowledgements

Firstly, I must thank my supervisors, Professor John Bridgeman and Dr Cynthia Carliell-Marquet, for their support and insight throughout this research. Additionally, I am grateful for the EPSRC-CASE Award in conjunction with Severn Trent Water that has allowed me to cover the costs of the past four years. Thanks too to Pete Vale, my sponsor at Severn Trent.

There have been so many people who have helped with this wide-ranging research. Thank you to Mark Carter for extensive assistance in the lab. Thank you to Goff, Jimmy, Farryad, Raf and Gav for their help with various lab tests and for their camaraderie. Thank you to Mark Simmons and Federico Alberini for allowing me access to PIV equipment and to David Parker, Tom Leadbeater and Joseph Gargiuli for allowing me to play with their PEPT equipment. Both bits of kit helped remind me that science is cool! Thanks too, to Julie Williams for processing my qPCR samples and to Sandra Esteves for letting me take advantage of the microbiological community analysis expertise at Glamorgan. Away from the lab, Nainesh, Dom and Justin have been my technical wizards, dealing with a huge variety of CFD, Excel and Matlab questions. Thank you to my officemates, Chris, Roger, Neil, Sally, Shahad, Ashley, Davide and Martin along with others mentioned above who have distracted me and cheered me up over many cups of tea and long lunch breaks.

Last, but by no means least, I owe a great deal of thanks to my family. Dad, the original Dr R. Sindall, deserves recognition as the (probably unwitting) inspiration for this PhD. John has always been willing to remind me that having a “real” job is just as challenging as academic research and is the best little brother I could wish for. Finally, Mum has not only proof-read every word of this thesis but has always supported me through every challenge I have had thrown at me and she has consoled, advised and encouraged me even when she had no understanding of the problems involved. Thank you!

# Contents

Abstract.....	i
Acknowledgements.....	ii
List of figures.....	ix
List of tables.....	xvi
Abbreviations and notation.....	xviii
Abbreviations.....	xviii
Notation.....	xix
CHAPTER 1 Introduction.....	1
1.1 Background and Motivation.....	1
1.2 Research Relevance.....	3
1.3 Layout of thesis.....	3
CHAPTER 2 Anaerobic digestion.....	5
2.1 Aims of anaerobic digestion.....	5
2.2 Biogas as green energy.....	6
2.3 Biochemical processes.....	7
2.4 Factors affecting AD.....	9
2.4.1 Temperature.....	9
2.4.2 Retention time.....	10
2.4.3 Nutrients.....	11
2.4.4 Alkalinity and pH.....	12
2.4.5 Inhibitors.....	13

2.5	Mixing and anaerobic digestion.....	15
2.5.1	Purpose of mixing .....	15
2.5.2	Methods of mixing .....	16
2.5.3	Industrial application of mixing.....	16
2.6	Effects of mixing on biogas production .....	17
2.6.1	Effect of mixing regime .....	18
2.6.2	Effect of mixing method.....	35
2.6.3	Review of literature .....	39
2.7	Effects of mixing on digester microbiology.....	41
2.8	Microbiological community analysis of anaerobic digestion.....	46
2.9	Review of previous research and knowledge gaps.....	49
CHAPTER 3	Fluid flow and CFD modelling .....	52
3.1	Fluid flow.....	52
3.1.1	Governing equations.....	52
3.1.2	Turbulence .....	53
3.1.3	Turbulent mixing .....	54
3.1.4	Boundary layer theory .....	57
3.1.5	Flow patterns .....	59
3.1.6	Velocity gradient.....	60
3.2	Computational fluid dynamics modelling.....	62
3.2.1	General methodology .....	63
3.2.2	Governing equations of computational fluid dynamics.....	63

3.2.3	Turbulence modelling and the Boussinesq hypothesis .....	65
3.2.4	Modelling mixing.....	73
3.2.5	Modelling sludge rheology.....	77
3.2.6	Discretisation .....	79
3.2.7	Mesh generation.....	80
3.2.8	Results of previous work.....	80
3.3	Review of previous research and knowledge gaps.....	101
CHAPTER 4	Aim and objectives.....	103
CHAPTER 5	Materials and Methods.....	104
5.1	Experimental set-up and methods.....	104
5.1.1	Digestibility batch tests.....	104
5.1.2	Semi-continuous laboratory-scale digester tests .....	105
5.2	General analytical methods .....	109
5.2.1	Total and volatile solids.....	109
5.2.2	pH.....	109
5.2.3	Alkalinity and Ripley's ratio.....	110
5.2.4	Ammonia.....	111
5.2.5	Volatile fatty acids.....	111
5.2.6	Viscosity .....	111
5.3	Quantitative polymerase chain reaction .....	112
5.4	Particle image velocimetry (PIV).....	114
5.5	Positron emission particle tracking (PEPT) .....	116

5.5.1	Tracer preparation .....	118
CHAPTER 6	Synthetic sludge assessment .....	120
6.1	Sludge composition.....	120
6.2	Sludge preparation.....	120
6.3	Synthetic sludge rheology.....	121
6.3.1	Rheology of digesting sludge .....	122
6.4	Nutritional properties of synthetic sludge.....	124
6.5	Summary .....	126
CHAPTER 7	Positron Emission Particle Tracking .....	128
7.1	Experimental conditions .....	128
7.2	Tracer particle suitability .....	129
7.3	Particle location and path lines.....	130
7.4	Velocity magnitude .....	138
7.5	Azimuthally-averaged occupancy .....	139
7.6	Azimuthally-averaged velocity.....	143
7.7	Particle trajectory length analysis.....	151
7.8	Summary .....	154
CHAPTER 8	CFD modelling .....	156
8.1	Model geometry .....	156
8.2	Numerical method .....	157
8.2.1	High performance computing facility .....	157
8.2.2	Software.....	158

8.2.3	Discretisation schemes .....	158
8.2.4	Modelling rotating flows.....	158
8.2.5	Boundary conditions .....	159
8.2.6	Mesh generation.....	160
8.2.7	Turbulence models.....	160
8.3	Model verification and validation .....	161
8.3.1	Model verification: mesh density .....	161
8.3.2	Model validation: turbulence model selection against PIV .....	163
8.3.3	Model validation: comparison to PEPT .....	168
8.4	Velocity contours .....	171
8.5	Velocity magnitude analysis.....	178
8.6	Particle trajectories.....	182
8.7	Turbulent kinetic energy and turbulent intensity.....	184
8.8	Velocity gradient .....	188
8.9	Summary .....	193
CHAPTER 9	Mixing, digester stability and gas production .....	196
9.1	Experimental set-up.....	196
9.2	Feedstock differences .....	197
9.3	Effect of mixing on digester stability .....	198
9.4	Effect of mixing on digester performance .....	206
9.5	Effect of mixing on gas production .....	209
9.6	Effect of mixing on microbiological communities.....	221

9.7	Summary .....	229
CHAPTER 10	Discussion.....	232
10.1	Flow visualisation.....	233
10.2	CFD modelling strategy.....	235
10.3	Experimental method .....	240
10.4	Microbiological community analysis.....	245
10.5	Coupling of CFD and experimental findings.....	247
10.6	Implications for full-scale anaerobic digestion .....	250
10.7	Summary .....	251
CHAPTER 11	Conclusions and recommendations.....	254
11.1	Conclusions .....	254
11.2	Recommendations for further work .....	257
References	.....	259

## List of figures

Figure 2.1 - Food web of methanogenic anaerobic digestion, showing four major steps and five physiologically distinct groups of micro-organisms: a - fermentative bacteria, b - hydrogen-producing acetogenic bacteria, c - acetogens, d - hydrogenotrophic methanogens, and e – acetoclastic methanogens. Reproduced from Angenent et al. (2004).....	7
Figure 3.1 – Idealised visualisation of the energy cascade, adapted from Stanley and Smith (1995) .	55
Figure 3.2 - Flow of fluid over a flat plate depicting the development of the boundary layer, taken from Frei (2013) .....	58
Figure 3.3 – Turbulent boundary layer structure showing viscous sub-layer, buffer region and turbulent log region, adapted from (Versteeg and Malalasekera, 2007).....	59
Figure 3.4 - Flow patterns generated by a radial-flow impeller (left) and an axial-flow impeller (right) .....	60
Figure 3.5 – Steps involved in CFD flow analysis .....	63
Figure 3.6 – Velocity for stationary turbulence .....	64
Figure 3.7 – Sliding mesh across a two-dimensional grid interface, reproduced from ANSYS-Fluent (2012).....	76
Figure 3.8 – Stress-strain curves for Newtonian and non-Newtonian fluids.....	77
Figure 5.1 - Lab-scale digester .....	107
Figure 5.2 - Schematic of PIV technique showing light source illuminating plane through seeded flow, image capture and subsequent processing of consecutive images to determine flow vectors, reproduced from (Isoda et al., 2003).....	115
Figure 5.3 - Detection of particle location using a series of photon pair detections .....	118
Figure 6.1 - Rheological properties of synthetic sludge compared to digested sewage sludge with varying solids concentrations .....	121

Figure 6.2 - Rheology of digesting sludge over a 72 hour period, at mixing speeds of i) 0 rpm, ii) 40 rpm and iii) 300 rpm ..... 123

Figure 6.3 - Mean gas production from batch tests using synthetic sludge and sewage sludge as feedstock..... 125

Figure 7.1 – Path line followed by a single radioactive particle over a 20 minute period in a lab-scale anaerobic digester mixing real sludge at i). 50 rpm, ii). 100 rpm, iii). 150 rpm, and iv). 200 rpm. Black dashed line shows sludge level in vessel and red dashed line shows centre line of impeller..... 131

Figure 7.2 – Path line followed by a single radioactive particle over a 20 minute period in a lab-scale anaerobic digester mixing synthetic sludge at i). 50 rpm, ii). 100 rpm, iii). 150 rpm, and iv). 200 rpm. Black dashed line shows sludge level in vessel and red dashed line shows centre line of impeller. . 132

Figure 7.3 – x, y, and z co-ordinates of a single radioactive particle over a 20 minute period in a lab-scale anaerobic digester mixing real sludge at i). 50 rpm, ii). 100 rpm, iii). 150 rpm, and iv). 200 rpm ..... 135

Figure 7.4 – x, y, and z co-ordinates of a single radioactive particle over a 20 minute period in a lab-scale anaerobic digester mixing synthetic sludge at i). 50 rpm, ii). 100 rpm, iii). 150 rpm, and iv). 200 rpm..... 137

Figure 7.5 - Central differencing method..... 138

Figure 7.6 - Production of an azimuthal grid scheme for spatial averaging of data, taken from Chiti et al. (2011) ..... 139

Figure 7.7 – Azimuthally-averaged occupancy in a lab-scale anaerobic digester mixing real sludge at i). 50 rpm, ii). 100 rpm, iii). 150 rpm, and iv). 200 rpm..... 140

Figure 7.8 – Azimuthally-averaged occupancy in a lab-scale anaerobic digester mixing synthetic sludge at i). 50 rpm, ii). 100 rpm, iii). 150 rpm, and iv). 200 rpm ..... 141

Figure 7.9 – Azimuthally-averaged velocity magnitude, normalised by tip speed, in a lab-scale anaerobic digester mixing real sludge at i). 50 rpm, ii). 100 rpm, iii). 150 rpm, and iv). 200 rpm ..... 145

Figure 7.10 – Azimuthally-averaged velocity magnitude, normalised by tip speed, in a lab-scale anaerobic digester mixing synthetic sludge at i). 50 rpm, ii). 100 rpm, iii). 150 rpm, and iv). 200 rpm .....	146
Figure 7.11 – Azimuthally-averaged axial velocity, normalised by tip speed, in a lab-scale anaerobic digester mixing real sludge at i). 50 rpm, ii). 100 rpm, iii). 150 rpm, and iv). 200 rpm .....	147
Figure 7.12 – Azimuthally-averaged axial velocity, normalised by tip speed, in a lab-scale anaerobic digester mixing synthetic sludge at i). 50 rpm, ii). 100 rpm, iii). 150 rpm, and iv). 200 rpm .....	148
Figure 7.13 – Azimuthally-averaged radial velocity, normalised by tip speed, in a lab-scale anaerobic digester mixing real sludge at i). 50 rpm, ii). 100 rpm, iii). 150 rpm, and iv). 200 rpm .....	149
Figure 7.14 – Azimuthally-averaged radial velocity, normalised by tip speed, in a lab-scale anaerobic digester mixing synthetic sludge at i). 50 rpm, ii). 100 rpm, iii). 150 rpm, and iv). 200 rpm .....	150
Figure 7.15 – Mean frequency of circulation in a lab-scale anaerobic digester mixing real or synthetic sludge .....	153
Figure 7.16 – Mean circulation velocity in a lab-scale anaerobic digester mixing real or synthetic sludge .....	153
Figure 7.17 – Agitation index in a lab-scale anaerobic digester mixing real or synthetic sludge .....	153
Figure 8.1 – Geometry of i). the digester vessel and ii). the impeller .....	156
Figure 8.2 – Comparison of velocity magnitude from varying grid densities along a line, $r/R = 0.6$ ..	162
Figure 8.3 - $u$ velocity vector plots of CMC mixed in a lab-scale digester at 100 rpm, measured using PIV .....	164
Figure 8.4 - $v$ velocity vector plots of CMC mixed in a lab-scale digester at 100 rpm, measured using PIV .....	164
Figure 8.5 – $u$ velocities along a line at $r/R = 0.6$ modelled using four different turbulence models, as compared to results from PIV .....	166
Figure 8.6 – $v$ velocities along a line at $r/R = 0.6$ modelled using four different turbulence models, as compared to results from PIV .....	166

Figure 8.7 – Turbulent kinetic energy, $k$ , along a line at $r/R = 0.6$ modelled using four different turbulence models, as compared to results from PIV .....	168
Figure 8.8 - CFD contour plots of normalised velocity magnitude for synthetic sludge mixed at i). 50 rpm, ii). 100 rpm and iii). 200 rpm .....	170
Figure 8.9 - CFD contour plots of normalised axial velocity for synthetic sludge mixed at i). 50 rpm, ii). 100 rpm and iii). 200 rpm .....	170
Figure 8.10 - CFD contour plots of normalised radial velocity for synthetic sludge mixed at i). 50 rpm, ii). 100 rpm and iii). 200 rpm .....	170
Figure 8.11 – Contour plots of velocity magnitude for digesters mixed at i). 50 rpm, ii). 100 rpm and iii). 200 rpm .....	172
Figure 8.12 – Vector plots of velocity coloured by velocity magnitude for digesters mixed at i). 50 rpm, ii). 100 rpm and iii). 200 rpm .....	173
Figure 8.13 – Contour plots of axial velocity for digesters mixed at i). 50 rpm, ii). 100 rpm and iii). 200 rpm .....	175
Figure 8.14 – Contour plots of radial velocity for digesters mixed at i). 50 rpm, ii). 100 rpm and iii). 200 rpm .....	176
Figure 8.15 – Contour plots of tangential velocity for digesters mixed at i). 50 rpm, ii). 100 rpm and iii). 200 rpm .....	177
Figure 8.16 – Change in proportion of digester volume experiencing high, medium and low velocity magnitudes with increasing mixing speed .....	180
Figure 8.17 – Mean velocity magnitude in different zones and in the digester overall at modelled mixing speeds .....	181
Figure 8.18 – Particle trajectories of ten neutrally buoyant particles for digesters mixed at i). 50 rpm, ii). 100 rpm and iii). 200 rpm .....	183
Figure 8.19 – Contour plots of TKE for digesters mixed at i). 50 rpm, ii). 100 rpm and iii). 200 rpm .....	185
Figure 8.20 – Contour plots of TI for digesters mixed at i). 50 rpm, ii). 100 rpm and iii). 200 rpm .....	187

Figure 8.21 – Mean TI in different zones and in the digester overall at modelled mixing speeds .....	188
Figure 8.22 – Contour plots of velocity gradient for digesters mixed at i). 50 rpm, ii). 100 rpm and iii). 200 rpm .....	190
Figure 8.23 – Vector plots of velocity coloured by velocity gradient for digesters mixed at i). 50 rpm, ii). 100 rpm and iii). 200 rpm .....	191
Figure 8.24 - Histogram of local velocity gradient in a lab-scale digester at mixing speeds of 50, 100 and 200 rpm .....	193
Figure 9.1 – RR of four digesters over the course of the first experiment (mixing changes made on Day 65 indicated by vertical line) .....	198
Figure 9.2 – RR of four digesters over the course of the second experiment (mixing changes made on Day 59 indicated by vertical line) .....	199
Figure 9.3 – pH of four digesters over the course of the first experiment (mixing changes made on Day 65 indicated by vertical line) .....	201
Figure 9.4 – TA of four digesters over the course of the first experiment (mixing changes made on Day 65 indicated by vertical line) .....	201
Figure 9.5 - pH of four digesters over the course of the second experiment (mixing changes made on Day 59 indicated by vertical line) .....	202
Figure 9.6 - TA of four digesters over the course of the second experiment (mixing changes made on Day 59 indicated by vertical line) .....	202
Figure 9.7 – VFA concentrations in four digesters over the course of the first experiment (mixing changes made on Day 65 indicated by vertical line) .....	204
Figure 9.8 - VFA concentrations in four digesters over the course of the second experiment (mixing changes made on Day 59 indicated by vertical line) .....	205
Figure 9.9 – TS concentration of four digesters over the course of the first experiment (mixing changes made on Day 65 indicated by vertical line) .....	207

Figure 9.10 – VS concentration of four digesters over the course of the first experiment (mixing changes made on Day 65 indicated by vertical line) .....	207
Figure 9.11 – TS concentration of four digesters over the course of the second experiment (mixing changes made on Day 59 indicated by vertical line) .....	208
Figure 9.12 – VS concentration of four digesters over the course of the second experiment (mixing changes made on Day 59 indicated by vertical line) .....	208
Figure 9.13 - Cumulative biogas production of four digesters over the course of the first experiment (mixing changes made on Day 65 indicated by vertical line).....	210
Figure 9.14 - Daily biogas production of four digesters over the course of the first experiment (mixing changes made on Day 65 indicated by vertical line) .....	210
Figure 9.15 - Cumulative biogas production of four digesters over the course of the second experiment (mixing changes made on Day 59 indicated by vertical line) .....	211
Figure 9.16 - Daily biogas production of four digesters over the course of the second experiment (mixing changes made on Day 59 indicated by vertical line).....	211
Figure 9.17 – Percentage of methane in biogas produced by each of four digesters over the course of the first experiment (mixing changes made on Day 65 indicated by vertical line) .....	217
Figure 9.18 – Percentage of methane in biogas produced by each of four digesters over the course of the second experiment (mixing changes made on Day 59 indicated by vertical line) .....	217
Figure 9.19 – Mean daily gas production over RT either side of the change in mixing speed during the first experiment .....	219
Figure 9.20 – Mean daily gas production over RT either side of the change in mixing speed during the second experiment .....	220
Figure 9.21 – Total eubacteria present in each of four digesters over the course of the second experiment (mixing changes made on Day 59 indicated by vertical line) .....	222
Figure 9.22 – Abundance of <i>Methanosaeta</i> present in each of four digesters over the course of the second experiment (mixing changes made on Day 59 indicated by vertical line).....	223

Figure 9.23 – Abundance of *Methanomicrobiales* present in each of four digesters over the course of the second experiment (mixing changes made on Day 59 indicated by vertical line) ..... 224

Figure 9.24 – Abundance of *Methanobacteriales* present in each of four digesters over the course of the second experiment (mixing changes made on Day 59 indicated by vertical line) ..... 224

Figure 9.25 - Comparison of samples taken from the top (left) and bottom (right) of the unmixed digester, using SEM..... 229

Figure 9.26 - Comparison of samples taken from the bottom of digesters mixed at 200 rpm (left) and 100 rpm (right), using SEM ..... 229

Figure 10.1 - Average daily gas volume produced in the second retention time after a change in mixing speed, measured during experiments, against average velocity gradient, calculated from CFD models of the digester ..... 248

Figure 10.2 - Percentage change in gas production volume produced in the second retention time after a change in mixing speed, measured during experiments, against average velocity gradient, calculated from CFD models of the digester, for lab-scale, mechanically-mixed digesters fed with nutrient-stressed and non-stressed feedstock ..... 249

## List of tables

Table 2.1 - Inhibitory effects of cations on anaerobic digestion .....	14
Table 2.2 - Average kinetic values for mesophilic growth of Methanosarcina and Methanosaeta from literature. Average values given with standard deviations in parentheses. Reproduced from Conklin et al. (2006).....	42
Table 3.1 – Advantages and disadvantages of two-equation turbulence models and the Reynolds Stress Model (Wilcox, 1998, ANSYS-Fluent, 2012) .....	73
Table 5.1 - Digester feeding regime.....	106
Table 5.2 - Oligonucleotide sequences used as calibration standards for the quantification of total eubacteria and key methanogenic groups. ....	113
Table 6.1 - Composition of synthetic digester sludge.....	120
Table 6.2 - Composition of synthetic sludge based on nutritional information given about components. N.B. toilet paper is assumed to contribute only cellulose equivalent to the weight added. ....	125
Table 6.3 – ICP-MS results of a semi-quantitative metals sweep on synthetic sludge (results are approximate: $\pm 20\%$ ). N.B.: Concentrations are listed as dry/dry weight. ....	126
Table 7.1 - Comparison of viscous properties and total solids of real and synthetic sludges used in PEPT .....	128
Table 7.2 – Mean and standard deviation of velocity magnitude (m/s) calculated from PEPT data for real and synthetic sludge at a range of mixing speeds .....	138
Table 8.1 - Dimensions of the digester vessel and impeller .....	157
Table 9.1 – ICP-MS results of a semi-quantitative metals sweep on synthetic sludge (results are approximate: $\pm 20\%$ ). N.B.: Concentrations are listed as dry/dry weight. ....	197
Table 9.2 – Gradients and R-squared values for linear regression performed on biogas production curves in four digesters before and after a change in mixing speed during the first experiment. N.B.:	

Mixing speeds for each digester are given before and after the change in mixing speeds with the mixing speed in bold relating to the curve whose gradient is calculated ..... 212

Table 9.3 – Gradients and R-squared values for linear regression performed on biogas production curves in four digesters before and after a change in mixing speed during the second experiment.

N.B.: Mixing speeds for each digester are given before and after the change in mixing speeds with the mixing speed in bold relating to the curve whose gradient is calculated ..... 213

## Abbreviations and notation

### Abbreviations

AD	Anaerobic digestion
ADC	Analogue-to-digital converter
CARPT	Computer-automated radioactive particle tracking
CAT	Computer aided tomography
CCD	Charged coupled device
CFD	Computational fluid dynamics
CHP	Combined heat and power
CMC	Carboxymethyl cellulose
COD	Chemical oxygen demand
CT	Cycle threshold
DEFRA	Department of the Environment, Food and Rural Affairs
DGGE	Denaturing gradient gel electrophoresis
DNA	Deoxyribonucleic acid
DNS	Direct numerical simulation
DS	Dissolved solids
EPS	Extracellular polymeric substances
FFT	Fast Fourier transform
FISH	Fluorescence in situ hybridisation
GCI	Grid convergence index
HPLC	High performance liquid chromatography
HRT	Hydraulic retention time
IA	Intermediate alkalinity
ICP-MS	Inductively coupled plasma mass spectrometry
IUPAC	International Union of Pure and Applied Chemistry
LDA	Laser Doppler anemometry
LEL	Lower explosive limit
LES	Large eddy simulation
MEL	Mixing energy level
MRF	Multiple rotating frames
MSW	Municipal solid waste
N	Nitrogen
OLR	Organic loading rate
P	Phosphorus
PA	Partial alkalinity
PBT	Pitched blade turbine
PCR	Polymerase chain reaction
PEPT	Positron emission particle tracking
PET	Positron emission tomography
PIV	Particle image velocimetry
qPCR	Quantitative real-time polymerase chain reaction

RANS	Reynolds-averaged Navier-Stokes
RNA	Ribonucleic acid
RNG	Re-normalisation group
RO	Renewables obligation
RR	Ripley's ratio
RSM	Reynolds stress model
RT	Retention time
RTD	Residence time distribution
SBR	Strong base anion exchange resin
SEM	Scanning electron microscopy
SFAS	Saturated fatty acid- $\beta$ -oxidising syntrophs
SGS	Sub-grid scheme
SIMPLE	Semi-implicit method for pressure-linked equations
SM	Sliding mesh
SPOB	Syntrophic propionate-oxidising bacteria
SRT	Solids retention time
SST	Shear stress transport
STW	Sewage treatment works
TA	Total alkalinity
TDS	Total dissolved solids
TGGE	Temperature gradient gel electrophoresis
TI	Turbulence intensity
TKE	Turbulent kinetic energy
TLD	Trajectory length distribution
T-RFLP	Terminal restriction fragment length polymorphism analysis
TS	Total solids
UPW	Ultrapure water
USEPA	United States Environmental Protection Agency
VFA	Volatile fatty acid
VOF	Volume of fluid
VS	Volatile solids

## Notation

$A$	Volume of acid
$B, C_1, C_2, C_\mu$	Constants
$D$	Characteristic dimension
$d_i$	Impeller diameter
$d_p$	Particle diameter
$D_\omega$	Cross-diffusion term
$F$	Mean frequency of circulation
$\bar{F}$	Body forces
$F_s$	Factor of safety
$G$	Velocity gradient
$\bar{G}$	Average velocity gradient

$\check{G}_k$	Modified generation term
$G_k, G_\omega$	Generation terms
$H$	Number of cells
$\bar{l}$	Mean trajectory length
$I$	Agitation index
$I_{mix}$	Macromixing index
$K$	Turbulent kinetic energy
$L$	Characteristic dimension of a vessel
$N$	Rotational velocity
$N$	Normality of acid
$N_t$	Total number of trajectories
$P$	Pressure
$PA$	Volume of acid to reach partial alkalinity end point
$P_{ave}$	Average mixing power input to vessel
$P_{in}$	Power of mixing input to vessel
$Re$	Reynolds number
$s_{ij}$	Mean strain rate tensor
$S_k, S_\epsilon$	Source terms
$St$	Stokes number
$T$	Time
$TA$	Volume of acid to reach total alkalinity end point
$TS$	Total solids
$U$	Characteristic velocity
$\bar{U}$	Average velocity
$u'$	Fluctuating component of velocity
$u, v, w$	Velocity
$u^+$	Dimensionless velocity
$u_g$	Mesh velocity of moving mesh
$u_i, u_j$	$i^{th}, j^{th}$ component of velocity
$u_i', u_j'$	$i^{th}, j^{th}$ component of fluctuating velocity
$u_K$	Kolmogorov velocity scale
$u_r$	Velocity of the rotating frame
$u_T$	Friction velocity
$u_{tip}$	Tip velocity
$V$	Volume
$VS$	Volatile solids
$W_1, W_2, W_3$	Weights
$x, y, z$	Cartesian co-ordinates
$x_i, x_j$	Cartesian co-ordinates
$Y$	Distance from the wall
$y^+$	Dimensionless wall coordinate
$Y_k, Y_\omega$	Dissipation due to turbulence

$\alpha^*$	Damping coefficient
$\Gamma_k, \Gamma_\omega$	Effective diffusivity
$\delta_{ij}$	Kronecker delta
$E$	Specific energy dissipation
$K$	Von Kármán constant
$\lambda_K$	Kolmogorov length scale
$M$	Dynamic viscosity
$N$	Kinematic viscosity
$\nu_t$	Turbulent eddy viscosity
$P$	Density
$\rho_p$	Particle density
$\sigma_k, \sigma_\varepsilon$	Prandtl numbers
$\bar{\tau}$	Stress tensor
$\tau_f$	Fluid response time
$\tau_K$	Kolmogorov time scale
$\tau_p$	Particle response time
$\Phi$	Power dissipation
$\Phi$	General scalar
$\Omega$	Specific dissipation rate
$\tilde{\omega}$	Angular velocity of rotating frame

## **CHAPTER 1      Introduction**

### **1.1 Background and Motivation**

Each day, the UK water industry collects, treats, and returns to the environment over 10 billion litres of wastewater at over 9000 wastewater treatment sites. Sewage sludge is a by-product of this treatment process (WaterUK, 2012). In 2010/11, 1.5 million tonnes of dry solids were produced as sewage sludge (WaterUK, 2012) and it is expected that the volumes of sludge that the industry must deal with in the future is likely to increase. Factors affecting this increase include population increase, increased property connection to the sewer network, and the continued implementation of the European Urban Waste Water Treatment Directive (91/271/EEC) and related legislation, which requires tighter controls on what nutrients can be released from wastewater treatment facilities (WaterUK, 2012).

Sewage sludge can be disposed of or recycled in a number of ways, including thermal destruction and disposal to landfill, with the most common route in UK being recycling of sludge to land. 70.8 % of sludge in the UK is disposed of in this manner. Disposal to land, which includes agricultural use, land reclamation and composting, is considered to be one of the most sustainable sludge disposal routes. Disposal to land can reduce the need to apply artificial fertiliser to agricultural land and can improve the nutritional quality of the soil for arable farming (WaterUK, 2012). In order for sludge to be disposed to land in this way, it must first be considered pathogenically safe and biologically stable. The EU Directive on the protection of the environment, and in particular of the soil, when sewage sludge is used in agriculture (86/278/EEC) stipulates that sludge must have “undergone biological, chemical or heat treatment, long-term storage or any other appropriate process so as to significantly reduce its fermentability and the health hazards resulting from its use” before it can be applied to land. Anaerobic digestion (AD) is one method of stabilising the sludge in line with this

legislation and has been practised for over 100 years (Brade and Noone, 1981); today 66 % of sewage sludge in UK is treated in this way (WaterUK, 2009).

Biogas, the main by-product of AD, can be used as a renewable source of heat and power through the use of combined heat and power (CHP) units. Thus, there is a value attached to this by-product and increasing the biogas production of an anaerobic digester becomes desirable. This desire to increase biogas production, and to increase the percentage of methane in the biogas that is produced, must be balanced against the operational costs of the anaerobic digester.

The major energy requirement for operation of an anaerobic digester is heating. However, the effects of temperature variation within the mesophilic anaerobic digestion range are well understood, with temperature increases between 22 and 41 °C increasing the efficiency of the digestion process and increasing the biogas production. Temperature increases above 41 °C resulting in a decrease in biogas production (Chae et al., 2008, Agler et al., 2010). Hence, decreasing the operating temperature of a digester to reduce the operational costs is not considered to be feasible on sites where biogas is used as an energy source, as it negatively impacts biogas production.

Estimates for the energy usage of mixing in a digester vary widely with Owen (1982) stating that the mixing of an anaerobic digester accounts for between 17 and 37 % of the total energy usage, whilst Lübken et al. (2007) calculate that the mixing requirements of their pilot-scale biogas reactor account for only 2.5 to 5 % of energy usage. At Severn Trent Water's Minworth sewage treatment works (STW), a site that serves approximately 1 million people, energy for mixing is reported to be approximately 3.1 W/m<sup>3</sup> of digester (Griffin, 2009). As operators and designers aim to decrease the costs and environmental impacts of anaerobic digestion, reducing the level of mixing can appear to be a feasible option for reducing energy usage. Unlike the effects of heating, the effects of reduced mixing on biogas production are not clear.

As such, conflict arises between the desire to increase biogas production, which according to the conventional wisdom requires mixing to maximise the energy production from the digester (USEPA, 1976), and the desire to limit the energy input to the digester in the form of mixing.

Whilst mixing is understood to be a key parameter in maximising gas production, little to no design information, other than that made available by suppliers, exists to aid engineers in designing digester mixing systems, evaluating tenders or rating existing systems, and the design values that are used are based on rules of thumb rather than on specific mixing theory (Dawson and Ozgencil, 2009). The Design Guide for Digester and Sludge Tank Mixing Systems (Dawson and Ozgencil, 2009) recommends that mixing systems are sized relative to the sludge active volume (volume of the digester in which sludge is actively mixed excluding volumes occupied by grit at the base of the digester) and the sludge blend time (time taken for the concentration of an injected tracer to be within 10 % of the mean concentration in the digester at all points in the digester). However, there is no clear link to gas production and the underpinning science is not clearly understood.

## **1.2 Research Relevance**

The work reported in this thesis focuses on physical and numerical analyses of mechanically mixed laboratory scale anaerobic digesters, in order to better understand the link between mixing and gas production. The work reported here uses positron emission particle tracking (PEPT) and computational fluid dynamics (CFD) to investigate the flow patterns established in digesters mixed at different speeds. Experimental work is carried out to determine the effects of these flow patterns on the biochemical environment, microbiological communities within the digesters and gas production at laboratory scale.

## **1.3 Layout of thesis**

Following on from this Introduction (Chapter 1) is a review of the literature relating to anaerobic digestion (Chapter 2), fluid flow and the modelling of mixing using CFD (Chapter 3). From this understanding of the current literature, the aim and objectives of the research are set out in Chapter

4. The wide variety of materials and methods used in order to fulfil these objectives are outlined in Chapter 5. Chapter 6 gives details of the synthetic sludge developed for this research and its relevant properties. Chapter 7 considers the digester flow patterns established in a digester analysed using the experimental technique of PEPT, whilst Chapter 8 considers these flow patterns, and their associated turbulent characteristics, using CFD modelling techniques. A comparison of the experimental and numerical results is also carried out. The effect of mixing on anaerobic digestion in terms of digester stability and biogas production are considered in Chapter 9, along with an analysis of the microbiological communities present using a quantitative polymerase chain reaction (qPCR) study. A general discussion of all of the results and their implications is presented in Chapter 10 and finally, conclusions and recommendations for future research are drawn in Chapter 11.

## **CHAPTER 2      Anaerobic digestion**

Within this chapter, the aims and process of AD are considered along with factors that are known to affect the digestion process. In particular, the literature relating mixing to gas production and digester stability is reviewed. Finally, the growing use of qPCR as a tool to understand the microbiology of digesters is discussed.

### **2.1 Aims of anaerobic digestion**

AD involves the biological decomposition of organic and inorganic molecules, in the absence of oxygen, in an airtight container (Tchobanoglous and Burton, 1991). In the wastewater treatment industry, AD is used to stabilise sewage sludge so that it can be applied to land as a valuable source of fertiliser instead of going to landfill. Additionally, the process reduces sludge transportation costs due to the reduction in the sludge volume that occurs. As such, the green credentials of AD are considered to be significant. In addition to reducing the volume of waste sent to landfill and reducing the carbon footprint linked with the transportation of waste, AD reduces the methane emissions generated by waste material from the wastewater treatment process. This lowers the carbon footprint of the wastewater treatment process and the industry as a whole. This is achieved by the extraction of valuable energy from the sludge in the form of biogas. As such, the main aims of anaerobic digestion can be summarised as:

1. Sludge stabilisation – To obtain a stable and safe end-product by reducing the organic content and the pathogen concentration of the sludge (van Haandel and van der Lubbe, 2007)
2. Sludge volume reduction – To increase the concentration of solids so that the final volume of sludge to be disposed of is kept to a minimum (van Haandel and van der Lubbe, 2007)

3. Biogas production – More recently, biogas has been used as a source of renewable energy and this has become a valuable by-product of the anaerobic digestion process (WaterUK, 2009)

## **2.2 Biogas as green energy**

The majority of biogas (60 %) produced by AD in the UK water industry is used to generate renewable heat and power in CHP units (WaterUK, 2009). This makes up a large percentage of the 877 GWh renewable electricity generated by the UK water industry in 2010-11, as well as accounting for some of the renewably generated heat that companies use. This accounts for 9.7 % of the total energy used by the industry (WaterUK, 2012). Whilst this does not sound like a great deal, it is significant enough for AD to be an economically favourable option for most, if not all, companies in the UK wastewater treatment industry. Economically, increasing the biogas production of an anaerobic digester is beneficial as long as the CHP capacity is available for that biogas to be used (Harvie, 2007).

DEFRA guidelines (DEFRA and DECC, 2011) promote the use of anaerobic digestion to produce green energy from waste products. Incentives such as the Renewables Obligation (RO), which provide financial support for generators of renewable electricity, mean that wastewater treatment companies benefit both internally and externally from increasing the production of high quality biogas from their anaerobic digesters. Energy use per unit volume across the UK wastewater treatment industry has increased over the 2008-11 period (WaterUK, 2009, 2012) mostly due to the necessity to treat water to higher final effluent quality (Cave, 2009, Howe, 2009). Additionally, the industry has commitments to reduce its contribution to climate change through greenhouse gas emissions. Reduced energy usage and increased renewable energy generation both play a significant role in this (WaterUK, 2012).

## 2.3 Biochemical processes

In order to appreciate the effects of process parameters on AD and biogas production, an understanding of the microbiological processes involved is vital. The microbiology of anaerobic digesters, though complex, is well understood. Most texts (Borja et al., 2005, Garcia-Ochoa et al., 1999, Siles et al., 2008) consider the breakdown of sludge to stabilised sludge and biogas as consisting of three main stages: hydrolysis, acidogenesis and methanogenesis. Acetogenesis is sometimes included as an intermediate step between acidogenesis and methanogenesis (Tchobanoglous and Burton, 1991, Tiehm et al., 2001) as shown in Figure 2.1, and the process can be broken down into a greater number of stages, especially for modelling purposes (Myint et al., 2007).

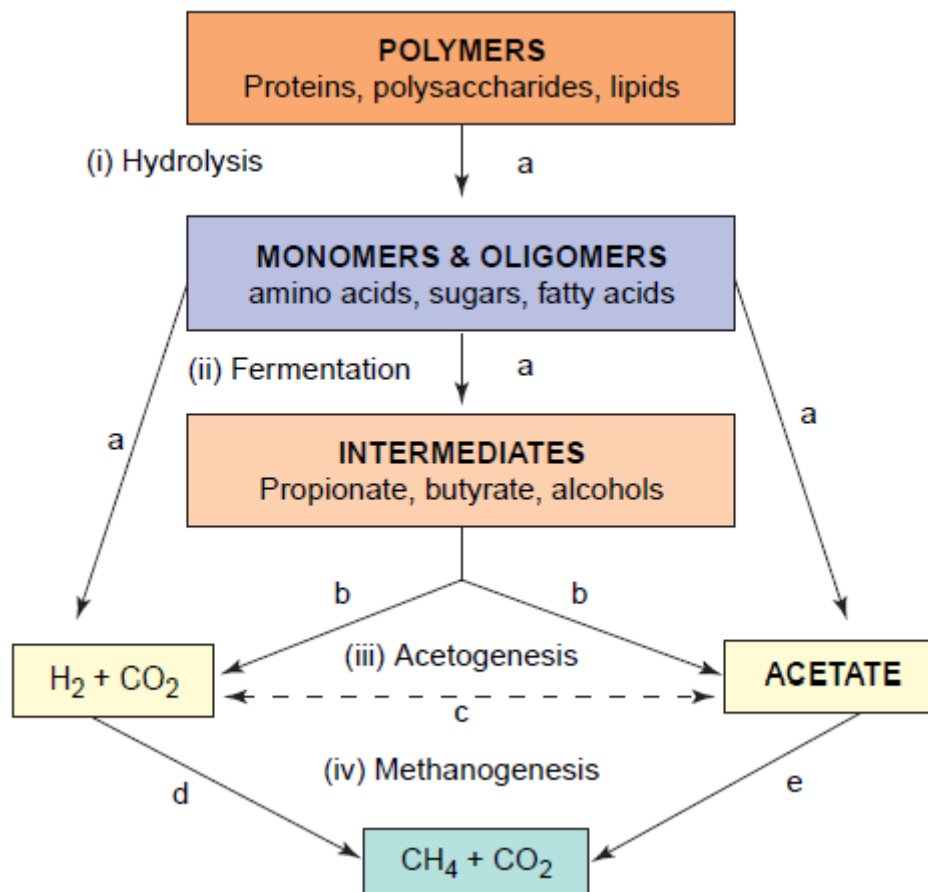


Figure 2.1 - Food web of methanogenic anaerobic digestion, showing four major steps and five physiologically distinct groups of micro-organisms: a - fermentative bacteria, b - hydrogen-producing acetogenic bacteria, c - acetogens, d - hydrogenotrophic methanogens, and e - acetoclastic methanogens. Reproduced from Angenent et al. (2004)

The hydrolysis step breaks down insoluble organic material and high molecular weight compounds, such as proteins, lipids, polysaccharides and nucleic acids, into soluble organic components including amino acids and fatty acids. This is carried out by hydrolases excreted by obligate or facultative anaerobes (Liu et al., 2004). For sewage sludge, this is considered to be the rate-limiting step and hence chemical, mechanical or thermal pre-treatment of the sludge can be employed to improve the digestion efficiency (Park et al., 2005, Tiehm et al., 2001, Vavilin et al., 1996).

The lower weight intermediate products of hydrolysis are then converted into hydrogen, carbon dioxide and acetic acid by acidogens, which are obligate and facultative anaerobes (Tchobanoglous and Burton, 1991). Higher order acids such as propionic, butyric and lactic acids, ketones and alcohols are also formed by the acidogens (Cooney et al., 2007). Acidogenesis has a high energy yield and acidogens are generally considered to be both faster growing and less sensitive to environmental conditions than methanogenic bacteria (Lin, 1993).

The higher order acids that are formed by acidogenesis are broken down by obligate acetogenic bacteria. This is a low energy yield process, and the acetogens are slow-growing and more sensitive to changes in environmental conditions than acidogens (Liu et al., 2004).

The final stage of the process, methanogenesis, converts hydrogen and carbon dioxide, acetate, methanol and formate into methane via the following typical reactions:



This is the slowest stage of the process once the sludge has been hydrolysed (Rincon et al., 2010, Siles et al., 2008).

## 2.4 Factors affecting AD

Whilst AD is a widely-used and well-accepted sludge stabilisation technique, it is a complex process that is sensitive to a wide range of factors. Some of the factors that affect AD are better documented than others and some of the more important of these factors are briefly reviewed here.

### 2.4.1 Temperature

Anaerobic digestion can take place in three temperature ranges: psychrophilic (below 20 °C), mesophilic (30-40 °C) and thermophilic (50-60 °C). At psychrophilic temperatures, the rate of digestion is slow. As such, the majority of sewage treatment plants operate in the mesophilic range. Whilst thermophilic digesters have higher organic loading rates and a higher pathogen destruction rate, the mesophilic range is preferable due to the reduced operational costs of heating, and the lower sensitivity of micro-organisms to toxic substances at lower temperatures (Gerardi, 2003). The structure of the microbial communities that are active in each of the temperature ranges are different, and a change between mesophilic and thermophilic temperatures can cause a severe reduction in the biogas produced by the digester until the populations in the digester have stabilised and grown. Even changes in temperature of 2 °C have been shown to reduce the rate of biogas production (Chae et al., 2008).

Temperature changes have different effects on different stages of the digestion process because of the communities of micro-organisms that are involved. The first stages of the digestion process (hydrolysis and acidogenesis) suffer very few ill effects from changes in temperature due to the mixed population involved in the process. This helps to ensure that at any temperature, there are some micro-organisms that are operating within their preferred temperature range. The later stages of the digestion process (acetogenesis and methanogenesis) require more specialised micro-organisms and thus are more likely to be adversely affected by temperature changes (Ward et al., 2008). As such, methane production is strongly temperature dependant. Moreover, fluctuations in temperature have a greater effect on the activity of methanogens than operating temperature itself.

As the micro-organisms involved in anaerobic digestion all have different optimum operating temperatures, fluctuations in temperature can adversely affect some groups whilst being advantageous to others. Hence, fluctuations can cause changes in the activity of different micro-organism groups, which in turn can lead to changes in the concentration of intermediary digestion products, such as organic alcohols and acids. This in turn will affect the overall performance of the digester (Gerardi, 2003). As such, it is important to maintain a stable operating temperature and process failure can occur if temperature changes are in excess of 1 °C/day. It is recommended that changes in temperature should be kept at less than 0.6 °C/day in order to avoid this situation arising (Appels et al., 2008).

#### **2.4.2 Retention time**

The retention time of a digester can be defined by the solids retention time (SRT), which indicates the average time that solids, and the micro-organisms that live on them, are in the anaerobic digester, or the hydraulic retention time (HRT), which is the average time that the liquid sludge is in the anaerobic digester. In a digester without a recycle, the HRT and SRT are equal. However, by recycling solids to the digester, the SRT and HRT can be decoupled and may vary considerably. As methanogens are slow-growing micro-organisms, the SRTs used in anaerobic digesters tend to be a minimum of 12 days, and often much longer. At lower SRTs, the wash-out of methanogens can have a detrimental effect on the long-term stability and performance of the digester. Furthermore, high SRTs provide the digester with a degree of buffering against the effects of shock or toxic loading. However, higher retention times require larger digestion vessels and as such there is a capital cost associated with an increased retention time. (Gerardi, 2003)

The degradation of volatile solids to methane and carbon dioxide in a digester are dependent on the HRT. In simple terms, the longer the HRT, the greater the volatile solids reduction will be, though it has been shown that increases in HRT greater than 12 days do not significantly increase the destruction of volatile solids. However, if the digested sludge is to be applied to land, the retention

time must be sufficiently high to ensure that the volatile solids and indicator pathogen counts in the end product are low enough to comply with legislation. (Gerardi, 2003)

### 2.4.3 Nutrients

The nutrients required for the micro-organisms involved in anaerobic digestion can be split into two groups, macronutrients and micronutrients. Macronutrients are those nutrients which are required in relatively large quantities by all micro-organisms, nitrogen and phosphorus. These are only available to micro-organisms in soluble form as ammonical nitrogen ( $\text{NH}_4^+\text{-N}$ ) and orthophosphate-phosphorus ( $\text{HPO}_4^-\text{P}$ ). The exact nutrient requirements of the digester vary greatly depending on the organic loading rate. As a rule of thumb, a COD:N:P ratio of 1000:7:1 is used for high strength wastes and a ratio of 350:7:1 for low loadings. These ratios are based on the common empirical formula for cellular material,  $\text{C}_5\text{H}_7\text{O}_2\text{NP}_{0.1}$ , and therefore assume that approximately 12 % of the dry weight of the bacterial cells in the sludge is nitrogen and 2 % is phosphorus. As such, the concentration of nitrogen and phosphorus in a digester can be estimated based on the COD of the influent and the COD removal in the digester. Alternatively, residual concentrations of 5 mg/l  $\text{NH}_4^+\text{-N}$  and 1-2 mg/l  $\text{HPO}_4^-\text{P}$  are recommended for digester effluent from a stable digester. By ensuring that there is residual nitrogen and phosphorus in the effluent, a check is made that bacterial growth is not limited by these elements in the digester. (Gerardi, 2003)

Micronutrients are those nutrients that are required in relatively small quantities for microbiological growth and enzyme systems. For those micro-organisms involved in the conversion of acetate to methane, the critical inorganic micronutrients are cobalt, nickel, iron and sulphur. Methanogens also need traces of selenium, tungsten, molybdenum, barium, calcium, magnesium and sodium. These micronutrients are present in most municipal wastewater in sufficient concentrations for an anaerobic digester to run stably, though for industrial wastewater, it is often necessary to dose digesters with additional micronutrients in order to prevent digester upsets. (Gerardi, 2003)

#### 2.4.4 Alkalinity and pH

As with temperature, different micro-organisms have different optimum operating pH. Whilst most fermentative bacteria can function in a range between pH 4.0 and 8.5, the change in pH does have an effect on the products of fermentation. At low pH, the main products are acetic and butyric acid and at a pH of 8.0, the main products are acetic and propionic acid. Meanwhile, the micro-organisms involved in methanogenesis are more sensitive to pH, with an optimum range of pH 6.8-7.2 (Appels et al., 2008). For this reason, the digestion process is sometimes split into a two-stage process so that a more acidic pH can be maintained in the first stage thereby optimising hydrolysis and acidification, whilst the second stage is optimised for methanogenesis. The pH in an anaerobic digestion is normally maintained between pH 6.8 and 7.2, in order to prevent the predominance of acidogens which may cause the accumulation of volatile fatty acids (VFAs), causing a reduction in pH and eventually, process failure (Rajeshwari et al., 2000), commonly known as souring.

In a stable digester, the reduction of pH caused by VFA accumulation is countered by the activity of methanogens which produce alkalinity in the form of carbon dioxide, ammonia and bicarbonate. Alkalinity can be considered as the buffering capacity of a digester to prevent rapid changes in pH. A stable digester will have a high alkalinity concentration in the form of carbon dioxide and bicarbonate ions. This makes it a useful indicator of stability and impending failure, as the accumulation of VFAs in a digester will result in a drop in alkalinity before the pH of the digester starts to drop (Ward et al., 2008). A molar ratio of bicarbonate:VFA of at least 1.4:1 is recommended in order for a digester to remain stable and well-buffered. However, it has been shown that the stability of the ratio is of greater importance than the exact level of the ratio itself (Appels et al., 2008).

### 2.4.5 Inhibitors

A huge number of substances have been reported in the literature as being inhibitory to anaerobic digestion. In order to be considered as inhibitory, a substance must cause an adverse shift in the microbial population or cause the inhibition of bacterial growth. This is usually identified by a decrease in biogas production and the accumulation of VFAs. For most inhibitory substances there is considerable variation in the inhibition levels reported in the literature. This is mainly due to the complexity of the processes involved in anaerobic digestion and the effects of other factors discussed within this section (Chen et al., 2008). In particular, acclimation and pH can have a strong effect on the inhibitory effects of chemicals at different concentrations. A slow increase in inhibitor concentration allows greater time for micro-organisms to acclimate than a sudden spike in concentration which increases the tolerance of a system to an inhibitor (Angelidaki and Ahring, 1993). pH can affect the level of ionisation of the inhibitor, thereby affecting the 'active' concentration which can produce inhibitory effects on the microbiological community (Koster and Lettinga, 1988).

Ammonia is produced during the degradation of nitrogenous material, found in urea and proteins. Methanogenic populations are the most likely to be damaged by ammonia inhibition. Several mechanisms for this inhibition have been proposed, including changes in intracellular pH, inhibition of specific enzyme reactions or increase of the energy required for cell maintenance. It is generally accepted that ammonia concentrations below 200 mg/l are beneficial to anaerobic digestion as nitrogen is an essential nutrient for the micro-organisms involved. However, at higher concentrations, inhibition occurs. Literature has reported a wide range of inhibitory concentrations ranging from 1.7 to 14 g/l, causing a 50 % reduction in methane production. The inhibitory concentration is affected by pH, temperature, the presence of cations such as sodium ( $\text{Na}^+$ ), calcium ( $\text{Ca}^{2+}$ ) and magnesium ( $\text{Mg}^{2+}$ ), and the speed at which ammonia concentration has increased, allowing acclimation of the micro-organisms as mentioned above. (Chen et al., 2008)

**Table 2.1 - Inhibitory effects of cations on anaerobic digestion**

<b>Cation</b>	<b>Concentration</b>	<b>Result</b>	<b>Reference</b>
Al <sup>3+</sup>	1000mg/l Al(OH) <sub>3</sub> for 59 days	Specific activity of methanogens and acetogens decreased by 50% and 72% respectively	Cabirol et al., 2003
	2500 mg/l	Tolerated after acclimation	Jackson-Moss and Duncan, 1991
Ca <sup>2+</sup>	Up to 7000 mg/l	No inhibitory effect	Jackson-Moss et al., 1989
	200 mg/l	Optimal for methanation of acetic acid	Kugelman and McCarty, 1964
	2500-4000 mg/l 8000 mg/l	Moderately inhibitory Strongly inhibitory	
Mg <sup>2+</sup>	720 mg/l	Optimal	Ahring et al., 1991
	400 mg/l	Growth ceases	Schmidt and Ahring, 1993
K <sup>+</sup>	< 400 mg/l	Enhance performance	Kugelman and McCarty, 1964
	> 400 mg/l	Inhibitory	
Na <sup>2+</sup>	100-200 mg/l	Beneficial	McCarty, 1964
	230 mg/l	Optimal for acetoclastic methanogens	Kugelman and Chin, 1971
	350 mg/l	Optimal for hydrogenotrophic methanogens	Patel and Roth, 1977
	3500-5500 mg/l 8000 mg/l	Moderately inhibitory Strongly inhibitory	McCarty, 1964

Salt toxicity causes bacterial cells to dehydrate due to osmotic pressure. This has been found to be predominantly determined by the cation. Cations such as aluminium (Al<sup>3+</sup>), sodium (Na<sup>+</sup>), potassium (K<sup>+</sup>), calcium (Ca<sup>2+</sup>) and magnesium (Mg<sup>2+</sup>) are present in sewage sludge and are released by the breakdown of organic matter. Additionally, they may be added as chemicals intended to adjust digester pH. Whilst they are required for microbial growth, high levels of these cations slow down the growth rate and can even cause severe inhibition. Information about the effects of aluminium on anaerobic digestion is limited. Similarly, very little is known about the toxicity of calcium, and the toxic effects of potassium are rarely discussed. More importantly, the concentration at which elements are inhibitory is not well-understood and various authors have stated a wide range of

inhibitory concentrations. Some of these are laid out in Table 2.1 to give an indication of the discrepancies in the data.

## **2.5 Mixing and anaerobic digestion**

### **2.5.1 Purpose of mixing**

Mixing is defined in the Handbook of Industrial Mixing: Science and Practice (Paul et al., 2004) as “the reduction of inhomogeneity in order to achieve a desired process result. The inhomogeneity can be one of concentration, phase, or temperature. Secondary effects, such as mass transfer, reaction, and product properties are usually the critical objectives.” Mixing in anaerobic digesters is necessary to bring bacteria in the biomass and food sources in the sludge together, so that sludge stabilisation can occur (USEPA, 1976). Furthermore, mixing promotes the establishment of a homogeneous environment for anaerobic digestion, by reducing temperature, pH, and concentration gradients within the reactor (Appels et al., 2008). This may prove to be important if spikes in temperature or toxin concentration occur in the influent sludge, which would have damaging effects on the microbiological community in the digester. According to the USEPA’s Anaerobic Sludge Digestion Operations Manual (1976), another aim of mixing is to minimise the formation of grit and scum layers in the reactor to ensure that the highest possible active volume is achieved. Vera and Lavelle (2005) showed that the elimination or control of grit and scum accumulation requires up to 10 times as much mixing as is required for maintenance of homogeneous temperature and solids concentration within the sludge, and it is not clear as to whether this degree of mixing is actually achieved in commercial digesters. Edgington (2001) drew attention to the fact that despite Severn Trent’s anaerobic digesters varying widely in hydraulic performance, all of those that used unconfined gas mixing had an effective volume of 80% or greater, which they considered to be acceptable. This suggests that eliminating grit and scum accumulation is not the main aim of mixing in anaerobic digesters operated in the UK wastewater industry.

### **2.5.2 Methods of mixing**

Mechanical mixing, gas mixing and mixing by recirculation can all be used to mix anaerobic digesters.

Mechanical mixing, despite being the most efficient form of mixing in terms of power consumed per volume mixed (Brade and Noone 1981), is not common due to issues of maintenance and wear and tear created by moving parts within the digester. Recirculation mixing most commonly uses mechanical pumps mounted on the outside of the digester to remove sludge from the digester and re-inject it at another point within the digester.

Gas mixing systems can be classified as unconfined or confined. Unconfined gas systems collect generated biogas at the top of the digesters, compress it and then pump it back in at the bottom of the digester through diffusers. The bubbles rise to the surface, forcing movement of the sludge as they pass up through the digester. Confined gas systems collect and compress gas in the same manner but discharge it through confined tubes. This forces the upward movement of sludge in the tubes, which creates convection currents within the digester (Tchobanoglous and Burton, 1991). Severn Trent Water use unconfined gas mixing in the majority of their anaerobic digesters.

All of these mixing technologies are represented in the literature, though impeller mixing dominates (Kaparaju et al., 2008, Ong et al., 2002, Gomez et al., 2006, Hoffman et al., 2008, Karim et al., 2005a, Karim et al., 2005b) due to its ease of application in a laboratory environment.

### **2.5.3 Industrial application of mixing**

Although the importance of mixing for achieving optimum process performance and gas production is well recognised (Appels et al., 2008), there is no clear consensus as to what constitutes an optimal mixing regime. A report for Severn Trent Water (Auty and Marquet, 2009) showed that across the wastewater treatment industry in the UK, there is a huge variation in how anaerobic digesters are operated, with some digesters mixed for only five minutes in an hour with no apparent detrimental effect on biogas yield, whilst others are mixed continually and achieve similar yields. Furthermore, the review highlighted the wide range of variables that must be considered when designing a mixing

system for a digester, including the shape of the digester, the mixing technology to be used, operating times, mixing energy and sludge rheology, which is in turn affected by the temperature, solids concentrations, biological loading and treatment of the sludge prior to digestion.

The only example of a full-scale trial of the effects of mixing on gas production from digesters was carried out within Severn Trent Water. Work carried out at full-scale with digesters in Loughborough concluded that continuous mixing of mesophilic anaerobic digesters produced more gas than periodic mixing (Harvie, 2007). As can be seen in Section 2.4, this finding agrees with the results of (Karim et al., 2005a), but not with other results from lab-scale trials published in the literature (Kaparaju et al., 2008).

## **2.6 Effects of mixing on biogas production**

The literature relating to the mixing of sewage sludge alone at full-scale is limited to Edgington (2001) who demonstrated that although the hydraulic performance of Severn Trent Water's anaerobic digesters vary widely, those with unconfined gas mixing achieve an effective volume of 80 % or greater, with other mixing systems exhibiting a lower effective volume after prolonged periods of operation.

Also considering the mixing of sewage sludge alone, but at lab-scale, Stafford (1982) compared the effects of mixing intensity on gas production by mixing a 3 litre digester intermittently (1.75 min mixing per 5 min) at low mixing speed (140 rpm) and at high mixing speed (1000 rpm). No information is given about the impeller blade, such as the impeller type or its diameter, so the mixing intensity is unclear. The digester was fed primary sludge and designed to have an HRT of 10 days. It was kept at a temperature of  $35 \pm 2$  °C. The gas volume was measured using an unspecified wet gas meter. There is no mention of the gas volume being corrected to STP and so discrepancies of up to 5 % may arise in the recorded gas volumes dependent on ambient conditions (Walker et al., 2009). Additionally, the results cannot be directly compared to other studies. Furthermore, it has been shown that unless acidified saturated saline solution is used as a barrier

solution, measurement by liquid displacement can incur biogas losses of up to 10 % (Walker et al., 2009) to the barrier solution and hence increase the level of error in gas measurements. It was shown that gas production rate was 12.5 % lower in the digester at the higher mixing speed. However, the higher mixing speed did increase the initial rate of gas production on commencement of mixing, suggesting that the higher mixing speed was beneficial for releasing trapped gas bubbles in the sludge. Further information about the rheology of the sludge would have helped to determine if this is likely but this data is not provided.

Indeed, the vast majority of research carried out on mixing of anaerobic digesters relates to manure slurries or the co-digestion of sewage sludge with municipal solid waste (MSW) fractions, such as fruit and vegetable waste. This is still very relevant as manure slurries, like sewage sludge, are non-Newtonian fluids whose properties are linked to solids concentration and require the presence of similar acetogenic and methanogenic bacteria to be digested anaerobically.

### **2.6.1 Effect of mixing regime**

Hoffman et al. (2008) operated four lab-scale digesters (volume = 4.5 litres) at different impeller speeds during the mesophilic digestion of cow manure, diluted to 50 g VS/l. Each digester was equipped with a 62 mm diameter Lightnin A310 axial flow impeller and mixed at speeds of 50 rpm, 250 rpm, 500 rpm or 1500 rpm. The temperature was maintained at  $34 \pm 1$  °C. Gas volume was measured using a commercial gas meter of unspecified design and corrected to STP of 0 °C and 1 atm. Without more details of the gas measurement equipment, the size of the error associated with the gas measurement is impossible to quantify. The digesters were fed daily so that OLR increased from 0.6 g VS/d to 3.5 g VS/d, with each OLR maintained for at least 1 HRT before OLR was further increased. It was shown that methane production was similar at all mixing speeds, with production rates of 0.24 l CH<sub>4</sub>/g VS fed or 0.56 l CH<sub>4</sub>/g VS consumed and methane accounting for 67.4 ± 5 % of the produced biogas. During start-up, the digester at 1500 rpm produced little biogas, a result that was linked to the high VFAs in the digester (>4000 mg/l acetic acid), whereas the other

digesters had low VFA concentrations and produced 0.6-1.0 l/d biogas during the same period. A similar upset was seen in the digester at 500 rpm when the OLR was increased from 0.6-1 g VS/d. This fits well with the hypothesis that high mixing speeds are beneficial for hydrolysis but that low mixing speeds favour methanogenesis. Hence, an imbalance in the process would be expected when high mixing speeds are used during digester start-up.

After 150 days of operation, the digesters at 250 rpm and 500 rpm were accidentally fed 3.3 times their usual feed. The digester at 500 rpm was better able to deal with this shock loading than the digester at 250 rpm, consuming all of the excess substrate in four days, whilst the digester at 250 rpm took 20 days to recover. This was attributed to the fact that the digester at 500 rpm had experienced an upset when the OLR had increased from 0.6 g VS/l to 1.0 g VS/l. After 260 days of operation, the OLR was doubled from 3.5 g VS/d to 7.0 g VS/d for one day to assess the effects of shock loading on the digesters. Once again, the digester at 500 rpm was best able to deal with the shock, followed by the digesters at 250 rpm which had by then also experienced shock loading, 50 rpm and finally, 1500 rpm. Whilst this gives little information about the effect of mixing speed on the ability to handle loading, it does demonstrate that digesters that have experienced unstable operation previously appear to operate more robustly when experiencing further unstable episodes.

Hoffman et al. (2008) is the only paper to date that considers the physical effects of mixing in an anaerobic digester in conjunction with experimental work linking mixing to gas production. Computer automated radioactive particle tracking (CARPT) and CFD were used to map shear distribution in the digester and estimate local shear intensities at different mixing speeds. This demonstrated that the absence of baffles in the digester promoted high levels of shear due to the high azimuthal velocity. The maximum axial shear stress was 1000 dynes/cm<sup>2</sup> (100 Pa) at 500 rpm and 800 dynes/cm<sup>2</sup> (80 Pa) at 250 rpm, whereas the maximum radial shear stress was 14000 dynes/cm<sup>2</sup> (1400 Pa) at 500 rpm and 9000 dynes/cm<sup>2</sup> (900 Pa) at 250 rpm, although these maxima were always confined to the impeller region. The spatially averaged velocity gradient was

also calculated in the digester and was found to be 3500, 630, 210 and  $17 \text{ s}^{-1}$  for 1500, 500, 250 and 50 rpm respectively. A microbiological analysis of the methanogenic communities present in the digesters under different mixing regimes was also carried out. More details of the hypotheses linking mixing to acetoclastic methanogen population and the results of this part of the research carried out by Hoffman et al. (2008) is given in Section 2.7.

Ong et al. (2002) studied the anaerobic digestion of cow manure with a VS concentration of 72 g/l at an HRT of 10 days. The 10 litre digesters were fed for 15 minutes in every hour and were kept at a temperature of  $35 \pm 1 \text{ }^\circ\text{C}$ . Digesters were equipped with two 6-blade disk-type turbine impellers, one at a fifth of the digester height above the base and the other at two thirds of the digester height above the base. The gas production was measured using liquid displacement with a barrier solution of acidified sodium chloride solution, measured at atmospheric pressure and  $26 \text{ }^\circ\text{C}$ . Several experiments were carried out. The first of these compared continuous mixing at 100 rpm to intermittent mixing at 160 rpm for four 30-minute periods throughout the day. This makes it difficult to distinguish between differences attributed to the mixing speed or to the mixing duration (i.e. continuous or intermittent). The digester was operated for 4-5 HRT after start-up before results were collected so no effects on start-up can be quantified. It was shown that there were no significant differences in the gas production from the continuously and intermittently mixed digesters. In both cases, methane accounted for 45-46 % of the biogas. It is suggested that this similarity was due to passive mixing in the intermittently mixed digester occurring due to bubbles of biogas lifting solids from the lower layers of the digester as they rose. No details of the sludge rheology are given so the likelihood of this hypothesis being accurate is difficult to judge. However, it is noted that spikes in the gas production from this digester coincided with the periods of mixing suggesting that not all gas was able to escape from the sludge under unmixed conditions, so passive mixing does not appear to have been wholly effective.

In the second experiment, two impeller configurations were tested at 100 rpm and at 200 rpm. The first was that used in the first experiment, with one impeller at a fifth of the digester height above the base and the other at two thirds of the digester height above the base, whilst the second configuration had one impeller at a third of the digester height above the base and the other at two thirds of the digester height above the base. In the second configuration, at 100 rpm, gas production was increased from 13 l/d to 16 l/d. This was attributed to the fact that it left a layer of solids intact at the base of the digester, thereby avoiding solids removal and increasing the SRT of the digester. This was associated with a lower level of methanogen washout and a corresponding lack of accumulation of VFAs.

Finally, to determine whether mixing has a benefit not linked to changes in SRT, a comparison of digestion in mixed and unmixed batch digesters was carried out. The mixed digester had an impeller speed of 200 rpm. It was shown that the unmixed digester produced 6 % more gas over the 70 days of the experiment and that the initial gas production rate was higher in the unmixed digester than in the mixed digester. There was also a higher concentration of extracellular polymeric substances (EPS) in the unmixed digester which has been shown to increase adhesion of bacteria to form aggregates and to increase the level of biomass retention (Lin et al., 2014). After 21 days of operation, the mixing in the mixed digester was switched off, stratification was seen to take place and gas production was shown to increase. This implies a lack of mixing is good for digestion, though part of the benefit likely stems from an increased SRT.

Kaparaju et al. (2008) studied the effects of mixing on thermophilic digestion of cattle slurry at lab-scale (volume = 3.6 litres) and at pilot-scale (volume = 500 litres). In lab-scale tests, homogenized cow manure diluted with water to 8.1 % TS was subjected to continuous mechanical mixing for 20 days after start-up and was then changed to either minimal mixing (10 minutes of mechanical mixing before extraction and feeding), intermittent mixing (continuous mechanical mixing withheld for 2 hours prior to extraction and feeding) or left as continuous mixing. After 23 days under this

regime, mixing was changed back to continuous in all digesters. The impeller dimensions and mixing speed are not stated making it impossible to comment on the effects of the mixing intensity. The digesters were fed every 12 hours and had an HRT of 15 days. The digesters were kept at 55 °C and gas volume was measured semi-continuously by liquid displacement, with a count recorded for every 100 ml of gas collected. The errors associated with this method of gas measurement are not quantified but are discussed in relation to the research of Stafford (1982) and apply equally in this case. The results are not converted to STP and similarly, there is an error associated with this that has been discussed previously. The results of these lab-scale tests showed that there was an increase in biogas production of 12.5 % for minimal mixing and 1.3 % for intermittent mixing when compared to biogas production from the continuously mixed digester over the same period. No analysis of the level of error in these measurements is given and, whilst the minimally mixed digester may actually represent an increase in biogas production, it is almost certain that the increase in the biogas production from the intermittently mixed digester is within the level of experimental error. VFA levels in the intermittently mixed digester were higher than those in the other digesters, at concentrations of 1.5 g/l as compared to 0.1-0.2 g/l in the continuously mixed and minimally mixed digesters. Specific biogas yield, measured as m<sup>3</sup>/kg VS, increased in all digesters in the second period, when the digesters were operated under different mixing regimes, but this increase was highest in the minimally mixed digester, which showed a 13 % increase.

Fluorescence in situ hybridisation (FISH) was used to study the microbial communities in the lab-scale digesters and it was seen that whilst *Methanosarcina* was present in all of the digesters, there was a higher abundance of short rods in the continuously and minimally mixed digesters, whilst long rods were abundant in the intermittently mixed digester. This implies that mixing has an effect on the morphology of methanogens, a hypothesis which is fully explored in Section 2.7.

Pilot-scale tests were carried out with 6.5-7.5 % TS cow manure slurry at a temperature of 54±1 °C. In this case, the digester was fed every 8 hours giving an HRT of 20 days. Mixing was performed by

two impellers and was either continuous (5 minutes on, 5 minutes off) or intermittent (5 minutes on, 5 minutes off, but with no mixing for 2 hours prior to extraction/feeding). Again, details of the impeller dimensions and mixing speed are not given so the effect of mixing intensity is difficult to quantify and the results are not easily compared to other studies. In this case, mixing was continuous for the first 7 days (i.e. for start-up) and then was intermittent for days 8-45, continuous for days 46-102, intermittent for days 103-135 and continuous for days 136-150. Gas volume was measured using a residential diaphragm gas meter. Whilst such gas meters often account for changes in temperature and pressure, it is not clear what STP are used and so direct comparison to other pilot-scale work is difficult. The results of the pilot-scale study showed that biogas yield was 2.5-14.6 % higher during intermittent mixing than during continuous mixing, with an average increase of 7 % when considering the change in mixing only across each feed batch. It was also shown that effluent VS concentration fell during intermittent mixing at a higher rate than explained by the increase in gas production, which may indicate that stratification occurred, hence increasing the SRT of the digester under intermittent mixing conditions, as seen in Hoffman et al. (2008). FISH analysis of the microbial communities present in the sludge under the two mixing regimes demonstrated that *Methanobacteriales* were dominant in the continuously-mixed digester and that there was no stratification with short rod bacteria present throughout the digester. Conversely, in the intermittently mixed digester, stratification was apparent with *Methanobacteria* dominant in the top layer of the digester, *Methanomicrobiales* dominant in the middle layer and *Methanosarcina* and *Methanomicrobiales* both abundant in the bottom layer. Methane potential tests carried out on sludge taken from these layers in both the continuously and intermittently mixed digesters showed higher methane potential in the top (floating solids) and bottom (settled solids) layers of the intermittently mixed digester (5.86 ml/ml and 6.33 ml/ml respectively) than in the continuously mixed digester (4.6-5.0 ml/ml). It is not surprising that the middle layer in the intermittently mixed digester had a lower methane potential of 4.0 ml/ml, though without further information about the

depth of the three layers, it is not possible to determine whether the intermittently mixed digester has a higher total methane potential.

Finally, Kaparaju et al. (2008) carried out batch tests in 400 ml digesters, run for 160 days and mixed on a shaker table. The digesters were tested under vigorous and continuous mixing (35 times/min with 3.5 cm stroke), gentle and continuous mixing (35 times/min with 1.2 cm stroke) or minimal mixing (thoroughly shaken by hand for 1 min before sample taken) at substrate to inoculum ratios of either 10:90 or 40:60. After 73 days, the mixing intensity in the two continuously mixed digesters was switched so that the gently mixed digester was subjected to vigorous mixing and vice versa for the remainder of the experiment. It was noted that vigorous mixing during start-up caused low gas production for the first 25 days at the higher loading rate (substrate to inoculum ratio of 40:60) but that reducing the level of mixing allowed the methane yield to increase. This is in agreement with Hoffman et al. (2008), who similarly found that high levels of mixing were detrimental during start-up, despite the difference in digestion temperature. Based on these results, Kaparaju et al. (2008) suggested that minimal mixing increases methane production rate through the improvement of syntrophic associations between hydrogen producers and consumers. It is further suggested that vigorous mixing could have inhibited biomass growth in methanogenic centres due to the diffusion of VFAs from acidogenic zones.

Kowalczyk et al. (2013) considered the effect of continuous and intermittent mixing on the co-digestion of cow manure with energy crops. The temperature of digestion and even the digestion temperature range is not stated. Given the huge impact of temperature on the digestion process, this is a huge oversight and makes the effects of mixing impossible to uncouple from the effects of temperature when comparing the results to other literature. Twenty-two litre digesters were mixed with three 3-blade propellers of 150 mm diameter and samples were taken from the base of the digester. Gas volume was collected in a sampling bag and then measured using a drum type gas meter which works on the principle of liquid displacement. The choice of barrier liquid is not clear

but it seems likely that gas loss does occur. Further gas losses may be incurred during the transfer of gas from the digester to the gas bag and then to the gas flow meter. Uncertainties of  $\pm 0.263$  l/h are stated. Results were then reported at STP of 273.15 K and 1.01325 bar.

In the first experiment, cow manure was co-digested with corn cobs and the mixing modes used were continuous mixing, or intermittent mixing with 2 h of mixing on, followed by 1 h off or 7 h on, followed by 1 h off. The mixing speed used is not mentioned so mixing intensity is unclear. The digesters were fed once a day and the OLR was increased in stages from 0.1-3.5 kg VS/m<sup>3</sup>/d. All digesters were mixed continuously for the first 15 days of operation to demonstrate that they were operating in a similar manner. There was no difference in the gas production between the digesters under different mixing regimes and the gas production rate was stable until the OLR was increased to 3.5 kg VS/m<sup>3</sup>/d, at which point fluctuations occurred. There was seen to be no significant increase (<5 %) in power consumption during the start-up of the mixer after it was turned off and Kowalczyk et al. (2013) determined that energy savings of 29 % could be made by operating with intermittent mixing rather than continuous mixing. However, it was noted that the digesters did show evidence of foaming during periods when they were not mixed. This is a reminder that mixing can serve multiple purposes during digestion and that ideal conditions for one purpose may not be ideal for other purposes. Without knowledge of the mixing intensity or the temperature range used for this experimental work, both of which may affect foaming (Ganidi et al., 2009), it is not possible to further comment on the link between mixing and foaming.

In a second experiment, cow manure was co-digested with maize silage. The mixing modes used were continuous mixing, or intermittent mixing with 10 min of mixing on, followed by 230 min off or 10 min on, followed by 50 min off. Again, the mixing speed used and temperature of digestion are not given, making the comparison of these results to those published elsewhere in the literature challenging. In this case, the different mixing regimes were applied from the first day and OLR was 2.3-2.4 kg VS/m<sup>3</sup>/d. There were significant differences in the gas production during start-up, with

the intermittently mixed digesters producing 20 % more gas than the continuously mixed digester. This was the case for the first 14 days of operation, supporting the benefits of low mixing during start-up as seen by Hoffman et al. (2008) and Kaparaju et al. (2008). After the first 14 days, no advantage in the intermittently mixed digesters was seen. From that point onwards, methane accounted for 56-58 % of the biogas produced, though this had been lower in the continuously mixed digester during start-up. Evidence of foaming was still present during periods when mixing was switched off in the intermittently mixed digester.

In a third experiment, the layering of micro-organisms in the digester was investigated in 400 ml batch digesters fed with cow manure and corn cobs and kept at 40 °C. No mixing was applied and it was seen that within 24 hours micro-organisms were more abundant in the lower layers of the unstirred digester. This abundance of micro-organisms concurs with the observation of Kaparaju et al. (2008) that methanogens were abundant in the lower layers of the digester.

Gomez et al. (2006) considered the mesophilic co-digestion of primary sludge (22 % of feedstock) and the fruit and vegetable fraction of MSW (78 % of feedstock) in lab-scale digesters (volume = 3 litres). Two of the digesters were operated with a primary sludge only feed whilst the other two were operated under a co-digestion regime. Digesters were subjected to a high level of mixing (continuously mixed at 200 rpm), a low level of mixing (continuously mixed at 80 rpm, except before wasting and after feeding when mixing was increased to 200 rpm) or static conditions (only mixed at 200 rpm prior to wasting and after feeding). The dimensions and type of impeller used in the experiments are not stated so mixing intensity is unclear and the results are not easily comparable to other research. At 200 rpm, complete homogenisation of the sludge was deemed to take place, though no justification of this statement was given. At 80 rpm, it was observed that there was some stratification but that there were also solids that remained in suspension in the upper part of the digester. Biogas production was measured daily by liquid displacement and corrected to STP, though the conditions denoted as STP are not stated so a direct comparison of the

results of this work to that of others is not possible. Similarly, the temperature of digestion is not stated making comparison to existing literature challenging, though it is indicated that digestion took place in the mesophilic range. As stated previously, errors may arise from the use of water as a barrier solution when using liquid displacement to measure gas production. No details of the liquid displacement system are given and thus the impact of these errors cannot be assessed further.

It was shown that biogas production from co-digestion was higher than that of primary sludge alone due to the increased VS in the feed, though the specific gas production (measured as  $\text{m}^3/\text{kg VS}$ ) was similar for both feedstocks. At an OLR of 2.5 g VS/d, reducing the level of mixing from high to low was shown to have no effect on gas production; therefore an energy saving could be made based on the reduced cost of mixing at lower mixing speeds. However, under static conditions, it was shown that the biogas yield and the specific gas production were lower than under low mixing conditions, so mixing cannot be stopped completely. It should be noted that changes to the mixing regime in this work took place rapidly, with some mixing regimes operating for less than 10 days. As such, digesters were operated for less than 1 HRT (37-47 days depending on OLR) under each regime. Thus, the results are unlikely to give a clear picture of the success of digestion under different mixing regimes at steady-state as the microbial communities in the digesters are not given sufficient time to acclimate to the new regime before conditions are changed (Gerardi, 2003).

Stroot et al. (2001) carried out experiments to compare the effects of vigorous and minimal mixing on the co-digestion of the organic fraction of MSW, primary sludge and waste activated sludge at 37 °C. pH was controlled when it fell below pH 7, first by the addition of chemicals and then by reducing the feeding rate. The feeding rate was also reduced when VFA concentrations increased above 1000 mg/l. This resulted in an increased retention time (RT) and decreased OLR for poorly performing digesters, which allowed failing digesters to continue to function for a greater period of time than if feeding continued at a constant rate. This skewing should be noted when considering the results though it does describe a more realistic feeding regime in an industrial setting. The gas

was collected in bags and measured daily by liquid displacement. No mention of the barrier solution is made so the size of potential errors is unclear. The increased error associated with transfer to and from the gas bags is also not quantified. The digesters had a volume of 2 litres and were fed in such a way that the RT was kept at 20 days but the OLR ranged from 3.5 g VS/l/d to 9.4 g VS/l/d. The digesters were subjected to continuous (continuous and vigorous shaking on mixer table at an estimated power of 1.5 W/l) and minimal (thoroughly shaken by hand for 1 min before wasting and 1 min before feeding each day) mixing conditions. The continuously mixed digester performed poorly compared to the minimally mixed digester, demonstrating levels of VFAs that required a suspension of feed, particularly at the higher OLR. At the higher OLR, the minimally mixed digester showed a greater variability in the level of VFAs, which could have been accounted for by the formation of distinct pockets within the digester environment.

Smaller 500 ml digesters were then started from the most stable and least stable digesters in the previous experiment in order to observe the effect of changing the level of mixing. As such, four digesters were operated, two that had originally been operated at an OLR of 9.4 g VS/l/d under continuous mixing (unstable) and two that had originally been operated at an OLR of 3.5 g VS/l/d under minimal mixing (stable). For each pair of digesters, one was left under the original mixing regime and the other was changed to the alternative mixing regime. After 18 days, the unstable continuously mixed digester that had been changed to minimal mixing had a reduced VFA concentration which allowed feeding of the digester to resume. No such change was seen in the digester that remained under continuously mixed conditions. The stable minimally mixed digester that had remained under minimally mixed conditions continued to perform well, whilst the digester that had been changed to a continuously mixed regime demonstrated an immediate increase in VFA concentration and had to be stabilised by withholding feed. Hence, Stroot et al. (2001) draw the conclusion that unstable operation can lead to greater resilience to overloading as seen in Hoffman et al. (2008). Furthermore, it appears that unstable continuously mixed digesters can be stabilised by reducing the level of mixing.

Vavilin and Angelidaki (2005) tested three mixing regimes at three OLRs for the co-digestion of manure and MSW, and compared the results to a simplified co-digestion model. The digesters were operated in batch mode, with a volume of 500 ml, and were kept at 37 °C. They were mixed under one of three regimes: vigorously and continuously (shaker table at 105 times per min, 5 cm length), gently and continuously (shaker table at 58 times per min, 17 cm length) or minimally (shaken by hand 1 min every 1-2 days). No mention is made of the gas measurement method used so the errors involved cannot be quantified. The simplified computer model treated co-digestion as a two-stage process consisting of acidogenesis and methanogenesis, with VFAs acting both as a precursor for methane production and also as an inhibitor for both processes, when at high concentrations. The model ignored hydrogenotrophic methanogenesis and as such, all methanogenesis is assumed to follow the acetoclastic methanogenesis pathway. This is inaccurate as acetoclastic methanogenesis accounts for approximately 70 % of the methane produced from digestion (FAO, 1997).

At low OLR (4.5 g/g), no significant difference was found in methane production under different mixing intensities and biogas production was low. In a batch process, the initial biomass concentration determines the methane production and when the biomass concentration is initially low, there is a long delay in methane production as there is insufficient feedstock to support high levels of micro-organism growth. At a moderate OLR (23 g/g), higher methane production was shown under minimal mixing conditions. The computer model predicted that there was no apparent inhibition of the biomass growth in methanogenic centres of the sludge, despite the high levels of VFAs outside of these regions. Such methanogenic centres could help to avoid acidification from high concentrations of VFAs and enhance solids decomposition at a moderate OLR and under minimal mixing conditions.

At high OLR (41 g/g), the computer model predicted that methanogenesis would be strongly inhibited by high concentrations of VFAs as methanogenic centres dissipate. This appeared to be

true under all mixing conditions, with pH of 6.05-6.85 measured in all of the samples, compared to pH 7.05-7.50 in samples taken from digesters at lower OLR.

The comparison of the experimental results and the simplified computer model led to the conclusion that only under imperfect mixing conditions are methanogens able to remain in sites that are protected from rapid acidogenesis and hence the accumulation of, and inhibition by, VFAs. This is in agreement with the distinct pockets identified in the minimally mixed digester of Stroot et al. (2001). As such, vigorous mixing is not suitable for systems where methanogenesis is rate-limiting, including during start-up, as shown previously in Hoffman et al. (2008) and Kaparaju et al. (2008). However, if hydrolysis were to become rate-limiting, under conditions where the population of methanogens was high, then mixing may improve hydrolysis and so increase the rate of the digestion process.

Ghanimeh et al. (2012) studied the thermophilic digestion of the source-segregated organic fraction of MSW at lab-scale (volume = 9 litres) under mixed and unmixed conditions. The digesters were kept at 55 °C and were operated for 235 days. They were seeded with non-acclimated cattle manure and then fed three times per week with organic MSW with a TS content of 7.5-8.0 %. The first digester was mixed continuously at 100 rpm whilst the other was not mixed except for a few minutes after feeding and prior to sludge wasting. There are no details given of the impeller used, or the duration or speed at which the unmixed digester is mixed around feeding and wasting, so it is difficult to draw direct comparisons with the results of other studies. Gas volume was measured by water displacement and was not converted to STP. This method of gas measurement incurs errors of up to 10 % because of the loss of carbon dioxide to the barrier solution (Walker et al., 2009). At an initial OLR of 0.45-0.46 g VS/l/d, the unmixed digester reached a maximum gas yield of 2 l CH<sub>4</sub>/g VS within 20 days, whilst the mixed digester achieved a maximum gas yield of 1 l CH<sub>4</sub>/g VS within 18 days. These results agree with those of Hoffman et al. (2008) and Kaparaju et al. (2008), which showed that mixing was detrimental during start-up, despite the fact that the work of Hoffman et al. (2008) was carried out under mesophilic conditions. However, over the first month of operation, the

average methane yield in the mixed digester was higher than that in the unmixed digester (0.60 l CH<sub>4</sub>/g VS and 0.45 l CH<sub>4</sub>/g VS respectively).

The OLR in the mixed digester was dropped to 0.28 g VS/l/d after 33 days of operation and was then increased to 2.5 g VS/l/d after 159 days of operation, with no signs of instability being reported. However, after 167 days of operation, the concentration of VFAs in the digester increased, the biogas and methane production of the digester fell and feeding was suspended for 5 days before being resumed at an OLR of 0.31 g VS/l/d. This was maintained for two weeks but VFA concentrations continued to rise and feeding was suspended again after 191 days of operation for 26 days. Feeding was resumed on Day 203 with an OLR of 0.24 g VS/l/d, then reduced to 0.10 g VS/l/d due to high VFA concentrations persisting. The authors were forced to terminate the experiment after 235 days.

In the unmixed digester, OLR increased from 0.28 g VS/l/d to 1.35 g VS/l/d after 33 days of operation and VFA concentration immediately increased, alongside a drop in the percentage of methane in the biogas and a falling pH. This suggested the presence of instabilities due to VFA build-up. Feeding was stopped for 2 days and resumed at an OLR of 0.8 g VS/l/d. It was then increased to an OLR of 1.9 g VS/l/d. When the load increased to 2.1 g VS/l/d, the VFA concentration doubled and methane yield fell sharply. As such, feeding was stopped on Day 190 and resumed at an OLR of 0.8 g VS/l/d after 12 days. The high VFA concentration persisted and so OLR was reduced to 0.6 g VS/l/d. The experiment was terminated on Day 242.

During the increase in OLR, the mixed digester was able to cope with a higher OLR (2.5 g VS/l/d) than the unmixed digester (1.9 g VS/l/d) and still had a lower total VFA concentration, lower propionate concentration and a lower Ripley's Ratio (RR). This suggests that mixed digesters are better able to cope with high loading rates. When overloading did occur, the mixed digester showed signs of methanogenic inhibition caused by a washout of microbial flora, identified by an increased TS removal compared to the unmixed digester, whilst the unmixed digester appeared to suffer

overloading simply because the digester's capacity had been exceeded. This suggests that digester stability is sensitive to HRT as well as OLR, and that a higher OLR could have been digested if the HRT had been held constant, rather than being reduced as OLR increased.

Tian et al. (2013) attempted to characterise the effects of digester mixing on gas production without the effects of sedimentation under thermophilic conditions (50-54 °C) using batch digestion at lab-scale (volume = 5 litres) under mixed and unmixed conditions. The mixed digester was equipped with a 50.8 x 9.5 mm magnetic bar and agitated by a large volume magnetic stirrer set to 100 rpm. An inert bulking agent was added to the unmixed digester to prevent sedimentation. The gas volume was measured using a positive displacement gas meter filled with anti-freeze solution and was converted to STP, though there is no mention of what temperature and pressure constitutes STP.

In Run 1, 0.3 kg beet tailings and 2 kg bulking agent were added to 3 l of inoculum in the unmixed digester, whilst 0.3 kg tailings were added to 3 l of inoculum in the mixed digester. At the end of the run, the liquors from the two digesters were mixed and used to restart both digesters for Run 2. For Run 3, the liquors from the mixed digester were used to start the unmixed digester and vice versa. For Run 4, the liquors from the unmixed digester were diluted and used to start both digesters. For Run 5, the liquors from the unmixed digester were used to restart the unmixed digester and liquors from the mixed digester were used to restart the mixed digester. This was repeated for Run 6. The digesters were run until biogas production dropped to 100 ml/d; each run lasted 15-20 days.

During the first two runs, the methane yield from the unmixed digester was 0.35-0.36 m<sup>3</sup> CH<sub>4</sub>/kg VS removed, whilst in the mixed digester, it was 0.23-0.27 m<sup>3</sup> CH<sub>4</sub>/kg VS removed. The unmixed digester also showed a higher maximum production rate which was achieved sooner in the experiment. This is akin to the lower gas production rate associated with mixing during start-up found by Hoffman et al. (2008), Kaparaju et al. (2008), Kowalczyk et al. (2013) and Ghanimeh et al. (2012). During Run 3, after the liquors from the mixed digester were used to restart the unmixed

digester and vice versa, the cumulative methane yield from the unmixed digester remained similar to Runs 1 and 2, but the daily production rate fell. This may be due to the micro-organisms taking longer to acclimate to the new mixing regime. For the mixed digester, the methane yields and daily production rates were similar to Runs 1 and 2.

During Runs 4-6, the unmixed digester showed similar yields to Runs 1 and 2 but the mixed digester showed a lower maximum methane production rate, though the cumulative yields were similar. In all cases, the unmixed digester exhibited a higher methane yield and maximum methane production rate than the mixed digester. The mixed digester also experienced higher levels of VFAs (1.2 g/l acetate compared to 0.9 g/l acetate) which were persistent in the digester for longer. This agrees with the results of Vavilin and Angelidaki (2005) who suggest that mixing is beneficial for increasing the rate of hydrolysis, but may be detrimental for methanogenesis.

The microbiological communities present in the original inoculum and in the digester liquors taken on the third day of Run 6 from each of the two digesters were assessed using polymerase chain reaction (PCR) analysis. The communities in the three samples were distinct, with abundant methanogens (*Methanobacteriales*, *Methanomicrobiales* and *Methanosarchinales*) present in the inoculum and the unmixed digester whilst much lower concentrations of *Methanobacteriales* were found in the mixed digester. This fits well with the hypothesis of Vavilin and Angelidaki (2005). This suggests that mixing has an effect on the microbial community of a digester, though whether this is a direct result of the mixing (e.g. shear stress) or a result of the environmental conditions associated with mixing (e.g. VFA concentration) is not clear.

The results of this work were compared to the work of others with similar mixing intensities measured in  $W/m^3$  (Stroot et al., 2001). Whilst the results compare favourably in this instance, a comparison based on power gives no indication of the mixing patterns established in the digester and the link between mixing and rheology. This oversimplifies digester mixing and implies that a constant power per volume input will provide a constant level of mixing, which is not the case when

different mixing methods and feedstocks are used (Brade and Noone, 1981). It is further noted that part of the improvement in performance of the unmixed digester may be attributed to the addition of the bulking agent which may have provided additional inert media for microbiological communities to colonise and form syntrophic communities.

Ong et al. (2002) investigated the behaviour of an unmixed digester fed with reconstituted cattle manure. The digesters had a volume of 10 litres and were kept at 35 °C. They were started in batch mode and were then operated semi-continuously with a 10 day HRT. The feed had a TS concentration of 80 g/l. Gas volume was measured using a wet gas meter though no mention is made of whether the results were adjusted to STP and again, there is an unknown level of error associated with the choice of barrier solution. The first of the two digesters was operated for 40 days (4 RT) after start-up, with the slurry fed to the top of the digester and discharged from the bottom of the digester. This was followed by 4 RT operated with the feed added to the top of the digester and the slurry discharged from the centre height of the digester. This change in discharge point was found to increase the gas production rate from 12 l/d to 17 l/d. The increase was attributed to digester stratification causing a build-up of solids at the base of the digester and a corresponding increase in SRT, as it was noted that once the solids reached the height of the discharge point, the gas production stabilised. The second digester was operated for 10 days (1 RT) after start-up, with the slurry fed at the base and discharging from the top of the digester. This was problematic due to the presence of a scum layer which was too thick to discharge and it was found that biogas was being pumped out of the digester in preference to the scum. As such, the operation of the digester was changed so that the discharge point was at the centre height of the digester, but the digester was mixed continuously at 160 rpm. The digester was operated under these conditions for a further 20 days (2 RT). Under these operating conditions the gas production rate was 16 l/d. No data is given about the size or type of impeller used for mixing so no direct comparisons can be drawn between results of this and other work. The difference in the time spent under each set of operating conditions further complicates the possibility of assessing the effect of mixing on the gas

production from the digester. However, it is clear that unmixed cattle manure stratifies into three layers, namely a floating scum layer, a thick sludge layer at the bottom of the digester and a watery fraction in the middle that is low in particulate matter. This is in agreement with the work of Kaparaju et al. (2008), who identified different layers in the digester and additionally showed that these were associated with different methane potentials. By selecting which layer slurry is discharged from, it is possible to affect the SRT of the digester and therefore affect the overall gas production of the digester.

### **2.6.2 Effect of mixing method**

The research discussed until this point has compared the effects of mixing regimes (intermittent or continuous mixing, speed of mixing) under mechanical mixing conditions, either impeller mixing or through the use of a shaker table. This section now considers other mixing methods, such as gas or slurry recirculation.

Karim et al. (2005a) studied the operation of a confined gas-mixed lab-scale digester (volume = 3.73 litres) at different biogas recycle rates and with different draft tube heights. The digesters were kept at  $35 \pm 2$  °C and were fed manure with 5 % solids once every two days in order to achieve an HRT of 16.2 days and an OLR of 3.37 g COD/l/d. The gas produced from the digester was collected in a gas bag and recirculated to the digester to provide mixing. The digester was operated at gas recirculation rates of 0, 1, 2, and 3 l/min through a draft tube with a clearance of 40 mm, and at 1 l/min through draft tubes with clearances of 40 mm, 26 mm and 13 mm. The gas production was measured using a wet gas test meter, though no mention is made of the barrier solution or of a conversion to STP. The issues with this have been mentioned previously and will not be reiterated here. The digesters ran for 20-30 days after start-up, which represents less than 2 RT. As such, there may have been insufficient time for the microbial communities in the digester to fully acclimate to the different mixing conditions to which they were subjected. Regardless of mixing speed, all of the digesters produced biogas at a rate of 0.40-0.45 l/l/day, with methane accounting

for approximately 65 % of the biogas produced. There was no VFA accumulation recorded in any of the digesters, suggesting that the digestion process was stable. The clearance height of the draft tube similarly had no effect on gas production. As such, the authors concluded that mixing conditions do not have an effect on gas production. Whilst this clearly disagrees with other published results, such as those of Kaparaju et al. (2008), Gomez et al. (2006) and Stroot et al. (2001), Karim et al. (2005a) suggested that all of the digesters studied may have achieved a well-mixed state due to the production of biogas within the sludge and the subsequent rising of that gas through the sludge. Without further details on the rheology of the sludge or results that attempt to visualise the flow patterns within the digester, it is impossible to verify the accuracy of this statement.

Karim et al. (2005b) operated the same lab-scale digesters (volume = 3.73 litres) to compare the effects of different mixing methods (confined gas recirculation at 1 l/min, confined mechanical mixing using a Lightnin A310 impeller with a diameter of 62 mm at 275 rpm, confined slurry recirculation at 0.82 l/min, or no mixing) on gas production from manure with a range of TS concentrations (5 %, 10 %, 15 % TS). Mixing by slurry recirculation at 15 % TS was not tested as the pump was unable to handle such a viscous liquid. The same temperature and HRT were used as in Karim et al. (2005a) and again biogas was collected in gas bags and measured using a wet gas test meter, though results were not converted to STP. As before, digesters were fed once every two days. The mixing conditions in each digester were selected to provide a constant energy input of  $8 \text{ W/m}^3$ . When fed with 5 % TS sludge, all of the digesters behaved similarly, with a methane production of 0.26 - 0.28 l/g VS. At 10 % TS, the unmixed digester produced 22 % less biogas than that mixed by slurry recirculation, whilst the gas-mixed digester produced 10 % less than the slurry-mixed digester. The mechanically-mixed and slurry-mixed digesters showed comparable gas production. At 15 % TS, the unmixed digester took less time to achieve stable digestion after start-up than the mixed digesters, with the mixed digesters taking more than 10 days longer, and displaying low pH and low biogas production in the first 30 days of operation. This agrees well with

the results of Hoffman et al. (2008) who similarly found that mixing was detrimental during digester start-up.

After one month of operation, it was noted that the gas-mixed digester was producing more biogas than the other digesters at 15 % TS, although it was also noted that severe accumulation of solids was taking place in the digester. This suggests that gas-mixing was ineffective at 15 % TS and as such, an increase in biogas production would be expected in conjunction with the increase in the SRT of the digester. The mechanically-mixed digester did not demonstrate signs of solids accumulation but also experienced an increase in biogas production as compared to the unmixed digester. This suggests that there is a benefit to mixing, although care must be taken in selecting the mixing method, particularly at high solids concentrations.

Whilst all the mixing regimes considered had an equal power input to the system, no indication is given of the effectiveness of these regimes, e.g. the presence of dead zones, though it seems likely that not all mixing was equally effective as indicated by the solids accumulation in the gas-mixed digester. No indication is given of the shear stress imparted to the sludge either, a parameter which is likely to affect the ability of mixing to increase gas production.

Karim et al. (2005c) continued the work described in Karim et al. (2005b) by subjecting the four digesters to a change in feed. After 30 days of operation at steady-state, with a 10 % TS manure feed, the digesters were fed a 3.5 % TS manure for 9 days and then returned to the 10 % TS manure feed. All four of the digesters became unstable and produced less biogas when the feed concentration was changed. The unmixed digester was most badly affected and the reduced gas production from this digester continued for 10 days longer than the other digesters after feeding of a 10 % TS manure was resumed. Whilst all digesters did return to their original level of gas production, the mixed digesters were better able to handle the shock loading, as demonstrated by the quicker return to normal gas production levels.

Lee et al. (1995) compared mechanical mixing to mixing by gas recirculation. A 1.5 litre digester equipped with a triple impeller and a gas diffuser was fed 100 ml of swine waste once daily, giving an HRT of 15 days. The OLR was 3.9 g VS/l/d and the digester was kept at 38 °C. The digester was initially run for 15 days under continuous mixing. It was then operated for 14 days under each of four mixing regimes: mechanical mixing (30 rpm) for 10 mins in every 3 hours, mechanical mixing (30 rpm) for 10 mins in every 6 hours, gas recirculation (2.4 l/min) for 10 mins in every 3 hours and gas recirculation (2.4 l/min) for 10 mins in every 6 hours. The gas volume was measured using a wet gas meter during the last three days of each mixing regime when the digester was assumed to have stabilised and adapted to the regime. They showed that gas production was similar under all mixing regimes, except for gas recirculation at 10 min in every 6 hours where gas production was higher. No reasoning for this is given and with no detail on rheology or the mixing systems employed, it is difficult to determine the cause for this difference.

The importance of sludge rheology is highlighted by Benbelkacem et al. (2013), who studied the residence time distribution (RTD) of solids and liquids in a 43 litre anaerobic digester mixed by biogas recirculation and fed with MSW or synthetic green waste. Given the effect of increasing SRT in a digester, as shown by Ong et al. (2002) and Karim et al. (2005c), the RTD is likely to have a major effect on the gas production of a digester, though Benbelkacem et al. (2013) do not consider gas production in this work. The digester was equipped with an inner wall across half of the digester, with an inlet at the top on one side of the wall and an outlet at the bottom on the other side of the wall. There were 14 injectors at the base, which released 2 s sequential injections of biogas every 30 minutes to provide mixing, and the digester was kept at 35 °C. The digester was fed five days a week with either MSW (TS = 22 %, 26 %, 30 %) or synthetic green waste (TS = 23 %); centrifugal liquor from the same plant was added to achieve the desired TS concentration. The RT was approximately 20 days and the biogas recycle ratio was 0.6. The rheology of the digestate was tested using a slump test in order to calculate the yield stress.

The RTD was calculated in order to provide a measure of the level of mixing achieved in the digester. An iodide tracer was used for the liquid phase and 500 tracer beads of 8 mm diameter were used for the solid phase. Tested tracer materials were polypropylene, polyamide, glass and Bioflow 9. The effective working volume of the digester was lower than expected, with the volume of dead zone increasing as TS concentration increased. At 30 % TS, dead zone accounted for approximately 18 % of the total liquid volume and the liquid mixing approached a plug flow behaviour.

For the solids RTD, the density of the particles had a strong effect on the fraction of particles that were extracted from the digesters, with the extraction of the densest particles being lowest at low TS concentrations. This suggests that sedimentation of solids occurs in the lower solids concentration sludges, with the densest particles settling out most quickly. At 30 % TS, similar recovery was observed for all of the tracers, indicating that less sedimentation, even of dense particles, occurs when the yield stress of the sludge is high. The source of the feedstock as well as the total solids concentration has a strong influence on the sludge rheology, indicated by the green waste, with a TS concentration of 23 % producing a similar tracer curve to that of MSW at 26-30 % TS. This demonstrates the difficulties of comparing results of other research undertaken in the field of anaerobic digestion where the effects of rheology are suggested by the TS concentration of the feedstock but are not implicitly measured. When comparing sludge from different sources, this is likely to introduce errors, as identical TS concentrations do not imply identical rheological properties.

### **2.6.3 Review of literature**

From this review, it can be seen that the intensity of the mixing, in terms of mechanical mixing speed or recirculation rate of gas or slurry, as well as whether the operation of the mixing is intermittent or continuous, have an effect on the biogas production of a digester. Additionally, and often overlooked, the rheology of the feed, which is dependent on both the solids concentration and the

source of the feed, also plays an important role in determining the success of mixing and the associated gas production and release.

It can be seen that mixing appears to increase biogas production when compared to the non-mixed scenario (Karim et al., 2005a, Karim et al., 2005b), but only when the solids concentration is above 5 %. At solids concentrations of 5 % or less, it has been suggested that the sludge is thin enough that adequate mixing is achieved by the production of biogas and therefore mixing has little to no effect on the performance of the digester (Karim et al., 2005a, Karim et al., 2005c, Hoffman et al., 2008). However, as the mixing intensity increases from low mixing speeds of less than 100 rpm to higher mixing speeds of 100 to 200 rpm for impeller mixing, or from 1 l/min to 2-3 l/min for biogas recirculation, the biogas production falls (Karim et al., 2005c, Kaparaju et al., 2008). Furthermore, at higher mixing speeds, it is demonstrated by Karim et al. (2005c) that digesters are better able to deal with shock loading conditions, though Gomez et al. (2006) showed that previous exposure to shock was more valuable than a low mixing speed for increasing the robustness of a digester.

Stroot et al. (2001) found that when sewage sludge was continuously and vigorously mixed on a shaker table, the system had a higher ratio of VFA concentration to bicarbonate alkalinity, indicating that it was less stable than when it was shaken by hand for two minutes each day. The continuously mixed digesters could be stabilised by reducing the mixing regime from continuous to minimal. There is a body of literature that suggests that anaerobic digestion may work most efficiently with minimal mixing. However, due to the wide range of variables involved in anaerobic digester mixing experiments, from the feed and its rheology to the mixing method, duration, intensity and the impact of mixing on the sludge, there is no definitive conclusion across the whole body of literature as to what constitutes minimal mixing and what constitutes an optimum mixing regime. Further difficulties arise from comparing the results of experiments where different gas measurement methods have been used or when gas production rates have not been converted to STP. A set of

comparable parameters is required to provide greater clarity of the degree of mixing that is applied to sludge under different mixing regimes and with different mixing methods.

This gap in the literature makes it difficult to predict the effects of changing the mixing regime of an anaerobic digester on sludge stabilisation, biogas production and energy yield of a digester.

## 2.7 Effects of mixing on digester microbiology

As the rate-limiting step in producing methane-rich biogas once hydrolysis has been overcome, it is methanogenesis that forms the focus of the analysis of the effects of mixing on microbiology. This requires some understanding of the micro-organisms involved in the process. Methanogens can be split into two main groups: acetoclastic methanogens which convert acetate to methane and hydrogenotrophic methanogens which convert hydrogen and carbon dioxide to methane (Griffin et al., 1998). Nearly all known methanogens are capable of converting hydrogen and carbon dioxide into methane, whilst very few known methanogens are capable of the conversion of acetate to methane. The only known acetoclastic methanogenic strains are *Methanosarcina spp.* and *Methanosaeta spp.*, and whilst Montero et al. (2007) demonstrated that the hydrogenotrophic methanogens are important during the start-up process, they are commonly displaced by acetoclastic methanogens at steady-state. Research has shown that due to the high concentrations of acetate found in anaerobic sludge (a range of 50-900 mg l<sup>-1</sup> across 30 digesters in USA is given in Speece (1988)), acetoclastic methanogens are responsible for approximately 70 % of all methane production in domestic sludge digestion (FAO, 1997). *Methanosaeta* and *Methanosarcina* have different kinetic coefficients as shown in Table 2.2. This shows that *Methanosarcina* has a greater maximum rate of acetate utilisation ( $K_{COD}$ ) and maximum growth rate ( $Y \cdot K_{COD}$ ), a greater half-saturation coefficient ( $K_S$ ) and a greater yield coefficient ( $Y$ ) compared to *Methanosaeta* (Conklin et al., 2006). This would suggest that *Methanosaeta* will dominate when acetate concentrations are low or when SRT is high, with *Methanosarcina* dominating when the reverse is true.

**Table 2.2 - Average kinetic values for mesophilic growth of *Methanosarcina* and *Methanosaeta* from literature. Average values given with standard deviations in parentheses. Reproduced from Conklin et al. (2006)**

	Methanosaeta		Methanosarcina	
	All data	-Outlier	All data	-Outlier
Maximum rate of acetate utilisation, $K_{COD}$ (mg COD/ mg VSS.d)	10.1 (16)	3.1 (1.8)	12.2 (5.5)	
Half-saturation coefficient, $K_s$ (mg COD/l)	49 (19)		280 (77)	
Cell yield coefficient, $Y$ (mg VSS/mg COD)	0.019 (0.002)		0.048 (0.032)	0.036 (0.013)

In most cases, *Methanosaeta* is the dominant acetoclastic methanogen in anaerobic digesters (Conklin et al., 2006). However, in rapid start-up reactors which have very high acetate levels (peaking at 66-83 mM acetate) and in reactors with an HRT of less than or equal to 10 days, the fast-growing *Methanosarcina* is dominant (Conklin et al., 2006) as predicted by the kinetic yields. The greater acetate utilisation rate of *Methanosarcina* suggests that *Methanosarcina*-dominated reactors would be better able to convert acetate to methane, especially when dealing with high loading rates, which could result in a higher volume of produced methane. However, most digesters are not dominated by *Methanosarcina* but by *Methanosaeta*. Whilst reducing the SRT of anaerobic digesters may not be a feasible method of increasing *Methanosarcina* dominance when considered in conjunction with other aims of digestion such as sludge stabilisation, increasing the acetate concentration locally within the digester could potentially be engineered by limiting the mixing of the digester (Conklin et al., 2006).

There is limited literature that has considered the effects of mixing on the microbial population of an anaerobic digester. Vavilin and Angelidaki (2005) suggested that the spatial separation of initial methanogenic zones from the active acidogenic zones is of key importance at high organic loading rates. Hence, if methanogenesis is considered to be the rate-limiting step during start-up, vigorous mixing will suppress growth and propagation of these methanogenic centres, limiting biogas production. This suggests that limited mixing is beneficial at least during digester start-up.

A further possible explanation for variations in the microbiological community structure of anaerobic digesters lies in the morphology of the acetoclastic methanogens. *Methanosarcina* grow as single coccoidal cells with a diameter of up to 2  $\mu\text{m}$  (Ni et al., 1994), or in groups with an appearance similar to that of a bunch of grapes that can be up to 3 mm in diameter (Schmidt and Ahring, 1999), whilst *Methanosaeta* are square-ended rod-shaped cells, which form filaments of 8 to <100  $\mu\text{m}$  long, which in turn form tangled flocs of up to 20 to 30 mm in diameter (Janssen, 2003). Cells can be expected to be affected by turbulence within a mixing vessel if they are of a comparable size to the scale of the turbulent Kolmogorov eddies that form in the vessel (Amanullah et al., 2004). These are of the order of 10-100  $\mu\text{m}$  in agitated bioreactors (Amanullah et al., 2004) and so it is not unreasonable to consider that the filaments formed by *Methanosaeta* are more likely to be adversely affected by mixing than the single coccoidal cells of *Methanosarcina*. The effects of shear stress on filamentous cells have been shown to include changing the structure of the filaments through breakage, changing the cell development of the filaments and reducing mass transfer into the cells by changing the cell morphology (Joshi et al., 1996). If the filamentous *Methanosaeta* are likely to suffer greater adverse effects in these ways when the level of mixing is increased, this would lead to *Methanosarcina* outperforming *Methanosaeta* at high mixing intensities.

Membrane hybridisation and FISH were used to track changes in the methanogenic population in the digesters of Hoffman et al. (2008). It was seen that mixing intensity did not have an effect on bacterial abundance. However, the relative levels of methanogens did change. Over the first 50 days, there was an increase in *Methanobacteriaceae* in the digesters at 1500 rpm and 500 rpm, after which this population fell. This may have been linked to the poor start-up in the digesters at the higher mixing speeds. In the digesters at a lower mixing speed, the concentration of *Methanobacteriaceae* was level throughout this period. The level of *Methanococcaceae* was low and decreased throughout the experiment in all digesters, though there were peaks in the population in the digester at 1500 rpm on Day 20 and in the digester at 500 rpm on Day 77. These

peaks coincided with peaks in VFA concentrations. The population of *Methanomicrobiales* was low throughout in all digesters.

The competition between acetoclastic methanogens appeared to be most affected by mixing speed. The levels of acetoclastic methanogens were highest at the highest mixing intensities. However, *Methanosaeta* was virtually non-existent in the digester at 1500 rpm, whilst the levels of *Methanosarcina* increased during the first 77 days of operation. A similar increase in *Methanosarcina* was seen in the digesters at 500 rpm and 250 rpm, though levels remained low at 50 rpm. This is likely to be accounted for by *Methanosarcina* outperforming *Methanosaeta* at high acetate levels in digesters that suffered an upset during start-up, but also by the higher shear rates at high mixing intensities being more disruptive to the filamentous *Methanosaeta*. Further evidence for this is given by the higher levels of *Methanosaeta* in the digesters at 50 rpm and 250 rpm than in those at 500 rpm and 1500 rpm toward the end of the experiment. This agrees with Conklin et al. (2006) who showed that rapid start-up reactors were often unstable (i.e. high in acetate) during start-up and were dominated by *Methanosarcina*. Interestingly, they further suggest that although vigorous mixing was found to disrupt syntrophic micro-organisms, they may have implemented sufficient mixing to overcome diffusion limitations and thus remove the need for close spatial associations between the syntrophs (Hoffman et al., 2008). This suggests that there may be a mixing intensity threshold above which the destruction of such pockets of micro-organisms no longer has a negative effect on the methanogenesis of the anaerobic digester.

McMahon et al. (2001) carried out an analysis of the microbiological communities present in the digesters of Stroot et al. (2001) using polyacrylamide gel electrophoresis, membrane hybridisation and PCR. Generally, they found that *Methanosarcina* was the most abundant acetoclastic methanogen in unstable digesters with high concentrations of acetate, while *Methanosaeta* was dominant in stable digesters with low concentrations of acetate. The digesters under continuous mixing regimes demonstrated much lower levels of Archaea than those under minimal mixing

regimes. After the change in mixing, the population of Archaea increased in the digester where mixing had been reduced, with *Methanosarcina* being the dominant Archaea, although *Methanobacteriaceae* population also increased once propionate levels had fallen. Conversely, the Archaea population fell in the digester where mixing was increased. This was followed by an increase in Archaea levels as feeding was withheld to maintain digester stability. In this case, a sharp increase in *Methanosarcina*, accompanied by a small drop in *Methanosaeta*, was linked to the rising acetate levels in the digester. *Methanobacteriaceae* activity also increased during the VFA degradation that followed the withholding of mixing.

In the digester where mixing was reduced, the population of methanogens increased as VFA was consumed. This was attributed to the reduced level of VFA inhibition and the break-down of propionate to acetate providing an increased level of feed for the acetoclastic methanogens. This was matched by a rise in gas production. In the case of both digesters, *Methanosarcina* was more abundant when acetate concentrations were high and *Methanosaeta* was dominant when the opposite was true. This agrees with the acetate utilisation rates of the two methanogens and was predicted by Conklin et al. (2006). The population of *Methanobacteriaceae* increased as VFAs were degraded due to the plentiful formation of hydrogen and formate.

McMahon et al. (2001) also studied the levels of syntrophic bacteria in the digester. During periods of propionate consumption, syntrophic propionate-oxidising bacteria (SPOB) appeared to be dependent on methanogens to consume their metabolic products, which suggests that minimal mixing regimes which support syntrophic relations may be beneficial. Furthermore, the continuously mixed digester which had a history of instability initially had high populations of saturated fatty acid- $\beta$ -oxidising syntrophs (SFAS). This was attributed to the diversity of the substrate available during instability and the wide substrate utilisation range of SFAS. Whilst the levels of SFAS remained high in the digester that continued to be mixed continuously, in the digester changed to minimal mixing the population of SFAS decreased as digester stability was restored.

It is unlikely that either the creation or destruction of localised pockets of syntrophic micro-organisms creating high localised acetate concentrations, or the morphology of methanogens alone, is responsible for the variation in microbiological community structure under changing mixing conditions. The relative importance of these effects is likely to be dependent on the specific mixing regime employed, the digester volume and the feed composition.

## **2.8 Microbiological community analysis of anaerobic digestion**

In order to better understand the effect of physical and chemical characteristics of different feeds and operating procedures, it is important to be able to study the microbiological communities involved in anaerobic digestion. In the early days of microbial community analysis, culture-based approaches, which depended on the isolation and cultivation of a limited number of cultures, were used. However, this led to a distorted view of the microbial communities involved, as the majority of the micro-organisms involved in anaerobic digestion cannot be cultivated *ex situ* (Amann et al., 1995). More recently, culture-independent molecular techniques have allowed this stumbling block to be overcome. These techniques fall into four categories: clone library, molecular fingerprinting, hybridization and quantitative real-time polymerase chain reaction (qPCR). Clone libraries have been widely used in analysis of wastewater treatment systems and are still used when comprehensive taxonomic information is required (Kim et al., 2013). However, the method is costly and time-consuming, and is not suited to dealing with large numbers of samples.

Molecular fingerprinting techniques, such as denaturing gradient gel electrophoresis (DGGE), temperature gradient gel electrophoresis (TGGE) and terminal restriction fragment length polymorphism analysis (T-RFLP), take polymerase chain reaction (PCR) fragments of different sequences or sizes, and separate them by their different mobility on gels or in capillaries (Gilbrade et al., 2006). By assuming that each band or peak represents a single microbial species, the molecular fingerprint of a sample can be used to determine the diversity of the communities present. At the same time, sequencing the deoxyribonucleic acid (DNA) fragments recovered from the bands or

peaks of interest can offer further information about the specific micro-organisms. This information is limited by the sequence length.

FISH can be used to visualise the abundance and distribution of micro-organisms in microbial communities. This is an improvement on ex situ hybridisation methods, such as nucleic acid hybridisation, which requires the extraction of nucleic acids. However, hybridisation techniques suffer from being low-throughput methods. Since the late 1990s, qPCR has been used to not only detect the presence of target sequences but also to quantify their absolute numbers (Kim et al., 2013). It is widely considered the most precise method currently available for detecting and quantifying nucleic acids and, as it has become more affordable and more widely available, it has been applied extensively to wastewater treatment (Zhang and Fang, 2006).

Conventional PCR amplifies a target sequence, ideally exponentially, and then measures the final concentration of that sequence. However, the end-point is not proportional to the initial concentration of the template DNA or ribonucleic acid (RNA). qPCR, on the other hand, monitors the progress of the amplification process in real time, allowing the visualisation of the exponential amplification. It is this that allows the absolute quantification of target sequences. This is achieved by continuously measuring the fluorescence emitted as the target sequences accumulate.

A number of papers have made use of qPCR to consider the micro-organisms involved in methanogenesis. Only six methanogenic orders have been identified to date, all of which belong to the phylum *Euryarchaeota*. In 2005, the work of Yu et al. (2005) provided an array of primer and probe sequences for the selective detection of methanogen groups, which have become a valuable resource, leading to further work in assessing the structure and dynamics of the methanogenic community in a range of anaerobic digestion systems.

Lee et al. (2009) investigated the changes in methanogenic community structure in batch tests fed with treated synthetic glucose medium, whey permeate and liquefied sewage sludge. The

methanogenic community was analysed using qPCR at the order and family level, and it was found that *Methanosarcinaceae* and *Methanomicrobiales* were the dominant methanogens in the acetate-rich and acetate-depleted regions of the digester respectively, in all digesters. Each digester showed significantly different methanogen community pattern shifts despite having the same seeding source and operating conditions, which suggests that the feed composition has an important effect on the methanogenic community in a digester. Lee et al. (2009) used qPCR to ascertain which methanogens were present in the digestion of protein-, lipid-, and cellulose-rich feeds at batch scale. They demonstrated that protein-rich feeds led to the highest production of methane and that for all feed types, hydrogenotrophic methanogens were more abundant than acetoclastic methanogens. *Methanoculleus sp.* was generally the most abundant methanogen. The findings of Wagner et al. (2013) agree with the work of Lee et al. (2009) in that feed composition has an important effect on the methanogenic community in a digester.

Traversi et al. (2012) considered the methanogenic communities in a pilot-scale reactor and how they related to the biogas production of the digester when operating with two different pre-treatment processes, pressure extrusion and turbo-mixing. They found a positive and significant correlation between biogas production rate and abundance of methanogens. This was true when considering both pre-treatment processes, though pressure extrusion gave a higher biogas yield with higher methane content. Accordingly, samples taken when pressure extrusion was used as a pre-treatment process had the higher concentration of methanogens.

Williams et al. (2013) used qPCR to study the methanogenic populations in a full-scale anaerobic digester fed on food waste over 18 months. The methanogenic communities were dominated by *Methanosaetaceae*, suggesting that acetoclastic methanogenesis was the main route for production of methane. A sudden drop in *Methanosaetaceae* was followed by a spike in acetate, which in turn stimulated the *Methanosarcinaceae* family. Later, a build-up of ammonium inhibited *Methanosaetaceae*, causing a shift from acetoclastic to hydrogenotrophic methanogenesis. This

demonstrates the importance of the effects of the physicochemical environment of the digester on its microbiology.

Cardinali-Rezende et al. (2012) also used qPCR to study the methanogenic populations in a full-scale anaerobic digester, in this case being fed on municipal solid waste over 2 years of start-up. They found that methane production was dominated by the hydrogenotrophic *Methanomicrobiales* (> 90 %) in preference to the acetoclastic *Methanosarcinaceae*, and *Methanosaetaceae* were only measured in very low numbers.

Whilst the research discussed in this section has increased the understanding of how qPCR can be used to link methanogenic population structure to environmental characteristics within a digester, particularly the presence of VFAs, and the gas production of a digester, it is not directly linked to the effects of mixing. To date, qPCR has not been used to assess the effects of mixing on gas production although other techniques have been used to consider the effects of mixing on digester microbiology as seen in Section 2.7.

## **2.9 Review of previous research and knowledge gaps**

This literature review has considered the many factors that affect the production of biogas from anaerobic digestion and in particular, the effects of mixing on both gas production and the micro-organisms that degrade organic material to produce that gas. It is clear that increasing biogas production from digesters used in wastewater treatment is beneficial not only to the environment but also to the wastewater treatment company, through the reduction of greenhouse gas emissions and the production of renewable heat and power. Whilst the biochemical processes involved in anaerobic digesters are complex, they are well-understood. The many factors that affect the process are well-documented in the literature, with some better understood than others. The effects of temperature are widely accepted, whilst the concentrations of inhibitory chemicals and organic compounds required to affect digester stability and gas production are more contentious.

It is recognised that mixing in anaerobic digesters brings micro-organisms and substrate into contact in the sludge, so that the digestion process can take place. Additional benefits, such as reducing temperature, pH and concentration gradients, are widely cited. However, no consensus has been reached in the literature regarding what constitutes an optimal mixing regime. A review of the literature in this field allows the following outline conclusions to be drawn:

- Mixing anaerobic digesters is preferable to not mixing in terms of gas production
- Mixing at low mixing speeds allows greater digester stability and, in some cases, greater gas production than mixing at high speeds
- Similarly, intermittent mixing appears to have positive results on digester stability and gas production when compared to continuous mixing
- At low solids concentration, the effects of mixing are less obvious as self-mixing may occur, due to the produced gas rising through the digester

Considering methanogenesis as the rate-limiting step in the production of methane-rich biogas, once hydrolysis has been overcome, the effects of mixing on methanogens is important in understanding the effects of mixing on gas production. qPCR can be used to investigate the micro-organisms involved in methanogenesis, and whilst its popularity and application in the field of wastewater treatment is increasing, to date there is no literature that makes use of the technique to consider the effects of mixing on methanogens. It is suggested that a *Methanosarcina*-rich digester is preferable to a *Methanosaeta*-rich digester for increasing biogas yields due to its greater acetate utilisation rate, though the literature to back up this hypothesis is limited. However, the effects of mixing on methanogens could be considered to be the result of the creation or destruction of localised pockets of syntrophic micro-organisms creating high localised acetate concentrations, which would favour *Methanosarcina* at low mixing speeds and *Methanosaeta* at high mixing speeds. The morphology of these methanogens offers an alternative hypothesis whereby filamentous *Methanosaeta* are more likely to be adversely affected by mixing than the single coccoidal cells of

*Methanosarcina*. These are competing hypotheses and there is a lack of agreement as to the effects of mixing on methanogenic population structure.

## CHAPTER 3      Fluid flow and CFD modelling

This chapter is split into two sections. The first considers the science of fluid flow. In particular it gives a mathematical description of turbulence and of the boundary layer, and discusses how the flow patterns in a vessel are formed and how they have effects down to the smallest scales. In the second section, the governing theory of CFD is examined and its application to the study of flow patterns in anaerobic digesters is reviewed.

### 3.1 Fluid flow

#### 3.1.1 Governing equations

The flow of fluid with the absence of heat transfer is governed by two sets of equations. The first of these is the continuity equation, which is derived from the law of conservation of mass, which states that the mass of a closed system remains constant over time. When considering an arbitrary control volume of a time-varying, compressible flow, the continuity equation is given in Cartesian coordinates as:

$$\frac{\partial \rho}{\partial t} + \frac{\partial(\rho u)}{\partial x} + \frac{\partial(\rho v)}{\partial y} + \frac{\partial(\rho w)}{\partial z} = 0 \quad \text{Equation 3-1}$$

where  $\rho$  is density,  $t$  is time and  $u$ ,  $v$  and  $w$  are velocities in the  $x$ ,  $y$  and  $z$  directions respectively. In the case of an incompressible flow, density is assumed to be constant. Hence, in tensor form, the continuity equation becomes:

$$\frac{du_i}{dx_i} = 0 \quad \text{Equation 3-2}$$

The second set of governing equations is the momentum equations which are a mathematical expression of the application of Newton's Second Law to fluid motion. Newton's Second Law states

that the net force on an object is equal to the rate of change of its momentum. When considering incompressible flow in an arbitrary control volume, the equations for momentum are given in tensor form as:

$$\frac{\partial u_i}{\partial t} + u_j \frac{\partial u_i}{\partial x_j} = -\frac{1}{\rho} \frac{\partial p}{\partial x_i} + \nu \frac{\partial^2 u_i}{\partial x_j \partial x_j} \quad \text{Equation 3-3}$$

where  $p$  is pressure.

The equations were derived independently by French engineer, Claude-Louis Navier, and Irish mathematician, Sir George Gabriel Stokes, in the early to mid- nineteenth century and hence are referred to collectively as the Navier-Stokes equations.

### 3.1.2 Turbulence

Flow is characterised as laminar or turbulent on the basis of the dimensionless Reynolds number, which is the ratio of inertial to viscous forces in a flow, expressed as:

$$Re = \frac{\rho u D}{\mu} \quad \text{Equation 3-4}$$

where  $Re$  is Reynolds number,  $u$  is characteristic velocity,  $D$  is characteristic length, and  $\mu$  is dynamic viscosity.

For mixing, the characteristic velocity is taken as  $ND$ , where  $N$  is the rotational velocity of the impeller and  $D$  is the characteristic length, taken as the impeller diameter. This gives a Reynolds number of:

$$Re = \frac{\rho N D^2}{\mu} \quad \text{Equation 3-5}$$

where  $N$  is rotational velocity and  $D$  is impeller diameter.

Turbulence is the chaotic state of flow that occurs when inertial forces dominate. The original experiment carried out by Reynolds (1883), considered flow in a pipe and used pipe diameter as the characteristic length. In this case, laminar flow occurs below a Reynolds number of 2000, with fully developed flow occurring at Reynolds numbers greater than 4000. Between 2000 and 4000, a transitional flow regime exists which exhibits an increasing level of turbulent flow characteristics as Reynolds number increases. For mixing, Reynolds numbers less than 10 indicate that flow is laminar; for Reynolds numbers greater than  $2 \times 10^4$ , flow is turbulent and for Reynolds numbers between 10 and  $2 \times 10^4$ , flow is transitional.

Turbulent flow is time-independent, apparently chaotic and non-deterministic, i.e. there is no unique solution to describe the flow (Davidson, 2004). To describe the mixing that is caused by this type of flow, it is necessary to consider all the length and time scales of the mixing process, thereby allowing the calculation of when the system is fully mixed. The apparently random nature of turbulent flow leads to more effective transfer of fluid particles in all directions than in laminar flow and this in turn promotes faster mixing. For fully developed turbulent flow, away from boundaries, the structure of the flow is independent of translations or rotation and is known as isotropic flow, which by its nature is also homogeneous. Although this flow appears to be unpredictable, the velocities involved are normally distributed. Hence, although the flow is unsteady with time, it is steady-on-average and the statistical properties of the turbulent flow are reproducible even if the detailed properties are not.

### **3.1.3 Turbulent mixing**

In order to examine how mixing occurs in a turbulent flow, it is necessary to give the turbulence a nominal structure. Hence, a turbulent flow is considered as consisting of a series of eddies at different length scales. An eddy is any event in the flow which can have time and length scales assigned to it. The length scale of the largest possible eddy in a vessel will be the diameter of the vessel itself as all fluid is contained within it. In the underlying structure of the flow in the vessel,

there will be flow structures on smaller length scales, leading to the concept of an energy cascade as shown in Figure 3.1. The largest eddies are the most energetic, whilst the smallest eddies have less energy.

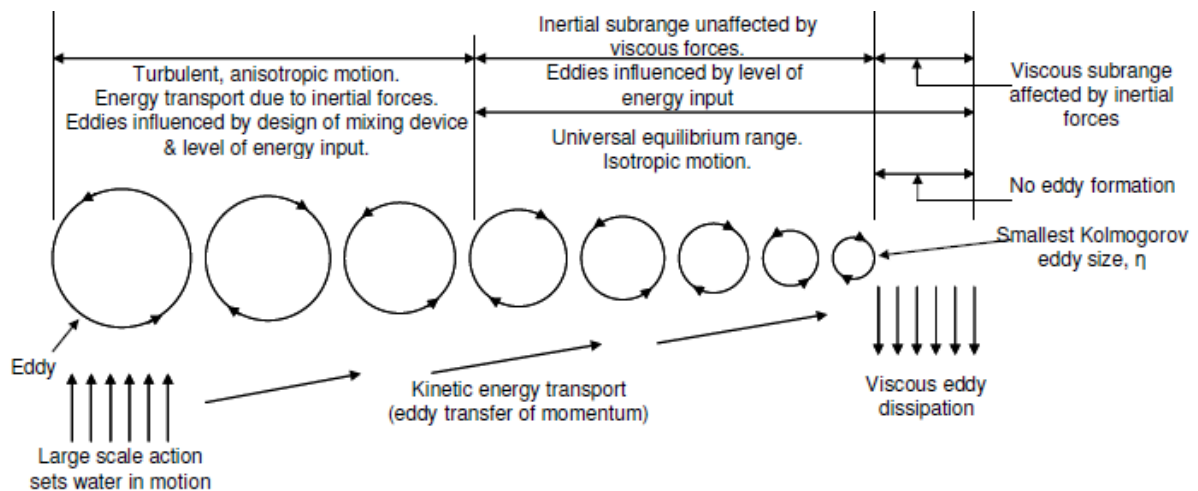


Figure 3.1 – Idealised visualisation of the energy cascade, adapted from Stanley and Smith (1995)

Energy at the large scales is extracted from the mean flow (Tennekes and Lumley, 1982) and drives macromixing, for example by stirring with an impeller or through large scale convection due to temperature differences in the vessel. This energy is passed down through to smaller and smaller eddies, through which mesomixing takes place in the form of turbulent diffusion and the disintegration of eddies. Finally, at the smallest scales, micromixing takes place through mixing at the smallest scales of motion and the dissipation of heat due to viscous friction beyond that. Eddies above a cut-off length scale are anisotropic with those below assumed to be isotropic, i.e. having the same statistical properties in all directions. The Kolmogorov length scale is the length scale for which the Reynolds number is equal to one and Kolmogorov reasoned that in the region of this length scale, eddies decay to heat due to viscous dissipation (friction between the molecules due to the molecular viscosity). At these length scales, the flow will be isotropic and so the nature of the turbulence only depends on the energy input to the flow and the fluid properties i.e. specific energy dissipation rate

and kinematic viscosity (Pope, 2000). Hence the Kolmogorov length scale, velocity scale, and time scale are defined based on these variables:

$$\lambda_K = \left( \frac{\nu^3}{\varepsilon} \right)^{1/4} \quad \text{Equation 3-6}$$

$$u_K = (\varepsilon \nu)^{1/4} \quad \text{Equation 3-7}$$

$$\tau_K = \left( \frac{\nu}{\varepsilon} \right)^{1/2} \quad \text{Equation 3-8}$$

where  $\lambda_K$  is Kolmogorov length scale,  $\nu$  is kinematic viscosity,  $\varepsilon$  is specific energy dissipation rate,  $u_K$  is Kolmogorov velocity scale and  $\tau_K$  is Kolmogorov timescale.

The Kolmogorov length scale gives a representation of the smallest eddies that can exist within the flow and therefore indicates the smallest scale at which mixing can take place in turbulent flows. Mixing down to the Kolmogorov scale is achieved by fluid mechanics. Below this scale, mixing down to the molecular scale occurs by diffusion (Amanullah et al., 2004). The efficacy of micro-mixing at the Kolmogorov scale can be the limiting factor in biological initiation processes, as it is an important mechanism for bringing micro-organisms and reactants together locally (Lehwald et al., 2012). When particles or cells are smaller than the eddies surrounding them, the eddies carry the particles along. As such, particle rising and settling velocity in a vessel is dependent on the ratio of the Kolmogorov length scale and the particle diameter and actually independent of the impeller type (Fajner et al., 2008, Pinelli et al., 2004). However, if cells are of the same order of magnitude as the Kolmogorov scale, it is suggested that the kinetic energy of turbulence may be transferred from eddies to the cell surface of micro-organisms and this can lead to cell damage (Kawase and Moo-Young, 1990). Whilst the Kolmogorov scale gives a useful indication of whether cells are likely to be damaged by turbulence in the vessel, it is a concept that should be used with care, due in part to the large range of energy dissipation rates measured by different workers using the same mixing systems (Nienow et al., 2013). This may be attributed to the variations in energy dissipation rates across a stirred vessel

with dissipation rates in the impeller region being up to 1000 times higher than in the bulk of the fluid (Kilander and Rasmuson, 2005). Furthermore, although this approach has worked well for several single cell entities including bacteria, yeast and animal cells (Nienow et al., 2013), Kolmogorov's theory does not give any indication of the mechanisms with which cell damage can occur (Amanullah et al., 2004) and therefore may not be applicable in all systems.

### 3.1.4 Boundary layer theory

At high Reynolds numbers, the bulk flow of a viscous fluid behaves increasingly like an inviscid or ideal fluid. The most notable shortcoming of this approximation to an ideal fluid is that the no-slip condition, of zero velocity at the wall, is not satisfied. The viscosity must be taken into account so that a transition from a finite velocity close to the wall to zero velocity at the wall can be achieved. At large Reynolds numbers, this happens in a thin layer of fluid close to the wall called the boundary layer or frictional layer. (Schlichting and Gersten, 2000)

Boundary layers can be laminar or turbulent. Within a laminar boundary layer, the layers of fluid slip over one another without mixing and so momentum transfer takes place by shear forces acting between the layers. In most engineering applications, boundary layers quickly develop from laminar to turbulent. In the case of flow over a flat plate, at a critical distance from the leading edge of the plate, instabilities start to form in the boundary layer which spread as the distance increases until the whole of the boundary layer is turbulent. The turbulent boundary layer is further broken down into three regions (Schlichting and Gersten, 2000) as shown in Figure 3.2. These regions can be described mathematically by the relationship between the dimensionless velocity, and the dimensionless wall coordinate,  $y^+$ , defined as:

$$u^+ = \frac{u}{u_\tau} \quad \text{Equation 3-9}$$

$$y^+ = \frac{yu_\tau}{\nu} \quad \text{Equation 3-10}$$

where  $u^+$  is dimensionless velocity,  $u_\tau$  is the friction velocity,  $y^+$  is dimensionless wall coordinate and  $y$  is the distance from the wall.

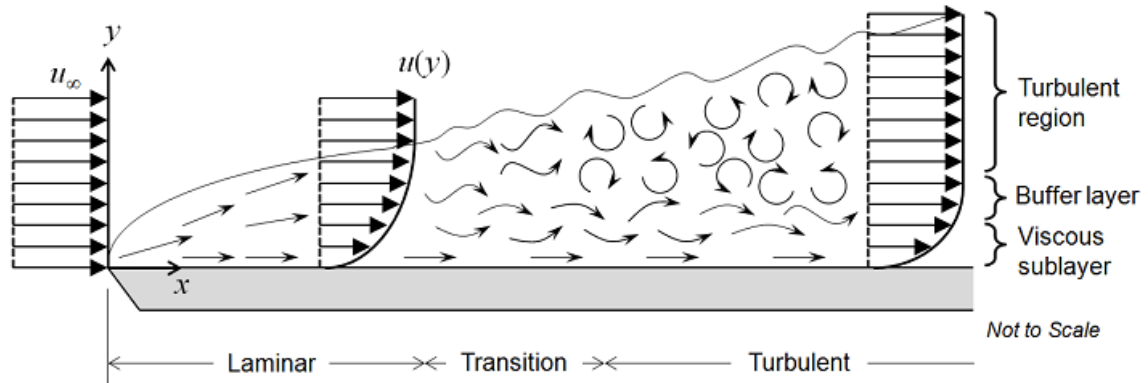


Figure 3.2 - Flow of fluid over a flat plate depicting the development of the boundary layer, taken from Frei (2013)

The viscous sub-layer is found along the wall, where  $y^+$  is less than 5. Here, the flow of the slowest moving fluid closest to the wall is dominated by the viscous stresses on the fluid and  $u^+ = y^+$ . In the turbulent log region, where  $y^+$  is greater than 30, flow is mathematically described using the log law:

$$u^+ = \frac{1}{\kappa} \ln y^+ + B \quad \text{Equation 3-11}$$

where  $\kappa$  is the Von Kármán constant and  $B$  is a constant. For a smooth wall, experiments have shown that  $\kappa \approx 0.41$  and  $B \approx 5.0$ .

A buffer region exists between the viscous sub-layer and the turbulent log region, i.e. where  $y^+$  is between 5 and 30. A mathematical description of these layers is shown in Figure 3.3. Finally, above approximately  $y^+ = 100$ , the log region gives way to the wake region which is the outer region of flow in which mixing occurs. It is essential that the boundary layer is resolved in CFD simulations as it is here that most turbulent kinetic energy is generated and this in turn can have a strong effect on the bulk flow of the fluid.

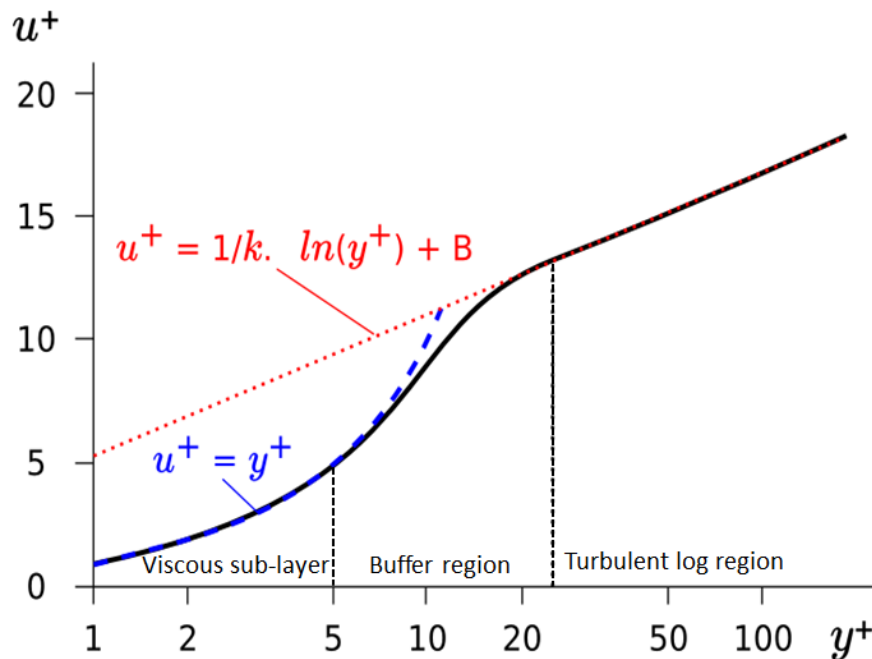


Figure 3.3 – Turbulent boundary layer structure showing viscous sub-layer, buffer region and turbulent log region, adapted from (Versteeg and Malalasekera, 2007)

### 3.1.5 Flow patterns

The flow patterns that are generated in a mixing vessel are dependent on the geometry of the vessel, the mixing method, the location of inflows and outflows to the vessel and the physical properties of the fluid contained within the vessel. In turn, the flow patterns have an effect on the contact of fluid particles, the formation and location of dead zones in the vessel and the presence of floating or settled layers in the vessel.

Impellers used for mechanical mixing can be separated into two categories based on the flow patterns that they induce within a vessel: radial-flow impellers, like a flat-blade impeller, and axial-flow impellers, like a pitched-blade impeller. Radial-flow impellers produce two circulating loops of fluid, one above and one below the impeller, whilst axial-flow impellers produce a single circulation loop which extends above and below the impeller as shown in Figure 3.4. It has been shown that axial-flow impellers, particularly the pitched blade turbine (PBT) or Rushton turbine impellers, have been subjected to far greater study than axial-flow impellers, due to their wide adoption as a

general-purpose impeller in industries ranging from food and beverage to pharmaceutical and fast-moving consumer goods. (Hemrajani and Tattersson, 2004)

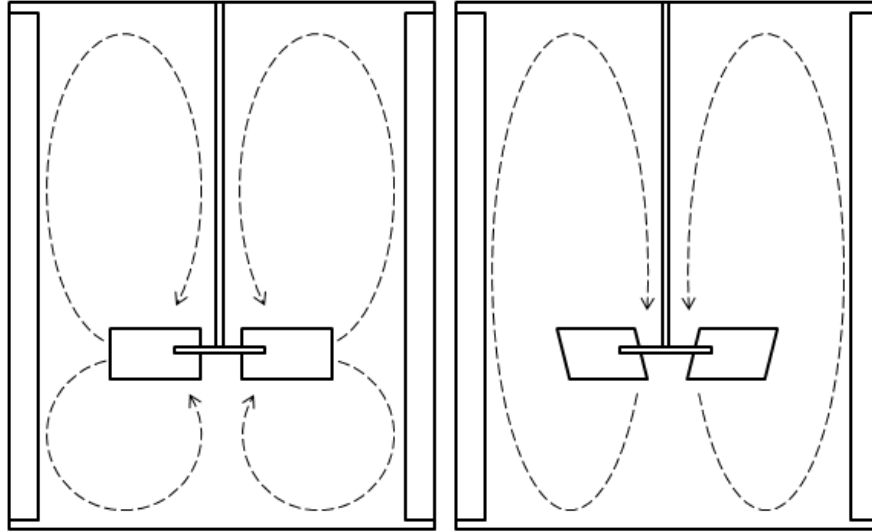


Figure 3.4 - Flow patterns generated by a radial-flow impeller (left) and an axial-flow impeller (right)

### 3.1.6 Velocity gradient

Camp and Stein (1943) considered the angular distortion of an elemental volume of water arising from the application of tangential surface forces and defined  $G$  as the root mean square velocity gradient in a mixing vessel, expressed algebraically as:

$$G = \sqrt{\left(\frac{\partial u}{\partial y} + \frac{\partial v}{\partial x}\right)^2 + \left(\frac{\partial u}{\partial z} + \frac{\partial w}{\partial x}\right)^2 + \left(\frac{\partial v}{\partial z} + \frac{\partial w}{\partial y}\right)^2} \quad \text{Equation 3-12}$$

where  $G$  is the root mean square velocity gradient.

This absolute velocity gradient is related to the work done per unit volume per unit time by:

$$\Phi = \mu \left[ \left(\frac{\partial u}{\partial y} + \frac{\partial v}{\partial x}\right)^2 + \left(\frac{\partial u}{\partial z} + \frac{\partial w}{\partial x}\right)^2 + \left(\frac{\partial v}{\partial z} + \frac{\partial w}{\partial y}\right)^2 \right] = \mu G^2 \quad \text{Equation 3-13}$$

where  $\Phi$  is power dissipation, equal to the total work done by shear per unit volume per unit time.

From this,

$$G = \sqrt{\frac{\Phi}{\mu}} = \sqrt{\frac{P_{in}}{\mu V}} = \sqrt{\frac{\varepsilon}{\nu}} \quad \text{Equation 3-14}$$

where  $P_{in}$  is the power of mixing input to the vessel and  $V$  is the volume of the vessel.

In theory, the absolute velocity gradient,  $G$ , can be calculated at any point within a mixing vessel, provided that the energy dissipation at that point is known. In practice, energy dissipation, along with other flow characteristics, varies across the vessel, making velocity gradient a function of time and location. Given these complications, the average velocity gradient throughout the vessel,  $\bar{G}$ , is often approximated as:

$$\bar{G} = \sqrt{\frac{P_{ave}}{\mu V}} \quad \text{Equation 3-15}$$

where  $\bar{G}$  is the average velocity gradient and  $P_{ave}$  is the average mixing power input to the vessel.

Camp and Stein originally applied the concept of the  $G$  value to the design and analysis of mixing, coagulation and sedimentation processes but since its introduction it has found use describing mixing in a wide range of engineering applications (Metcalf and Eddy, 2003, Crittenden et al., 2005).

The value of  $\bar{G}$  is often used in the design of mixing vessels with Tchobanoglous and Burton (1991) recommending a value of 60-80  $s^{-1}$  for the design of an anaerobic digester. However, it has been argued that the concept of  $\bar{G}$  is flawed as it attempts to represent a complex flow field with a single number (Clark, 1985; Luo, 1997). Neither the distribution of velocity gradients nor the distribution of power inputs within a digester is uniform as areas of high power input, (e.g. close to impeller), are likely to experience high levels of turbulence and hence, velocity gradients several orders of magnitude greater than areas of low turbulence. As such, although a useful parameter to

approximate overall conditions, the average velocity gradient does not sufficiently describe the fluctuations in local velocity gradient within a vessel. Nonetheless, CFD models of a digester can be used to determine the local values of velocity gradient and consider the range of local velocity gradients that are experienced across a vessel. It is these local variations that occur down to the Kolmogorov scale which can have an effect on microbiological communities and thereby may be used to determine the effect of mixing on gas production at a local scale within the digester.

### **3.2 Computational fluid dynamics modelling**

CFD is the use of numerical algorithms to solve the governing equations of fluid flow. In order to calculate the velocity and pressure at any specific point in a fluid flow, it is necessary to also know the velocity and pressure at adjacent points. As such, the Navier-Stokes equations must be solved for all points in a flow simultaneously, a highly demanding exercise without the use of a computer. Despite starting life in the aerospace industry, the use of CFD has now found applications in a wide range of industries from chemical processing, to hydrodynamics, meteorology and biomedical engineering. Within this section, the theory underpinning computational fluid dynamics is presented.

### 3.2.1 General methodology

The process of performing flow analysis using CFD follows the steps shown in Figure 3.5.

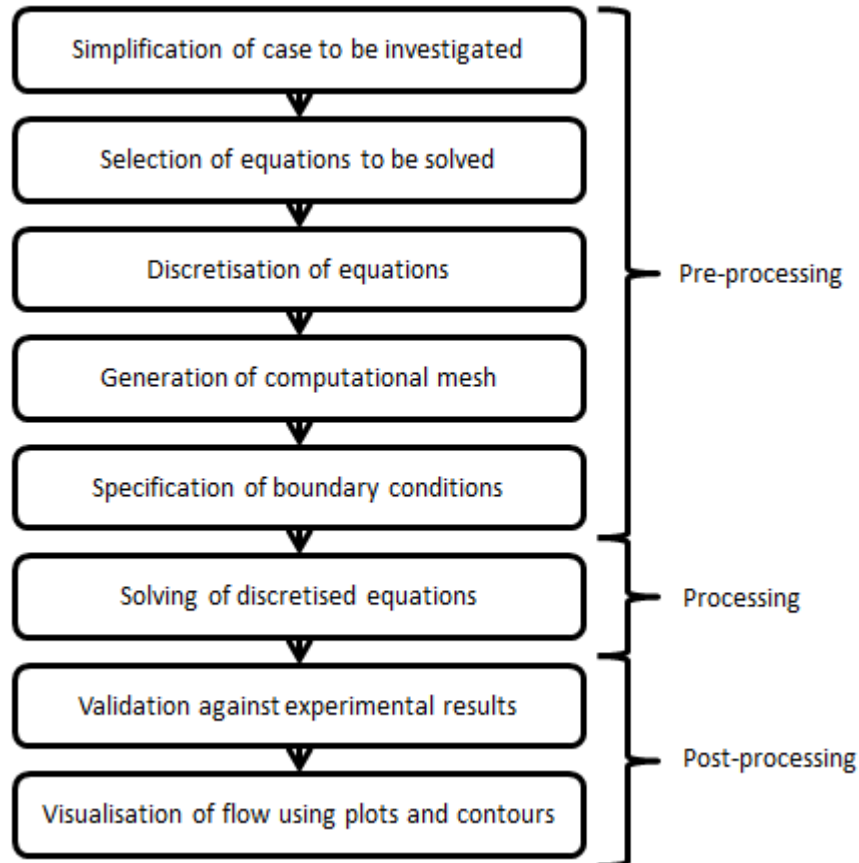


Figure 3.5 – Steps involved in CFD flow analysis

### 3.2.2 Governing equations of computational fluid dynamics

The continuity equation and the momentum equations introduced in Section 3.1 form the foundation of advanced fluid dynamics analysis. If a Newtonian fluid with a constant viscosity is considered and body forces are incorporated into the pressure term, then only four flow variables appear in the Navier-Stokes momentum equations and hence, with the help of the continuity equation, a solution can be found. Due to the large range of length scales in turbulent flows, it is computationally very demanding to resolve them all and thus researchers often describe the flow statistically. When measuring the velocity at a point in a fully developed turbulent flow, it can be seen that the velocity fluctuates around a mean value, as shown in Figure 3.6. Reynolds concluded

that the velocity of the flow at any point in time could be considered as the sum of this average velocity and a fluctuating component (Tennekes and Lumley, 1982):

$$u = \bar{u} + u' \quad \text{Equation 3-16}$$

where  $\bar{u}$  is the mean velocity and  $u'$  is the fluctuating component at time  $t$ .

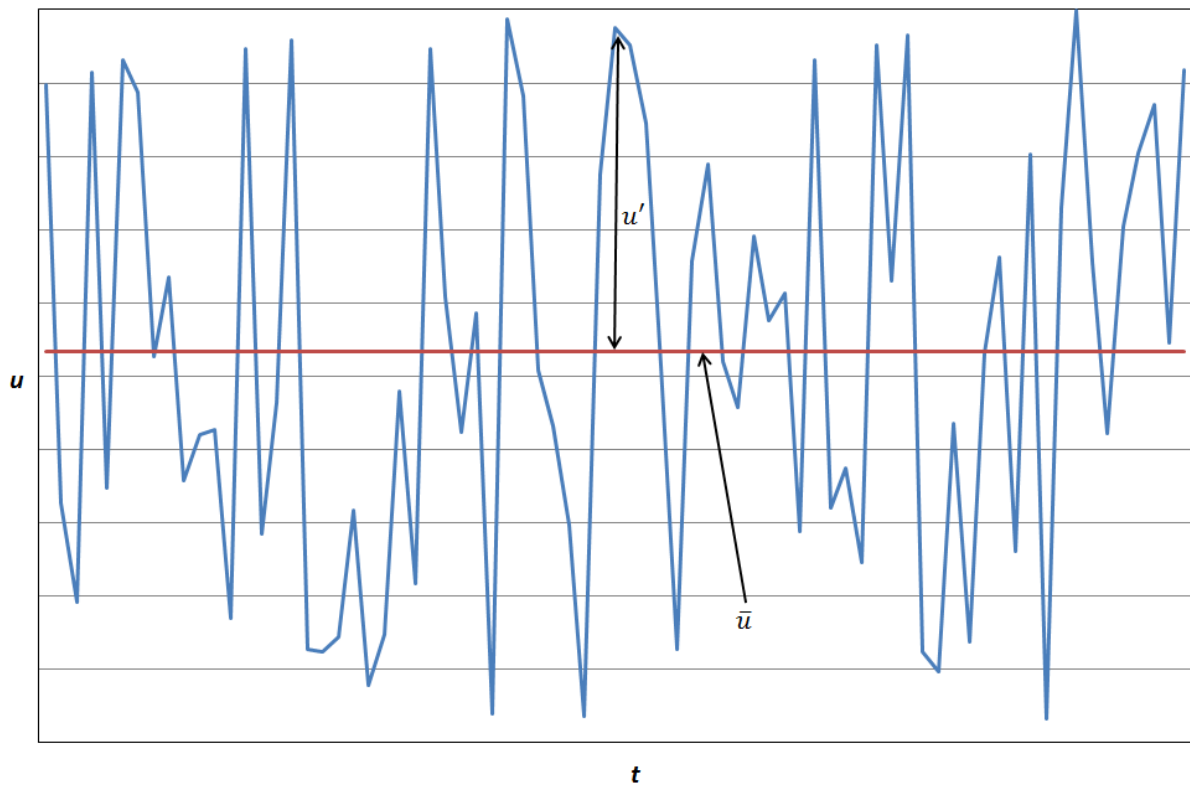


Figure 3.6 – Velocity for stationary turbulence

By integrating the velocity over time,  $\Delta t$  and dividing by  $\Delta t$ , the time-averaged velocity is given as:

$$\bar{u} = \frac{1}{\Delta t} \int_t^{t+\Delta t} (u - u') dt \quad \text{Equation 3-17}$$

Time-averaging the instantaneous velocity gives the mean velocity whilst the time-averaged fluctuating component has a value of zero (Tennekes and Lumley, 1982). Applying this technique to the Navier-Stokes equations, as stated in Section 3.1.1, gives the Reynolds Averaged Navier-Stokes

(RANS) equations (Reynolds, 1895). However, the product of two fluctuating components is not necessarily zero and therefore, whilst the time-averaged continuity equation may be written as:

$$\frac{\partial \bar{u}_i}{\partial x_i} = 0 \quad \text{Equation 3-18}$$

the time-averaged momentum equation must be rewritten as:

$$\frac{\partial \bar{u}_i}{\partial t} + \bar{u}_j \frac{\partial \bar{u}_i}{\partial x_j} = -\frac{1}{\rho} \frac{\partial \bar{p}}{\partial x_i} + \frac{1}{\rho} \frac{\partial}{\partial x_i} \left( \nu \frac{\partial \bar{u}_i}{\partial x_j} - \overline{u'_i u'_j} \right) \quad \text{Equation 3-19}$$

The additional terms are known as the Reynolds stresses and account for the turbulent fluctuations in the mean flow. Hence, in turbulent flows, the fluctuating velocity components increase the number of unknowns in the equation set and further equations are required in order to close and solve the set of equations (Versteeg and Malalasekera, 2007).

### 3.2.3 Turbulence modelling and the Boussinesq hypothesis

Turbulence models are sets of equations that are used to model the Reynolds stresses in the RANS equations. The choice of model is dependent, amongst other things, on the computing power available and the accuracy of the solution required. The most commonly adopted turbulence models are based on the eddy viscosity model, which in turn, are based on the Boussinesq hypothesis. Boussinesq (1877) postulated that the momentum transfer caused by turbulent eddies, i.e. the link between the Reynolds stresses and local shear, can be modelled with an eddy viscosity, in the same way that molecular viscosity is used to model momentum transfer caused by molecular movement in a gas. It is important to note that the eddy viscosity hypothesis has no physical grounding. The eddy viscosity model states that:

$$-\overline{u_i u_j} = \nu_t \left( \frac{\partial u_i}{\partial x_j} + \frac{\partial u_j}{\partial x_i} \right) - \frac{2}{3} k \delta_{ij} = 2\nu_t s_{ij} - \frac{2}{3} k \delta_{ij} \quad \text{Equation 3-20}$$

where  $\nu_t$  is the turbulent eddy viscosity,  $k$  is the turbulent kinetic energy,  $\delta_{ij}$  is the Kronecker delta and  $s_{ij}$  is the mean strain rate tensor:

$$s_{ij} = \frac{1}{2} \left( \frac{\partial u_i}{\partial x_j} + \frac{\partial u_j}{\partial x_i} \right) \quad \text{Equation 3-21}$$

The equation for the turbulent eddy viscosity is dependent on the two-equation model used.

### 3.2.3.1 Two equation models

The two-equation turbulence models are a family of eddy viscosity models that solve two separate equations for turbulent viscosity and length scales.

#### 3.2.3.1.1 Standard $k$ - $\epsilon$ model

The standard  $k$ - $\epsilon$  model, proposed by Launder and Spalding (1972), is one such model and is regularly used in CFD simulations due to its robustness and reasonable accuracy for a wide range of turbulent flows. It is a semi-empirical model based on the model transport equations for turbulent kinetic energy ( $k$ ) and its dissipation rate ( $\epsilon$ ), with the model transport equation for  $k$  being derived from the exact equation, whilst the transport equation for  $\epsilon$  is based on physical reasoning. The model assumes that flow is fully turbulent and that the effects of molecular viscosity are negligible. The following transport equations are used to calculate  $k$  and  $\epsilon$ , respectively:

$$\frac{\partial}{\partial t}(\rho k) + \frac{\partial}{\partial x_i}(\rho k u_i) = \frac{\partial}{\partial x_j} \left[ \left( \mu + \frac{\mu_t}{\sigma_k} \right) \frac{\partial k}{\partial x_j} \right] + G_k - \rho \epsilon + S_k \quad \text{Equation 3-22}$$

$$\frac{\partial}{\partial t}(\rho \epsilon) + \frac{\partial}{\partial x_i}(\rho \epsilon u_i) = \frac{\partial}{\partial x_j} \left[ \left( \mu + \frac{\mu_t}{\sigma_\epsilon} \right) \frac{\partial \epsilon}{\partial x_j} \right] + C_1 \frac{\epsilon}{k} (G_k) - C_2 \rho \frac{\epsilon^2}{k} + S_\epsilon \quad \text{Equation 3-23}$$

where  $G_k$  = generation of turbulent kinetic energy due to mean velocity gradients,  $\mu_t$  = turbulent kinetic energy,  $C_1 = 1.44$ ,  $C_2 = 1.92$ ,  $\sigma_k$  and  $\sigma_\epsilon$  = Prandtl numbers for  $k$  and  $\epsilon$  with values of 1.0 and 1.3 respectively and  $S_k$  and  $S_\epsilon$  are source terms.

The generation of turbulent kinetic energy due to mean velocity gradients is calculated using:

$$G_k = \mu_t \left( \frac{\partial u_i}{\partial x_j} + \frac{\partial u_j}{\partial x_i} \right) \frac{\partial u_j}{\partial x_i} \quad \text{Equation 3-24}$$

and the turbulent eddy viscosity,  $\mu_t$ , is calculated by combining  $k$  and  $\varepsilon$ :

$$\mu_t = \rho C_\mu \frac{k^2}{\varepsilon} \quad \text{Equation 3-25}$$

where  $C_\mu = 0.09$ .

### 3.2.3.1.2 Realisable $k$ - $\varepsilon$ model

As the strengths and weaknesses of the standard  $k$ - $\varepsilon$  model have been documented, adjustments have been made to improve its performance in various situations. The realisable  $k$ - $\varepsilon$  model, proposed by Shih et al. (1995), is such a model, which contains a formula for the turbulent viscosity which involves a variable  $C_\mu$  and an equation for the dissipation rate that is derived from the dynamic equation for the mean-square vorticity fluctuation. This allows the model to satisfy certain mathematical constraints on the Reynolds stresses, making the model more consistent with the physics of turbulent flow. In this model, the equation for dissipation rate becomes:

$$\frac{\partial}{\partial t}(\rho\varepsilon) + \frac{\partial}{\partial x_i}(\rho\varepsilon u_i) = \frac{\partial}{\partial x_j} \left[ \left( \mu + \frac{\mu_t}{\sigma_\varepsilon} \right) \frac{\partial \varepsilon}{\partial x_j} \right] + \rho C_1 S_\varepsilon - \rho C_2 \frac{\varepsilon^2}{k + \sqrt{\nu\varepsilon}} + S_\varepsilon \quad \text{Equation 3-26}$$

where  $C_2 = 1.9$ ,  $\sigma_k$  and  $\sigma_\varepsilon =$  Prandtl numbers for  $k$  and  $\varepsilon$  with values of 1.0 and 1.2 respectively and  $S_k$  and  $S_\varepsilon$  are source terms. Additionally,

$$C_1 = \max \left[ 0.43, \frac{\eta}{\eta + 5} \right] \quad \text{Equation 3-27}$$

where

$$\eta = S \frac{k}{\varepsilon} \quad \text{Equation 3-28}$$

where

$$S = \sqrt{2S_{ij}S_{ij}} \quad \text{Equation 3-29}$$

The realisable  $k$ - $\varepsilon$  model more accurately predicts the spreading rate of jets and is likely to provide superior performance for rotating flows, boundary layers under strong adverse pressure gradients, separation and recirculation. One limitation of the realisable  $k$ - $\varepsilon$  model is that it produces non-physical turbulent viscosities when the computational domain contains both rotating and stationary sub-domains. Despite this, several authors have successfully demonstrated its use in modelling anaerobic digesters (Bridgeman, 2012, Wu, 2010c, Wu, 2011).

### 3.2.3.1.3 $k$ - $\omega$ model

Another set of two-equation turbulence models exist. These are again semi-empirical models, this time based on the model transport equations for turbulent kinetic energy ( $k$ ) and the specific dissipation rate ( $\omega$ ), which can be thought of as the ratio of dissipation rate to turbulent kinetic energy. The standard  $k$ - $\omega$  model frequently used in commercially available CFD software is based on the Wilcox  $k$ - $\omega$  model (Wilcox, 1998), which incorporates modifications for low-Reynolds-number effects, compressibility, and shear flow spreading. The following transport equations are used to calculate  $k$  and  $\omega$ , respectively:

$$\frac{\partial}{\partial t}(\rho k) + \frac{\partial}{\partial x_i}(\rho k u_i) = \frac{\partial}{\partial x_j} \left[ \Gamma_k \frac{\partial k}{\partial x_j} \right] + G_k + Y_k + S_k \quad \text{Equation 3-30}$$

$$\frac{\partial}{\partial t}(\rho \omega) + \frac{\partial}{\partial x_i}(\rho \omega u_i) = \frac{\partial}{\partial x_j} \left[ \Gamma_\omega \frac{\partial \omega}{\partial x_j} \right] + G_\omega - Y_\omega + S_\omega \quad \text{Equation 3-31}$$

where  $G_k$  = generation of turbulence kinetic energy due to mean velocity gradients,  $G_\omega$  = generation of  $\omega$ ,  $\Gamma_k$  and  $\Gamma_\omega$  = effective diffusivity of  $k$  and  $\omega$  respectively,  $Y_k$  and  $Y_\omega$  = dissipation of  $k$  and  $\omega$  due to turbulence,  $S_k$  and  $S_\omega$  = source terms.

The effective diffusivity of  $k$  and  $\omega$  respectively are calculated as

$$\Gamma_k = \mu + \frac{\mu_t}{\sigma_k} \quad \text{Equation 3-32}$$

and

$$\Gamma_\omega = \mu + \frac{\mu_t}{\sigma_\omega} \quad \text{Equation 3-33}$$

The turbulent or eddy viscosity,  $\mu_t$ , is calculated by combining  $k$  and  $\omega$ :

$$\mu_t = \alpha^* \frac{\rho k}{\omega} \quad \text{Equation 3-34}$$

where the coefficient  $\alpha^*$  damps the turbulent viscosity causing a low-Reynolds-number correction.

#### 3.2.3.1.4 SST $k$ - $\omega$ model

The shear-stress transport (SST)  $k$ - $\omega$  model was developed by Menter (1994) as a combination of the robust and accurate  $k$ - $\omega$  model in the near-wall region and the free-stream independent  $k$ - $\epsilon$  model in the far field. This is achieved by converting the  $k$ - $\epsilon$  model into a  $k$ - $\omega$  format. The SST  $k$ - $\omega$  model uses a blending function that allows it to behave as the standard  $k$ - $\omega$  model in the near-wall region and as the transformed  $k$ - $\epsilon$  model away from the surface. Additionally, the SST  $k$ - $\omega$  model incorporates a damped cross-diffusion derivation term in the equation for  $\omega$ , uses different modelling constants and the definition of the turbulent viscosity is modified to account for the transport of the turbulent shear stress.

These modifications enable the SST  $k$ - $\omega$  model to more accurately and more reliably predict a wider range of flows than the standard  $k$ - $\omega$  model. The following transport equations are used to calculate  $k$  and  $\omega$ , respectively:

$$\frac{\partial}{\partial t}(\rho k) + \frac{\partial}{\partial x_i}(\rho k u_i) = \frac{\partial}{\partial x_j} \left[ \Gamma_k \frac{\partial k}{\partial x_j} \right] + \tilde{G}_k + Y_k + S_k \quad \text{Equation 3-35}$$

$$\frac{\partial}{\partial t}(\rho \omega) + \frac{\partial}{\partial x_i}(\rho \omega u_i) = \frac{\partial}{\partial x_j} \left[ \Gamma_\omega \frac{\partial \omega}{\partial x_j} \right] + G_\omega - Y_\omega + D_\omega + S_\omega \quad \text{Equation 3-36}$$

where  $\tilde{G}_k$  = modified generation of turbulent kinetic energy due to mean velocity gradients and  $D_\omega$  = cross-diffusion term.

### 3.2.3.2 Reynolds Stress Model

The Reynolds Stress Model (RSM) is a far more complicated turbulence model than the two-equation models. Rather than using the isotropic eddy-viscosity hypothesis, RSM closes the RANS equations by solving transport equations for the Reynolds stresses, along with an equation for the dissipation rate. This means that seven additional transport equations must be solved when dealing with three-dimensional models. RSM deals with the physics of flow phenomena in a far more rigorous manner than the two-equation models so has greater potential to accurately represent complex flows. The equations for the transport of the Reynolds stresses,  $\overline{\rho u'_i u'_j}$ , in an incompressible flow without body forces and ignoring transport due to rotation may be written as:

$$\begin{aligned} \frac{\partial}{\partial t}(\overline{\rho u'_i u'_j}) + \frac{\partial}{\partial x_k}(\rho u_k \overline{u'_i u'_j}) \\ = \frac{\partial}{\partial x_k} \left[ \overline{\rho u'_i u'_j u'_k} + \overline{p'(\delta_{kj} u'_i + \delta_{ik} u'_j)} \right] \\ + \frac{\partial}{\partial x_k} \left[ \mu \frac{\partial}{\partial x_k} (\overline{u'_i u'_j}) \right] - \rho \left( \overline{u'_i u'_k} \frac{\partial u_j}{\partial x_k} + \overline{u'_j u'_k} \frac{\partial u_i}{\partial x_k} \right) \\ + \rho' \left( \frac{\partial u'_i}{\partial x_j} + \frac{\partial u'_j}{\partial x_i} \right) - 2\mu \frac{\partial u'_i}{\partial x_k} \frac{\partial u'_j}{\partial x_k} \end{aligned} \quad \text{Equation 3-37}$$

where the terms on the left hand side are the local time derivative and the convection term and the terms on the right hand side of the equation are, in order, terms for turbulent diffusion, molecular diffusion, stress production, pressure strain and dissipation.

The model is still limited by the closure assumptions employed to model certain terms in the transport equations for the Reynolds stresses. The modelling of pressure strain and dissipation rate terms in particular poses a problem. Furthermore, the requirement to solve seven instead of two additional equations means that RSM is significantly more computationally expensive than the two-equation models, and the issues involved in modelling certain terms mean that the results may not be sufficiently superior to the simpler models to warrant the extra computing expense. However, if the flow features of interest are the result of anisotropy in the Reynolds stresses, as is likely to be the case in highly swirling flows, it is important that the model is considered.

### 3.2.3.3 Direct numerical simulation

As laid out in Section 3.1.2, turbulence can be considered as eddies characterised by a spectrum of length and time scales. In theory, it is possible to resolve the entire spectrum by numerically integrating the Navier-Stokes equations, a process called direct numerical simulation (DNS). As such, DNS requires no modelling; it is a direct resolution of the Navier-Stokes equations. However, in practice, this is not feasible due to the prohibitively high computational costs of such a simulation.

The number of grid points required to construct a DNS simulation is proportional to  $Re^{9/4}$  and hence is also proportional to the smallest length scale in the flow. Additionally, a time step must be selected that allows the smallest time scales to be resolved. Consequently, the DNS approach is limited to applications with low Reynolds numbers and simple geometries. As such, it is not applicable to this work and will not be considered further.

### 3.2.3.4 Large eddy simulation

Large eddy simulation (LES) offers a compromise between the accuracy of DNS and the lower computational cost of turbulence model-based solutions. The large energy-containing eddies in the flow are resolved directly, while smaller eddies are modelled using a subgrid-scale model. This allows the use of a coarser mesh and a larger time step that would be possible for a DNS solution. However, LES still requires a substantially finer mesh than a RANS model. This is due in part to the issue that near the wall, even the large eddies become relatively small and, where  $y^+ < 1$ , require a mesh resolution that is once again dependent on the Reynolds number. The computational costs of resolving the boundary layer with LES increases proportionally with  $Re^{1.8}$  (Piomelli, 2008). Additionally, a LES model must be run for sufficient time to ensure that stable statistics of the flow are obtained. This leads to a computational cost for LES that is normally orders of magnitude higher than that for a steady RANS calculation.

### 3.2.3.5 Model selection

Each of the turbulence models available has advantages and disadvantages in certain applications and there is no one universally applicable turbulence model that is the right choice for every situation. As such, it is necessary to select turbulence models on a case-by-case data. When determining which model to use, considerations should include the physics of the situation, the level of accuracy required from the model, the computational resources and time available for running the simulation and guidance regarding best practice for problems of a similar nature. Table 3.1 gives an overview of the advantages and disadvantages of the turbulence models discussed in this chapter.

**Table 3.1 – Advantages and disadvantages of two-equation turbulence models and the Reynolds Stress Model (Wilcox, 1998, ANSYS-Fluent, 2012)**

<b>Model</b>	<b>Advantages</b>	<b>Disadvantages</b>
Standard $k-\varepsilon$	Simple to implement Stable calculations converge easily Reasonable predictions for many flows	Poor predictions of swirling or rotating flows, flows with strong separation, axisymmetric jets, unconfined flow and fully developed flow in non-circular ducts Only valid for fully turbulent flows Limited by the isotropic eddy viscosity assumption
Realisable $k-\varepsilon$	Improved performance for planar and round jets, boundary layers under strong adverse pressure gradients and separation, rotation and recirculation and strong streamline curvature	Limited by the isotropic eddy viscosity assumption Not recommended for use with multiple reference frames
Standard $k-\omega$	Valid throughout boundary layer (assuming sufficiently fine grid resolution)	Flow separation is over predicted
SST $k-\omega$	Suitable for adverse pressure gradients and separation Accounts for transport of principal turbulent shear stress	Less suitable for free shear flows
RSM	Physically most complete model Accounts for streamline curvature, swirl, rotation and high strain rates Accurately calculates mean flow properties and Reynolds stresses Superior results to $k-\varepsilon$ models for flows with stagnation points	Computationally expensive Tightly coupled momentum and turbulence equations makes it harder to obtain converged results May not be more accurate than two-equation models

### 3.2.4 Modelling mixing

There are two main methods for explicitly calculating the effects of a rotating flow, either employing multiple reference frames (MRF) or employing a sliding mesh (SM).

#### 3.2.4.1 Multiple reference frames

With the MRF method, the vessel is split into two regions, the impeller region and the bulk region, which incorporates the fluid in the remainder of the vessel. The flow within the impeller region is calculated according to a rotating reference frame which is associated with a rotational velocity equal to that of the impeller, whilst the flow within the bulk region is calculated according to a

stationary reference frame. An arbitrary point in the domain is located by a position vector  $\bar{r}$  from the origin of the moving frame. Fluid velocities in the moving frame are transformed from the stationary frame using:

$$\bar{v}_r = \bar{v} - \bar{u}_r \quad \text{Equation 3-38}$$

where

$$\bar{u}_r = \bar{\omega} \times \bar{r} \quad \text{Equation 3-39}$$

where  $\bar{v}_r$  is the relative fluid velocity viewed from the rotating frame,  $\bar{v}$  is the absolute fluid velocity viewed from the stationary frame,  $\bar{u}_r$  is the velocity of the rotating frame and  $\bar{\omega}$  is the angular velocity of the rotating frame.

For the rotating zone, the conservation of mass in an incompressible flow becomes:

$$\nabla \cdot \bar{v}_r = 0 \quad \text{Equation 3-40}$$

and the conservation of momentum becomes:

$$\nabla \cdot (\bar{v}_r \bar{v}) + [\bar{\omega} \times (\bar{v} - \bar{v}_t)] = -\nabla P + \nabla \cdot \bar{\tau} + \bar{F} \quad \text{Equation 3-41}$$

where  $\bar{\tau}$  = stress tensor and  $\bar{F}$  = body forces.

The momentum equations are solved in each of the two zones, with the acceleration of the fluid in the rotating reference frame being augmented by the additional terms indicated in the equations above, and a steady-state approximation is made at the interface between the two regions. This allows a mixing model to be approximated to a steady-state model by considering the flow patterns

that are established during a snapshot of the impeller's motion. Hence, this method is sometimes called the frozen rotor-stator method.

### 3.2.4.2 Sliding meshes

With the SM method, the vessel is again split into two regions, the impeller region and the bulk region. The mesh within the impeller region rotates at a rotational velocity equal to that of the impeller, whilst the mesh within the bulk region remains stationary.

The integral form of the conservation equation for a general scalar,  $\varphi$ , on an arbitrary control volume,  $V$ , whose boundary is moving, as in a sliding mesh is written as:

$$\frac{d}{dt} \int_V \rho \varphi dV + \int_{dV} \rho \varphi (\bar{u} - \bar{u}_g) \cdot \bar{dA} = \int_{dV} \Gamma \nabla \varphi \cdot \bar{dA} + \int_V S_\varphi dV \quad \text{Equation 3-42}$$

where  $\bar{u}$  is the flow velocity vector,  $\bar{u}_g$  is the mesh velocity of the moving mesh,  $\Gamma$  is the diffusion coefficient and  $S_\varphi$  is the source coefficient of  $\varphi$ . Note that  $dV$  is used to represent the boundary of the control volume,  $V$ .

The time derivative term in this equation can be written as:

$$\frac{d}{dt} \int_V \rho \varphi dV = \frac{[(\rho \varphi)^{n+1} - (\rho \varphi)^n] V}{\Delta t} \quad \text{Equation 3-43}$$

where  $n$  and  $n+1$  denote the current and subsequent time steps respectively.

The momentum equations are solved across the mesh for each time step, and at the end of the time step, the impeller region slides past that of the bulk region. For this to be possible, the interface between the two regions must be rotationally symmetrical and non-conformal. At the end of each

time step, the non-conformal interfaces are updated to reflect the new positions of the two zones relative to one another.

In order to calculate the flow across this ever-changing interface, an interior zone is created between the interface zones on either side of the interface as shown in Figure 3.6. Here, the interface zones are composed of faces A-B and B-C on one side and D-E and E-F on the other. The intersection of these zones produces faces a-d, d-b, b-e, e-c and c-f which are then grouped to form an interior where the cell zones overlap. Where cell zones do not overlap, the remaining faces are paired to produce a periodic zone. Hence flow into cell IV is calculated using faces d-b and b-e, thereby using information from cell I and III.

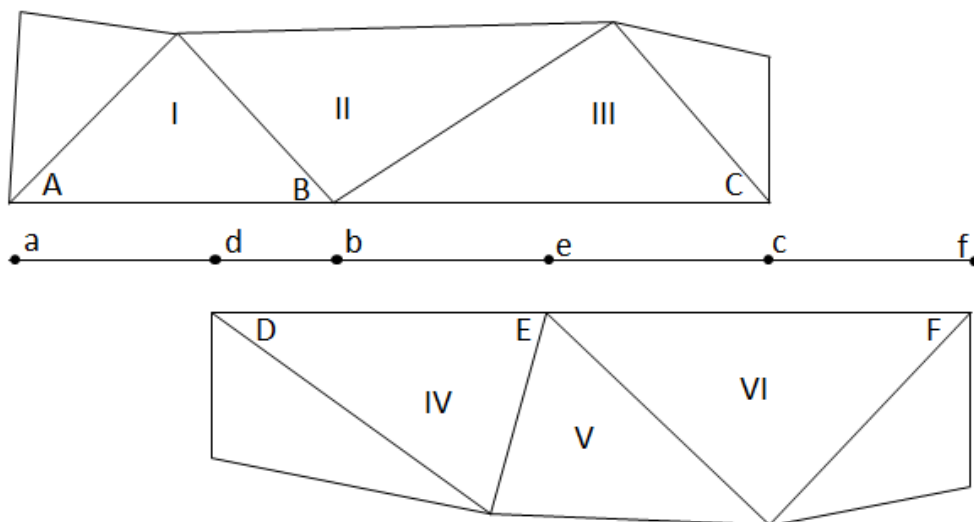


**Figure 3.7 – Sliding mesh across a two-dimensional grid interface, reproduced from ANSYS-Fluent (2012)**

This method allows the model to predict unsteady flows as they occur. In the case of a mixing vessel, this is beneficial if there is strong rotor-baffle interaction which is likely to have an important effect on the overall flow patterns developed. However, by running a transient simulation instead of a steady-state simulation, the computational expense of the SM method is higher than that of the MRF method.

### 3.2.5 Modelling sludge rheology

A fluid is said to be Newtonian if the shear stress arising from its flow is proportional to the shear strain rate applied to make it flow. As such, an incompressible Newtonian fluid can be described by the equation:

$$\tau = \mu \frac{du}{dy} \quad \text{Equation 3-44}$$

where  $\tau$  is shear stress and  $\frac{du}{dy}$  is the rate of strain.

Non-Newtonian fluids are those fluids that do not follow this linear relationship between shear stress and strain rate as shown in Figure 3.8. Non-Newtonian fluids include shear-thinning fluids, for which apparent viscosity decreases with increased stress, shear-thickening fluids for which apparent viscosity increases with increased stress, Bingham plastics, which have a linear stress-strain relationship but require the application of a yield stress before they will flow, and time-dependent thixotropic fluids, for which apparent viscosity decreases with the duration of stress.

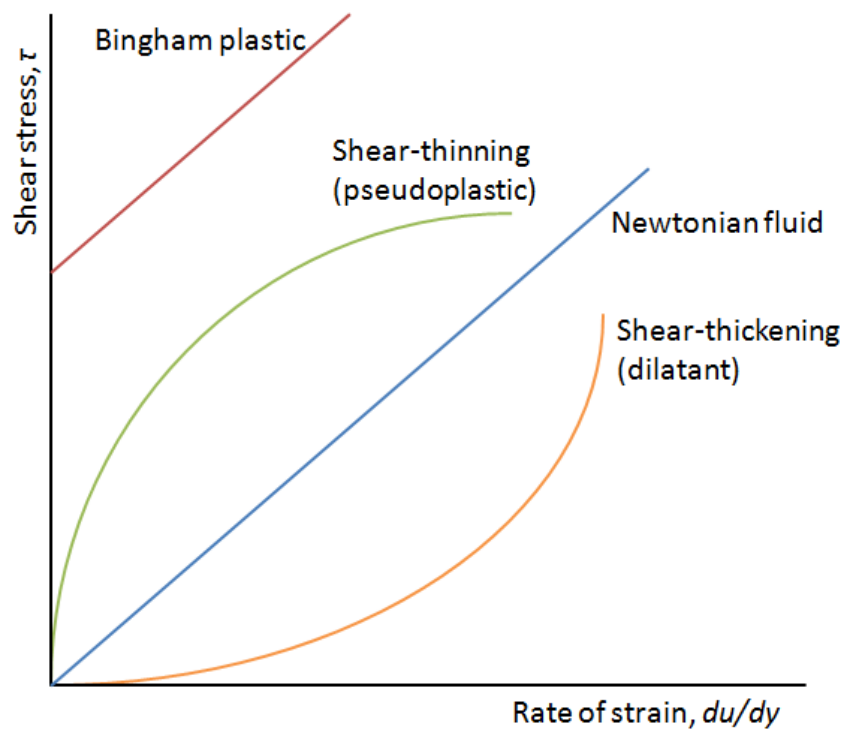


Figure 3.8 – Stress-strain curves for Newtonian and non-Newtonian fluids

Sewage sludge behaves as a non-Newtonian fluid that frequently exhibits a yield stress (Forster, 2002). The effects of sludge treatment processes and sludge properties on its rheology are complex and have been the subject of many studies.

Spinosa and Lotito (2003) determined that thin sludges behave like Newtonian fluids, whilst more concentrated sludges are non-Newtonian in their behaviour. Malczewska (2009) agreed that below a critical solids concentration, in the range of 0.58-2.41 % solids, sludge behaves as a Newtonian fluid. Above this critical concentration, behaviour becomes non-Newtonian and as solids concentration increases, yield stress and rigidity coefficient also increase.

Forster (2002) considered several sewage sludges which exhibited a yield stress that varied with both solids concentration and treatment type. Digested sludge had a yield stress an order of magnitude lower than activated sludge at the same solids concentration. Guibaud et al. (2004) similarly showed that the viscosity of sludge decreased when it underwent anaerobic digestion and that viscosity and shear stress were exponentially related to solids concentration. The sample origin was also deemed to be important in determining the rheological properties of the sludge. These findings were corroborated by Tixier et al. (2003). Moeller and Torres (1997) modelled primary and secondary sludges that had been digested aerobically and anaerobically and, likewise, were able to demonstrate that the sludge exhibited a dramatic change in rheological properties due to anaerobic digestion, with the apparent viscosity decreasing after digestion. Tixier et al. (2003) also demonstrated that viscosity was sensitive to changes in floc structure, a result that was replicated by Pevere et al. (2006, 2009).

Several standard non-Newtonian fluid models have been used to successfully describe the rheological properties of sewage sludge including a simple power law (also known as Ostwald-de Waele) (Moeller and Torres, 1997, Pollice et al., 2007, Hasar et al., 2004), Bingham (Guibaud et al., 2004, Pevere et al., 2007), Herschel-Bulkley (Mori et al., 2008, Yang et al., 2009) and Casson (Yang et

al., 2009) models. The equations for these are laid out below and commercial CFD software offers the ability to model the rheology of a fluid using these equations. Monteiro (1997) concluded that the best models were those that incorporate a yield stress such as Herschel-Bulkley and Bingham.

**Simple power law  
(Ostwald-de Waele):**

$$\tau = k \left( \frac{du}{dy} \right)^n$$

Equation 3-45

**Bingham:**

$$\tau = \tau_0 + \eta \left( \frac{du}{dy} \right)$$

Equation 3-46

**Herschel-Bulkley:**

$$\tau = \tau_0 + k \left( \frac{du}{dy} \right)^n$$

Equation 3-47

**Casson:**

$$\tau^{1/2} = \tau_0^{1/2} + k \left( \frac{du}{dy} \right)^{1/2}$$

Equation 3-48

where  $k$  is flow consistency index,  $n$  is flow behaviour index,  $\tau_0$  is yield stress and  $\eta_0$  is plastic viscosity.

Baudez et al. (2004) represented steady-state behaviour of pasty sewage sludges using a Herschel-Bulkley model and noted that for the same material, different models of rheological behaviour could be applied based on the range of data considered. Hence, it was concluded that any rheological model is only valid in the range over which it was determined and as such, care should be taken when selecting the appropriate rheological model for application within a CFD simulation.

### 3.2.6 Discretisation

Discretisation is the approximation of the governing equations to a set of linear algebraic equations that the CFD software can solve iteratively. One of the most common discretisation methods is the finite volume method to discretise the conservation form of the governing equations over discrete control volumes. The finite-volume method is popular in commercial CFD software as it rigorously

enforces conservation, it is flexible in terms of geometry and its ability to cope with a range of fluid phenomena, and it is directly relatable to physical quantities, such as mass flux.

### **3.2.7 Mesh generation**

The discretised governing equations are solved over a net of points across the fluid flow, which are selected by creating a mesh over the domain. The number of cells created in the mesh has an effect on the accuracy of the solution and the computational power required to reach that solution, with an increased number of cells increasing both the accuracy and the computational cost. As such, a balance must be reached between computational cost and accuracy. For this reason, generated CFD meshes often have a higher concentration of smaller cells around regions of high velocity or pressure gradients, such as on surfaces where there is a need to resolve the boundary layer, and a lower concentration of larger cells in regions which experience smaller gradients. Meshes can be structured or unstructured. In a structured mesh, every cell away from the wall has the same number of neighbouring cells. Structured meshes often require fewer cells than unstructured meshes which reduces the computational cost of simulations. Cells in a mesh can be tetrahedral or hexahedral. Hexahedral cells tend to provide greater accuracy as they can be better aligned to the flow whilst tetrahedral cells are useful for creating meshes around complex geometries.

### **3.2.8 Results of previous work**

Due to the highly variable nature of sludge and the difficulty of visualising flow patterns in an opaque medium, CFD models have long been seen as an alternative to laboratory-based experiments to simulate flow patterns in a number of different sludge mixing tanks, including anaerobic digesters. This literature is split into full-scale, pilot-scale and lab-scale models, and reviewed here.

#### **3.2.8.1 Full-scale models**

The flow patterns in a full-scale digester can be studied experimentally by the introduction of a tracer fluid at the inlet and its detection at the outlet. The resultant RTD curve describes how much time

each packet of the fluid spends in the digester. These experiments can be costly and only give a 'black box' representation of the flow through the digester. As such, CFD offers a more cost-efficient alternative.

Meroney and Colorado (2009) considered the flow of a tracer injection over time, through four full-scale cylindrical digesters of different volumes mixed by pumped recirculation and with different draft tube configurations. No-slip conditions were applied on all walls, inlets had a specified flow rate and outlets were treated as mass flow boundaries. No mention is made of the boundary condition applied at the liquid free surface. The pumps in the draft tubes were modelled as fan areas with a pressure increase of approximately 6500 Pa, tailored to give the desired draft tube flow rate. The sludge was assumed to have the same rheological properties as water and the RANS equations were closed with a standard  $k-\varepsilon$  turbulence model. They demonstrated that all four of the digesters modelled displayed no evidence of short-circuiting, dead volumes, plug flow behaviour or partial mixing, despite the difference in size and inlet/outlet arrangements.

The results of Meroney and Colorado (2009) are hampered by their selection of the standard  $k-\varepsilon$  turbulence model, which is known to give poor predictions of rotating flows (Wilcox, 1998); such flows are demonstrated to be present in the digesters modelled. Furthermore, the results demonstrate that fluid density can have a strong influence on the mixing patterns in a digester and yet the sludge is assumed to have the same density and rheological properties as water; based on the well-documented non-Newtonian properties of sludge (Forster, 2002), this is a poor assumption. Also of concern is the lack of validation. Whilst a model is validated against the experimental work of Cholette and Cloutier (1959), the model bears little relation to the digester models studied and makes use of a different geometry and a different turbulence model, the realisable  $k-\varepsilon$  model, which is known to give improved predictions of rotating flows when compared to the standard  $k-\varepsilon$  model (Wilcox, 1998). The model validation is further hindered by the unknown outlet placement and

mixer characteristics of the experimental vessel. As such, the results and conclusions of Meroney and Colorado (2009) have questionable validity.

Wu (2010b) studied the effect of mixing Newtonian (water) and non-Newtonian (sludge) fluids in a full-scale (volume = 4888 m<sup>3</sup>) egg-shaped digester with mechanical draft tube mixing. He made use of the MRF approach to model the impeller motion within the draft tube and a realisable  $k-\epsilon$  turbulence model to close the RANS equations. The sludge rheology was modelled using a simple power law and no-slip conditions were applied on all walls, with the liquid surface modelled as a symmetry plane. The convergence criteria for the model were set as residuals of  $10^{-3}$ , two orders of magnitude higher than recommended by best practice guidelines (ERCOFTAC, 2000). As such, the results of these simulations may be only partially converged, thereby introducing inaccuracies. The results of simulations at a range of mixing speeds and with sludges of varying solids concentrations demonstrated that mixing intensity, characterised by zones of low ( $<0.05$  m/s), medium ( $0.05 < v < 1$  m/s) and high ( $> 1$  m/s) velocities, increased with increased impeller rotational speed and decreased with increased sludge viscosity. At high viscosity (0.25-2.93 Pa.s), mixing was considered to be poor with up to 87 % of the digester experiencing velocities of less than 0.05 m/s. Finally, mechanical draft tube mixing was compared to external pumped circulation by calculating the power necessary to achieve the same average sludge velocity. In this way, mechanical draft tube mixing was shown to be 43.8-49.7 % more efficient in terms of power consumption depending on sludge viscosity.

The model was validated using water. Power number and flow number were calculated as shown below and were compared to full-scale measurements undertaken at the San Mateo Wastewater Treatment Facility in Arizona and to lab specifications for the draft tube made at Philadelphia Mixing Solutions.

$$N_p = \frac{P}{\rho N^3 D^5} \quad \text{Equation 3-49}$$

$$N_Q = \frac{Q}{ND^3} \quad \text{Equation 3-50}$$

where  $N_p$  is power number in a stirred vessel,  $P$  is power delivered to the fluid by the impeller,  $N$  is rotational speed,  $D$  is impeller diameter,  $N_Q$  is flow number in a stirred vessel and  $Q$  is flow rate through the draft tube.

The flow number of the impeller was predicted to be within 3 % of both the field tests and the lab specifications, suggesting that volumetric flow rate through the draft tube was correctly predicted. However, this provides no indication of the accuracy of the flow patterns generated in the bulk of the digester, particularly when considering the mixing of a non-Newtonian sludge. The power number showed an error of 38.2 % and 42.4 % when compared to full-scale measurements and lab specifications respectively. This error was attributed to numerical errors resulting from the simulated power and measurement inaccuracies arising from the experiments. The use of a RANS model, which has known limitations in predicting boundary layer development, is likely be a significant source of the error based on the development of the flow within the draft tube. No analysis of the wall roughness in the tube or its possible effects on the results is given. The mesh quality was similarly stated as affecting the accuracy of the simulation. Despite this, there is no mention of the number of cells used for the simulation and there is no evidence of grid independence tests being performed.

Terashima et al. (2009) considered the mixing of non-Newtonian sludge in a full-scale digester (volume = 1100 m<sup>3</sup>) with mechanical draft tube mixing. The rheology of the sludge was described using a power law for which the coefficients were determined experimentally. No-slip conditions were applied at the wall and a free surface condition was applied at the liquid surface. The impeller in the draft tube was modelled as an applied force on the sludge. This introduces an element of

error as the force has to be selected through trial and error until the correct mixing rate is achieved. No mesh density test is reported so it is unclear as to whether the results of the simulation are mesh-independent. Given that the mesh had only 10,000 cells, a relatively small number for a full-scale digester model when compared to other models in the literature, it seems unlikely that mesh independence was achieved. The simulation also makes use of a laminar flow model, which is an unrealistic assumption for mixing digested sludge.

Despite these limitations, the transient simulations of tracer mixing have good agreement with an experimental tracer curve at a sludge concentration of  $63 \text{ kg/m}^3$  and at a mixing rate of  $19 \text{ day}^{-1}$ . An indication of the level of mixing in the digester is calculated and called the uniformity index, a ratio of the number of the total cells in the mesh that contain tracer at any given time. This demonstrates that an increased rate of mixing leads to a more uniform concentration of tracer throughout the digester being achieved more quickly. It is noted that the lower half of the digester is the first to achieve uniform tracer concentration due to the effects of the outflow at the base of the draft tube. A comparison of the uniformity index across simulations with different sludge rheology shows that uniformity within the digester is achieved more quickly when mixing less viscous sludges rather than more viscous sludges.

Craig et al. (2013) investigated the effects of changing sludge rheology on impeller draft tube mixing in a full-scale (volume =  $1250 \text{ m}^3$ ) digester. The movement of the impeller was modelled using MRF, an SST  $k-\omega$  turbulence model was used and no-slip conditions were applied at the wall whilst a free-slip condition was applied at the liquid free surface. The assumption that the liquid free surface is flat was tested by running a two-dimensional volume of fluid (VOF) model to assess the level of impact the jet of fluid from the draft tube had on the surface 300 mm above. They demonstrated that whilst the surface profile was not in fact flat, if the steady-state profile of the surface was used in place of a flat surface in the three-dimensional model, it gave highly unusual flow patterns which

were not realistic and did not represent real-world flow physics as the fluid at the surface acted more like a jet impinging on a solid surface. The use of a transient 3D VOF simulation was considered too computationally expensive to more accurately predict the flow patterns and as such, the flat free surface was assumed to be a preferable assumption to the steady-state surface profile predicted by VOF.

The non-Newtonian sludge properties were modelled using a Hershel-Bulkley model with different coefficients to account for the different properties of raw and digested sludge. The model was also run with water in order to demonstrate the importance of correctly modelling sludge's non-Newtonian properties. The results of this comparison showed that whilst the measures of mixing used for validation by many researchers, such as impeller torque, were within 10 % of each other for water and sludge, the flow patterns generated were significantly different, with water experiencing higher velocities throughout the digester. This highlights the issues with single-point validation, as used by Wu (2010b), and with the poor selection of sludge rheology models, as seen in Meroney and Colorado (2009).

Convergence was considered to have been achieved when residuals fell below  $10^{-3}$ , two orders of magnitude higher than recommended by best practice guidelines (ERCOFTAC, 2000). As such, the results of the simulations may not have reached convergence. This is of particular concern when it is noted that the results of the simulations are not symmetrical around the centre of the digester, despite the digester geometry and the draft tube geometry both being rotationally symmetrical. This is further indication of a lack of convergence.

The results of Craig et al. (2013) show that when mixing the more viscous raw sludge, there are much larger dead zones at the base of the digester than for the less viscous digested sludge. Furthermore, they show that the less viscous sludge induces higher strain rate and therefore a higher associated shear stress than the more viscous sludge. A lack of comparison of the results from the models with

experimental data means that their validity is questionable, particularly given the issues with the non-symmetrical flow patterns and the convergence criteria mentioned above.

The literature making use of CFD simulations to model full-scale digesters demonstrates the difficulty of adequately validating a model at full-scale, due to the lack of experimental data available. The importance of running mesh independence tests at full-scale is often overlooked as fine meshes across large domains are time-consuming and computationally expensive to run. Similarly, poor assumptions such as laminar flow, Newtonian sludge rheology and inadequate convergence criteria may reduce the computational cost of these large simulations but have adverse effects on the accuracy of the results.

### 3.2.8.2 Pilot-scale models

There are very few papers which relate to CFD models of pilot-scale digesters and they are dominated by mechanical mixing.

Wu (2011) studied the effects of six turbulence models (standard  $k-\varepsilon$ , realisable  $k-\varepsilon$ , RNG  $k-\varepsilon$ , standard  $k-\omega$ , SST  $k-\omega$ , RSM) when carrying out CFD simulations of a 572-litre, mechanically-mixed, flat-bottomed digester equipped with four baffles and a PBT impeller (PMSL 3LS39). The simulations were initialised using a steady-state MRF model and were then changed to a transient SM model. No discretisation scheme is specified for the pressure term other than that it is a "standard scheme". For all other terms, first-order discretisation schemes were used. This will have the effect of mean vortices not being properly resolved by the model, increasing numerical dissipation and detrimentally affecting the accuracy of the predicted flow. This is observed when second-order schemes are later applied and the predicted flow is improved. A symmetry condition was applied at the liquid free surface but no indication of the boundary condition applied at the wall is given, though a no-slip condition is likely. The non-Newtonian sludge was modelled using a simple power law.

As with Wu (2010b), the simulations were compared to power and flow numbers calculated from lab specifications for the impeller. As previously stated, this technique provides no indication of the accuracy of the flow physics generated in the bulk of the digester and can lead to erroneously validated simulations (Craig et al., 2013). The results of this work demonstrated that for water and 2.5 % TS sludge, the standard  $k-\omega$  model was best for predicting flow number, whilst at higher solids concentrations (5.4 %, 7.4 %, 9.1 % and 12.1 % TS), the realisable  $k-\varepsilon$  model gives the most accurate prediction of flow number. It is further noted that in all cases, the RSM model was computationally more expensive to run when compared to the two-equation models. As TS increases, the error in the predicted flow number increases for all of the turbulence models. This may be a consequence of the increased mixing speeds used for the higher solid concentration sludge in order to ensure that the Reynolds number was always in the turbulent range or may indicate an increased level of error within the non-Newtonian sludge model at higher solids concentrations. The result is not commented on in the paper.

The CFD model in Wu (2011) is validated against the published results of experimental work carried out by Hoffman et al. (2008) in an unbaffled 4.3 litre, conical-based digester using a Lightnin A310 impeller and a 5.5 % TS sludge. The lack of geometrical similarity between the digesters and the impellers, and the differences in the rheology of the sludge in the simulated digester and that used for validation, means that the value of this validation exercise is highly questionable. This is particularly highlighted by a comparison of the azimuthally-averaged axial velocities which shows that simulated peak velocities are approximately a quarter of those recorded in the experimental work.

Wu (2012a) considers the mechanical mixing of high solids sludges in a pilot-scale digester (volume = 18.8 m<sup>3</sup>). The non-Newtonian fluid is modelled using a power law model and the flow is assumed to be laminar. This is an incorrect assumption as it is later demonstrated that the Reynolds

numbers calculated for the digester fall firmly in the transitional range. No-slip conditions are applied on the walls and the liquid free surface is modelled as a symmetry plane. The model is validated by plotting the power number against the Reynolds number for ribbon and anchor impellers and comparing the curves to those determined experimentally by Prajapati and Ein-Mozaffari (2009). There are differences in the impeller configuration between the CFD model and the experimental digester, and combined with the issues of using power number as a validation tool, as discussed earlier, the validation is of limited value.

Wu (2012a) considers the mixing of four types of manure at three TS concentrations greater than 12.1 % TS with six impellers (single-blade ribbon, flat-bottom anchor, dual-blade ribbon, arc-bottom anchor, curtain-type, three counterflow (CF-2) impellers), two modified high solidity (MHS 3/39°) impellers, two pitched blade turbines (PBT 4/45°) and at four mixing speeds (range from 4-18 rpm depending on impeller type). The mixing time required for a tracer to achieve a concentration with variance of less than 5 % across the digester ( $t_{95}$ ) and the mixing energy level (MEL) are calculated for each impeller. In order to achieve the same average velocity in the flow field ( $v = 0.22$  m/s), the three CF-2 impellers require the lowest mixing energy level whilst the two MHS 3/39° impellers have the shortest  $t_{95}$ . By considering the relationship between  $t_{95}$ , impeller speed and MEL, it is concluded that the two MHS 3/39° impellers are the preferred mixing method for sludge with 12.1 % TS.

It can be seen from the limited pilot-scale literature that pilot-scale models suffer from the same limitations of good quality validation noted for full-scale digesters. Additionally, the importance of selecting an appropriate turbulence model to close the RANS equations is demonstrated.

### 3.2.8.3 Lab-scale models

Lab-scale models represent the true testing ground for simulation parameters, such as turbulence model selection, the effects of different sludge rheology and the methods involved in modelling

mixing methods other than mechanical mixing. As such, there is significantly more literature available relating to lab-scale digester models than to full-scale or pilot-scale.

Wu and Chen (2008) were one of the first models to make use of a non-Newtonian power law fluid to model sludge rheological properties in an anaerobic digester. They used the standard  $k-\epsilon$  turbulence model and validated the flow of non-Newtonian fluids in a pipe (diameter = 0.0254 m) against experimental determined axial velocities from Pinho and Whitelaw (1990) who tested carboxymethyl cellulose (CMC) solutions of 0.1, 0.2, 0.3 and 0.4 %wt concentration. The model predicts axial velocities well, though it does underestimate the velocities in the near-wall region. This may be an issue with the mesh density in the wall region being insufficiently fine to accurately capture the flow there. This cannot be verified as no mesh independence tests are carried out and no indication of the mesh density is given.

Having ascertained that the CFD model is capable of predicting non-Newtonian pipe flow accurately, at least in the bulk flow, a cylindrical lab-scale digester (volume = 4 litres) is modelled with both water and 2.5 % TS sludge. The digester has an inflow pipe in the centre of the base and an outflow sidearm at the top of the digester. It was shown that different flow patterns arise for the two fluids, though the flow speeds are similar. This demonstrates the importance of accurately modelling sludge rheology.

Bridgeman (2012) considered the effects of mixing speed, sludge rheology and turbulence model on the results of steady-state CFD simulations of a 6-litre cylindrical vessel equipped with two 6-blade impellers. The model made use of no-slip conditions at the walls and a free slip plane at the liquid surface; sludge rheology was modelled using a power law. Five turbulence models (standard  $k-\epsilon$ , RNG  $k-\epsilon$ , realisable  $k-\epsilon$ , standard  $k-\omega$  and RSM) were tested by comparing the simulated power consumption integrated over the vessel when mixing 2.5 % TS sludge at 100 rpm, against the power input determined experimentally from torque measurements. This demonstrated that the RSM

model best predicted the power consumption, followed by the realisable  $k$ - $\epsilon$  model, both of which were accurate to within 20 %. The standard  $k$ - $\epsilon$  model was the least able to predict power consumption, with an error of 221 %. As such, the RSM model was used for further simulations. However, this validation against the power consumption provides no indication of the accuracy of the flow physics generated in the bulk of the digester, as discussed previously in relation to the papers of Wu (2010b) and Craig et al. (2013).

The flow was modelled at 100 rpm to assess the impact of total solids concentration (0 %, 2.5 %, 5.4 %, 7.5 %, 9.1 %, 12.1 % TS) on the mean velocity and it was demonstrated that mean velocity fell as solids content increased, in agreement with the full-scale results of Wu (2010b). This was explained by the increased solids content reducing the ability of the particles within the sludge to move and be mixed. The reduction in mean velocity was accompanied by an increase in the volume of dead zone (defined as volumes experiencing a mean velocity of less than 5 % of the maximum velocity magnitude), which could be modelled as a function of TS using a second order polynomial. Increasing mixing speed (30 rpm, 50 rpm, 100 rpm, 200 rpm) for a constant TS concentration of 5.4 % was shown to reduce dead zone volume in the digester; dead zone volume could be modelled as a function of mixing speed using a power law. The average local velocity gradient in the digester was found to be between 4 and 10  $\text{s}^{-1}$  at 100 rpm, depending on the TS of the sludge. This is an order of magnitude lower than average vessel velocity gradients suggested for effective anaerobic digestion in the existing literature (Tchobanoglous and Burton, 1991). This may be a consequence of the difference in the calculation methods used, with Bridgeman (2012) calculating the average local velocity gradient and Tchobanoglous and Burton (1991) potentially calculating the overall average velocity gradient from experimental work, though it is not stated what method is used.

Finally, Bridgeman (2012) considered the effect of mixing speed on gas production experimentally. This demonstrated that for 2.5 % TS sludge, increasing mixing speed from no mixing to 100 rpm had no effect on the gas production of the digester.

Wu (2010c) considered the ability of 12 turbulence models including six low Reynolds number models (standard  $k-\varepsilon$ , RNG  $k-\varepsilon$ , realisable  $k-\varepsilon$ , Abid low- $Re$   $k-\varepsilon$ , Lam-Bremhorst low- $Re$   $k-\varepsilon$ , Launder-Sharma low- $Re$   $k-\varepsilon$ , Yang-Shih low- $Re$   $k-\varepsilon$ , Abe-Kondoh-Nagano low- $Re$   $k-\varepsilon$ , Chang-Hsieh-Chen low- $Re$   $k-\varepsilon$ , standard  $k-\omega$ , SST  $k-\omega$  and RSM) to predict the frictional pressure drop of single-phase non-Newtonian fluids with TS concentrations of 2.5 %, 5.4 % and 7.5 % along a pipe (diameter = 0.02 m, length = 0.4 m). In all cases, the flow velocity was set to ensure that the Reynolds number was greater than 2000. As such, flow velocities of 2, 2, 3, 4, 5 and 6 m/s were set for TS = 0 %, 2.4 %, 5.4 %, 7.5 %, 9.1 % and 12.1 % respectively, giving a range of Reynolds numbers from 6300 to 2470. The sludge was modelled using a non-Newtonian power law.

Low Reynolds number turbulence models are an adapted form of the standard  $k-\varepsilon$  model, designed to improve the prediction of flow physics in boundary layers which are not fully turbulent. This may be applicable when the flow in a pipe is not sufficiently long for the growth of a fully-developed boundary layer. Due to the short length,  $L$ , of the modelled pipe in relation to its diameter,  $D$  ( $L < 60 D$ ), the boundary layer is unlikely to be fully-developed (Douglas et al., 2005) and as such the low Reynolds number models are applicable. The models were validated against the predicted pressure drop over the pipe length based on a number of empirical correlations for turbulent flow conditions. This validation gives no indication of the accuracy of the predicted flow patterns in the pipe but also assume a fully-developed turbulent flow. As such, high errors were found, regardless of turbulence model used.

The low Reynolds number models require a significantly finer near-wall mesh in order to capture the boundary layer (Versteeg and Malalasekera, 2007). For this reason, the Chang-Hsieh-Chen low

Reynolds number turbulence model using a mesh of 52,800 cells was compared to the standard  $k-\omega$  model using a mesh of 18,000 cells. The predicted velocities were identical for the centreline of the pipe and were within 10 % even within the boundary layer. The finer mesh required by the low Reynolds number models increased the computational expense for these simulations. As such, the standard  $k-\omega$  model was used in further models. Though no mesh independence test was carried out and the results are not validated, this approach was used to model a pilot-scale digester (volume = 792 m<sup>3</sup>) and the distribution of velocity gradients studied. This showed that 84.5 % of the digester experienced velocity gradients of less than 10 s<sup>-1</sup>, 7.9 % experienced velocity gradients of 10 – 70 s<sup>-1</sup> and 7.6 % velocity gradients of over 70 s<sup>-1</sup>. The average local velocity gradient was calculated to be 3.44 s<sup>-1</sup>, significantly lower than the overall average velocity gradient, calculated from the power input, which was 70.8 s<sup>-1</sup>. This finding is similar to that of Bridgeman (2012).

Wu (2012c) modelled a lab-scale (volume = 4.3 litres) digester equipped with mechanical mixing using both LES and RANS models. The sludge was modelled using a power law fluid. Due to the computational expense of LES simulations, only a third of the digester was modelled and no mesh-independence test was carried out. Given that the mesh has only 190,000 cells, it is unlikely that the mesh was sufficiently fine to suitably capture all aspects of the flow using LES. The use of an overly coarse mesh with LES gives high sub-grid viscosity to kinematic viscosity ratios that are unphysical. This would detrimentally affect the physicality of the simulated results. Furthermore, no indication of the  $y^+$  values is given; a low  $y^+$  is required for a mesh to be suitable for wall resolution within LES.

The LES model was validated against experimental results published by Hoffman et al. (2008). There are errors of up to 75 % in the axial velocities reported and, whilst Wu expresses concern about the physicality of the experimental results, no further attempt is made to validate the LES model. As such, the LES model is essentially unvalidated. The RANS model is validated against experimental results for mixing water reported by Bugay et al. (2002) using an RSM turbulence model and the MRF

approach. There is reasonable correlation between these results though the validation does not consider the effect of the non-Newtonian sludge model.

The flow number and power number are calculated for each of the models and compared to lab specifications. The issues with this validation method have been discussed previously in Section 3.2.8.1. These results demonstrate that LES gives slightly better predicted flow and power numbers than RANS models, though the lack of a mesh-independence test or any real validation mean that these results are questionable. The results further show that using the SM approach generally improves the flow field prediction when compared to the MRF approach for RANS simulations. This is to be expected when the intrinsically unsteady interaction between the impeller and the walls of the digester, especially when baffles are present, is considered.

Yu et al. (2011) considered the mechanical mixing of high solids sludge (>10 % TS) in lab-scale digesters (volume = 4.3 litres) mixed with an A310 impeller and a helical ribbon impeller, in the experimental work of Hoffman et al. (2008) and Karim et al. (2005b), respectively. The model uses an MRF approach to model the rotation of the impeller and a power law to describe the non-Newtonian sludge. A no-slip condition is applied at the walls but no mention is made of the boundary condition at the liquid free surface. The model uses a standard  $k$ - $\epsilon$  turbulence model when Reynolds numbers are greater than 1000, an unspecified low Reynolds  $k$ - $\epsilon$  turbulence model between Reynolds numbers of 10 and 1000, and a laminar model when Re is less than 10. Whilst this initially appears to be logical, it is expensive to implement and the turbulence models selected are inappropriate for modelling turbulence in digester mixing, as shown by Bridgeman (2012) and Wu (2010c).

The model is validated against axial flow velocities using results for the A310 impeller mixing water, for which there is good agreement, though this gives no indication of the applicability of the non-Newtonian fluid model. A comparison of the flow patterns generated by the A310 impeller when

mixing 10 % TS sludge and sludge of less than 5 % TS, modelled as Newtonian, demonstrates that at 10 % TS, 95 % of the digester volume acts as dead zone compared to only 5 % when mixing Newtonian sludge. This highlights the importance of accurately modelling the non-Newtonian properties of sludge, particularly as TS increases, in agreement with Craig et al. (2013), Wu and Chen (2008) and Bridgeman (2012). Due to the challenges of mixing high solids sludge using the A310 impeller, sludges with TS concentrations of 10 and 20 % were modelled with helical ribbon impeller mixing. The flow patterns generated at both TS concentrations were similar and approximately 5 % of the digester was considered to be dead zone. Increasing the mixing speed gave the same flow patterns but with increased flow velocities. As such, it was concluded that for sludge with a high TS, ribbon impellers provide improved digester mixing.

Vesvikar and Al-Dahhan (2005) simulated confined gas mixing of sludge in a lab-scale digester (volume = 7.2 litres) using a steady-state two-phase CFD model. The gas phase was modelled as air and the liquid phase was modelled as water, thereby neglecting the non-Newtonian properties of the sludge. Given that the sludge used in the experimental work had a solids content of 5 %, it is highly unlikely that it behaved as a Newtonian fluid (Forster, 2002), limiting the usefulness of the CFD results. The gas phase inlet was set as a mass flow inlet to represent a single-point sparger at the base of the draft tube. No-slip conditions were applied on the vessel walls and a free-slip condition was set at the liquid free surface. Above the liquid free surface, an outlet was set so that the gas phase could escape from the top of the digester. A first-order upwind discretisation scheme was used for the convection terms. This prevents the effect of mean vortices from being properly resolved, increasing numerical dissipation and detrimentally affecting the prediction of flow patterns in the digester. For the liquid, a standard  $k-\epsilon$  turbulence model is used, whilst for the gas phase, a zero-equation mixing length model is used. It has been seen from other papers discussed in this section (Bridgeman, 2012, Wu, 2010a) that the standard  $k-\epsilon$  is poorly equipped to predict flow under mixed conditions in anaerobic digesters. The zero-equation mixing length model is an even simpler

model which links a single length scale with a single velocity scale and is unlikely to produce accurate results (ANSYS-Fluent, 2012). These issues with the model are highlighted when it was validated against experimental CARPT data. Whilst the simulated and experimental results demonstrate qualitatively similar flow patterns, dead zones and circulation loops, the axial velocity of the fluid is less well-predicted with errors of up to 20 %.

By adapting the model to test the effects of different air flow rates, the results of Vesvikar and Al-Dahhan (2005) show that increasing gas flow rate does not affect the flow outside of the draft tube; this is likely to be partially a consequence of using a single-point sparger and partially due to the selection of a Newtonian fluid model and inappropriate turbulence models. Increasing the diameter of the draft tube was shown to reduce the velocity inside the draft tube but increase the velocity in the reduced annular cross-section of the digester. This had the effect of reducing the volume of dead zone in the digester. Changing the height of the draft tube and its clearance from the base of the digester had no effect on the overall flow patterns or the volume of dead zone. Finally, the flat base of the digester was compared to a conical base, which was shown to reduce the volume of dead zone near to the base of the digester, though not to the same extent as increasing the draft tube diameter.

Wu (2010a) used an Eulerian multiphase simulation to model two-phase gas mixing in a lab-scale digester. In this model, the liquid phase is first treated as water and then as sludge, with the rheological properties modelled with a non-Newtonian power law. The gas phase is assumed to consist of spherical bubbles of uniform diameter which do not coalesce or break up. Whilst this assumption may be accurate for highly viscous sludges, it is highly improbable when mixing less viscous sludges or water. Three high Reynolds number  $k-\epsilon$  turbulence models are tested alongside six low number Reynolds  $k-\epsilon$  turbulence models, two  $k-\omega$  models and RSM, for flow in a pipe (diameter = 0.02 m, length = 0.4 m). The model is hampered by the choice of convergence criteria as

residuals that are less than  $10^{-3}$ , which, as has been mentioned previously, is not low enough to ensure fully-converged solutions. Additionally, first-order scheme are used for convection terms, which increases numerical dissipation in the simulation and can detrimentally affect the accuracy of the predicted flow patterns.

The models are used to predict the pressure drop over a pipe, and compared to the pressure drop predicted by empirical correlations as in Wu (2010c). The issues with this validation method are discussed in relation to that paper. A comparison of the effects on predicted pressure drop of different bubble diameter, liquid flow rate, liquid viscosity (determined by % TS) and turbulence model is carried out. This shows that as bubble size increases, the error in the predicted pressure drop also increases, with the CFD model under-predicting pressure drop. The low Reynolds number models, which make use of a finer mesh than the high Reynolds number models, show similar centreline velocities in the pipe, though differences of up to 10 % are predicted in the near-wall region, particularly with more viscous sludges. The accuracy of these near-wall velocities cannot be validated using the current validation technique, nor can it be fully attributed to either the turbulence model used or the differences in the mesh.

The SST  $k-\omega$  turbulence model is selected for modelling confined gas mixing in the lab-scale digester (volume = 7.14 litres) used in the experimental work of Karim et al. (2004). The CFD model generally shows good agreement with the experimentally measured axial velocities, except close to the liquid surface and in the centre of the digester, close to the draft tube where axial velocities are under-predicted by up to 50 %. Using this model, Wu (2010a) shows that the average velocity of the liquid phase falls as TS concentration increases and that as TS increases, the mean circulation loops in the sludge decrease in size leading to greater dead zone formation at the base of the vessel. By removing the draft tube to model unconfined gas mixing, it is shown that unconfined gas mixing results in a higher average liquid velocity than with confined gas mixing but this is due to significantly

higher liquid velocity in the region of the central gas jets, with low velocity elsewhere in the digester. As such, although the average velocity increases, the volume of dead zones also increases, particularly at high TS concentrations. Hence, it is concluded that confined gas mixing is preferable to unconfined gas mixing at TS = 5.4 %. Finally, confined gas mixing is compared to draft tube impeller mixing and sludge recirculation to crudely determine their relative efficiencies. For this, the confined gas mixing model is adapted to draft tube impeller mixing and to sludge recirculation, and the impeller speed and sludge recirculation velocity are adjusted until all three mixing mechanisms achieve similar flow patterns. The MEL for each of the three mixing mechanisms is calculated and used to show that mechanical mixing is more efficient than confined gas mixing, which in turn is more efficient than sludge recirculation.

It can be seen that the literature on CFD models of lab-scale digesters is still dominated by mechanically-mixed digesters, though some models of gas mixing and sludge recirculation have been built. Once again, the importance of good quality validation is clear and is a stumbling block in much of the published research. As is shown at larger scales, the modelling of sludge rheology is also vital to obtaining accurate and realistic results. Several authors have considered the selection of appropriate turbulence models for digester mixing and it is shown that the realisable  $k-\varepsilon$  model and the standard or SST  $k-\omega$  models all provide good results. The standard  $k-\varepsilon$  model gives large errors and more complex models such as RSM, low Reynolds  $k-\varepsilon$  models and LES do not provide significantly improved results over the realisable  $k-\varepsilon$  model and the standard or SST  $k-\omega$  models, but do increase the computational cost of the simulation, in part due to the finer meshes required.

#### **3.2.8.4 CFD models including biochemical reactions**

Wu et al. (2009) is one of the first papers to consider the integration of biochemical reactions into a CFD model. They use a CFD model to solve the mass, energy and species transport equations in order to predict gas production from a full-scale plug-flow anaerobic digester (volume = 1593 m<sup>3</sup>).

The model assumes no turbulence and no bulk flow in the digester due to the low flow rate in plug-flow digesters. This is clearly an unrealistic assumption and as such, no mixing takes place. The manure is modelled as a Newtonian fluid which, whilst a poor assumption, is less important due to the assumption that the flow in the model is stationary. The walls of the digester are adiabatic and the temperature of the sludge is kept constant in the digester before reaction occurs. The digestion process is modelled as a single-step reaction:



It is estimated that after reaction 80 % of the organic matter remains. The rate of reaction is modelled using an Arrhenius equation with a first-order BOD removal rate based on that calculated for an ideal plug-flow reactor. This is a vast oversimplification of a complex multistage process which is dependent on numerous reactions and an even greater number of physical, chemical and microbiological parameters. The mesh contains 31,500 cells and no mesh-independence test is carried out. Whilst it is highly likely that this number of cells would be too low to accurately predict flow patterns in the digester, the assumption that there is no flow taking place reduces the significance of this poor assumption. The results are compared to the experimentally measured gas production of the digester and are shown to be within 5 %. However, this single point cannot be considered as a full or proper validation of the model and as such the results are of questionable value. However, the model does show the feasibility of integrating a biochemical model, albeit a vastly oversimplified one, into a simplified CFD model.

Wu (2012b) used a two-stage simulation to link a biochemical model to a physical mixing model. The first stage of the simulation was a steady-state flow pattern calculation to determine the effects of mixing and heat transfer. The temperature and residence time in each cell were then fed to a transient biochemical model which predicted the methane generation over a 15 day period.

The biochemical reaction kinetics were based on five equations for hydrolysis, acidogenesis, propionate degrading acetogenesis, butyrate degrading acetogenesis, and methanogenesis, and the yield coefficients and rate constants were based on those in Angelidaki et al. (1993) and Keshtkar et al. (2001, 2003). The biochemical model was validated against the experimental results of Mackie and Bryant (1995) with good agreement, albeit in a tight pH range of 6.8–7.2. A second validation of the biochemical model against Borja et al. (1994) agreed less well, particularly at very short (5.2 days) and very long (25 and 50 days) HRT. This was attributed to the pH falling outside the range accounted for by the model and indicative of stable digestion (pH 6.8–7.2). As such, further simulations were carried out at an HRT of 15 days and the pH was limited to the range indicative of stable digestion.

The CFD model used was that of a mechanically-mixed egg-shaped digester as simulated in Wu (2010b) and issues with this model are discussed in Section 3.2.8.1. The model used impeller speeds of 400–750 rpm mixing 5 % TS sludge, modelled using a non-Newtonian power law. This model was validated against power and flow numbers, and a discussion of this validation method is found in Section 3.2.8.1. The CFD model demonstrated that the digester was well-mixed with pH and temperature uniform throughout the digester. As such, the methane yield from the digester corresponded to residence time in each cell. This implies that in an egg-shaped digester, mixing has no impact on gas production and hence the lowest mixing speed is preferable to improve the overall digester energy balance. In reality, this is an oversimplification as mixing can have an effect on the digestion process not just through its effect on temperature gradients in the digester, but also on concentration gradients, which in turn may impact on microbiological communities, and the effects of turbulence on microbiological communities.

In order to assess the effect of temperature on the biochemical model, an unheated plug-flow digester (volume = 19,952 m<sup>3</sup>) was modelled over the course of a year, during which solar radiation

had an effect on the temperature, which ranged between 15 and 19 °C. Despite several issues with the plug-flow CFD model, including the low mesh density (cells = 470,000), the lack of a mesh-independence test and the assumption of laminar flow, all of which would adversely affect the accuracy of the results, the model showed that methane yield and pH were linked to temperature and as such, methane production in the warm summer months was nearly double that of the cold winter months. Whilst this model is an oversimplification because of the small number of factors linking the physical model to the biochemical model, it is a useful starting point for demonstrating the feasibility of connecting the two in a multi-stage simulation.

### **3.2.8.5 Summary of existing literature**

It can be seen that the existing literature considering the use of CFD to model anaerobic digester mixing is dominated by mechanically-mixed tanks. Some models of confined gas mixing have been created, but models of unconfined mixing are difficult to find. Many of the mechanically-mixed vessels make use of draft tubes, although Wu (2012a) considers the mixing of high solids sludge with a range of impeller types. Many of the models are limited by erroneous assumptions of laminar flow or sludge modelled as a Newtonian fluid. Across the literature, it can be seen that an accurate prediction of the rheological properties of sludge has a huge effect on the accuracy of a CFD model, as do the accurate modelling of inlet and outlet pipes and other tank geometries. Furthermore, validation is a key step in ensuring that a model is realistic but is often difficult to achieve because of the challenges of flow visualisation in an opaque fluid and mixing system.

Some research has considered how to link biochemical models to physical mixing models but this is in its infancy due to the complexity of the digestion process, the very different time steps required in the two sections of an interlinked model and the high number of ways in which mixing may impact on digestion.

### 3.3 Review of previous research and knowledge gaps

This chapter has examined the science of fluid flow and its application in CFD. Fluid flow is governed by the Navier-Stokes equations, an expression of the conservation of mass and momentum. The importance of turbulence in nearly all natural flows is to be noted. This apparently chaotic movement of fluid leads to the dissipation of energy within a system from the largest scales of the vessel to the smallest scales, known as the Kolmogorov scales, through an energy cascade. It is at this lowest level that damage is likely to occur to micro-organisms. A great deal of the turbulent kinetic energy that is generated in a flow is generated in the boundary layer, the structure of which is discussed. An understanding of the flow patterns in mechanically mixed vessels is also included as it is these flow patterns that are generated by mixing and which in turn exist at the highest levels of the energy cascade. The velocity gradient is considered as a tool for determining the level of turbulence within a vessel. Whilst the average velocity gradient is considered to be flawed as it attempts to represent a complex flow field with a single number, local velocity gradients can be calculated for every part of a vessel with the help of CFD.

The general methodology for CFD is broken into seven stages: simplification of the case to be modelled, discretisation of the relevant equations, generation of a computational mesh, selection of boundary conditions, solution of the discretised equations across that mesh and validation and visualisation of the results. The adaptation of the Navier-Stokes equations to the RANS equations and the subsequent need for turbulence models to close the equation set is discussed. A number of two-equation models, along with the RSM are discussed in detail with the advantages and disadvantages of each model being addressed. These two-equation models invariably rely on the Boussinesq hypothesis. More complex closure models such as LES and the concept of DNS are also briefly considered. The MRF and SM methods for modelling mixing are compared and it is clear that whilst the MRF model may overlook certain aspects of the flow by providing a steady-state solution, it is computationally less expensive than the transient SM model. The importance of creating an

appropriate computational grid for solving the discretised equations is made apparent as an insufficiently fine mesh may fail to capture vital aspects of the flow, whilst an overly fine mesh will have a significant impact on the computational expense of the model. A range of mesh types can be used to find a balance between these two extremes.

Finally, a review of existing literature relating to CFD modelling of anaerobic digestion was undertaken. This demonstrated that, whilst the literature is dominated by mechanically-mixed digesters, these models are often limited by the simplifying assumption of laminar flow or Newtonian sludge characteristics. In the cases where models are not limited by these assumptions, mechanical mixing of anaerobic digesters has been shown to be accurately modelled with the help of the RSM turbulence model, although computationally less expensive results of similar quality can be reached with the standard  $k-\omega$  model at low solid concentrations or the realisable  $k-\varepsilon$  model at higher solid concentrations. Very little literature has attempted to link gas production to CFD results, but in those cases that do, it was shown that increased mixing has no benefit to the gas production of a digester.

## **CHAPTER 4      Aim and objectives**

The aim of this research is to identify mixing regimes and associated flow patterns that increase biological activity and hence biogas output, whilst minimising energy input, for lab-scale anaerobic sludge digesters.

In order to meet this aim, four objectives have been set. These are as follows:

1. Quantify the relationship between mixing speed and flow patterns in laboratory-scale mechanically-mixed digesters experimentally, using positron emission particle tracking (PEPT).
2. Develop a CFD model of the laboratory digesters to visualise flow patterns and quantify turbulence effects that may impact biogas yield. Quantify zones in a digester according to the level of turbulence experienced, e.g. dead zones versus actively mixed zones.
3. Quantify the relationship between biogas yield and mixing in laboratory-scale, mechanically-mixed digesters for a range of sludge characteristics (e.g. viscosity and solid content) and energy input characteristics (i.e. mixing speed).
4. Characterise microbiological communities present in laboratory-scale, mechanically-mixed digesters at different mixing speeds, with a focus on the prevalence of methanogens in order to establish relationships between microbiological community structure and experimentally determined environmental conditions (e.g. pH, volatile fatty acids (VFAs)) in the digester.

## CHAPTER 5      **Materials and Methods**

Within this chapter, the main methods and materials used throughout the research are presented.

The chapter is split into five sections:

1. **Experimental set-up and methods** details the set-up of the laboratory digester tests
2. **General analytical methods** details the methods used for general sludge characterisation
3. **Quantitative polymerase chain reaction** details the experimental methods and protocol followed for the identification and quantification of methanogenic populations in the laboratory digesters
4. **Particle image velocimetry (PIV)** details the set-up of PIV tests
5. **Positron emission particle tracking** details the set-up of PEPT tests

### **5.1 Experimental set-up and methods**

This section is sub-divided into two sections, the first dealing with the batch digestibility tests used in developing the synthetic sludge and the second concentrating on the semi-continuous laboratory-scale digester tests.

#### **5.1.1 Digestibility batch tests**

During the development of the synthetic sludge, digestibility batch tests were carried out with digested sludge from Kidderminster STW as the inoculant and a range of synthetic sludges used as the feed. In order to minimise differences in the biomass content of the inoculant, the digested sludge was sieved to remove large lumps of biomass before it was added to the serum bottles. 30 ml of inoculant sludge was added to 70 ml of each type of synthetic sludge and placed in a 120 ml serum bottle. Tests were carried out in triplicate for each sludge and for the control which used a feed of deionised water. The bottles were sealed with a butyl rubber septum and an aluminium crimp and

kept at a constant temperature of 35 °C. The tests ended when the biogas production subsided to the base level of the non-feed control, which took approximately 13 days.

#### **5.1.1.1 Biogas volume measurement**

Biogas accumulated in the 20 ml headspace of the bottles and the pressure of gas was measured using a manometer and then converted into a volume using the ideal gas equation:

$$PV=nRT \qquad \text{Equation 5-1}$$

where P is pressure, V is volume, n is number of moles, R is the Universal Gas Constant and T is temperature.

The final biogas volumes reported were based on standard temperature and pressure, 25 °C and 1 atmosphere (101325 N/m<sup>2</sup>) respectively. In order to produce an accurate curve of biogas production, biogas volumes were measured several times a day during the initial stages but this was reduced to once a day as biogas production slowed. Gas was measured by piercing the septum with a needle connected to a tube, in turn connected to a manometer. Fine, short needles were used to ensure that the needle tip did not touch the sludge and that the pierced holes in the septum would reseal easily. Needles were replaced when they became blunt.

#### **5.1.2 Semi-continuous laboratory-scale digester tests**

This section describes the apparatus and feeding regime for the semi-continuous laboratory-scale digesters, the storage and preparation of the feed and the methods for biogas collection and analysis.

##### **5.1.2.1 Apparatus and feeding regime**

Four identical 6-litre digesters were used for semi-continuous tests, as shown in Figure 5.1. They were heated to 36 ± 1 °C by means of water jackets, fed by a circulating heater, and the temperature of the digestate was monitored with a thermometer placed in the digester. Additionally, the

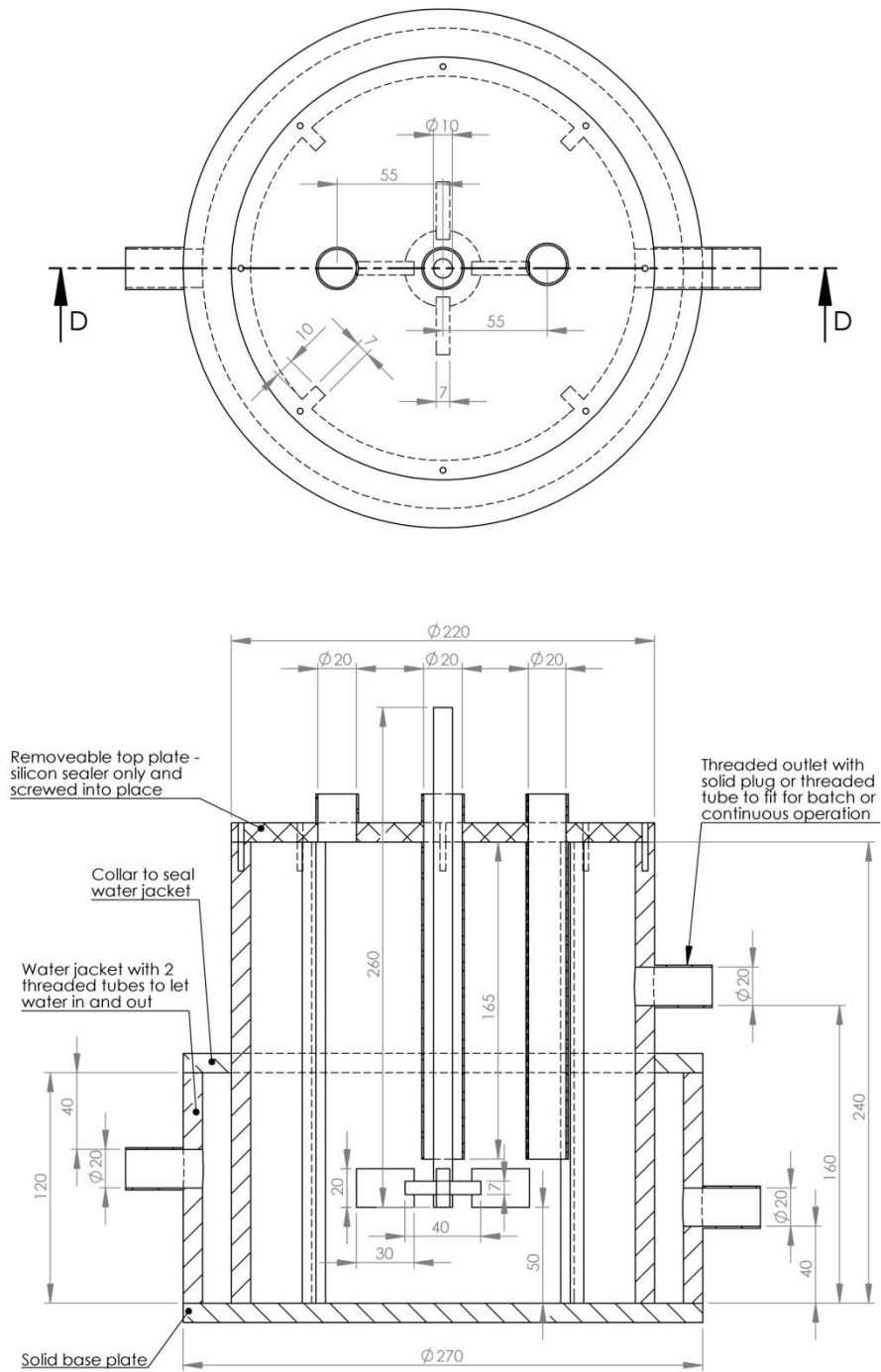
digesters were insulated using reflective radiator lining. Each digester was equipped with a 4-blade paddle for stirring, positioned 50 mm above the base of the reactor, and four baffles around the walls of the digester. The digesters were fed with 250 ml of feed five times per week (Monday to Friday). The retention time was affected by the fact that the digesters were only fed on weekdays, as shown in Table 5.1. Ten litres of synthetic sludge were made up every other week. The digester feed composition was developed during the course of the research as a synthetic feed source for the laboratory digestion experiments and further details of its composition, rheology and nutritional properties are given in Sections 6.1, 6.3, and 6.4 respectively.

**Table 5.1 - Digester feeding regime**

<b>Parameter</b>	<b>Daily feeding</b>	<b>Monday to Friday feeding</b>
<b>Concentration of VS in feed</b>		28.5 g/l
<b>Daily feed volume</b>	179 ml	250 ml
<b>Actual retention time</b>	33.6 days	24 days
<b>VS added per feed</b>	5.1 g	7.1 g
<b>Organic loading rate (OLR)</b>	0.85 g/l/d	1.18 g/l/d

### 5.1.2.2 Sludge sampling

Sludge samples were taken daily immediately prior to digester feeding. They were collected using the side arm of the digester and each sample consisted of 250 ml of sludge. If less sludge was required for analysis, any additional sludge was discarded. As far as possible, analysis was carried out on the sludge immediately after sampling. Where this was not possible, sample storage is detailed in the section relating to the relevant analysis.



N.B. All measurements in mm. All pipe diameters are nominal. Impeller should be plastic. Shaft will have to be brass. Paddle thickness determined by material.

Figure 5.1 - Lab-scale digester

### 5.1.2.3 Biogas collection

The volume of biogas produced by the digesters was measured using a semi-continuous gas flow meter. This was built to a design reported by the Water Research Council (WRC, 1975) and works by means of an inverted tipping bucket mechanism immersed in liquid. As the gas bubbles fill the bucket, it tips and a magnet activates a switch connected to a counting device. The flow meter used had a nominal bucket volume of 20 ml per count and was designed to measure gas flow rates of 1 to 20 l day<sup>-1</sup>. A more precise bucket volume was calculated by bubbling air through the gas flow meter and collecting it in an upturned measuring cylinder in a water bath. The barrier solution in the flow meter was acidified 75 % sodium chloride solution to prevent absorption of carbon dioxide and preserve the composition and volume of the biogas (Walker et al., 2009). A three-way valve at the top of each digester allowed venting, collection or sampling to take place. Gas was assumed to be at ambient air pressure when it passed through the gas flow meter. The final biogas volumes reported were based on standard temperature and pressure, 25 °C and 1 atmosphere (101325 N/m<sup>2</sup>) respectively and the volumes were converted using semi-continuous air pressure data collected from Birmingham Airport (UKMeteorologicalOffice, 2012). It was assumed that the collected gas was still at the temperature of the digester when its volume was measured.

### 5.1.2.4 Biogas analysis

Biogas composition was analysed daily whenever possible, using a handheld combustible gas meter (GMI GT44). The gas meter was calibrated by injecting five standard gas mixtures: 1) 100 % CH<sub>4</sub>, 0 % CO<sub>2</sub>; 2) 75 % CH<sub>4</sub>, 25 % CO<sub>2</sub>; 3) 50 % CH<sub>4</sub>, 50 % CO<sub>2</sub>; 4) 25 % CH<sub>4</sub>, 75 % CO<sub>2</sub>; 5) 0 % CH<sub>4</sub>, 100 % CO<sub>2</sub>. A 1 ml plastic syringe attached to a needle was used for sampling gas from ports at the top of each digester. The samples were injected into the gas meter and the % LEL reading recorded. The percentage methane was then calculated from the calibration curve. Samples were taken in triplicate and a mean of the three points was recorded.

## 5.2 General analytical methods

This section deals with the analytical methods used to assess the physiochemical and rheological properties of the sludge.

### 5.2.1 Total and volatile solids

TS and VS concentrations were measured in duplicate for sludge and synthetic sludge samples. The procedure follows that described in Standard Methods (2540 B and E) (Eaton et al., 2005). Nickel tins were cleaned, dried and put into the furnace for 30 minutes to burn off any residual volatile matter. The tins were then cooled and weighed ( $W_1$ ). 20 ml of sludge was measured into the tins, which were then placed in an oven at 105 °C for at least two hours, until all liquid had evaporated. The tins were placed in desiccators and once cooled, were weighed again ( $W_2$ ) before being transferred to the furnace at 500 °C for one hour. After cooling in the desiccators, the tins were weighed a final time ( $W_3$ ). Concentrations of TS and VS can be calculated using the following equations:

$$TS = \frac{W_2 - W_1}{V} \quad \text{Equation 5-2}$$

$$VS = \frac{W_3 - W_2}{V} \quad \text{Equation 5-3}$$

where  $TS$  is total solids concentration,  $VS$  is volatile solids concentration,  $W_1$ ,  $W_2$  and  $W_3$  are weights as indicated in method above, and  $V$  is sample volume.

### 5.2.2 pH

pH was measured using a Mettler Toledo Model 320 electrode and meter. The meter compensates for changes in temperature and was calibrated using buffer solutions of pH 4, 7 and 9. The electrode probe was rinsed with ultra-pure water (UPW) before and after each analysis to minimise cross-contamination of samples.

### 5.2.3 Alkalinity and Ripley's ratio

The method for measuring alkalinity and Ripley's ratio (RR) is based on the titration method described in Standard Methods (2320 B) (Eaton et al., 2005). 20 ml of the sample was placed in a beaker. The sample was titrated with 0.1 N sulphuric acid to end points of pH 5.75, 4.5 and 4.3. The end point of pH 4.5 is recommended for samples with high alkalinities such as wastewater (Eaton et al., 2005) and is the end point used for the calculation of total alkalinity (TA). The other two end points are used in the calculation of RR. TA, which is a measure of the ability of a solution to buffer acids, was calculated as mg CaCO<sub>3</sub>/l according to the following equation:

$$TA = A \times N \times \frac{5000}{V} \quad \text{Equation 5-4}$$

where *TA* is total alkalinity, *A* is volume of standard acid used to reach end point of pH 4.5, *N* is normality of standard acid used, and *V* is volume of sample used.

Alkalinity and VFAs are measured to gauge the stability of a digester. It is claimed that an end point of pH 4.3 takes into account the VFA buffering as well as the bicarbonate buffering (Jenkins et al., 1983). As such, Jenkins et al. (1983) suggested the measurement of partial alkalinity (PA) with an end point of pH 5.75, which allows for 80 % titration of the bicarbonate alkalinity, but only 20 % titration of the VFAs. Titrating to pH 4.3 gives the buffering of bicarbonate and VFAs and is termed TA. As such titrating from pH 5.75 to pH 4.3 gives an indication of the VFA buffering and this is called intermediate alkalinity (IA). RR is the ratio of IA:PA and acts as a measure of digester stability. The advantage of RR over direct measurement of alkalinity and VFAs is that it requires only one analytical procedure which reduces the introduction of error and is less time-consuming. Ripley et al. (1986) stated that RR values below 0.3 indicate a stable digester whilst values of 0.8 or higher indicate that a digester is under stress. The RR was calculated using the following equation:

$$RR = \frac{TA - PA}{PA} \quad \text{Equation 5-5}$$

where *RR* is Ripley's Ratio, *TA* is volume of standard acid used to reach end point of pH 4.3 and *PA* is volume of standard acid used to reach end point of pH 5.75.

#### 5.2.4 Ammonia

The method for measuring ammonia was based on the ion selective electrode method described in Standard Methods (4500-NH<sub>3</sub> D) (Eaton et al., 2005). 100 ml of the sample was placed in a beaker and a Thermo Scientific Orion 9512 ammonium ion selective electrode was immersed in the sample. 1 ml of 10 N NaOH solution was added to the sample to raise the pH above pH 11 and the reading was allowed to settle before it was recorded. A calibration curve was created using standard dilutions of stock ammonium chloride solution. Ammonia concentration of the sample was then calculated from the sample readings and the calibration curve.

#### 5.2.5 Volatile fatty acids

Lactate, acetate, propionate, butyrate and succinate were measured using a DIONEX LC30 chromatography oven equipped with an ED40 electrochemical detector, a GP50 gradient pump and an AS40 automated sampler. The column used for VFA analysis was an IonPac AS11-HC 4 x 250 mm. Samples were centrifuged at 6000 rpm for 15 minutes and then filtered using Whatman 540 filter paper. Samples were first diluted to 5 % with UPW. Standards containing a known concentration of each of the volatile fatty acids were used to calibrate the high-performance liquid chromatograph (HPLC) and the samples were then run, with blanks run every ten samples and standards every twenty samples. As it was not possible to run this analysis each week, samples were collected from each of the digesters on a weekly basis and were frozen until they were processed.

#### 5.2.6 Viscosity

Viscosity measurements were carried out using a Couette viscometer (Fann Model 35) which operates by shearing a known volume of fluid in a test cell. The torque required to turn the bob at a

known speed within the cup of fluid is a function of the viscosity of the fluid. The sample cup was filled with 350 ml of the test fluid and the cup was then raised so that the rotor sleeve was immersed in the sample to the marked line. The fluid was thus able to fill the rotor sleeve and surround the bob. Each fluid was mixed at known bob speeds of 100, 200, 300 and 600 rpm and, once the reading had stabilised, the needle deflection was recorded. Using the conversion factors given in the viscometer manual, the needle deflection was translated into a shear stress reading so that a viscosity curve could be produced for each sample.

### 5.3 Quantitative polymerase chain reaction

qPCR is a biochemical method used to measure the number of gene copies of a target DNA or RNA sequence made over time. This gives an indication of the quantity of that gene sequence in the original sample, which in turn can be used as an indicator of the microbiological communities present in the sample. The method relies on thermal cycling, where repeated heating and cooling allows DNA melting and enzymatic replication of the DNA to take place. The DNA extraction and qPCR analysis was carried out by the Wales Centre of Excellence for Anaerobic Digestion at the Sustainable Environment Research Centre at the University of Glamorgan.

Genomic DNA was extracted from 100 µl samples of digestate using PowerSoil® DNA Isolation Kits (Mo Bio Laboratories Inc.) according to manufacturer's instructions. Purified DNA was eluted from the spin column with 100 µl of 10 mM Tris and stored at -20 °C until they were used. The concentration of extracted DNA was determined based on absorbance at 260 nm using a NanoDrop 1000 Spectrophotometer (Thermo Scientific).

The numbers of total *eubacteria* were estimated by qPCR by targeting 16S ribosomal ribonucleic acid (rRNA) gene sequences as described by Suzuki et al. (2000). Assays with primer and probe sets targeting the methanogenic orders, *Methanobacteriales*, *Methanomicrobiales* and *Methanococcales*, as well as two family level aceticlastic methanogens, *Methanosarcinaceae* and *Methanosaetaceae*, were used as described by Yu et al. (2005). All DNA samples were analysed in triplicate.

Calibration curves relating cycle threshold (CT) values to the number of gene copies were produced using known amounts of single-stranded DNA oligonucleotides as shown in Table 5.2. Table 5.2 uses standard IUPAC nucleic acid notation, where the four nucleobases guanine, cytosine, adenine and thymine are represented by G, C, A and T respectively. Degenerate base symbols that represent a position for which multiple possible alternatives exist also follow the standard notation where W is nucleobase A or T, K is nucleobase G or T, R is nucleobase A or G, Y is nucleobase C or T and D is nucleobase A, G or T. Oligonucleotides were synthesized commercially and PAGE purified (Life Technologies). A 10-fold serial dilution series of known amounts of these oligonucleotides were amplified by qPCR with the corresponding primer and probe sets. Calibration curves were prepared in duplicate.

DNA extracted from pure cultures of *Methanosaeta concilii* (DSM 6752), *Methanosarcina barkeri* (DSM 800), *Methanobacterium bryantii* (DSM 863), *Methanomicrobium mobile* (DSM 1539), *Methanococcus voltae* (DSM 1537) and *Halorubrum saccharovorum* (DSM 1137) were used as controls. Strains were purchased from the Deutsche Sammlung von Mikroorganismen and Zellkulturen (DSMZ), Braunschweig, Germany. Real-time PCR was performed using a Biorad iQ5 system (Bio Rad Laboratories).

**Table 5.2 - Oligonucleotide sequences used as calibration standards for the quantification of total eubacteria and key methanogenic groups.**

<b>Microbial target group</b>	<b>Oligonucleotide sequences (5'-3')</b>
Total <i>eubacteria</i>	CGGTGAATACGTTTCYCGGGACTTGTACACACCGCCCGTCTCAAGTCGTAACAAGGTAWCC
<i>Methanosaetaceae</i>	TAATCCTYGARGGACCACCAGTACGGCAAGGGACGAAAGCTAGGACGKGTGTYGGTGCCGTAGG
<i>Methanosarcinaceae</i>	GAAACCGYGATAAGGGGAGTTTAGCAAGGGCCGGGCAAACCGTAAACGATGYTCGCTA
<i>Methanococcales</i>	TAAGGGCTGGGCAAGTACTAGCGGTGRAATGYGTTGATCCGTTAAACTYTGCGRACTAGGTG
<i>Methanomicrobiales</i>	ATCGRTACGGGTTGTGGGACTYCGACAGTGAGGRACGAAAGCTGGTGTAAACDATGYGCGTTAGGTG
<i>Methanobacteriales</i>	CGWAGGGAAGCTGTAAAGTGTAGCACCAACGCGTGGAACAAGGAGTGGACGACGGTA

## 5.4 Particle image velocimetry (PIV)

PIV is a flow visualisation technique that is used to obtain instantaneous velocity measurements from particles seeded within a fluid, resulting in the development of two- or three-dimensional vector fields. The basic components of a PIV system are seeding particles, laser beam, camera, synchroniser and image analysis software. The laser is used to illuminate a plane in the vessel and a camera perpendicular to the laser takes rapid consecutive pictures of that plane. Seeding particles are added to the flow and the flow vectors are calculated based on the positional change of these particles between consecutive pictures. A schematic of the PIV technique is shown in Figure 5.2.

The seeding particles are used to detect movement in a local region of the fluid flow field. As such, they must follow the fluid motion. For this to be the case, they must be small, neutrally buoyant, chemically inert and insoluble. They must also scatter enough light from the laser beam to be detected by the camera. For model validation in this work, 10  $\mu\text{m}$  silvered glass spheres were used. The concentration of particles used had to be sufficiently high to give reliable velocity measurements. The aim was to have around 10 pairs of particles present in a 32 x 32 pixel interrogation window.

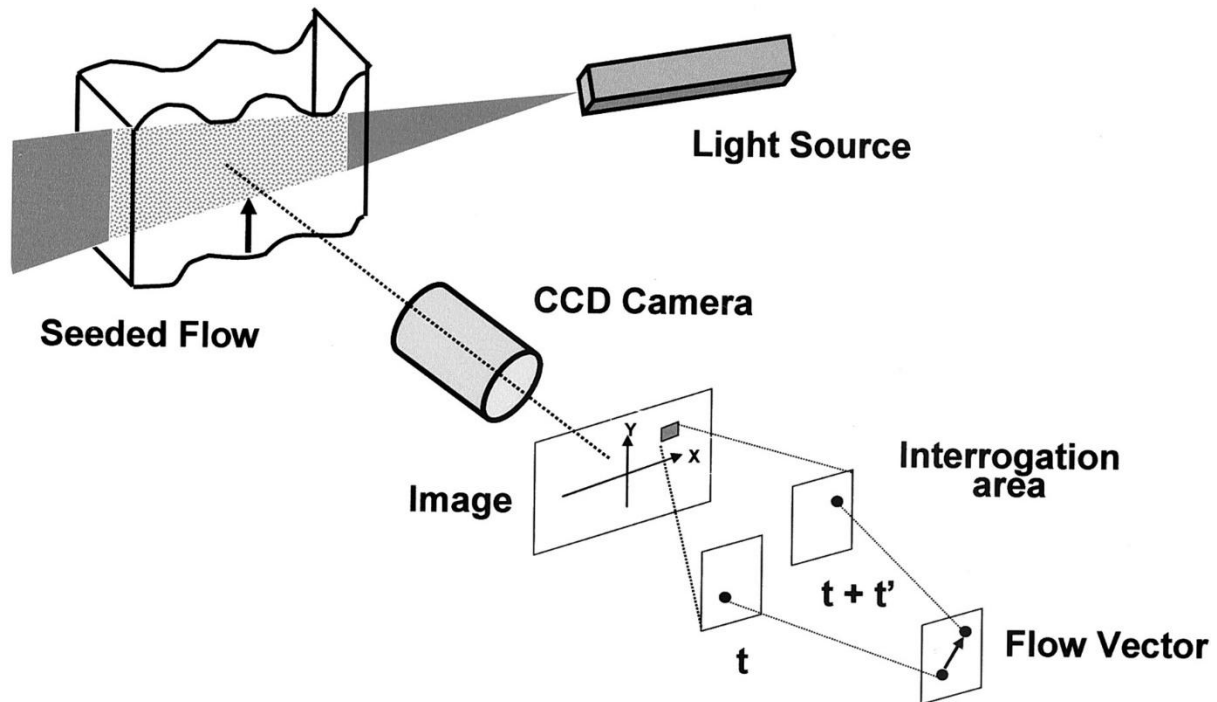


Figure 5.2 - Schematic of PIV technique showing light source illuminating plane through seeded flow, image capture and subsequent processing of consecutive images to determine flow vectors, reproduced from (Isoda et al., 2003)

An Nd:YAG (neodymium-yttrium aluminium garnet) laser was used to illuminate a plane through the mixing vessel. The beam thickness had to be kept to 1 mm or less as all particles within the volume of the beam will be illuminated and captured on the image, even if they are not focused. This can cause errors in the cross-correlation, as out-of-plane motion will still be considered.

A cross-correlation Charged Coupled Device (CCD) camera is used to record the images generated during PIV. The camera captures a sequence of PIV images with a very short time between them. A “frame straddling” technique is used so that two laser pulses are captured on consecutive frames separated by a known time interval set by a synchroniser. The synchroniser acts as a trigger for the lasers based on the frame rate of the camera.

Once the frames have been captured, image analysis is undertaken. Due to the high density of particles within the fluid, it is very difficult and often impossible to track the movement of individual particles from one image to the next. This makes it necessary to employ statistical methods to determine the most likely displacement of a group of particles. Images were divided up into interrogation windows of 32 x 32 pixels. Fast Fourier Transform (FFT) cross-correlation is used to

interrogate the image pairs. The cross-correlation function represents the probability distribution of all possible displacements of the particles within the interrogation window. Hence the maximum of the cross-correlation function represents the most probable displacement of the group of particles. A local velocity vector is determined from the distance travelled by the particles and the time interval between the two images. In this way, the velocity vectors for each interrogation window can be built up to give an image of the instantaneous flow field within the fluid. In this work, 400 image pairs were captured allowing the time-averaged flow field to be calculated. It is the time-averaged flow that can be compared to the results of CFD simulations in order to validate the CFD model.

For the purposes of PIV, it was necessary to use a transparent fluid which could accurately represent the non-Newtonian rheological properties of sewage sludge. CMC solution was selected as it has been shown to display rheological characteristics that can be modelled using a basic power-law, similar to that of real sludge in steady state and during pipe flow, mixing and aeration (Eshtiaghi et al., 2012). The CMC concentration required to match the rheological properties of the sludge were determined experimentally as described in Section 5.2.6.

## **5.5 Positron emission particle tracking (PEPT)**

The PEPT technique, is a flow visualisation technique based on the medical imaging technique, positron emission tomography (PET). It was developed at University of Birmingham and allows a single radioactive tracer particle moving inside a vessel to be tracked in three-dimensions over time. A radioactive particle is added to the liquid in which the flow is to be studied. By detecting the photons associated with the decay of this particle's nucleus, the location of the particle can be determined in three-dimensions, even in an opaque fluid or vessel. Tracking the position of the particle over time allows its velocity to be calculated and flow patterns within the vessel to be built up.

As the unstable nucleus of the tracer particle, a radioisotope, undergoes beta decay, it emits positrons. In a liquid or solid, the positron quickly annihilates with an electron in the surrounding matter and two photons, each of 511 keV, are emitted at  $180 \pm 0.5^\circ$  to one another. A positron camera can be used to detect this photon pair and simultaneous detection of the pair of photons determines a line along which the annihilation is assumed to have occurred. By considering a small number of photon pair detections, triangulation can be used to determine the position of the tracer in three dimensions as shown in Figure 5.3. It happens that some of the photons are scattered prior to detection. These are discounted by the tracking algorithm as they are not detected at  $180 \pm 0.5^\circ$  to one another.

The positron camera used is a Forte dual-headed gamma camera (Adac Laboratories) which consists of two heads on a motorised gantry which permits rotation about a horizontal axis and a separation of 250-800 mm between the detectors. Each head contains a single crystal of sodium iodide activated with thallium (NaI(Tl)) scintillator,  $500 \times 400 \text{ mm}^2$  and 16 mm thick, coupled to an array of 55 photomultiplier tubes (49 76-mm tubes and 6 50-mm tubes). Each photomultiplier is connected to a separate analogue-to-digital converter (ADC) and a single board computer in the head controls the 55 ADC channels. When scintillation occurs in the crystal, its centroid is determined via software allowing a spatial resolution of the camera for a point source of approximately 6 mm. The data are recorded event by event on a computer for subsequent processing.

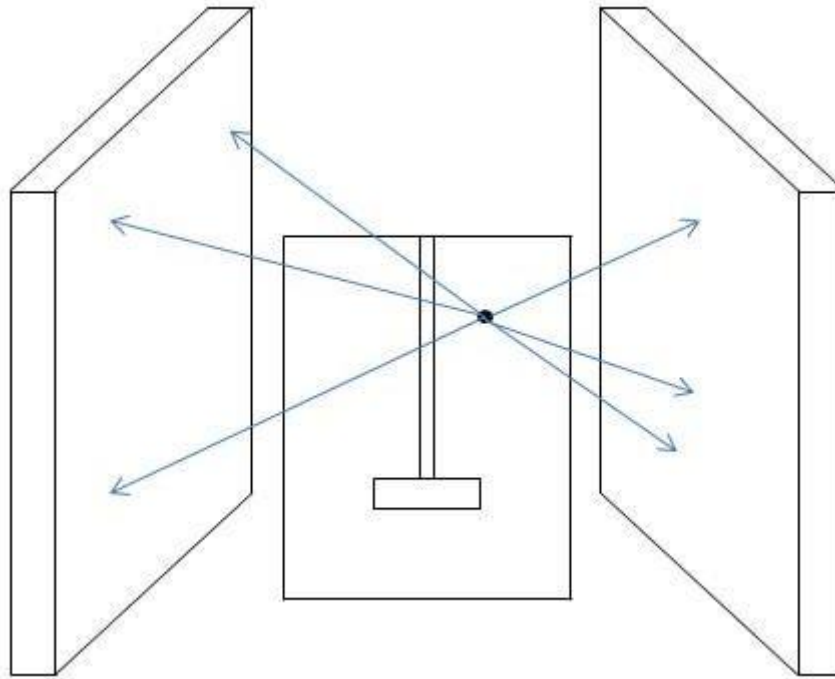


**Figure 5.3 - Detection of particle location using a series of photon pair detections**

The lab-scale digester was set up between the two detectors of the positron camera and a single radioactive tracer particle, prepared as described below was introduced into the lab-scale digester as it was mixed. At 1 m/s, a tracer can be located to within 0.5 mm, 250 times per second. By examining the changes in the tracer's position over time, an estimate of the particle's instantaneous velocity can be made, accurate to 10 %. The information gleaned from following a single particle using the PEPT technique can be used to extract further information about the flow field. First, the fraction of time that the tracer particle spends at each point in the fluid can be plotted. Over time, this comes to represent the time distribution of fluid in the digester. Over time, the instantaneous velocity of the particle as it moves through the digester enables a picture of the flow patterns to be built up. These can be compared to flow patterns developed using CFD.

### **5.5.1 Tracer preparation**

First, 3 ml of UPW was exposed to a 35 MeV  $^3\text{He}$  beam for a maximum of 2 hours, using a Scanditronix MC40 cyclotron. This allows the conversion of some of the  $^{16}\text{O}$  nuclei in the water molecules to radioactive  $^{18}\text{F}$  nuclei through the following nuclear reactions:



The resultant radioactive  $^{18}\text{F}$  nuclei are positron emitters with a half-life of 110 minutes. The  $^{18}\text{F}$  aqueous solution, which had an absolute activity of 60 mCi, was used to activate strong base anion exchange resin beads (SBR Dowex, purchased from Sigma-Aldrich). Five 600-700  $\mu\text{m}$  ion exchange beads were selected by sieving the bulk material and were placed in a cylindrical glass vial (diameter of 20 mm and height of 20 mm) and immersed in 1 ml of the  $^{18}\text{F}$  aqueous solution (activity of 20 mCi). The water was swirled for one hour at 75 rpm under a heated and dry nitrogen gas stream, flowing at 1.5 l/min, and a 250 W infrared lamp in order to slowly yet fully dry the ion exchange beads while promoting the exchange between  $\text{OH}^-$  and  $^{18}\text{F}^-$  ions on the surface of the functionalised SBR beads.

Once the beads were fully dried, they were individually coated with a thin layer (less than 100  $\mu\text{m}$ ) of fast-setting Araldite<sup>®</sup>, a commercially available epoxy resin, and left to set at room temperature for at least 30 minutes. The activity of each tracer particle was then measured and the most active tracer particle selected for use in the PEPT experiments.

## CHAPTER 6 Synthetic sludge assessment

Due to the highly variable nature of sewage sludge, it was decided that more consistent results could be achieved with synthetic sludge. This synthetic sludge would have to closely mimic sewage sludge in terms of both rheological properties and its ability to support microbiological population growth. This chapter considers the composition, preparation and suitability of the sludge to mimic sewage sludge.

### 6.1 Sludge composition

The synthetic sludge developed for this work was based on that used in Carliell-Marquet (2000). CMC was added in order to adapt the rheological properties of the sludge to make it a better match to that of sewage sludge collected at a local STW. The composition of the synthetic digester feed is given in Table 6.1.

**Table 6.1 - Composition of synthetic digester sludge**

<b>Feed constituent</b>	<b>Concentration (g/l)</b>
Corn flour (carbohydrate source)	6.3
Toilet paper (carbohydrate source)	9.0
Coffee creamer (fat and glucose source)	9.9
Bran flakes (fibre/lignin and carbohydrate source)	10.8
Yeast extract (protein source)	3.6
Peptone (protein source)	2.7
Sodium bicarbonate	2.7
Carboxymethyl cellulose (CMC)	0.1

### 6.2 Sludge preparation

The feed was made with deionised water, which was heated to 80 °C before CMC powder was dissolved. This had to be left overnight to ensure that the powder had dissolved completely to give a consistent viscosity throughout the feed. The water was heated again to a similar temperature when the corn flour was added. The toilet paper was shredded and then added to the warm starch mixture. The bran flakes were ground to powder before being added to the feed. The synthetic

sludge was well shaken before it was added to the digesters to ensure that solids did not settle out during storage. This synthetic sludge has a TS concentration of 30.5 g/l, a VS concentration of 28.5 g/l and a C:N ratio of 41.3 : 6.1 by weight. The feed was stored at 5 °C.

### 6.3 Synthetic sludge rheology

The rheological properties of the synthetic sludge were compared to those of anaerobically digested sewage sludge of varying solids concentrations collected at Kidderminster STW. These tests were carried out as described in Section 5.2.6 in triplicate to minimise errors arising from variation in the sludge. The results are shown in Figure 6.1.

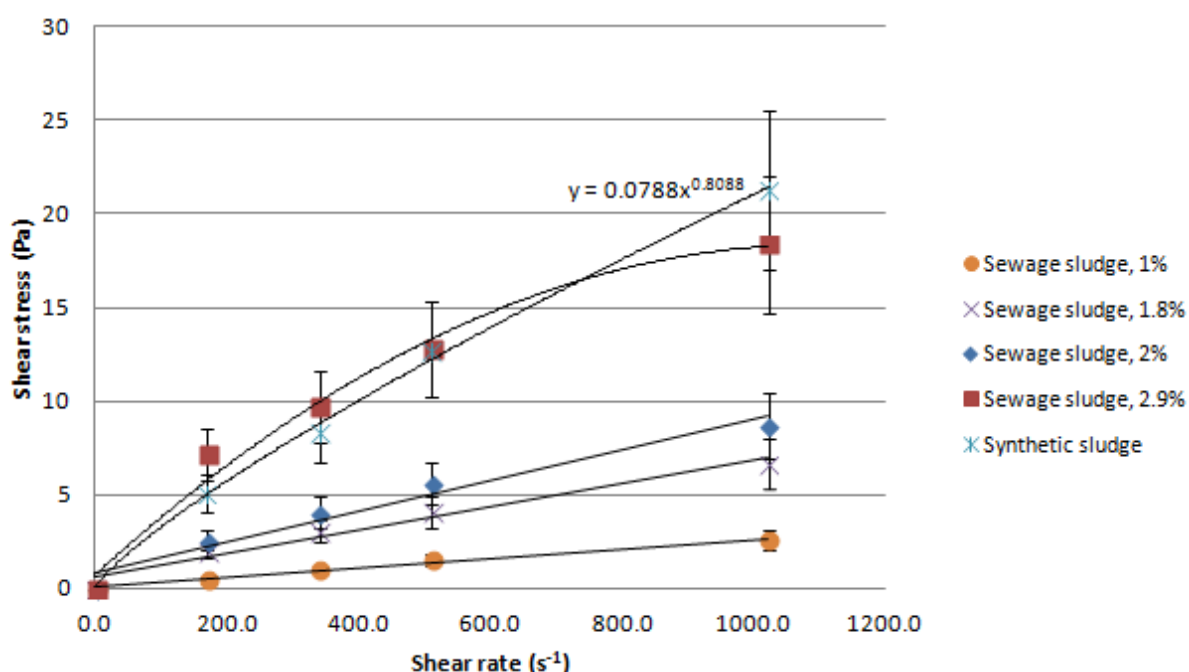


Figure 6.1 - Rheological properties of synthetic sludge compared to digested sewage sludge with varying solids concentrations

It can be seen that at solids concentrations up to 2 %, digested sewage sludge can be approximated to a Newtonian fluid within the tested range. At higher solids concentrations, the sludge behaves in a more non-Newtonian fashion and shear-thinning properties become apparent. The synthetic sludge is more viscous than the lower solids concentration sewage sludge and is similar in terms of viscous properties to the 2.9 % solids sludge. In comparison to the 2.9 % solids sewage sludge, the synthetic sludge demonstrates less shear-thinning properties and a more Newtonian profile, which

leads to a higher measured viscosity at the top end of the tested range of speeds but a lower viscosity than the 2.9 % solids sludge at the lower end of the range.

### **6.3.1 Rheology of digesting sludge**

It is well known that rheology of sludge is affected by the way in which it is processed (Moeller and Torres, 1997, Guibaud et al., 2004). Batch tests were carried out in laboratory-scale digesters to assess the importance of mixing speed on changes in rheology during the digestion process. Each of three digesters was fed with four litres of digested sludge from Kidderminster STW as the inoculant and 2.5 litres of synthetic sludge. The digested sewage sludge had a TS concentration of  $19.25 \pm 0.25$  g/l. Initially, the digesters were mixed vigorously at 550 rpm for 5 minutes to ensure that the feed was well mixed. The mixing in the three digesters were then turned off or lowered to 40 rpm or 300 rpm. A sludge sample was taken from each of the three digesters every 24 hours and the viscosity was measured as described in Section 5.2.6 before the sludge was returned to the digester. In order to ensure that the sample taken from each digester was representative of the sludge within that digester, each digester was mixed at 300 rpm for two minutes prior to the sample being taken. Based on the results of the biochemical potential test, which showed that gas production and therefore anaerobic digestion activity is highest within the first 72 hours of digestion under batch conditions, the viscosity measurements recorded in this time are shown in Figure 6.2.

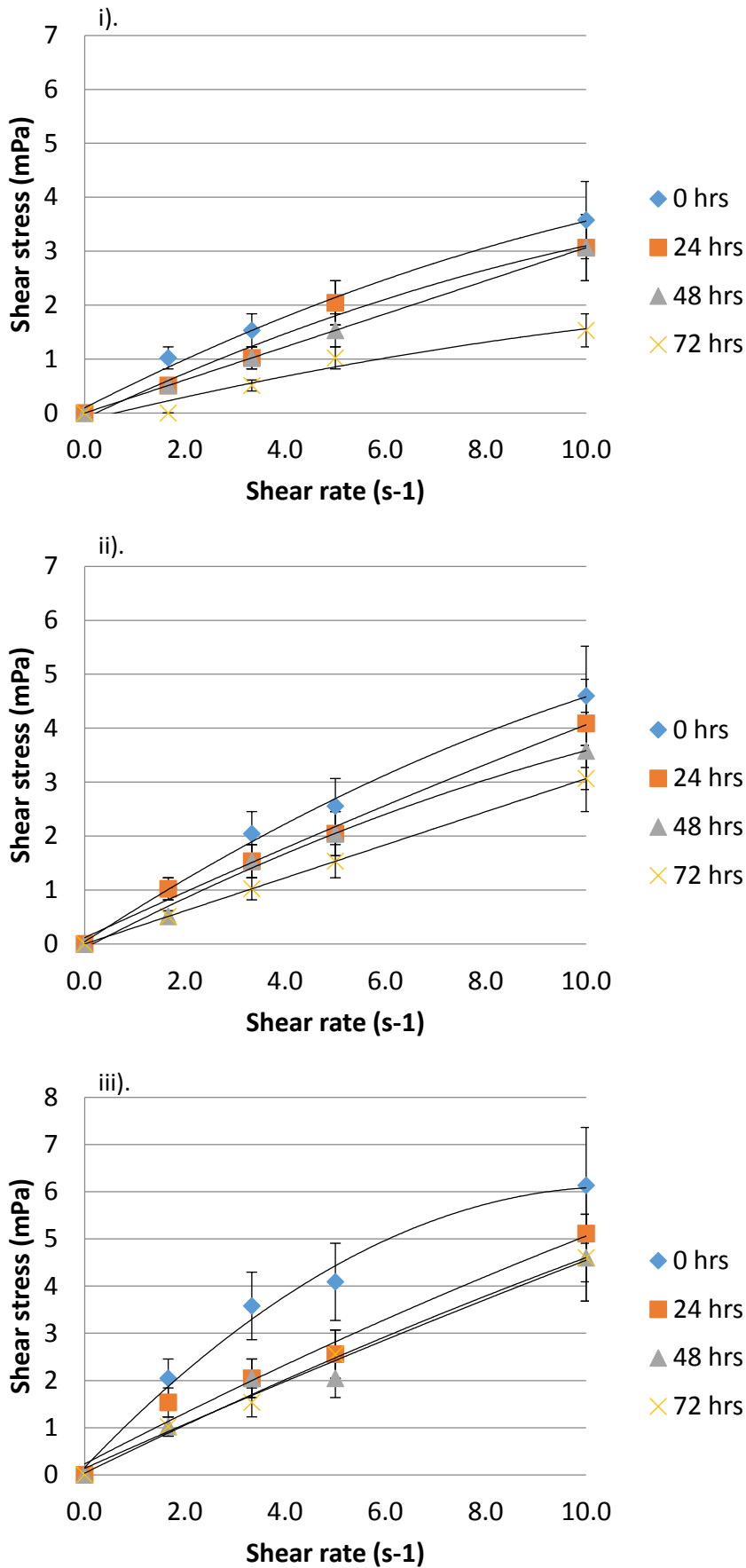


Figure 6.2 - Rheology of digesting sludge over a 72 hour period, at mixing speeds of i) 0 rpm, ii) 40 rpm and iii) 300 rpm

It can be seen that over the 72 hour test period, the viscosity of sludge in all three digesters fell demonstrating that the sludge is thixotropic, as previously shown by Moeller and Torres (1997) and Guibaud (2004). This thixotropic behaviour was most pronounced in the first 24 hours, for the sludge which experienced the highest mixing speed. Thixotropic behaviour is the time-dependent result of shear-thinning with the viscosity of a thixotropic fluid decreasing as it is exposed to shear for increasing periods of time. As a function of shear and time, it is expected that the sludge at the highest mixing speed, which is expected to experience the highest level of shearing in the impeller region, would have the greatest initial decrease in viscosity. Additionally, the non-Newtonian properties of the sludge are reduced over the course of the digestion, with the sludge behaving in a Newtonian fashion in all of the digesters within 48 hours. This is likely to be a consequence of a reduction in the TS concentration of the sludge as the VS is converted into biogas during the digestion process. As seen in Section 3.2.5, the non-Newtonian properties of sludge are often linked to TS concentrations (Guibaud et al., 2004, Spinosa and Lotito, 2003, Malczewska, 2009).

#### **6.4 Nutritional properties of synthetic sludge**

Whilst the rheological properties of the synthetic sludge are important for this research, it is also vital that the sludge acts as a source of macro- and micro-nutrients to allow microbiological growth within the digester. As such, batch tests to determine the biochemical potential of the synthetic sludge were carried out in triplicate according to the method described in Section 5.1.1 and the results compared to that of sewage sludge alone. The results of the biochemical potential tests can be seen in Figure 6.3. From this, it can be seen that the synthetic sludge seeded with sewage sludge allow the production of 6.5 times the volume of gas in 100 hours as compared to sewage sludge alone.

As the components of the synthetic sludge are largely food items, nutritional information was used to gain an understanding of the nutritional contents of the synthetic sludge feed. For this purpose, it

was assumed that the toilet paper contributed only cellulose to the feed, equivalent to the mass of toilet paper. Table 6.2 shows an estimate of the nutritional content of the synthetic sludge.

The main concern arising from this analysis was the concentration of sodium in the feed. However, it has been suggested that sodium concentrations of 3500 mg/L to 5500 mg/L were required for moderate inhibition of methanogenic bacteria under mesophilic conditions (Chen et al., 2008) so the addition of 900 mg/l should not cause significant issues to the stability of the digester.

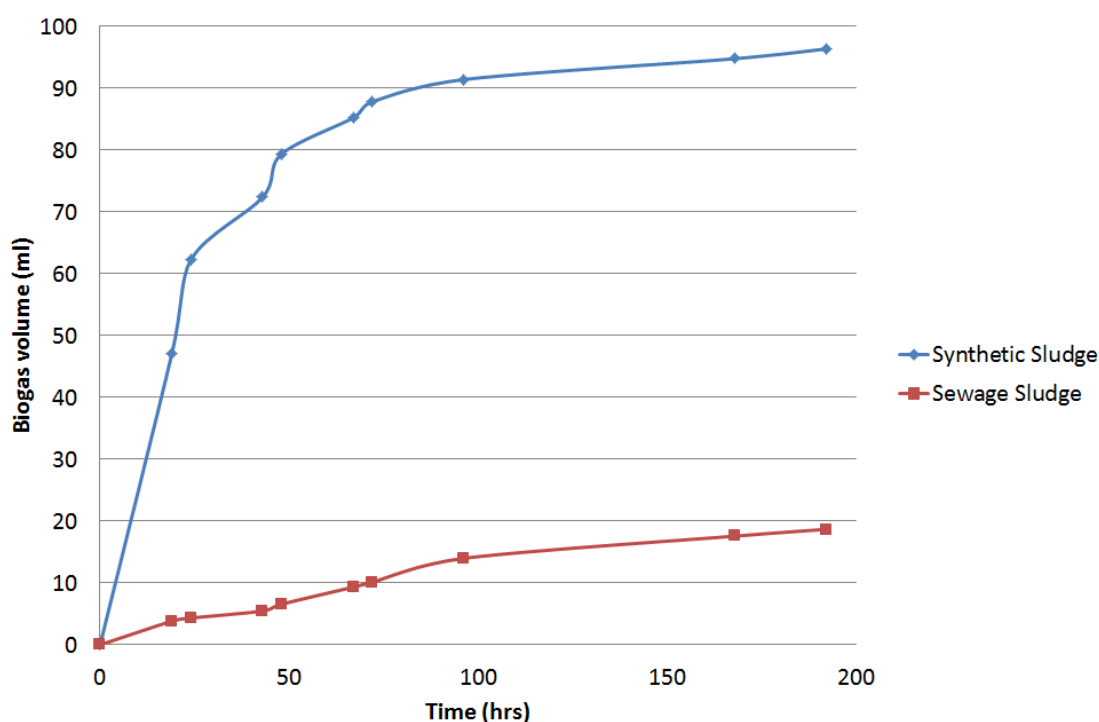


Figure 6.3 - Mean gas production from batch tests using synthetic sludge and sewage sludge as feedstock

Table 6.2 - Composition of synthetic sludge based on nutritional information given about components. N.B. toilet paper is assumed to contribute only cellulose equivalent to the weight added.

Component	Concentration
Protein	6.1 g/l
Carbohydrate	17.9 g/l
Sugar	3.9 g/l
Starch	8.6 g/l
Fat	3.8 g/l
Fibre	1.7 g/l
Salt	0.2 g/l
Sodium	0.9 g/l
Calcium	0.0 mg/l
Iron	1.5 mg/l
Cellulose	9.0 g/l

In order to assess what micro-nutrients are present in the digester feed, an acid digested synthetic sludge sample was filtered through a 0.45  $\mu\text{m}$  membrane and diluted to 1:10 and 1:100, and inductively coupled plasma mass spectrophotometry (ICP-MS) was used to identify the concentration of important micro-nutrient components in the sludge (Fe, Ca, Mg, K, Mn, Ni, Co, Cu, Zn, Se, P, W, Mo). The results of this semi-quantitative sweep are shown in Table 6.3.

**Table 6.3 – ICP-MS results of a semi-quantitative metals sweep on synthetic sludge (results are approximate:  $\pm 20\%$ ). N.B.: Concentrations are listed as dry/dry weight.**

Element	Concentration		Element	Concentration	
	ppb	mL/L		ppb	mL/L
Li	7.6	0.0076	As	5.1	0.0051
B	610	0.61	Se	3.3	0.0033
Na	83000	83	Rb	5.1	0.0051
Mg	2100	2.1	Sr	26	0.026
Al	400	0.4	Zr	2.5	0.0025
Si	2200	2.2	Mo	0.6	0.0006
P	9000	9	Ag	3.4	0.0034
K	9600	9.6	Sb	0.3	0.0003
Ca	6500	6.5	Ba	7.3	0.0073
Ti	30	0.03	Ce	1.5	0.0015
V	8.6	0.0086	Au	0.2	0.0002
Cr	3.8	0.0038	Pb	2.5	0.0025
Mn	36	0.036			
Fe	240	0.24			
Co	0.3	0.0003			
Ni	2.7	0.0027			
Cu	11	0.011			
Zn	110	0.11			
Ga	0.4	0.0004			
Li	7.6	0.0076			

## 6.5 Summary

This chapter has outlined the composition and preparation of the synthetic sludge developed in the course of this work. Below 2 % solids, it was shown that digested sewage sludge behaves as a Newtonian fluid. The synthetic sludge is non-Newtonian, and has similar rheological properties to a 2.9 % solids digested sewage sludge though it demonstrates less shear-thinning behaviour than digested sewage sludge. As sludge is digested under batch conditions, its viscosity decreases. This is most apparent at higher mixing speeds. Nutritionally, the synthetic sludge has sufficient nutrients to

produce 6.5 times the volume of gas over 100 hours as digested sewage sludge alone. An analysis of the macro- and micro-nutrients present in the synthetic sludge indicates that the sludge may suffer from high levels of sodium, although literature suggests that the concentration present is still well below levels required for moderate inhibition of methanogens.

## CHAPTER 7      Positron Emission Particle Tracking

This chapter considers the flow patterns generated by mechanical mixing in a lab-scale digester using the novel approach of PEPT as a visualisation technique. It aims to identify the particle coverage and flow patterns in the digester at a range of mixing speeds, and to recognise any differences between flow patterns at different mixing speeds.

### 7.1 Experimental conditions

The principles of PEPT and the preparation of the neutrally-buoyant radioactive particle are explained in Section 5.5. Two types of sludge were tested at four mixing speeds: 50 rpm, 100 rpm, 150 rpm and 200 rpm. The first sludge was anaerobically-digested sludge collected from the digesters at a local STW and is referred to in this chapter as real sludge. This is the first time that the mixing patterns present in an anaerobic digester have been visualised using real sludge, rather than a transparent model fluid. The second sludge was synthetic sludge and was the sludge used in the lab-scale digesters for the experimental work described in Chapter 8. Both sludges were considered as non-Newtonian fluids that follow a power law model,  $\eta = k\dot{\gamma}^n$ , and the consistency index,  $k$ , power law index,  $n$  and total solids content of the two sludges are shown in Table 7.1.

**Table 7.1 - Comparison of viscous properties and total solids of real and synthetic sludges used in PEPT**

Fluid	Consistency index, $k$	Power law index, $n$	Viscosity, mPa.s	Total solids content, g/l
Real sludge	0.0036	0.073	16	17.99
Synthetic sludge	0.2556	0.555	4	15.14

The activity of the radioactive tracer particle in the synthetic sludge was 560  $\mu\text{Ci}$ , whilst a weaker tracer with an activity of 340  $\mu\text{Ci}$  was used in the real sludge. The particle was tracked for 20 minutes at each mixing speed in each of the sludges, starting at the fastest mixing speed and finishing at the slowest mixing speed.

## 7.2 Tracer particle suitability

Stokes number,  $St$ , is a dimensionless number corresponding to the behaviour of a particle suspended in a fluid flow and is a measure of flow tracer fidelity in flow visualisation techniques. It is defined as the ratio of the characteristic time of the particle,  $\tau_p$ , to the characteristic time of the fluid,  $\tau_f$ .  $\tau_p$  is the time a particle takes to adjust to new forces acting on it and for most particles is very small. Mathematically,  $\tau_p$  and  $\tau_f$  are defined in a stirred tank as:

$$\tau_p = \frac{\rho_p d_p^2}{18\mu} \quad \text{Equation 7-1}$$

$$\tau_f = \frac{d_i}{\pi N d_i} = \frac{d_i}{u_{tip}} \quad \text{Equation 7-2}$$

where  $\rho_p$  is the density of the particle,  $d_p$  is the particle diameter,  $\mu$  is dynamic viscosity of the fluid,  $d_i$  is the impeller diameter,  $N$  is the frequency of rotation of the impeller and  $u_{tip}$  is the tip velocity of the impeller.

As such, the Stokes number in a stirred tank is defined as:

$$St = \frac{\tau_p}{\tau_f} = \frac{\rho_p d_p^2 u_{tip}}{18\mu d_i} \quad \text{Equation 7-3}$$

A large  $St$  indicates a situation in which the particle is slow to respond to changes in the forces acting upon it brought about by changes to the fluid velocity and will continue along its initial trajectory as its movement is dominated by its own inertia. For low  $St$ , the particle responds quickly to changes in the fluid velocity and hence, is able to track fluid streamlines well. As  $St$  approaches zero, the particle and fluid response times are identical and the particle will follow streamlines perfectly, a situation known as equilibrium flow. In practice, equilibrium flow is assumed for cases when  $St < 0.1$ . At a mixing speed of 200 rpm,  $St$  is in the range 0.011-0.195 depending on the viscosity used in the calculation. This represents the case that occurs at the tip of the impeller where velocities are highest and thus, for the majority of the digester,  $St$  is likely to be considerably lower. At a mixing

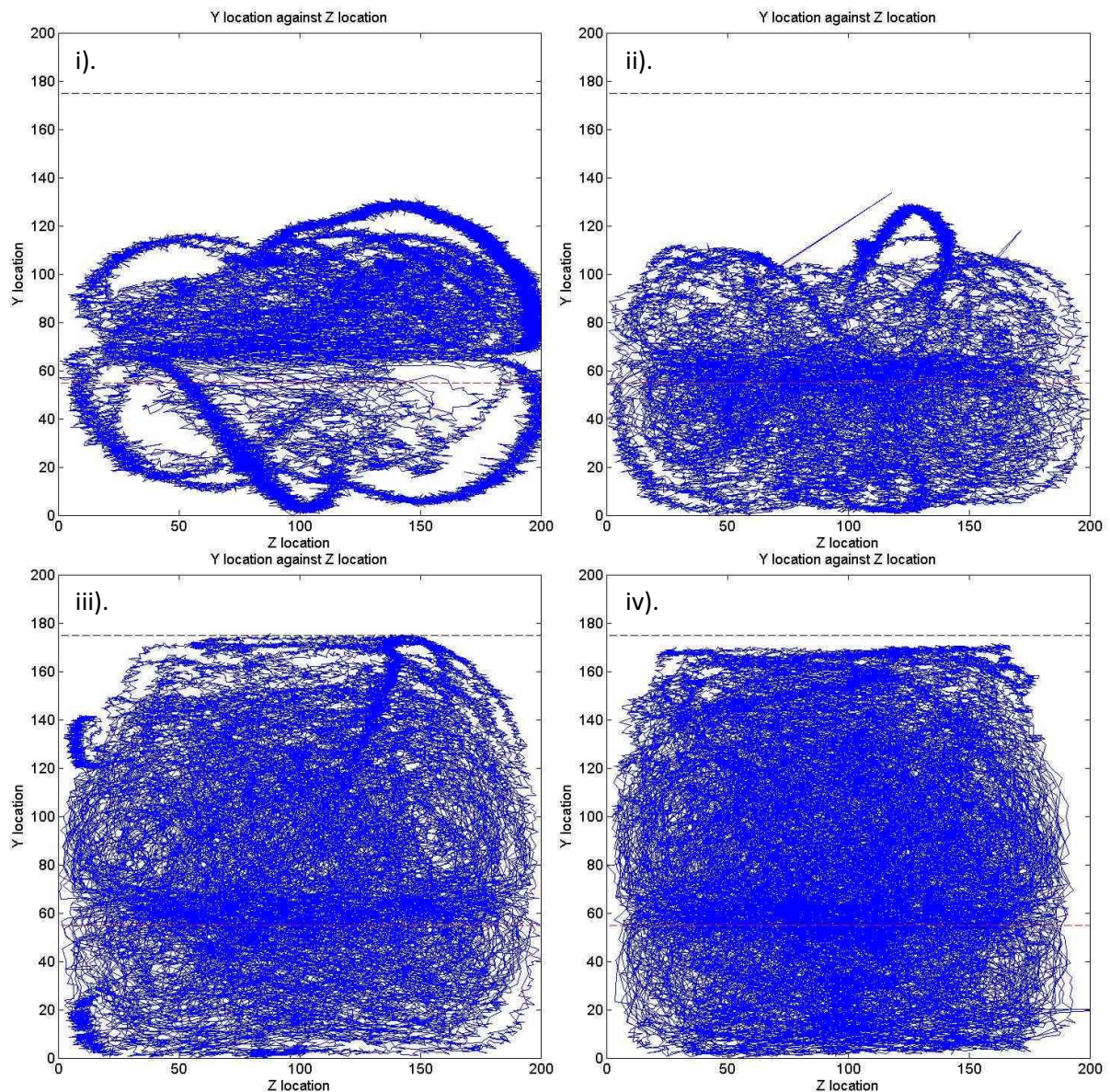
speed of 50 rpm,  $St$  falls to a range of 0.003-0.049, depending on the viscosity. Hence, the particle should be able to track the fluid streamlines well.

The estimated Kolmogorov length scale in the lab-scale digester was calculated using CFD models to be in the range  $8.6 \times 10^{-4}$ - $1.7 \times 10^{-2}$  m, depending on mixing speed. Hence, the diameter of the tracer particle is smaller than the smallest estimated Kolmogorov length scale, so it should follow the flow patterns of even the smallest eddies within the fluid.

The density of the particle was approximately  $1080 \text{ kg/m}^3$ , assuming that the process of coating the particle with Araldite<sup>®</sup> does not significantly change its density. The density of the two sludges was approximately  $955 \text{ kg/m}^3$ , slightly below that of water, giving a particle-fluid density ratio of 1.13. Given the turbulent nature of the fluid flow in the digester, even at the lowest mixing speed ( $Re = 2.6$ - $6.5 \times 10^4$  at 50 rpm), this nearly neutral buoyancy is likely to be sufficient to ensure that the particle follows the fluid flow rather than settling out. Combined with the low Stokes number and the small size of the particle compared to the Kolmogorov length scale, this suggests that the radioactive tracer particle is able to accurately track the fluid motion in the digester during PEPT experiments.

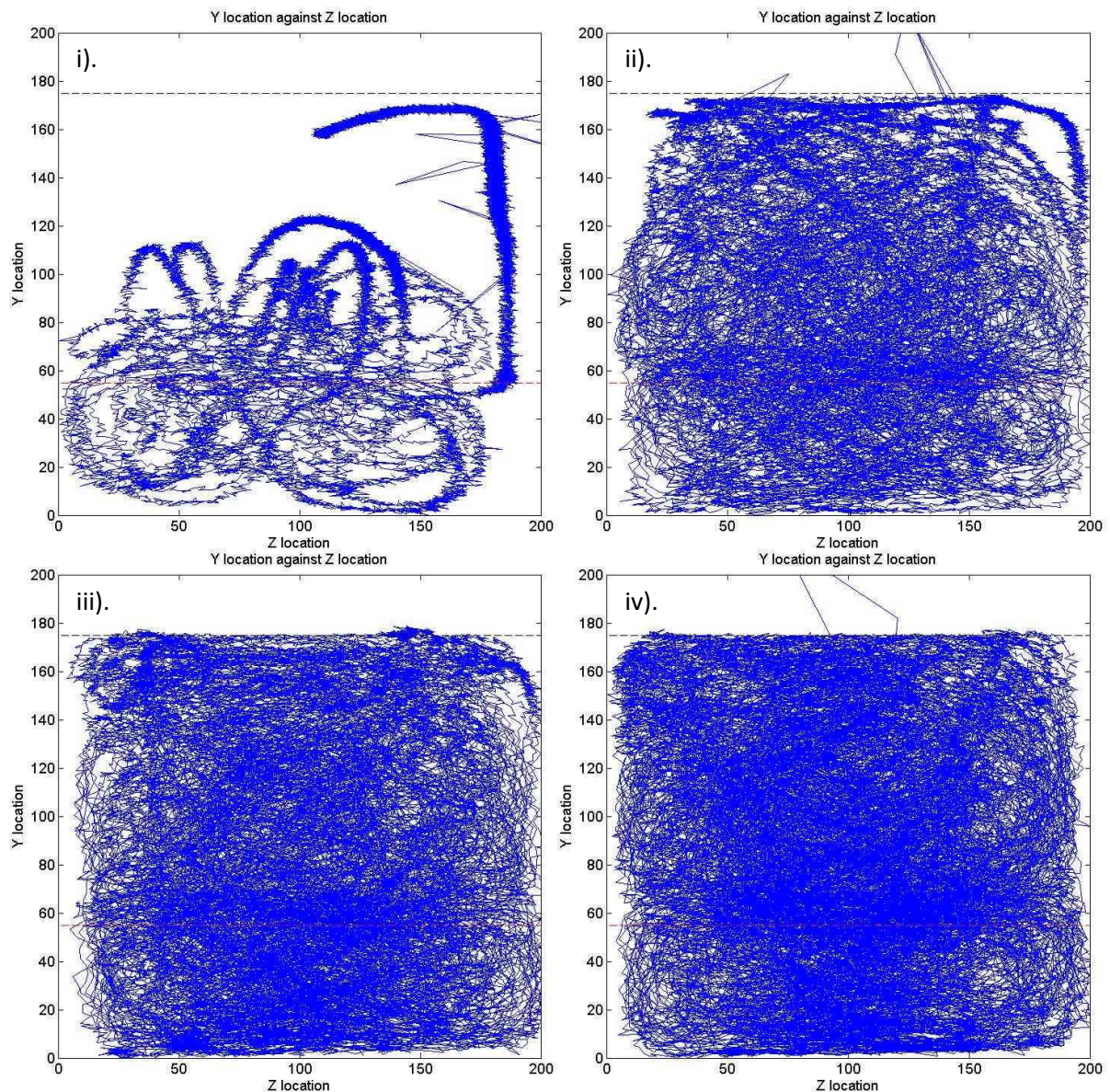
### 7.3 Particle location and path lines

Figure 7.1 and Figure 7.2 show the path lines followed by a single radioactive particle over a 20 minute period in a lab-scale anaerobic digester mixing real or synthetic sludge at a range of mixing speeds (50 rpm, 100 rpm, 150 rpm, 200 rpm). From these, it can be seen that for both real and synthetic sludge at mixing speeds of 150 rpm and 200 rpm, the contents of the digester is well-mixed. This is shown by the fact that over a 20 minute period, the particle effectively reaches all areas of the digester, which was filled to a height of 175 mm.



**Figure 7.1 – Path line followed by a single radioactive particle over a 20 minute period in a lab-scale anaerobic digester mixing real sludge at i). 50 rpm, ii). 100 rpm, iii). 150 rpm, and iv). 200 rpm. Black dashed line shows sludge level in vessel and red dashed line shows centre line of impeller.**

At 50 rpm, for both real and synthetic sludge, this is not the case and it appears that the digester is poorly-mixed, with the particle residing almost entirely in the bottom two thirds of the digester volume, between 0 and 120 mm above the base of the digester. In the case of the real sludge mixed at 50 rpm, the particle resides mostly in the volume above the impeller blades, the centreline of which is located at 60 mm above the base of the digester, and less frequently below the impeller.



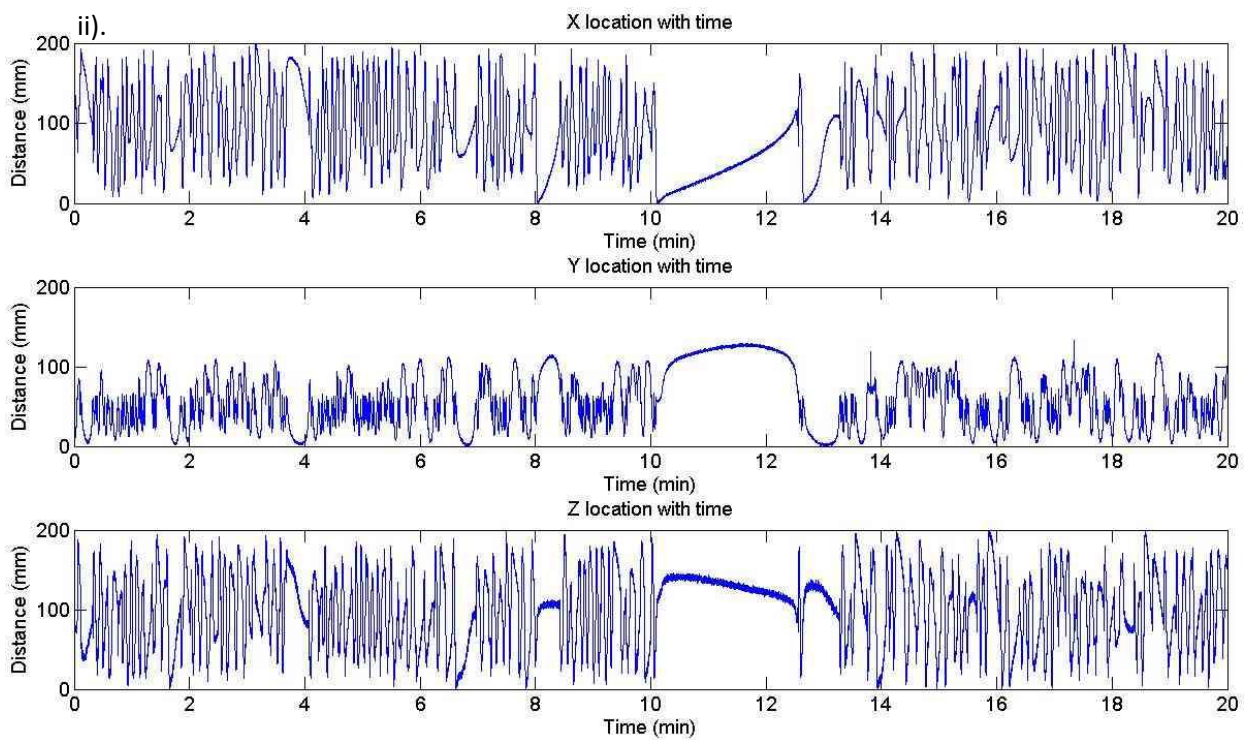
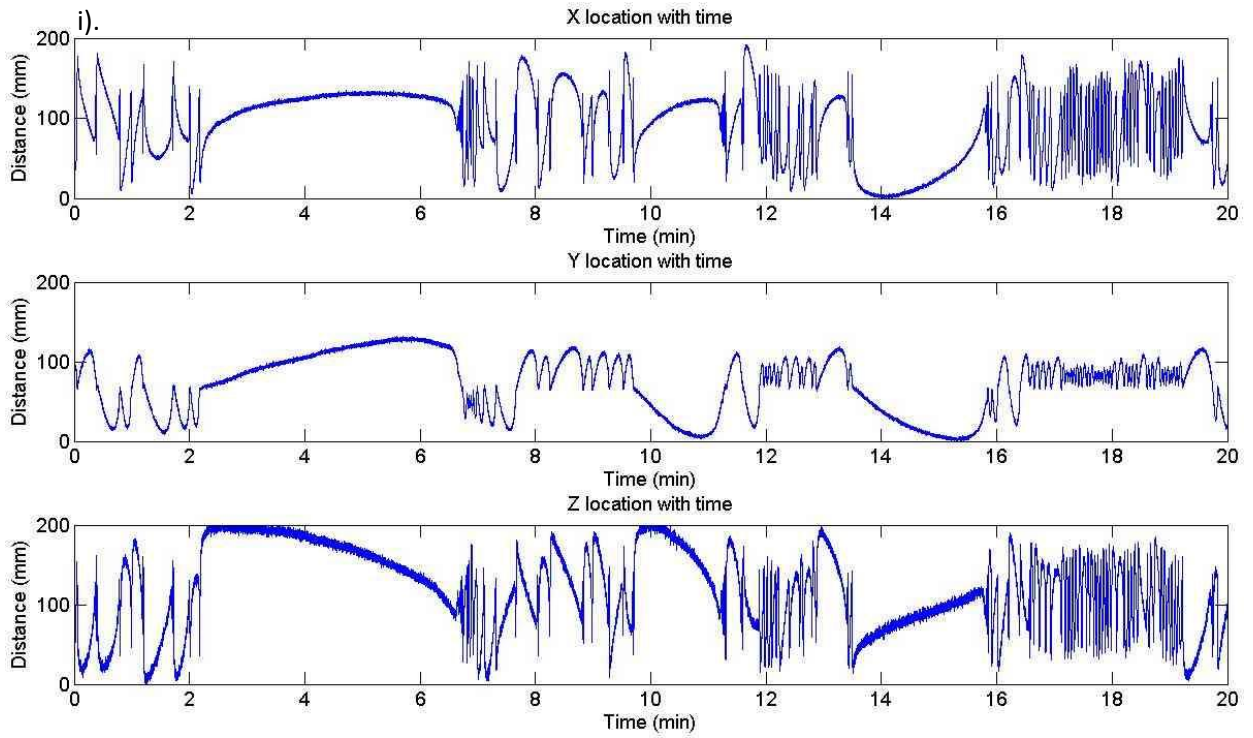
**Figure 7.2 – Path line followed by a single radioactive particle over a 20 minute period in a lab-scale anaerobic digester mixing synthetic sludge at i). 50 rpm, ii). 100 rpm, iii). 150 rpm, and iv). 200 rpm. Black dashed line shows sludge level in vessel and red dashed line shows centre line of impeller.**

At 100 rpm, there is a difference in the path lines of the particle in the synthetic and real sludge, with the synthetic sludge displaying a similar path line to the higher mixing speeds and the real sludge displaying a similar path line to the lower mixing speeds. This suggests that at 100 rpm, the synthetic sludge is well-mixed whilst the real sludge is poorly mixed, again with the particle residing almost entirely in the bottom two thirds of the digester volume between 0 and 120 mm. This difference can be attributed to the difference in the viscosities of the two fluids, with the real sludge having a greater viscosity than that of the synthetic sludge, as demonstrated in Table 7.1.

Figure 7.3 and Figure 7.4 show the  $x$ ,  $y$  and  $z$  co-ordinates of the particle plotted against time, and give a clearer picture of this behaviour. At high mixing speeds (150 rpm and 200 rpm), there are continuous fluctuations in the  $x$ ,  $y$  and  $z$  co-ordinates of the tracked particle. There are periods of time during which the co-ordinates of the particle do not change significantly, but these periods are less than 30 seconds at a time and this is not a common occurrence. The co-ordinates of these periods of slow movement correspond well to the location of the baffles in the digester, suggesting that they occur when the particle becomes stuck against a baffle for a number of seconds before it is carried away again by the bulk fluid flow in the digester. The fact that the particle does not remain stuck for very long indicates that particles that enter areas of recirculation behind baffles do not remain trapped there indefinitely.

At 50 rpm, the occurrence of these periods of almost stationary motion are more frequent and occur for longer times, with the particle experiencing periods of 5 minutes or more of slow movement in both the real and the synthetic sludge. In these cases, the co-ordinates of the particle during periods of slow movement occur when the particle is no longer close to the impeller blades, when the particle approaches the digester walls and is located either below the impeller or above 100 mm from the base of the digester (40 mm above the centre line of the impeller).

Once again, at 100 rpm, it can be seen that the synthetic sludge behaves more like the higher mixing speeds, with continuous fluctuations of the particle co-ordinates, whilst the particle in the real sludge experiences longer periods of slow movement when it is above 100 mm from the base of the digester.



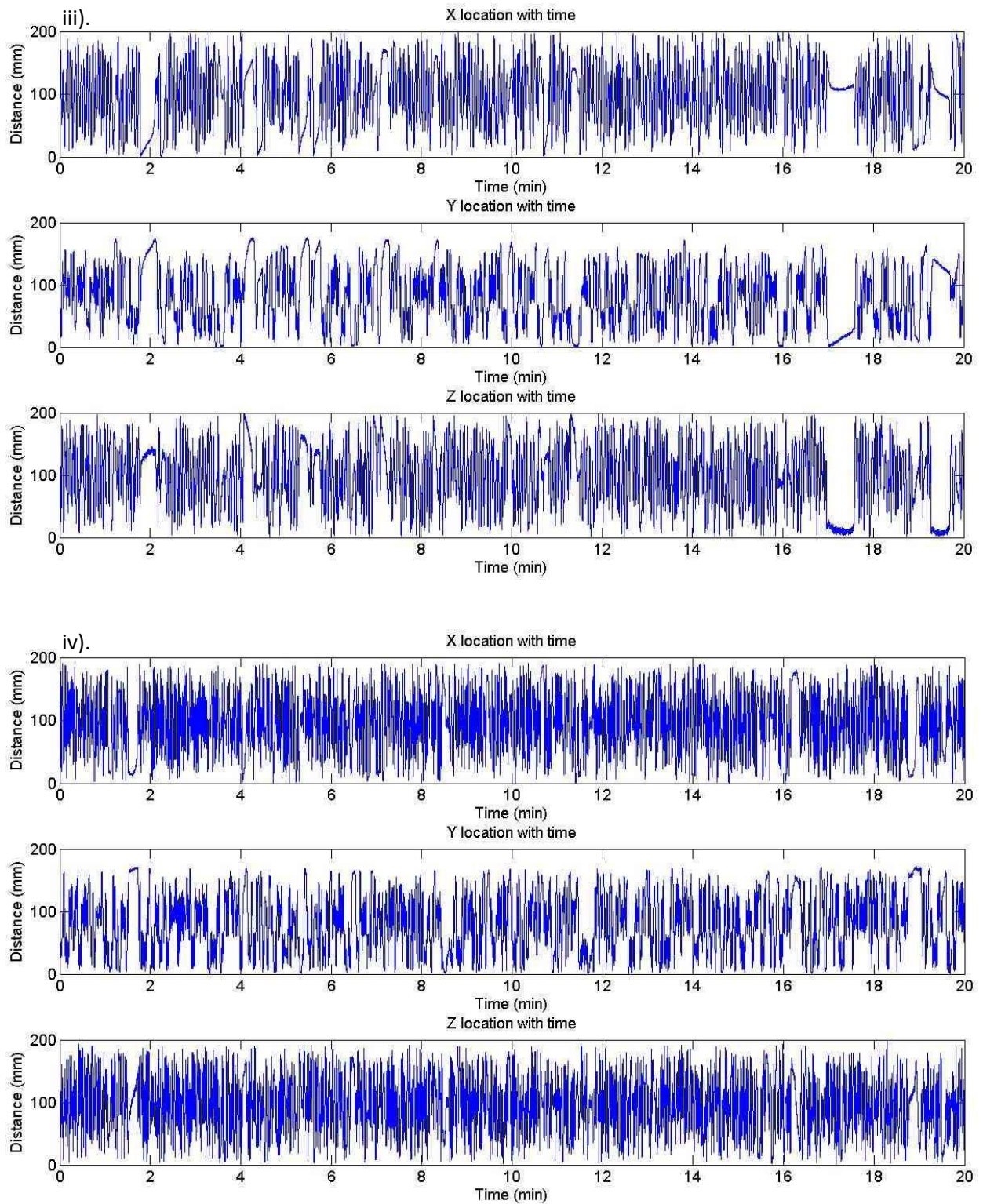
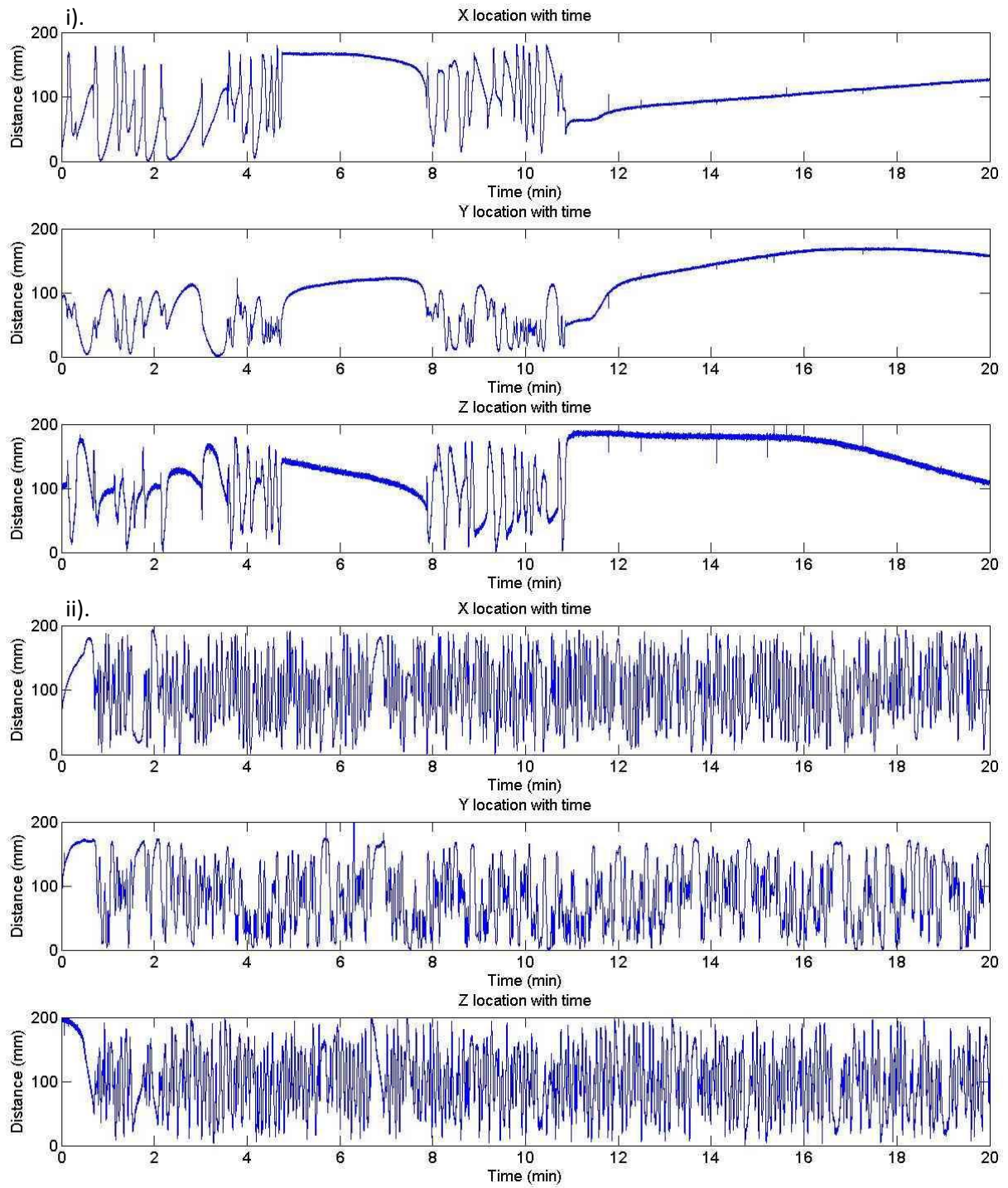


Figure 7.3 –  $x$ ,  $y$ , and  $z$  co-ordinates of a single radioactive particle over a 20 minute period in a lab-scale anaerobic digester mixing real sludge at i). 50 rpm, ii). 100 rpm, iii). 150 rpm, and iv). 200 rpm



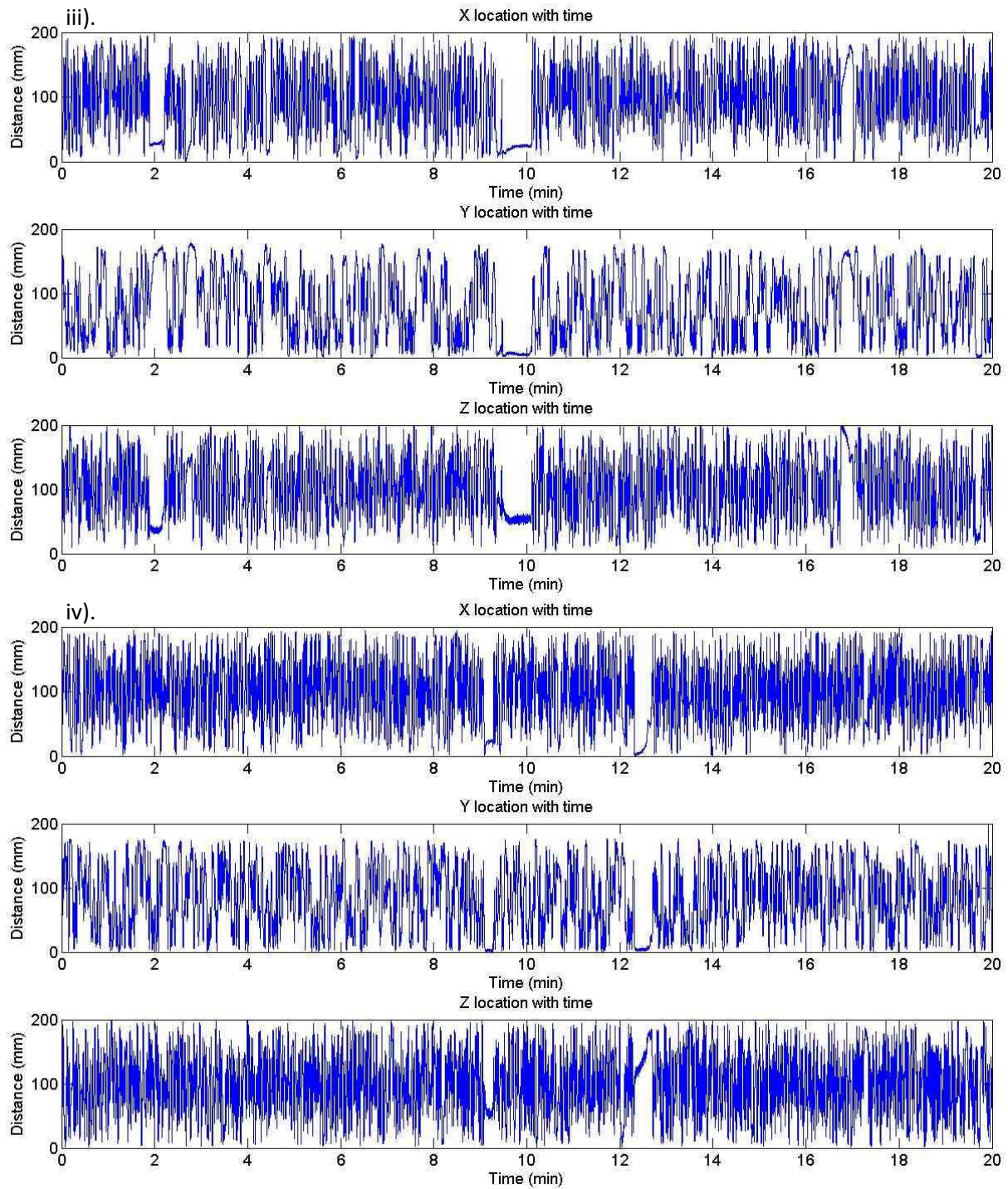


Figure 7.4 –  $x$ ,  $y$ , and  $z$  co-ordinates of a single radioactive particle over a 20 minute period in a lab-scale anaerobic digester mixing synthetic sludge at i). 50 rpm, ii). 100 rpm, iii). 150 rpm, and iv). 200 rpm

## 7.4 Velocity magnitude

From the time and location of the particle, the velocity was calculated at each of approximately 65,000 points along the path line for each of the eight twenty-minute experimental run. In order to calculate the velocity, it was assumed that the particle travelled in a straight line at constant velocity between any two consecutive points at which it was detected. The velocity of the particle was then calculated using a central differencing method as demonstrated in Figure 7.5 and Equation 7-4. The mean and standard deviation of these velocities are given in Table 7.2. The tip speed is included for comparison purposes.

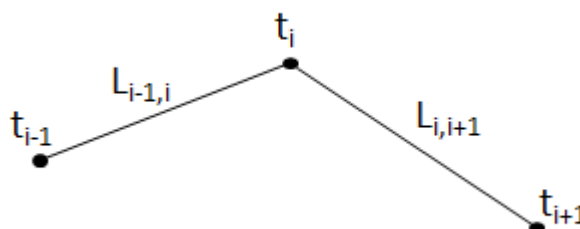


Figure 7.5 - Central differencing method

$$v_i = \frac{L_{i-1,i} + L_{i,i+1}}{t_{i+1} - t_{i-1}} \quad \text{Equation 7-4}$$

Table 7.2 – Mean and standard deviation of velocity magnitude (m/s) calculated from PEPT data for real and synthetic sludge at a range of mixing speeds

Mixing speed (rpm)	Tip speed (m/s)	Synthetic sludge		Real sludge	
		Mean (m/s)	Standard deviation	Mean (m/s)	Standard deviation
200	0.94	0.22	0.09	0.19	0.08
150	0.71	0.18	0.07	0.15	0.06
100	0.47	0.14	0.06	0.10	0.05
50	0.24	0.12	0.06	0.11	0.05

It is no surprise that the mean velocity magnitude of the particle increases as the mixing speed of the digester increases. Once again, the difference in viscosity between the synthetic and real sludge is apparent, with the mean velocity magnitude for the synthetic sludge being higher than that of the

real sludge at all mixing speeds. Furthermore, a comparison of the mean velocity in the sludge and the tip speed demonstrates the limited effects of increasing the mixing speed on the velocity at which the sludge moves, with the mean velocity in both sludges at 50 rpm being around 45-50 % of the tip velocity, but only 20-25 % at 200 rpm. This reduction in velocity as a percentage of tip speed, or normalised mean velocity, is most significant between 50 rpm and 100 rpm, where it falls from 45-50 % to 20-30 %. It then settles in the range of 20-25% for 150 and 200 rpm. The relative scarcity of data points in the digesters at 50 rpm allows the introduction of greater errors in the calculation of mean velocity, which may explain why there is a higher mean velocity in these digesters than in the digester mixing real sludge at 100 rpm.

### 7.5 Azimuthally-averaged occupancy

The Cartesian co-ordinates of the particle at each point on its path were changed to cylindrical co-ordinates in order to calculate azimuthally-averaged variables for the digester. Azimuthal averages are commonly used in literature relating to stirred vessels, due to the axial symmetry of a cylindrical vessel (Chiti et al., 2011). Once in cylindrical co-ordinates, a vertical two-dimensional grid was imposed on the digester between the axis of rotation (along the impeller shaft) and the wall of the digester. Each square in the two-dimensional grid represents all locations that fall within a three-dimensional toroidal cell, as shown in Figure 7.6.

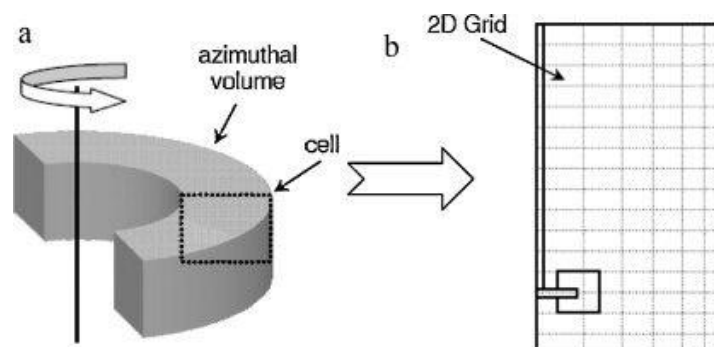


Figure 7.6 - Production of an azimuthal grid scheme for spatial averaging of data, taken from Chiti et al. (2011)

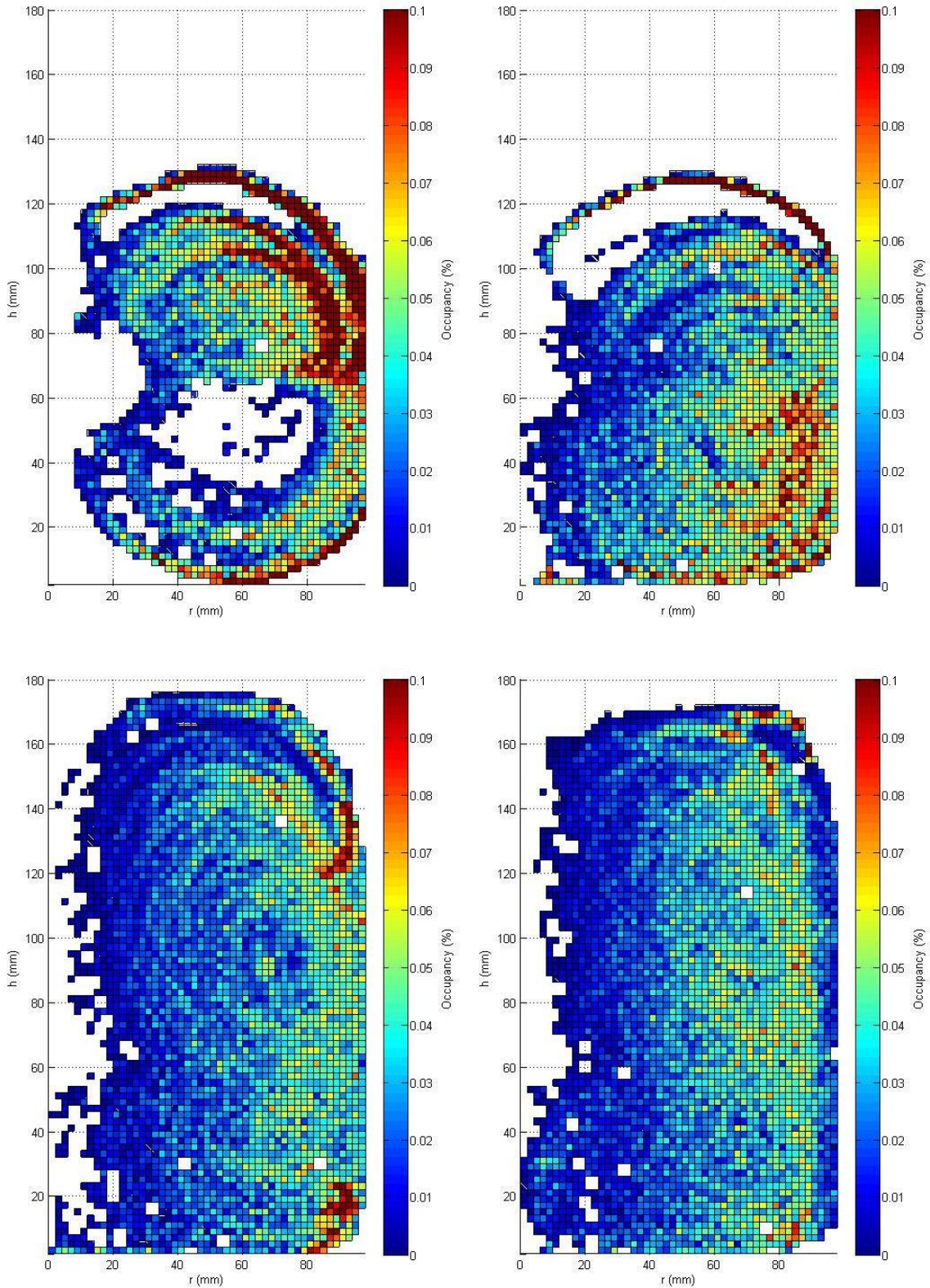


Figure 7.7 – Azimuthally-averaged occupancy in a lab-scale anaerobic digester mixing real sludge at i). 50 rpm, ii). 100 rpm, iii). 150 rpm, and iv). 200 rpm

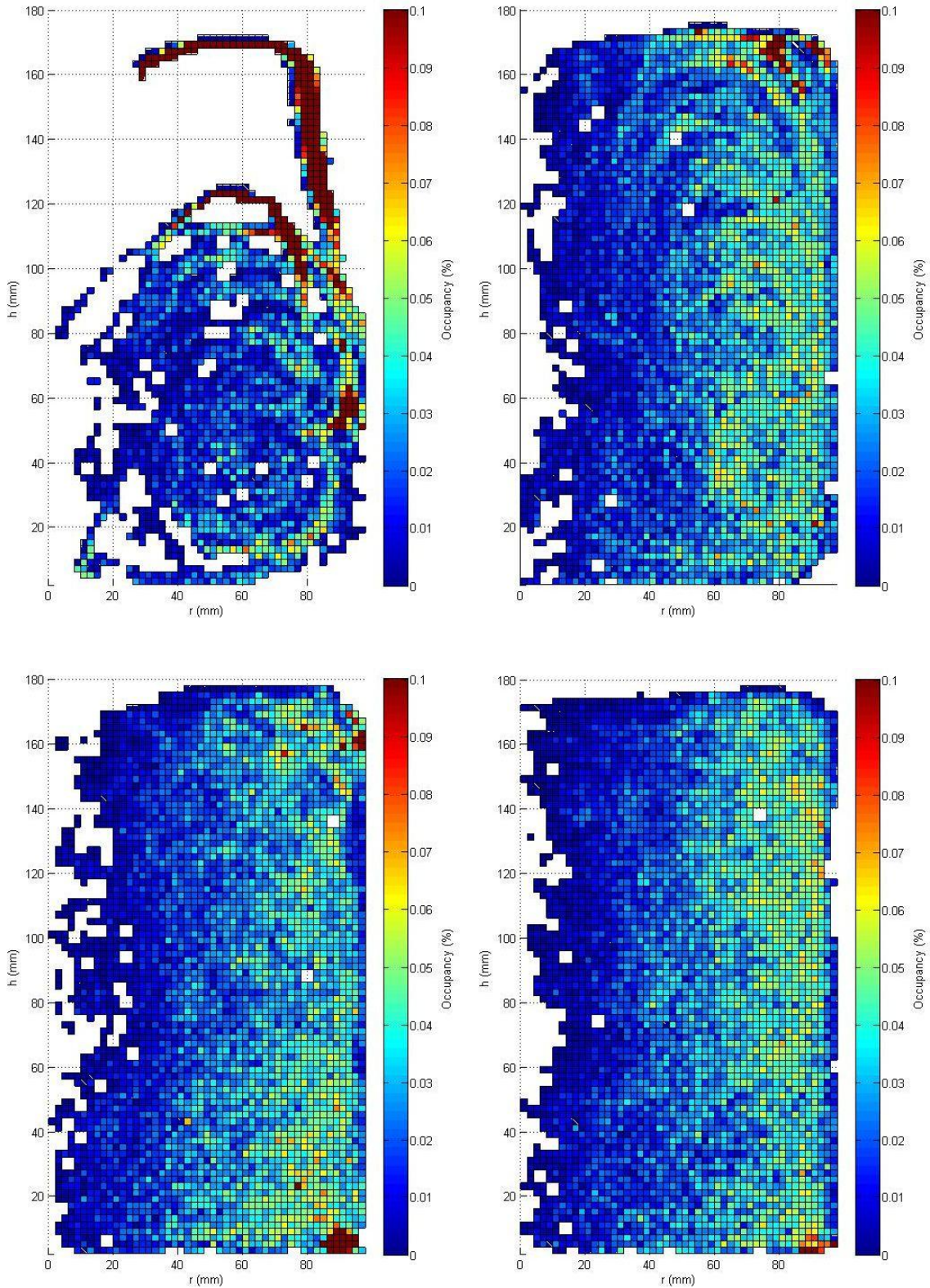


Figure 7.8 – Azimuthally-averaged occupancy in a lab-scale anaerobic digester mixing synthetic sludge at i). 50 rpm, ii). 100 rpm, iii). 150 rpm, and iv). 200 rpm

Figure 7.7 and Figure 7.8 show the azimuthally-averaged occupancy of the digester taken as the time the particle spent in each grid cell as a percentage of the total time. As such, the sum of all grid cells should add to 100 %, i.e. 20 minutes. It can be seen that at 200 rpm, the occupancy is well-distributed across the digester, though it is higher in the outer regions of the digester, close to the walls, than it is around the impeller and impeller shaft at the centre of the vessel. This can be explained by the fact that the flat-blade impeller acts as a radial flow impeller, pushing the fluid towards the walls of the digester before it moves around one of two circulation loops, above and below the impeller. Additionally, due to the speed at which the particle moves in regions close to the impeller, it is less frequently detected in this region, making it more difficult to accurately predict its location close to the impeller.

At 200 rpm, areas of high occupancy are minimal, indicating that particle coverage of the digester is fairly even. At 150 rpm, a very similar pattern to the occupancy plots at 200 rpm is seen, though the existence of a small high occupancy volume at the point where the wall meets the base of the digester can be seen. This is likely to be due to the particle becoming stuck against one of the baffles for a short period of time. At 100 rpm, for synthetic sludge, the plot is similar to that at 150 rpm. For real sludge at 100 rpm, the particle does not reach all parts of the digester, which explains the lack of data above 120 mm from the base of the digester and suggests that only some parts of the digester are effectively mixed by the movement of the impeller. On the occasions when the particle does move through this upper third of the digester, it is moving slowly and so spends a great deal of time in these cells. The occupancy plot for real sludge at 100 rpm is more similar to that of synthetic sludge and real sludge at 50 rpm than to synthetic sludge at 100 rpm.

At 50 rpm, for both synthetic and real sludge, the particle does not reach all parts of the digester, again providing little data above 120 mm above the base of the digester. As for the case of real sludge at 100 rpm, when the particle does move through the upper third of the digester, it is moving

slowly. For real sludge at 50 rpm, there is a gap in the data, level with the impeller blades, where the tracer particle has not been recorded in the 20 minute period. It is likely that the particle is moving at high velocity in this area and therefore does not spend a significant amount of time in the area, making it harder to detect, especially given that these measurements were carried out when the particle was at its lowest activity. As the particle moves at a lower velocity overall, compared to higher mixing speeds, the particle makes fewer “circuits” of the digester in the same amount of time. This is supported by the high occupancy tracks that the particle moves along between 60 and 120 mm above the base of the digester and also along the base of the digester. This low level of data capture close to the impeller, where the particle is moving at high velocity and is likely to be experiencing rapid changes in direction and velocity magnitude is a limitation of the PEPT technique, and has previously been noted by Chiti et al. (2011). Whilst this limitation will reduce the effectiveness of the technique, results may be improved by running the experiment for longer.

## **7.6 Azimuthally-averaged velocity**

The velocity magnitude, axial and radial velocities were also plotted as azimuthally-averaged variables, normalised by tip speed. These are shown in Figure 7.9 to Figure 7.14.

Whilst the lack of data points recorded at 50 rpm make it more difficult to build up a detailed picture of the flow patterns in the digester, it can be seen that, once normalised by tip speed, the flow patterns in the digester for both real and synthetic sludge at all mixing speeds are very similar. The mean normalised axial velocity plots demonstrate the upward flow of fluid along the wall of the digester directly above the impeller (centre line at 60 mm), with the fluid velocity reducing near the top of the digester. Directly above the impeller close to the impeller shaft, this flow is reversed, with the fluid moving down towards the impeller with a reduction in velocity away from the impeller near the top of the digester. The normalised axial velocity is close to zero near the liquid surface in the digester. Below the impeller, the mean axial velocity along the wall is negative as the fluid moves

towards the base of the digester, with the return flow towards the impeller taking place close to the centre line of the digester. These two loops of fluid circulation are representative of a radial flow impeller and can be seen with little difference across the mean normalised axial velocity plots at all mixing speeds.

The mean normalised radial velocity plots demonstrate that the highest flow rate towards the wall of the digester takes place level with and slightly above the impeller (in the range of 50-80 mm above the base of the digester). The rest of the digester experiences flow with little radial velocity, although a slight increase in negative radial velocity can be seen close to the base of the digester. This is more pronounced than the negative radial velocity in the recirculation loop above the impeller due to the limited space below the impeller. These results are limited by the low level of data capture in the impeller region, as explained in Section 7.5.

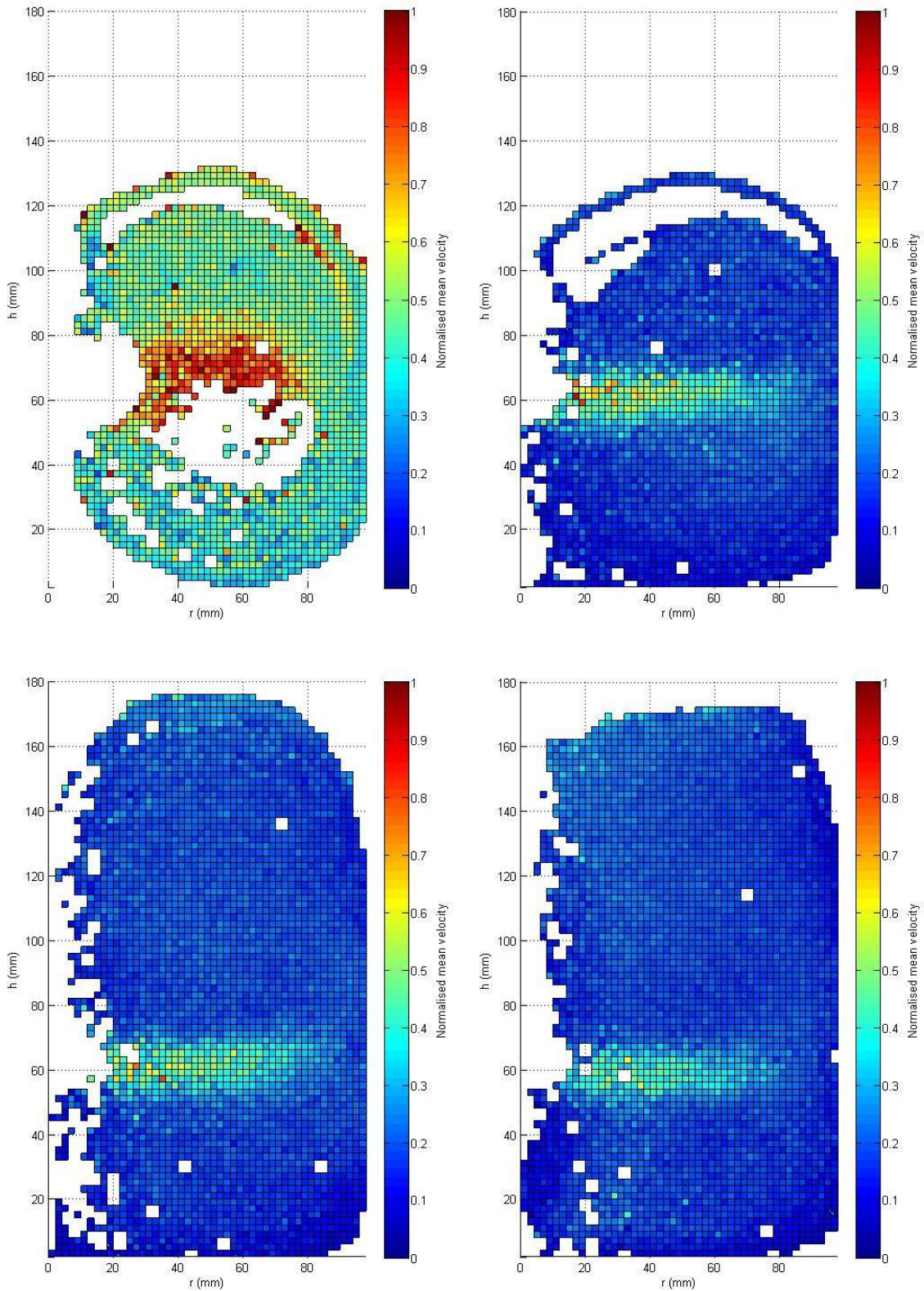


Figure 7.9 – Azimuthally-averaged velocity magnitude, normalised by tip speed, in a lab-scale anaerobic digester mixing real sludge at i). 50 rpm, ii). 100 rpm, iii). 150 rpm, and iv). 200 rpm

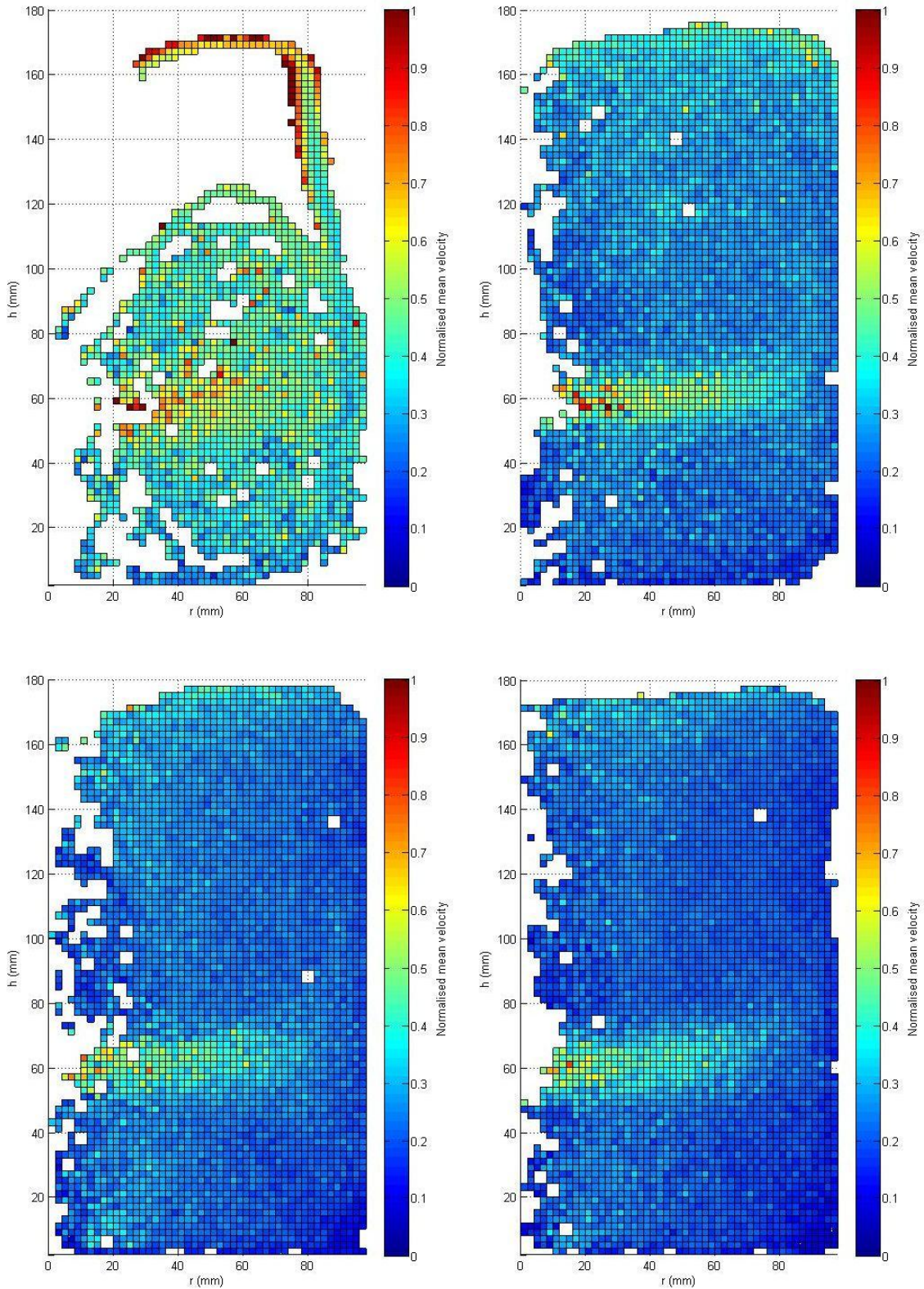


Figure 7.10 – Azimuthally-averaged velocity magnitude, normalised by tip speed, in a lab-scale anaerobic digester mixing synthetic sludge at i). 50 rpm, ii). 100 rpm, iii). 150 rpm, and iv). 200 rpm

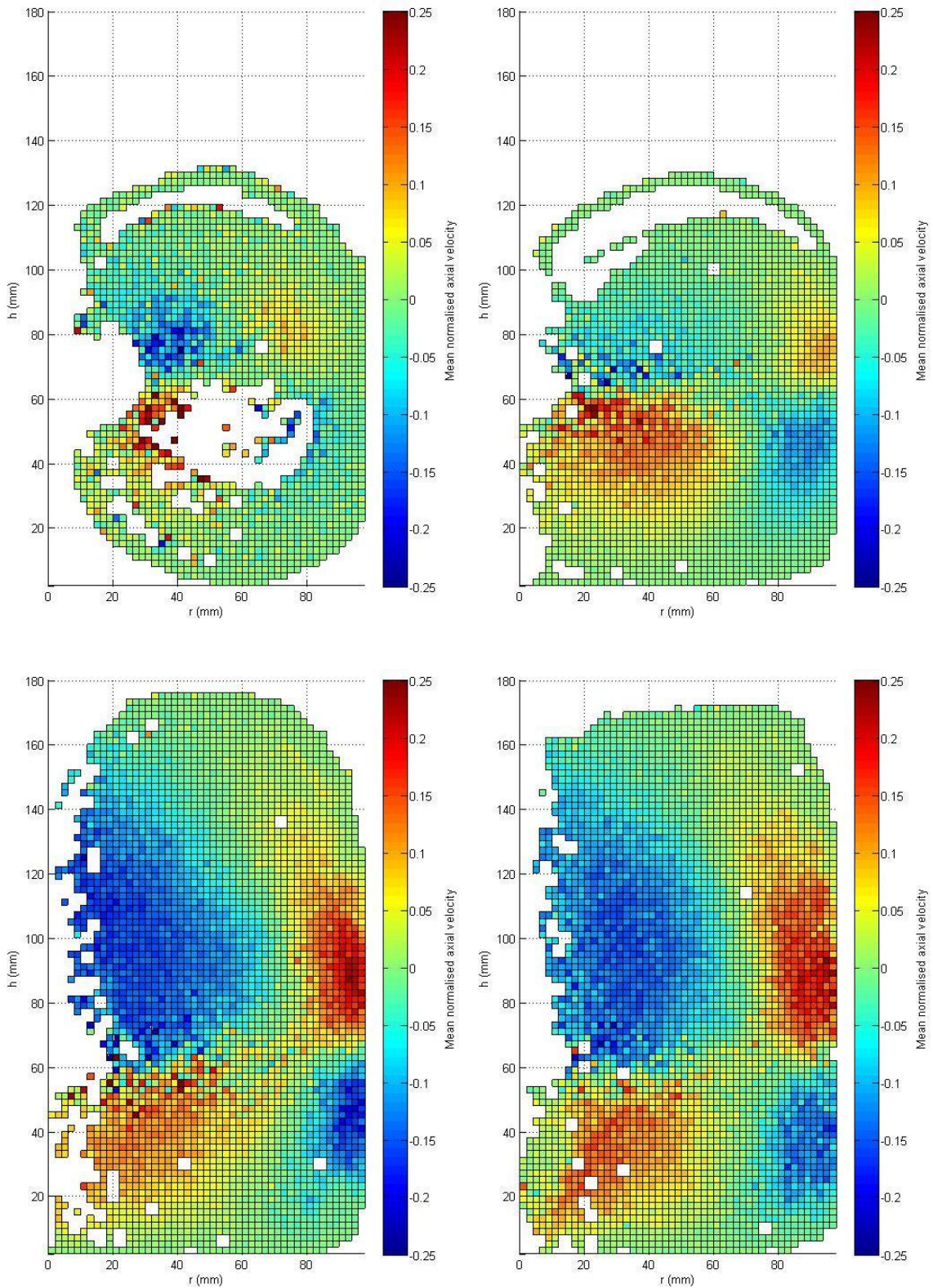


Figure 7.11 – Azimuthally-averaged axial velocity, normalised by tip speed, in a lab-scale anaerobic digester mixing real sludge at i). 50 rpm, ii). 100 rpm, iii). 150 rpm, and iv). 200 rpm

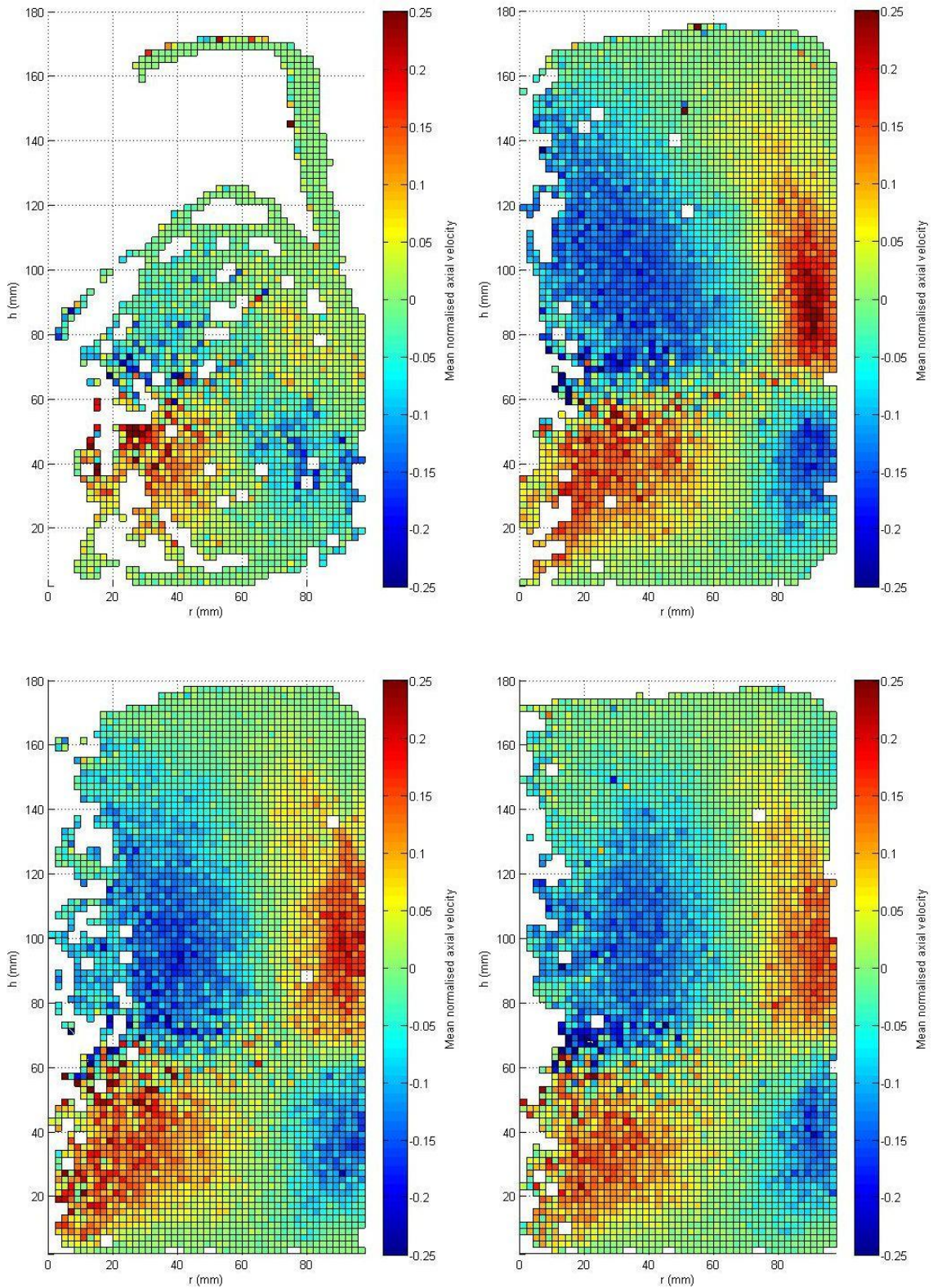


Figure 7.12 – Azimuthally-averaged axial velocity, normalised by tip speed, in a lab-scale anaerobic digester mixing synthetic sludge at i). 50 rpm, ii). 100 rpm, iii). 150 rpm, and iv). 200 rpm

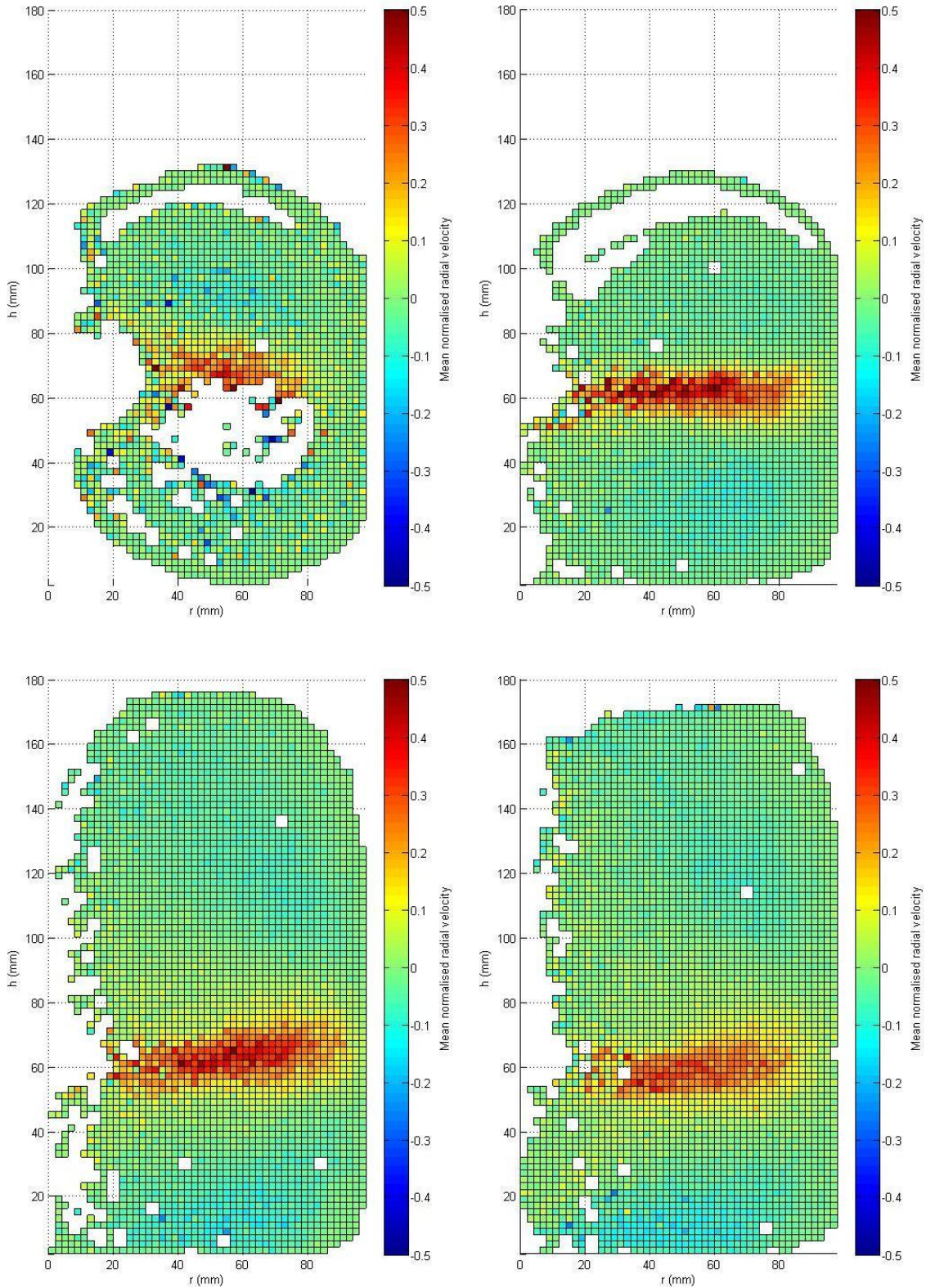


Figure 7.13 – Azimuthally-averaged radial velocity, normalised by tip speed, in a lab-scale anaerobic digester mixing real sludge at i). 50 rpm, ii). 100 rpm, iii). 150 rpm, and iv). 200 rpm

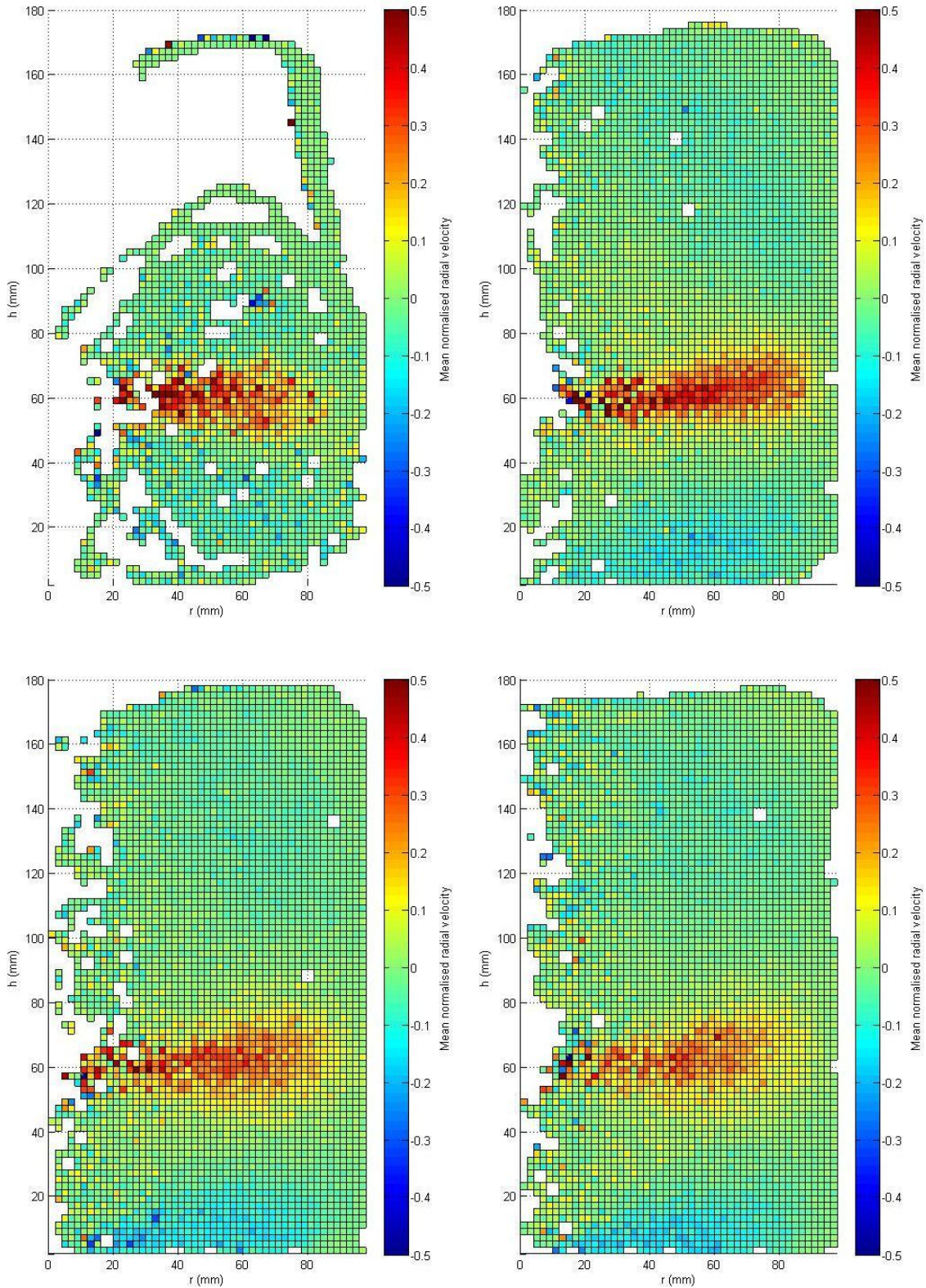


Figure 7.14 – Azimuthally-averaged radial velocity, normalised by tip speed, in a lab-scale anaerobic digester mixing synthetic sludge at i). 50 rpm, ii). 100 rpm, iii). 150 rpm, and iv). 200 rpm

## 7.7 Particle trajectory length analysis

PEPT lends itself well to analysis of mixing by use of the trajectory length distribution (TLD), a concept introduced by Villermaux (1996). The method depends on tracking a tracer particle within the flow over a significant period of time, and recording the length of the trajectories followed by the particle, from it leaving a reference surface to returning to that surface. From a high number of trajectories, a TLD can be built up and the mean trajectory length can be calculated. From this, Villermaux (1996) proposed a simple macromixing index,  $I_{mix}$ :

$$I_{mix} = \frac{\bar{l}}{L} \quad \text{Equation 7-5}$$

where  $\bar{l}$  is the mean trajectory length and  $L$  is a characteristic dimension of the vessel, for example, the vessel diameter.

A large value of  $I_{mix}$  would indicate efficient macro-mixing as the particle, which is assumed to accurately trace the fluid movement within the vessel, follows long trajectories compared to the size of the vessel.

In order to avoid the inherent uncertainty in the location of the tracer particle affecting the calculated trajectory length, a filtering method is used. All trajectories within the impeller region, i.e.  $50 < y < 70$  mm, were discarded and trajectories were considered to be the path taken by the particle from the last point at which it fell within this uncertainty band, to the next position within the band after the particle has visited other parts of the vessel. Following Fangary et al. (2000), the mean trajectory length,  $\bar{l}$ , was calculated for each experiment and the mean frequency of circulation,  $f$ , was calculated as:

$$f = \frac{N_t}{t} \quad \text{Equation 7-6}$$

where  $f$  is mean frequency of circulation,  $N_t$  is total number of trajectories, and  $t$  is total time of experiment. The mean circulation velocity of the fluid,  $\bar{v}$ , is then calculated as:

$$\bar{v} = f \times \bar{l} \quad \text{Equation 7-7}$$

This assumes that all fluid elements follow the mean trajectory length and circulate at the average frequency. Finally, by comparing the mean circulation velocity to the impeller tip speed,  $v_{tip}$ , an agitation index is calculated as:

$$I_{mix} = \frac{\bar{v}}{v_{tip}} \quad \text{Equation 7-8}$$

Figure 7.15 to Figure 7.17 show the mean frequency of circulation, the mean circulation velocity and the agitation index for the two sludges, plotted against mixing speed. Due to the lack of data points in the 40-50 mm reference surface at 50 rpm, the results suffer from inaccuracies as the start and end points of trajectories are more likely to be missed. This results in a smaller total number of trajectories with much longer trajectory lengths, thereby skewing the results.

As expected, it can be seen that as the mixing speed increases, so does the mean frequency of fluid circulation as the number of trajectories increases (Equation 7-6). The higher viscosity of the real sludge appears to reduce the magnitude of this effect in comparison to the synthetic sludge. In all cases, the mean circulation velocity (Equation 7-7) is higher than the mean velocity magnitude calculated in Section 7.4, though the general trend is still an increase in the mean circulation velocity as the mixing speed increases.

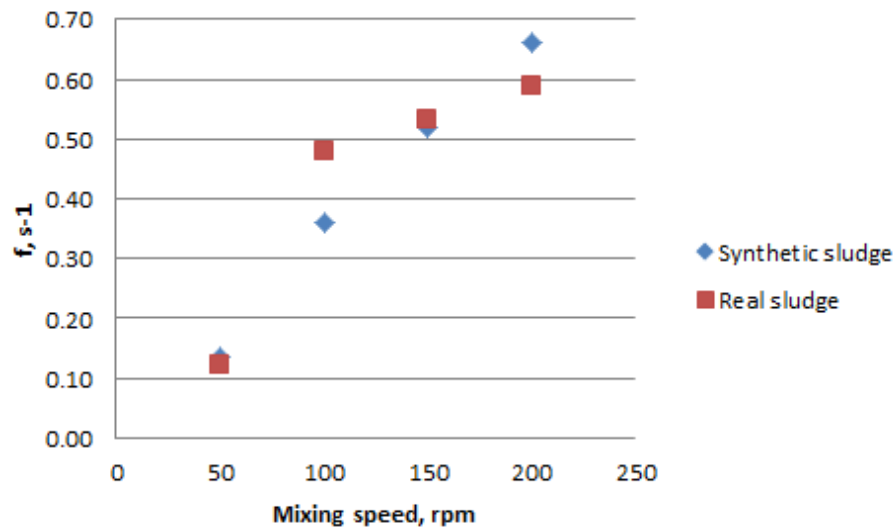


Figure 7.15 – Mean frequency of circulation in a lab-scale anaerobic digester mixing real or synthetic sludge

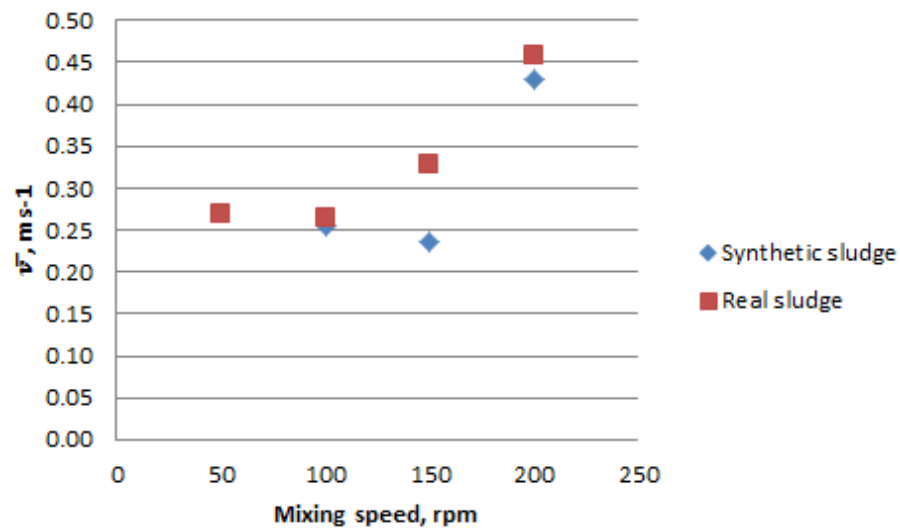


Figure 7.16 – Mean circulation velocity in a lab-scale anaerobic digester mixing real or synthetic sludge

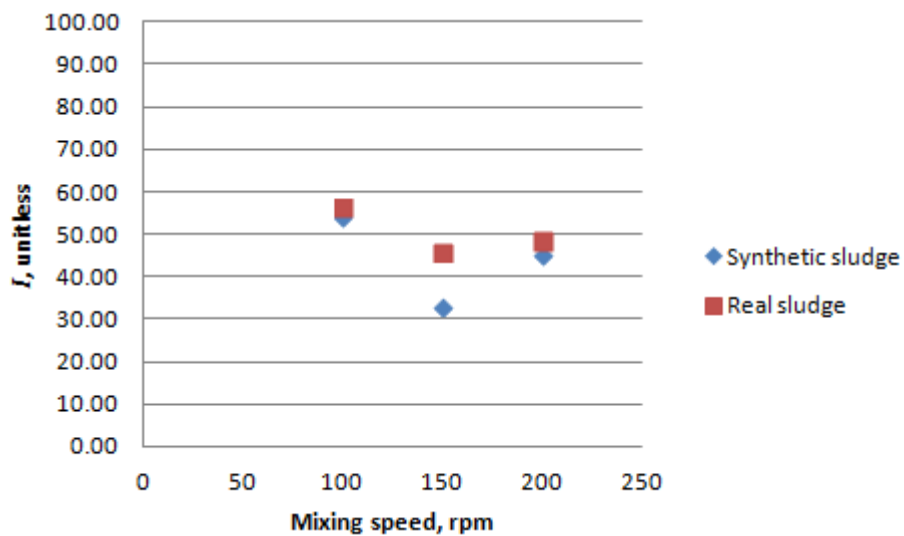


Figure 7.17 – Agitation index in a lab-scale anaerobic digester mixing real or synthetic sludge

With the exclusion of the data for 50 rpm, for the reasons stated above, the agitation index (Equation 7-8) is similar for all experiments, with an average of 44 % for the synthetic sludge and an average of 50 % for the real sludge. This agitation index is akin to the macromixing index proposed by Villiermaux (1996) and is an indication of the impeller's ability to impart motion to the fluid and is therefore a function of the impeller design and the fluid viscosity. These results suggests that the mixing is similarly efficient in the two sludges as the agitation index for the two sludges is within the 10 % maximum estimated error in calculating  $\bar{v}$ , based on the uncertainty associated with the location of the particle. As such, the difference in the sludge viscosity is not significant enough to produce large differences in the mixing efficiency of the impeller.

At 50 rpm when mixing both real and synthetic sludge and at 100 rpm when mixing real sludge, the low particle coverage of the digester demonstrates that the digester is poorly-mixed and under these conditions, it is likely that deposition of particles larger than the radioactive tracer particle will occur. This is likely to result in stratification of the digester, with a well-mixed and higher viscosity layer at the base of the digester and a less-well mixed and lower viscosity layer close to the top of the digester. This will have an impact on the gas production from different layers of the digester as food sources and micro-organisms are likely to be concentrated in the lower layer of the digester. The effects of the differences in the viscosity of stratified sludge on the results of this research are considered further in Section 10.2.

## 7.8 Summary

This chapter has used PEPT for the first time in order to assess the mixing patterns established at different mixing speeds in an anaerobic digester mixing real and synthetic sludge, both of which are opaque fluids. It has shown that the radioactive particle used in the PEPT experiments is small in relation to the Kolmogorov length scale in the digester and is nearly neutrally buoyant in both real

and synthetic sewage sludge. With the low Stokes number associated with the flow, the particle is likely to accurately track fluid motion in the digester during PEPT experiments.

The path line traced by the particle showed that at 150 and 200 rpm, the digester is well-mixed. At 50 rpm, the digester is poorly-mixed with the particle residing mainly in the bottom two-thirds of the digester. The top third of the digester is poorly covered by the particle, with the particle moving at low velocities, for extended periods of time, through the region. At 100 rpm, there is a difference in the behaviour of the real sludge and the synthetic sludge with the more viscous real sludge experiencing volumes of low particle coverage similar to both sludges at 50 rpm and the less viscous synthetic sludge appearing to be well-mixed. The effects of the difference in viscosity are also apparent when comparing the mean velocity magnitude of the two sludges.

Azimuthally averaged occupancy plots help to identify the location of volumes of poor particle coverage in the digesters, concentrated in the top third of the digester at 50 rpm and volumes where the particle becomes stuck, indicated by high occupancy, in very small areas close to the baffles and the base of the digester at higher mixing speeds. Azimuthally averaged velocity plots demonstrate the overall flow patterns in the digester, which are similar when normalised by tip speed. Areas of high axial velocity are found above and below the impeller as the sludge traces two circulation loops typical of a radial flow impeller. This is paired with a high radial velocity level close to the impeller as the sludge is pushed from the centre of the digester towards the walls.

The TLD analysis shows that the higher viscosity sludge results in a slower increase in fluid circulation as the impeller speed is increased but that at this magnitude, the difference has little effect on the agitation index, which is primarily a function of the impeller design.

## CHAPTER 8 CFD modelling

This chapter considers the simulation of the flow patterns generated by mechanical mixing in a lab-scale digester, using CFD. It will explain the numerical methods used to set up the model, and the verification and validation techniques used to test the accuracy and veracity of the simulated solutions against experimental data acquired during PIV and PEPT experiments. It aims to identify the flow patterns present in the modelled digester at different mixing speeds, and the distribution of turbulence and velocity gradients within the digester.

### 8.1 Model geometry

The CFD model is of a cylindrical vessel with a four-bladed flat impeller and four baffles spaced equally around the vessel wall. The geometry of the vessel and the detail of the impeller are shown in Figure 8.1. The dimensions of the vessel are given in Table 8.1.

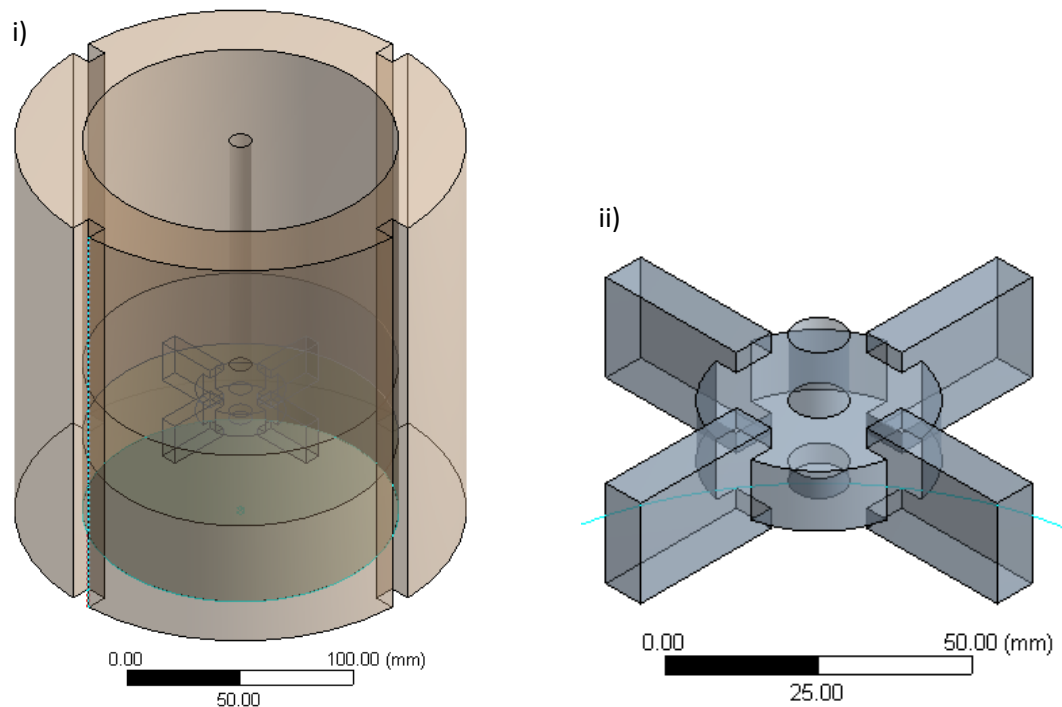


Figure 8.1 – Geometry of i). the digester vessel and ii). the impeller

**Table 8.1 - Dimensions of the digester vessel and impeller**

Vessel diameter	200 mm
Vessel height	200 mm
Impeller diameter	90 mm
Impeller height	20 mm
Impeller thickness	8 mm
Baffle depth	10 mm
Baffle thickness	10 mm
Inner section diameter	140 mm
Height of impeller centreline above base	60 mm

## 8.2 Numerical method

In order to develop a CFD model and use it to generate meaningful results, a number of settings must be determined, such as discretisation scheme, mesh density, turbulence model and boundary conditions. It is important that these are considered for each project as there are no universally applicable settings, and each CFD model represents its own challenges.

### 8.2.1 High performance computing facility

The high performance computing (HPC) facility at University of Birmingham, BlueBEAR, was used for all CFD simulations. BlueBEAR consists of 50 dual-processor 8-core (16 cores/node) 64-bit 2.2 GHz Intel Sandy Bridge E5-2660 worker nodes with 32 GB of memory, giving a total of 800 cores. Additionally there are 2 dual-processor 8-core (16 cores/node) 64-bit 2.2 GHz Intel Sandy Bridge E5-2660 log-on nodes as well as 2 dual-processor 8-core (16 cores/node) large memory (256 GB) nodes and 1 dual-processor 8-core (16 cores/node) log-on node with 64 GB of memory for applications that make use of graphical user interfaces (GUI). Simulations were set up using the BlueBEAR GUI node and then were run remotely on the worker nodes.

### 8.2.2 Software

Commercial CFD software, ANSYS Fluent 13.0 (ANSYS-Fluent, 2010a) was used to create the digester model. The geometry and mesh were created using ANSYS DesignModeler and ANSYS Meshing in ANSYS Workbench 13.0 (ANSYS-Fluent, 2010b).

### 8.2.3 Discretisation schemes

Fluent uses a finite volume method for discretisation of the governing equations. The simulations were run using a second-order upwind discretisation scheme for the convection terms, whilst the pressure terms were discretised using a central differencing scheme. The use of a second order convection scheme allows for better resolution of the gradients which in turn gives more accurate solutions than a first-order scheme. However, second-order schemes can take significantly longer to run. Following current best practice, simulations were run using a first-order convergence scheme until they were partially-converged and then a second-order convergence scheme was applied to reach a fully-converged solution.

The semi-implicit method for pressure-linked equations (SIMPLE) (Patanker and Spalding, 1972) was used for de-coupling pressure and velocity. This is an iterative scheme. It first solves the momentum equations and then solves the pressure-correction equation. This is used to correct velocity and pressure, and the momentum equations are resolved with these corrected variables. This loop is followed until convergence is reached. For all simulations, the residuals used to assess convergence (continuity, velocity components, turbulent kinetic energy, turbulent dissipation rate and Reynolds stresses) were set to  $1 \times 10^{-5}$  as recommended by best practice guidelines (ERCOFTAC, 2000).

### 8.2.4 Modelling rotating flows

The lab-scale digesters to be modelled in this work can be considered as a baffled cylindrical vessel mixed with a four-bladed rotating impeller. Clearly, the movement of the impeller within the vessel is vital to predicting the flow patterns that are established in the vessel. The two methods for

explicitly calculating the effects of a rotating flow are described in Section 3.2.4. In this work, the SM model is used in order to capture any unstable flows as the level of rotor-stator interaction is unknown, and using an MRF method would risk overlooking potentially important effects of this interaction on the overall flow patterns generated in the digester. For a model of this size, the increase in computational cost is not sufficiently large to make the SM model untenable when compared to the MRF approach.

### **8.2.5 Boundary conditions**

It is necessary to specify boundary conditions for all walls and the free surface in the digester model. All of the walls of the digester, including the base and the impeller blades, were specified using a no-slip condition. Accordingly, the velocity profile adjacent to the wall varies from zero at the surface to the free stream velocity in the bulk flow. In the region close to the wall, a boundary layer exists. The structure of this boundary layer is discussed in Section 3.1.4 and in order to capture this in the simulation, prism layer cells are used on all surfaces that are considered as walls. These cells are of similar dimensions to the cells nearby in the free stream, but have a very small thickness perpendicular to the wall so that the boundary layer is appropriately modelled. For the digester, five prism layer cells were used on each wall, with a growth rate of 1.2 and the thickness of the first cell being 0.1 mm. As the maximum  $y^+$  in the digester is 1.46, a wall function is not necessary.

The liquid free surface was modelled as a symmetry plane. This assumes that the surface is both flat and frictionless. Whilst some vortexing is likely to occur at the free surface, especially at higher mixing speeds, the extent to which this happens, and hence its effect on the overall flow patterns generated in the digester, is likely to be low. In order to model the shape of the liquid free surface, the VOF model could be used. This approach requires an expanded computational domain that includes the gas-liquid interface. The volume fraction of each phase is then determined throughout the domain by solving the continuity equation for the liquid phase. As such, a cell with a volume

fraction of one represents pure liquid and a volume fraction of zero represents pure gas. The interface between the liquid and gas that occurs at the liquid free surface is identified by cells with a volume fraction between zero and one (ANSYS-Fluent, 2012). The computational cost and complexity of modelling this phenomenon using a multiphase simulation is high. More importantly, Marshall and Bakker (2004) recommend that the VOF approach is not adopted for predicting vortex shape. Whilst they recognise that the VOF model can be applied to indicate whether vortexing will occur, they suggest that the model breaks down when the liquid-gas interface is broken, resulting in many small bubbles mixed with the liquid.

### **8.2.6 Mesh generation**

The mesh was generated using ANSYS Meshing in Workbench 13.0 (ANSYS-Fluent, 2010b). The unstructured mesh used was able to accommodate the complex geometry of the impeller, although the greater number of cells in the mesh as compared to a structured mesh increases computational time. Whilst hexahedral cells normally reduce the computational cost of the simulations, the complex nature of the geometry around the impeller means that cell size would have to be very small and hence the mesh would be very dense. Instead, the mesh makes use of tetrahedral cells. The number of cells required to ensure that the solutions are independent of the mesh density is determined in Section 8.3.1.

### **8.2.7 Turbulence models**

It was seen in Section 3.2.8 that the RANS model has been used extensively to accurately predict flow patterns in lab-scale digesters mixing non-Newtonian fluids. Whilst it is possible that the LES model may produce more accurate results, it has not been proven in the existing literature and that, combined with the high computational expense required for its implementation, do not make it an attractive option for this research. On the other hand, two-equation turbulence models of the  $k-\epsilon$  and  $k-\omega$  forms, have been shown to successfully model mechanical mixing of non-Newtonian sludge

previously (Bridgeman, 2012, Wu, 2010a). Hence, a RANS approach is used for this research. As such, the selection of the turbulence model used to close the RANS equations is important, as it ensures that the results of the simulations actually describe the real events that they are designed to model. The most applicable turbulence model is determined in Section 8.3.2. The models considered are the realisable  $k-\varepsilon$ , standard  $k-\omega$ , SST  $k-\omega$  and RSM, which are described in detail in Section 3.2.3. The standard  $k-\varepsilon$  model was not considered as existing literature has demonstrated that the realisable  $k-\varepsilon$  and standard  $k-\omega$  models are more applicable for this application (Bridgeman, 2012, Wu, 2010c, Wu, 2011).

### **8.3 Model verification and validation**

Before the results of the CFD model can be used, the model must be verified and validated. In short, verification can be described as “solving the equations right”, whilst validation shows that the model “solves the right equations” (Roache, 1998). Verification of the model requires a test that the mesh density is sufficient to capture the flow variations across the model and give some indication of what is considered to be a converged solution. Validation of the model requires that the underlying assumptions on which the model is based are justified and that the model results fit well with experimental or real-life results.

#### **8.3.1 Model verification: mesh density**

Verification of a model should convincingly demonstrate that it is capable of solving the equation to a suitable order of convergence. It then demonstrates that the equations have been solved to a rationally estimated accuracy or error band.

The Grid Convergence Index (GCI) (Roache, 1998) is a simple method to report grid convergence without being limited to doubling the number of cells in each consecutive grid as was the case with previous approaches to grid convergence. This allows the grid density to be analysed to provide an

indication of error bands. Velocity magnitude values were extracted for 500 individual points along a vertical line at  $r/R = 0.6$ , and the GCI was calculated as:

$$GCI = F_s \frac{e_{rms}}{r^2 - 1} \quad \text{Equation 8-1}$$

$$e_{rms} = \sqrt{\frac{\sum_{m=1}^{750} |(u_{m,1} - u_{m,2})/u_{m,2}|^2}{500}} \quad \text{Equation 8-2}$$

$$r = \left(\frac{h_2}{h_1}\right)^{1/3} \quad \text{Equation 8-3}$$

where  $u_m$  is velocity magnitude at point  $m$ ,  $h$  is the number of cells in the mesh and subscripts 1 and 2 refer to coarse and fine mesh respectively. A factor of safety of  $F_s = 1.25$  was applied in accordance with published recommendations for the comparison of multiple grids (Roache, 1998).

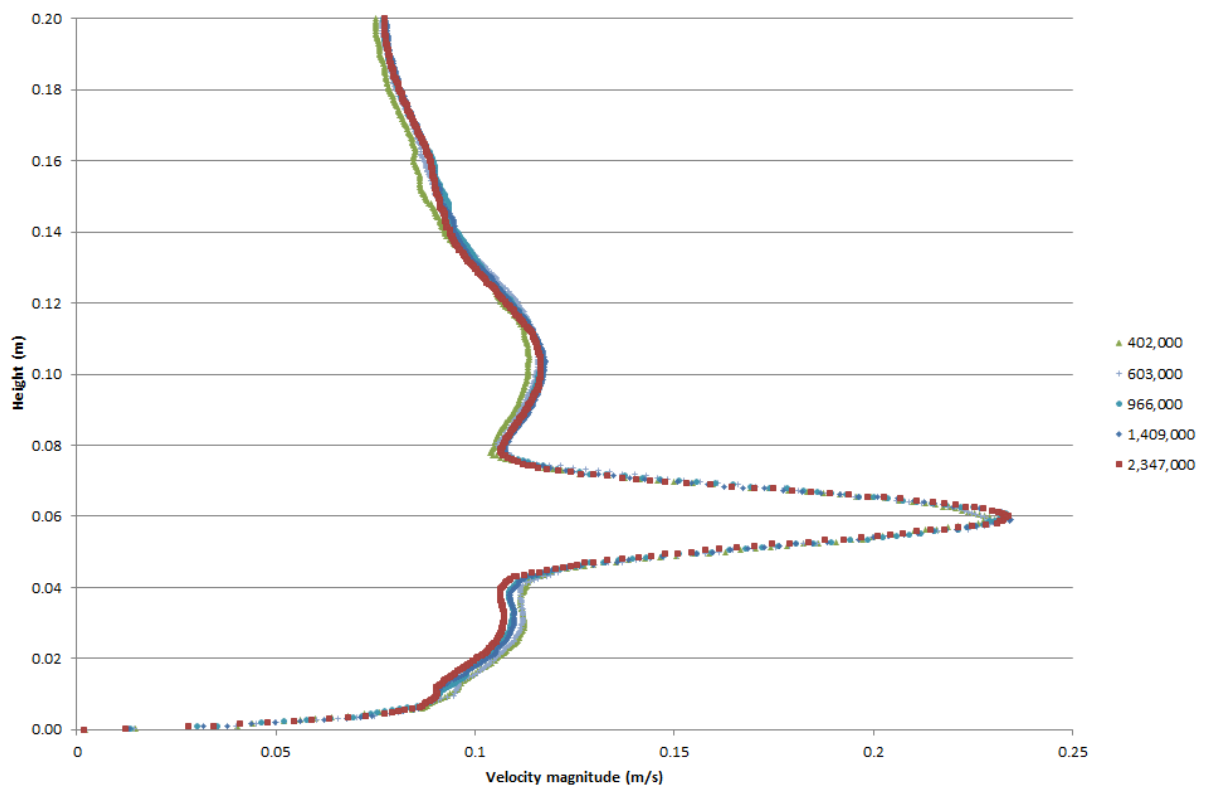


Figure 8.2 – Comparison of velocity magnitude from varying grid densities along a line,  $r/R = 0.6$

Five grid densities were tested: 402,000, 603,000, 966,000, 1,409,000 and 2,347,000 and the velocity magnitude along a line at  $r/R = 0.6$  was plotted in Figure 8.2. Taking the coarsest mesh as a baseline, GCIs were calculated for the finer grids as 9.6 % (603,000), 7.5 % (966,000), 5.9 % (1,409,000) and 5.7 % (2,347,000). From this, it can be seen that the solutions from the two finest grids approach solution convergence. Whilst the two grids fall slightly outside the 95 % confidence interval, the increase in computing time when increasing the mesh density from 1,409,000 to 2,347,000 was not considered to reflect a corresponding increase in the accuracy of the results and as such, the 1,409,000 cell grid was used to calculate flow patterns in the digester. Thus, error bars of 6 % can be attached to the results of the simulations undertaken.

### 8.3.2 Model validation: turbulence model selection against PIV

Validation is the process of showing that the results of the model are capable of describing the real events that they are designed to model. This is normally achieved by carrying out a number of experiments and comparing the results of the model to the results of the experiments. In this case, the results from a number of simulations which made use of various turbulence models were compared to the results of PIV experiments carried out in a clear plastic replica digester mixing 0.5 g/l CMC solution at 100 rpm.

The non-Newtonian fluid model used to model the viscosity of the CMC was calculated from viscosity measurements carried out as detailed in Section 5.2.6. The model uses a density of  $998 \text{ kg/m}^3$  and follows a non-Newtonian power law model,  $\eta = k\dot{\gamma}^n$ , with consistency index,  $k = 0.0707 \text{ Pa}\cdot\text{s}^{0.6052}$ , power law index,  $n = 0.6052$  and allowable viscosity range of 0.004-0.012 kg/m-s. The turbulence models tested were the realisable  $k-\varepsilon$ , standard  $k-\omega$ , SST  $k-\omega$  and RSM.

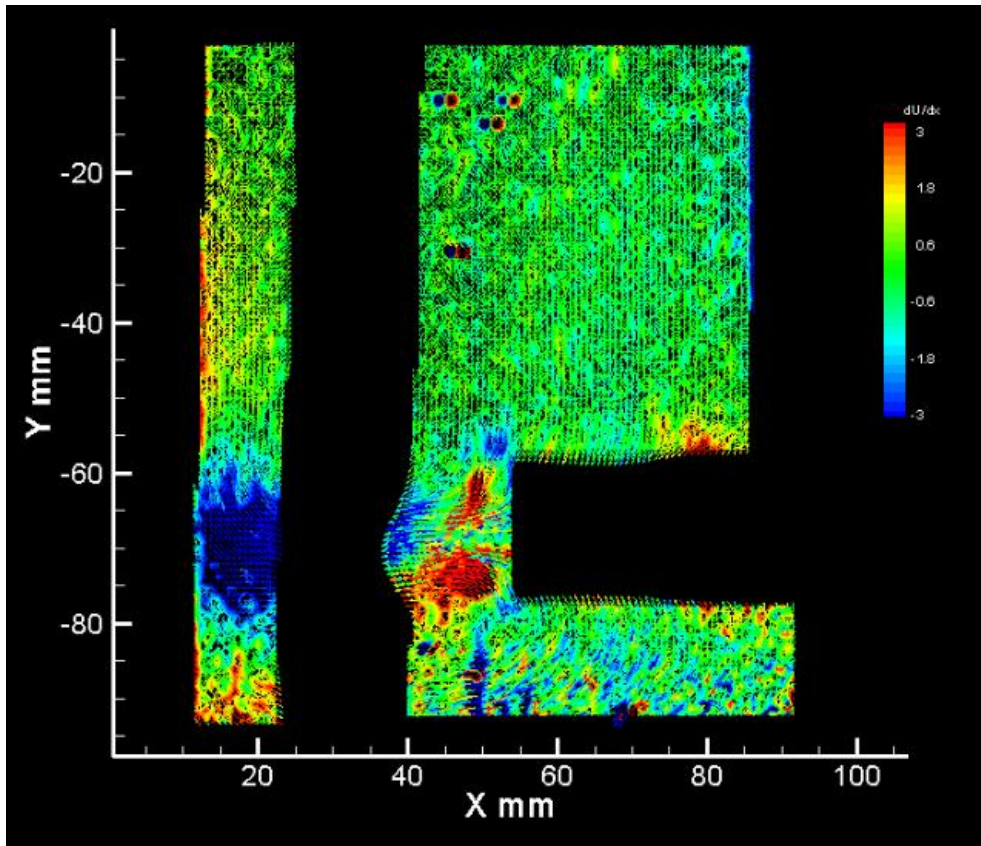


Figure 8.3 -  $u$  velocity vector plots of CMC mixed in a lab-scale digester at 100 rpm, measured using PIV

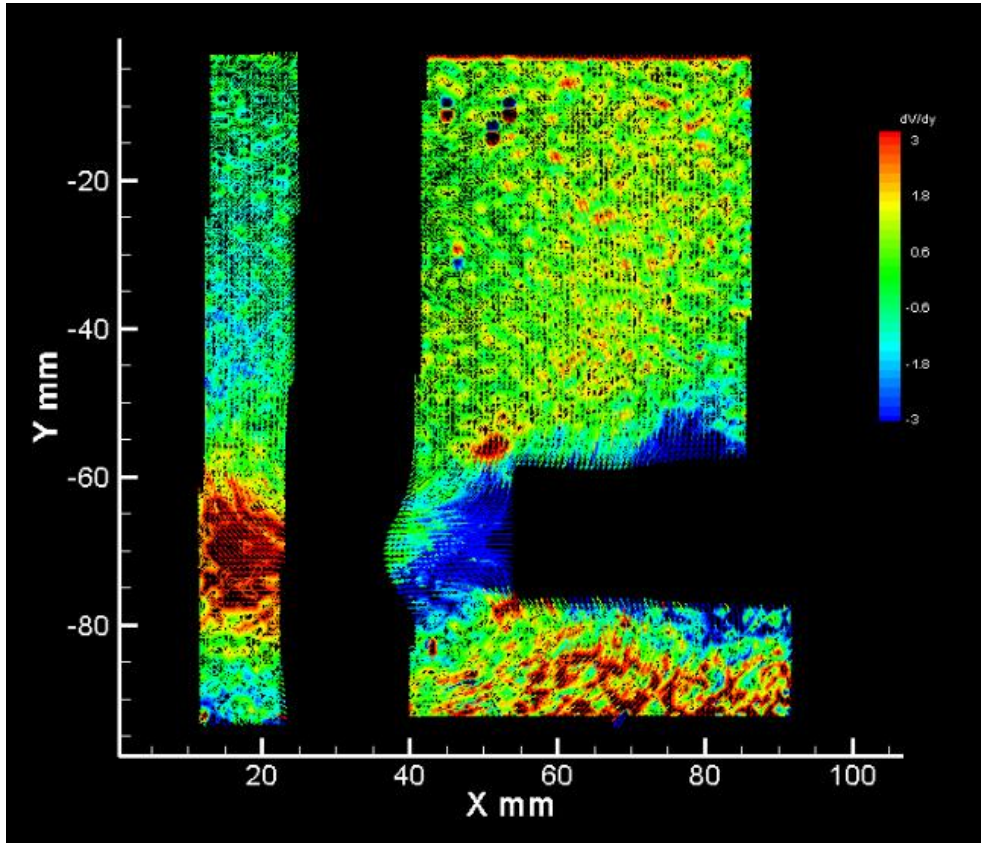


Figure 8.4 -  $v$  velocity vector plots of CMC mixed in a lab-scale digester at 100 rpm, measured using PIV

Figure 8.3 and Figure 8.4 show vector plots of the  $u$  and  $v$  velocities measured in the bottom two-thirds of the digester using PIV. It can be seen that the highest velocity particle movement occurs in the impeller region, where the fluid is pushed towards the digester wall and then moves either up or down along the wall to form two loops of fluid circulation. This is typical flow pattern of a radial flow impeller like the one used in this digester and agrees with the velocity contours measured using PEPT.

Figure 8.5 and Figure 8.6 show the  $u$  and  $v$  velocities along a line at  $r/R = 0.6$  with results extracted from the PIV results shown in Figure 8.3 and Figure 8.4 as well as from the CFD models. It can be seen that all four turbulence models are able to recreate the general shape of the  $u$  and  $v$  velocity plots for the PIV data. For all of the turbulence models, the peak  $u$  velocities in the impeller region are predicted to be slightly higher than the peak demonstrated by the PIV data. The magnitude of the peak  $u$  velocity is best predicted by the SST  $k-\omega$  model and the RSM. Both the standard  $k-\omega$  and the realisable  $k-\epsilon$  models underestimate the magnitude of the peak. Below the impeller, all four of the turbulence models follow the same curve and all four underestimate the magnitude of the  $u$  velocity.

There are significant differences between the four turbulence models considered above the impeller. Unfortunately, due to the limited frame used in the PIV data, the behaviour of the sludge in the top third of the digester was not monitored and no comparison between the CFD and PIV data can be made. Furthermore, the majority of literature does not give details of the velocity components away from the impeller near the top of the mixed vessels. However, results from a similar sized vessel, in which water was mixed using a six-blade Rushton turbine, show a similar velocity profile above the impeller to that modelled using the realisable  $k-\epsilon$  turbulence model (Rammohan et al., 2001). Whilst this does not take into account the non-Newtonian properties of the sludge, it has to serve as a best approximation in the face of a lack of more applicable data.

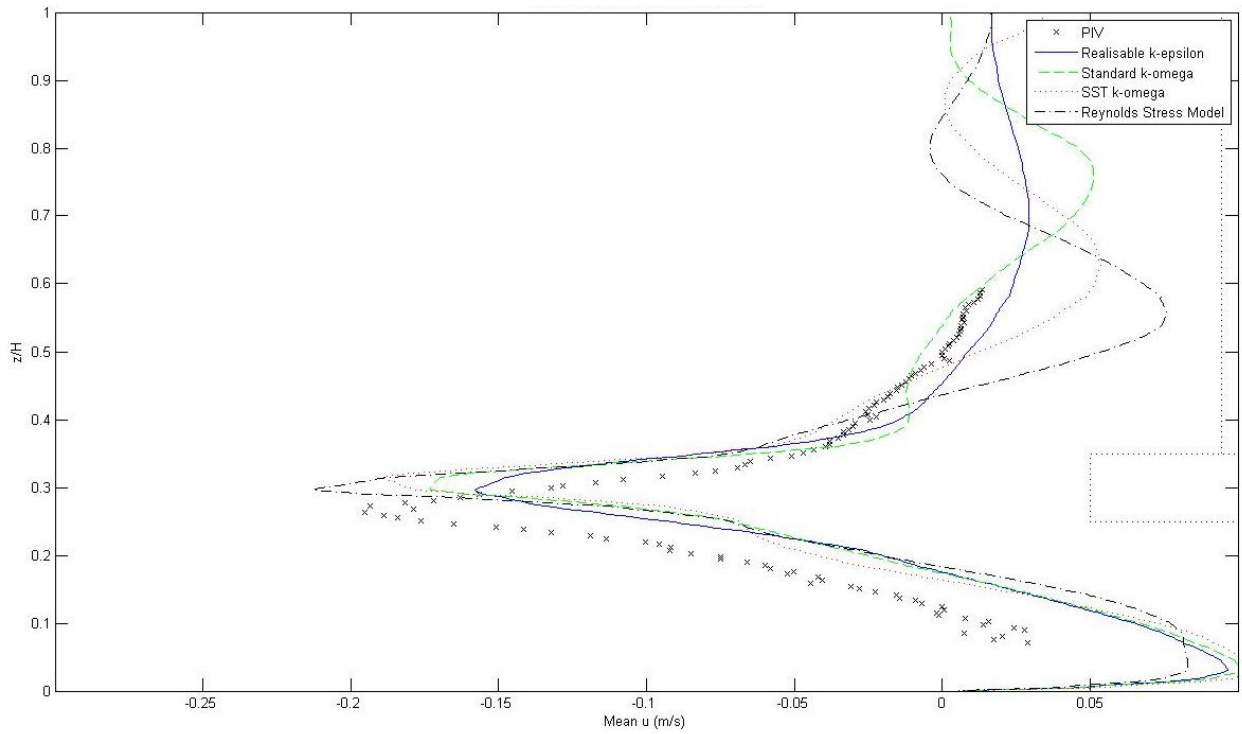


Figure 8.5 –  $u$  velocities along a line at  $r/R = 0.6$  modelled using four different turbulence models, as compared to results from PIV

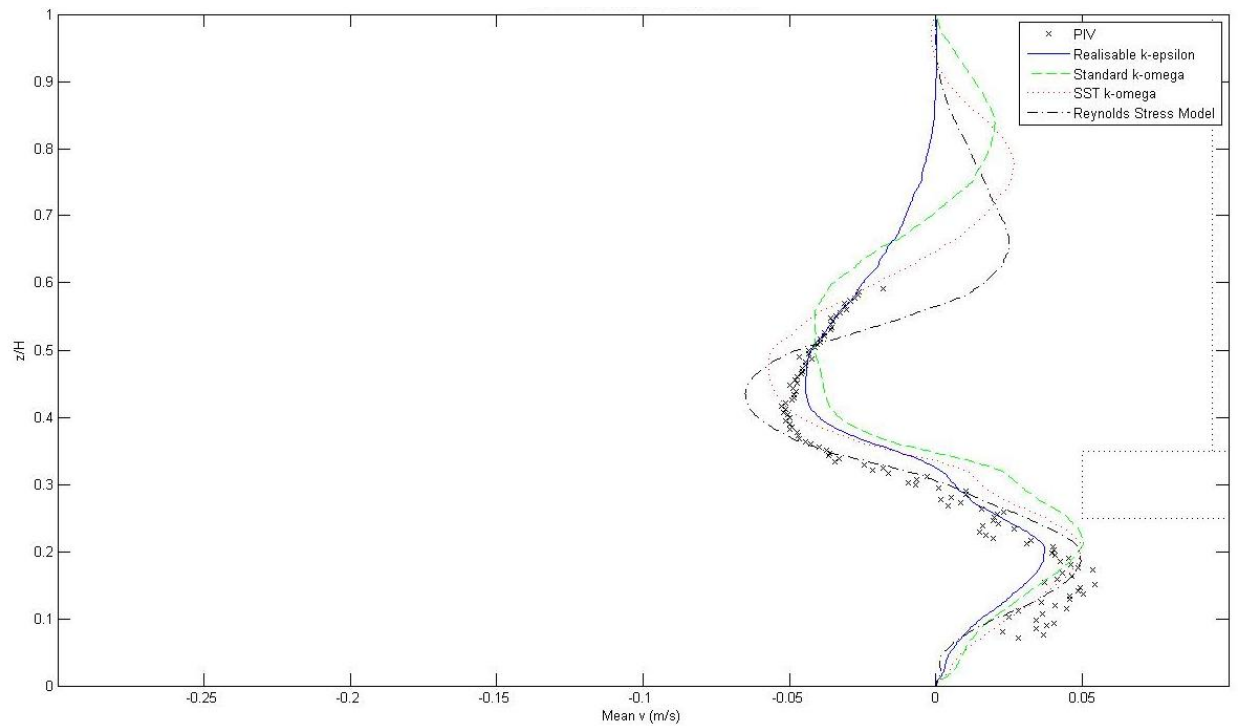


Figure 8.6 –  $v$  velocities along a line at  $r/R = 0.6$  modelled using four different turbulence models, as compared to results from PIV

In the area directly above the impeller, the  $u$  velocities predicted by the realisable  $k-\epsilon$  model are closest to the shape and magnitude of the PIV data. Whilst parts of this curve are well followed by

the standard  $k-\omega$  and the SST  $k-\omega$  models, the RSM does not predict the  $u$  velocities well in this area. Previous literature relating to CFD models of digesters have not made use of the RSM turbulence model due to the high computational cost of solving the extra equations involved and are often poorly validated using single data point techniques such as comparison to power number. As such, it is not clear if the RSM regularly overestimates peaks in velocity components of non-Newtonian sludge mixing away from the impeller region.

As for the  $u$  velocities, the location and magnitude of peak  $v$  velocities are well predicted by the CFD models, with the standard  $k-\omega$ , SST  $k-\omega$  and RSM all predicting the magnitude of the peak below the impeller very well despite placing it slightly higher in the digester than it is seen to occur from the PIV data. The realisable  $k-\varepsilon$  model is better at locating the peak, though it underestimates the magnitude. This is also true when considering the peak above the impeller. This is well-located by the SST  $k-\omega$  and RSM as well, though these models overestimate the magnitude of the peak. The standard  $k-\omega$  model underestimates the magnitude of this peak but predicts a wider peak than is identified by the PIV data. The realisable  $k-\varepsilon$  model predicts the uppermost PIV data points with a high level of accuracy.

From the  $u$  and  $v$  velocity PIV data, the turbulent kinetic energy (TKE) was calculated from two-dimensional data according to:

$$k = 0.75(\overline{(u')^2} + \overline{(v')^2}) \quad \text{Equation 8-4}$$

where  $u'$  and  $v'$  are the fluctuating components of velocity components in the  $x$  and  $y$  directions.

This was compared to the TKE predicted by the CFD models as shown in Figure 8.7. Whilst all four of the turbulence models are able to predict the location of the peak TKE, none of the models predict the magnitude of the peak well. The best of the models is the realisable  $k-\varepsilon$  model which predicts

approximately 65 % of the peak magnitude. The other three models predict less than 15 % of the peak magnitude.

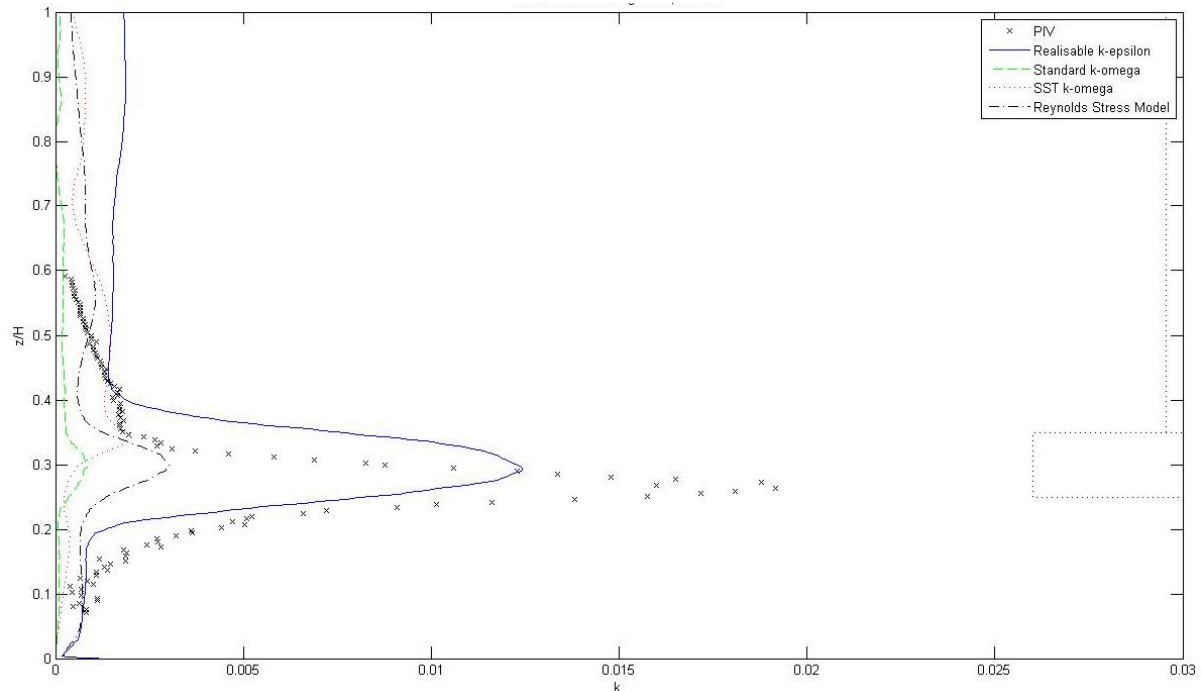


**Figure 8.7 – Turbulent kinetic energy,  $k$ , along a line at  $r/R = 0.6$  modelled using four different turbulence models, as compared to results from PIV**

Whilst the realisable  $k-\epsilon$  model underestimates the peak magnitudes of both velocity and TKE, it appears to be the best fit to the PIV data. It is also the best at predicting the TKE, which is of importance when predicting velocity gradients. As such, all further results are based on simulations which make use of the realisable  $k-\epsilon$  model unless otherwise stated. This is in agreement with the work of Wu (2011) and Bridgeman (2012), who both similarly found that the realisable  $k-\epsilon$  turbulence model was the most suitable for modelling sludge mixing.

### 8.3.3 Model validation: comparison to PEPT

CFD models of the digester were run using the realisable  $k-\epsilon$  model and a non-Newtonian fluid model that represents the sludge in the lab-scale digesters used in the experimental work. This follows a power law model,  $\eta = k\dot{\gamma}^n$ , and has consistency index,  $k$ , of  $0.0249 \text{ Pa}\cdot\text{s}^{0.555}$ , power law index,  $n$ , of 0.781, and allowable viscosity range of 0.004 – 0.009 kg/m-s. Figure 8.8 and Figure 8.10 show the

normalised velocity magnitude and normalised axial and radial velocity contour plots for sludge mixed at 50 rpm, 100 rpm and 200 rpm, as modelled using CFD. These results are plotted on a vertical plane through the centre of the impeller and can be directly compared to the azimuthally averaged normalised velocity magnitude and normalised axial and radial velocity plots measured using PEPT and shown in Figure 7.10, Figure 7.12 and Figure 7.14 respectively. As with the PEPT data, once normalised by tip speed, the CFD-generated flow patterns in the digester at all mixing speeds are very similar.

The plots of normalised velocity magnitude show that the bulk of the digester experiences a normalised velocity magnitude of approximately 0.3. Between the impeller blades and the digester wall is an area of higher normalised velocity magnitude. Whilst the distinction between low normalised velocities is not as easily seen on the PEPT plots as on the CFD plots, the contours on the two plots are very similar.

The normalised axial velocity plots from the CFD models demonstrate the two circulation loops, which are characteristic of a radial flow impeller and again, are a close match to those of the PEPT plots. The normalised radial plots from the CFD models demonstrate the areas of high normalised radial velocity between the impeller blades and the digester walls. Close to the base of the digester, an area of negative normalised radial velocity can be seen, as the fluid returns from the digester wall to the centre of the digester.

The high level of similarity between the CFD models and the PEPT data indicates that the CFD models are capable of giving a true and accurate representation of the velocity magnitude, radial velocity and axial velocity experienced by the synthetic sludge in the digester.

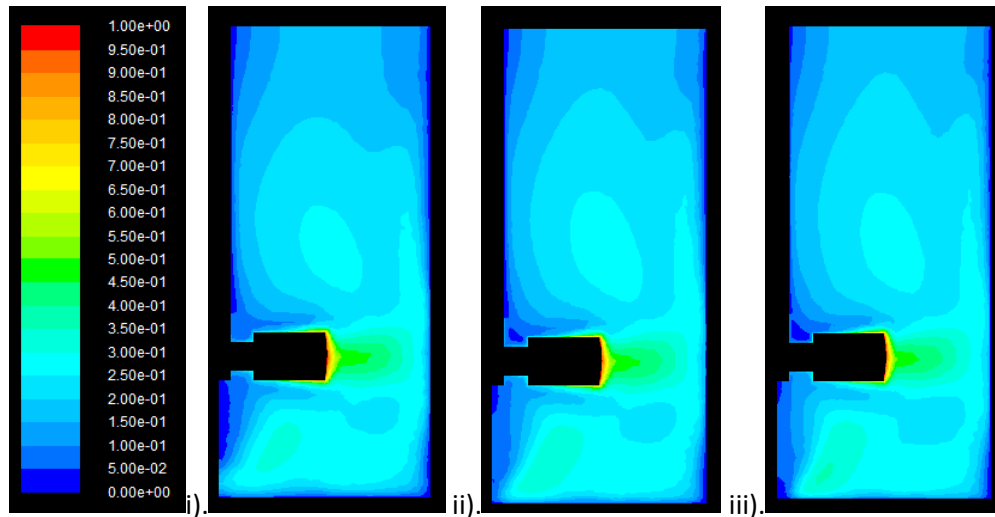


Figure 8.8 - CFD contour plots of normalised velocity magnitude for synthetic sludge mixed at i). 50 rpm, ii). 100 rpm and iii). 200 rpm

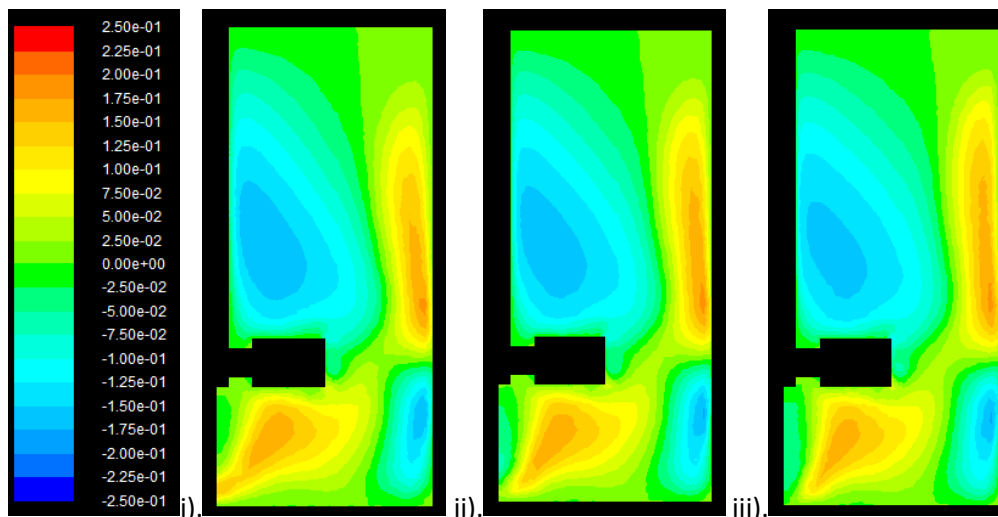


Figure 8.9 - CFD contour plots of normalised axial velocity for synthetic sludge mixed at i). 50 rpm, ii). 100 rpm and iii). 200 rpm

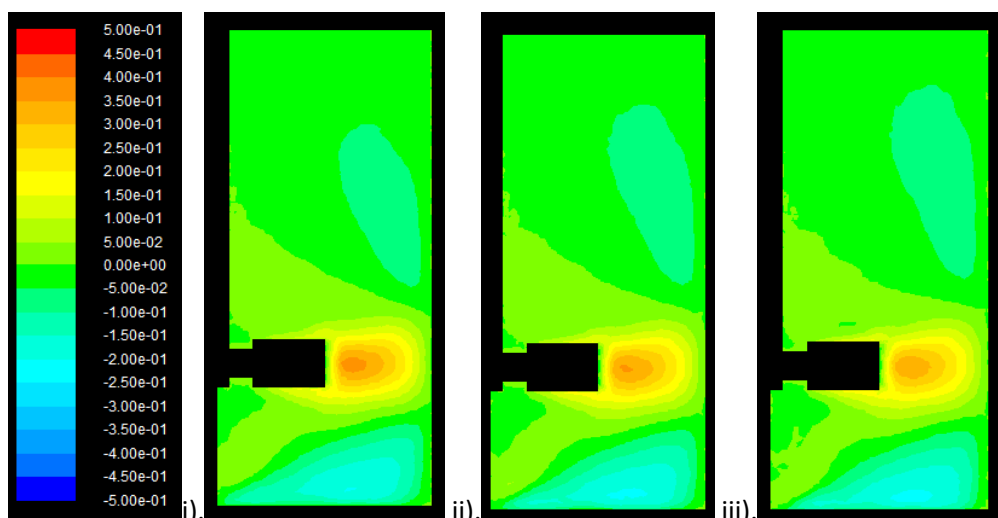


Figure 8.10 - CFD contour plots of normalised radial velocity for synthetic sludge mixed at i). 50 rpm, ii). 100 rpm and iii). 200 rpm

## 8.4 Velocity contours

Figure 8.11 shows contours of velocity magnitude in the digester at mixing speeds of 50, 100 and 200 rpm respectively on two planes through the digester: a vertical plane passing through the centre of the digester and a horizontal plane at  $y = 0.06$  m above the base of the digester, which passes through the centre of the impeller. From these, it can be seen that the highest velocity magnitude in the digester is found close to the impeller, with velocity magnitude decreasing towards the walls of the digester and above and below the impeller. The lowest velocities are found at the top of the digester, furthest from the impeller. These results are in agreement with published literature that describes the unconfined mechanical mixing of non-Newtonian sludge (Yu et al., 2011, Wu, 2012a).

In the impeller region, it is not surprising to find that the highest velocity magnitudes are found around the impeller tips. Velocity magnitude in the wake of the impeller blades is greater than that in front of the impeller blades. This is typical of a flat-blade impeller. In all cases, the highest velocity magnitude experienced in the digester is in the wake of the impeller blades and is approximately 17 % higher than the tip speed. This demonstrates the presence of a recirculation region behind the impeller blades.

A much smaller recirculation zone appears in front of the baffles, indicated by the small region of higher velocity magnitude, than that behind the baffles. Behind the baffles, the low velocity magnitude indicates the likely presence of a small dead zone. From the vertical plane through the digester, it can be seen that above the impeller, the velocity magnitude falls as the fluid moves higher up the digester and further from the impeller blades. Close to the top of the digester there are again small volumes close to the digester walls and the impeller shaft that experience very low velocity magnitude, suggesting the presence of dead zones. Similarly, below the impeller, there is an area of nearly stationary fluid directly below the impeller shaft.

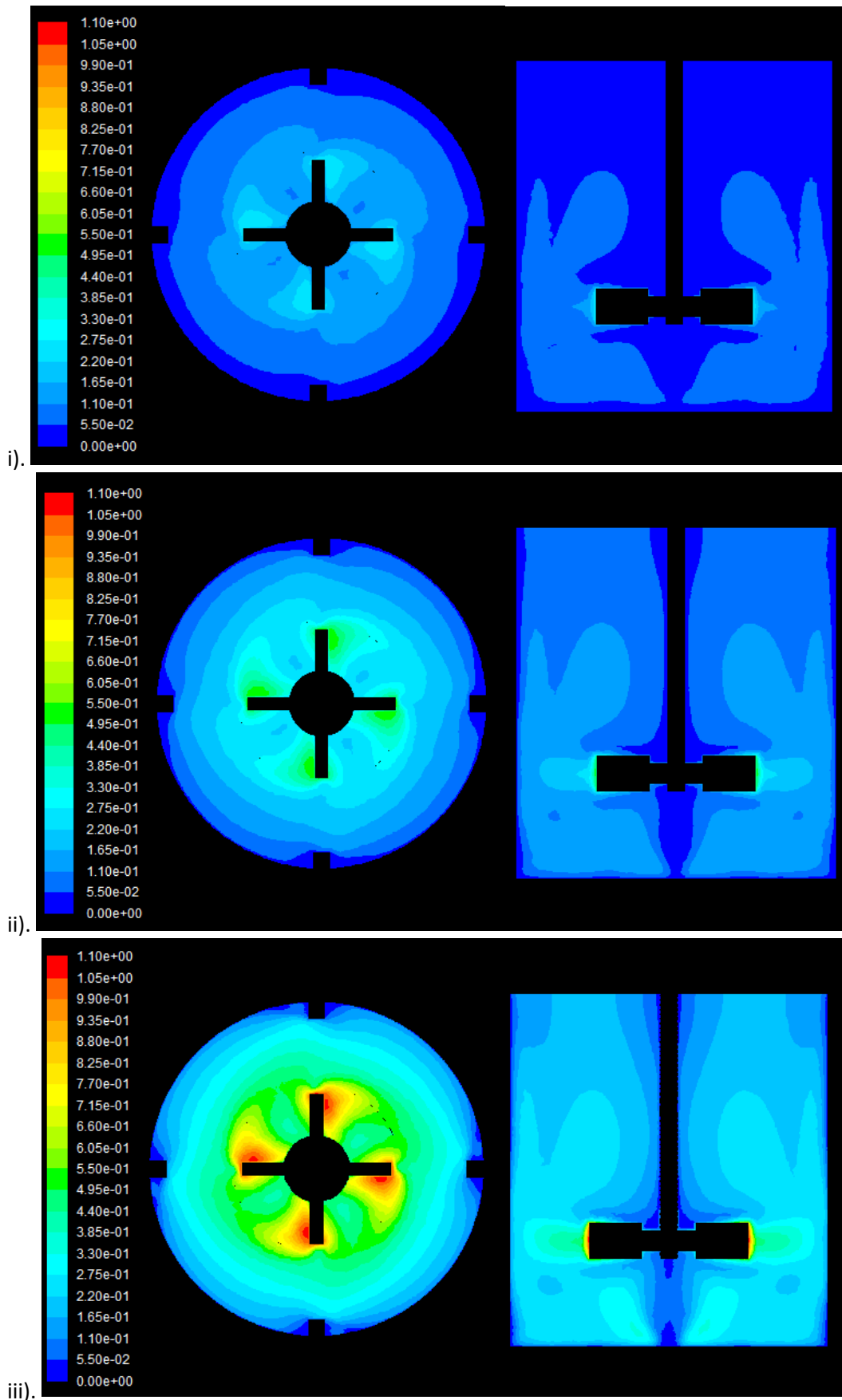


Figure 8.11 – Contour plots of velocity magnitude for digesters mixed at i). 50 rpm, ii). 100 rpm and iii). 200 rpm

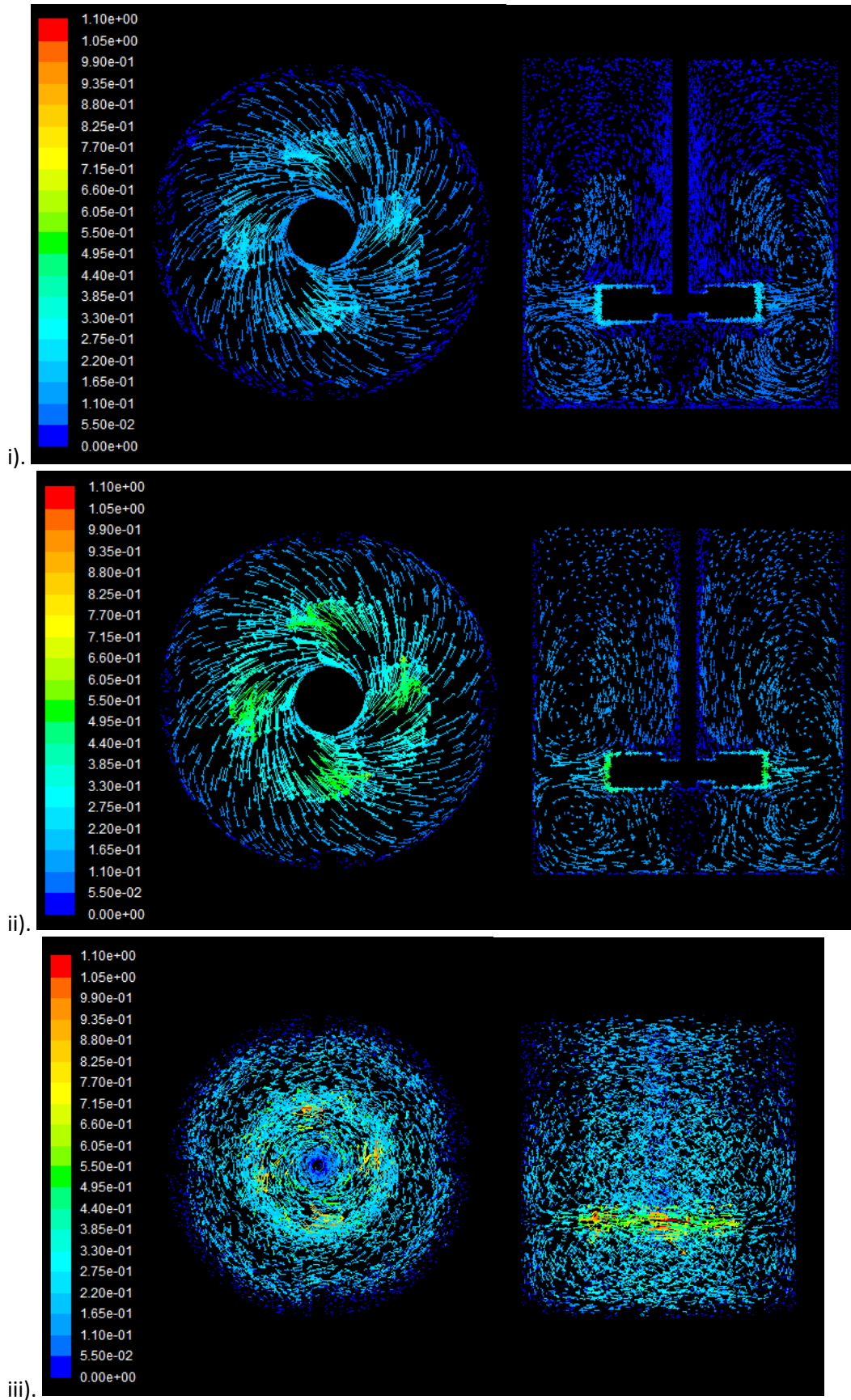


Figure 8.12 – Vector plots of velocity coloured by velocity magnitude for digesters mixed at i). 50 rpm, ii). 100 rpm and iii). 200 rpm

Whilst the velocity magnitude is proportional to the tip speed of the impeller, the contours that arise in the digester at each of the mixing speeds are similar. Velocity vectors coloured by velocity magnitude are shown in Figure 8.12 for the digesters at 50, 100 and 200 rpm respectively. From these, the circulatory loops above and below the impeller are clearly visible. At 50 and 100 rpm, fluid in the top third of the digester experiences velocity magnitudes of less than  $0.055 \text{ m s}^{-1}$ , suggesting the existence of extensive unmixed zones. This is corroborated by the PEPT results in Section 7.6. At 200 rpm, velocity magnitudes of  $0.275 \text{ m s}^{-1}$  are experienced throughout the digester, with the exception of small dead zones close to the walls at the top of the digester.

Figure 8.13 and Figure 8.15 show the axial, radial and tangential velocity contours respectively in the digester at mixing speeds of 50, 100 and 200 rpm respectively. Once again, the flow patterns that exist in the digesters at each of the three mixing speeds are similar, though the magnitude of the velocities involved increases as the mixing speed increases. It can be seen that, at all mixing speeds, the magnitude of the tangential velocity component is greater than the axial and radial velocity components. This can be attributed to the swirling motion set up in the digester by the movement of the impeller blades. As such, the tangential velocity component is highest in the region of the impeller and specifically, in the near wake of the impeller and close to the impeller tips. In the bulk of the digester, the tangential velocity is much lower than in the impeller region and is similar in magnitude to that of the axial velocity. The presence of small recirculation regions behind the baffles, highlighted in the velocity magnitude contour plots, is seen in the tangential velocity contour plots as regions of negative tangential velocity.

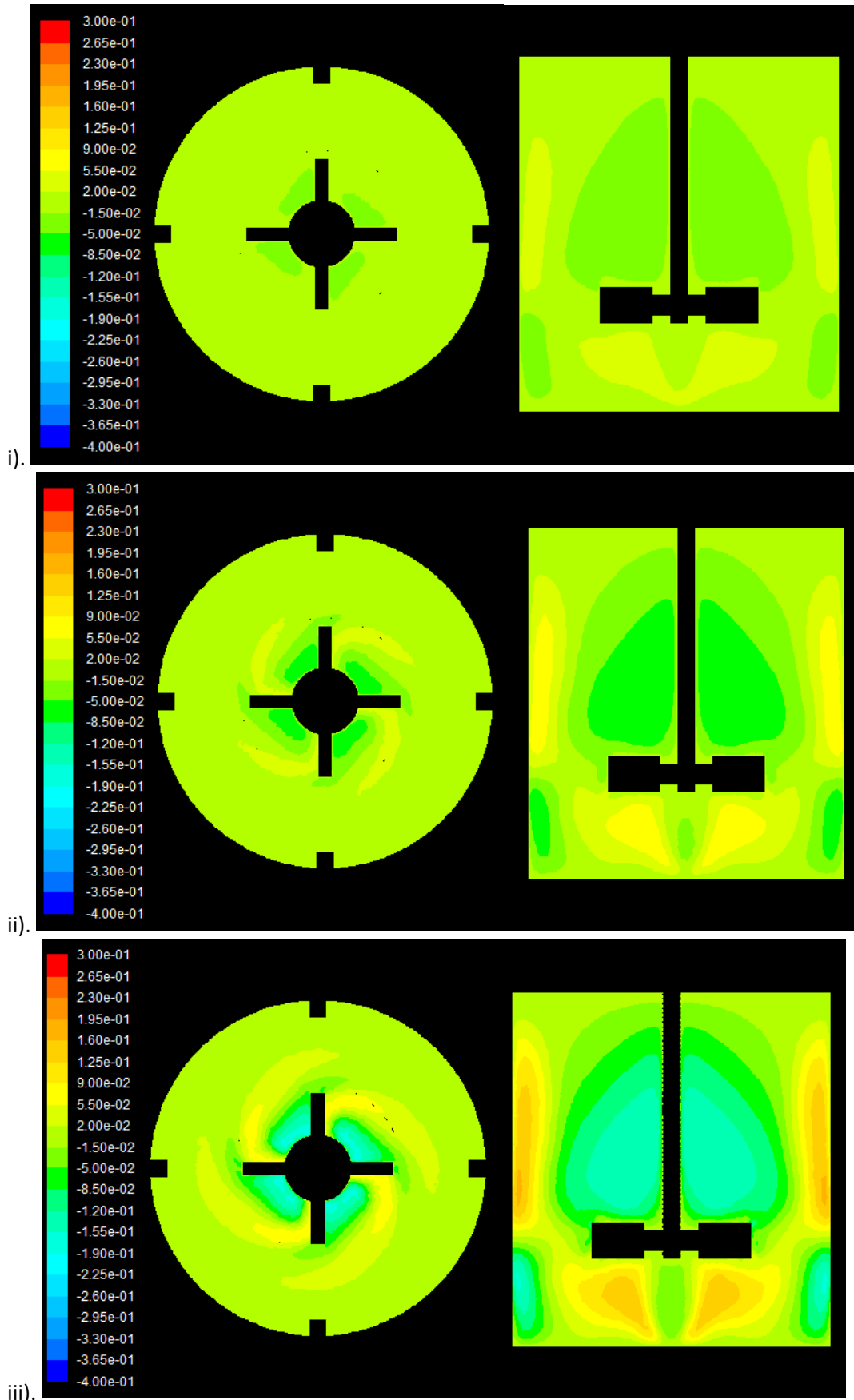


Figure 8.13 – Contour plots of axial velocity for digesters mixed at i). 50 rpm, ii). 100 rpm and iii). 200 rpm

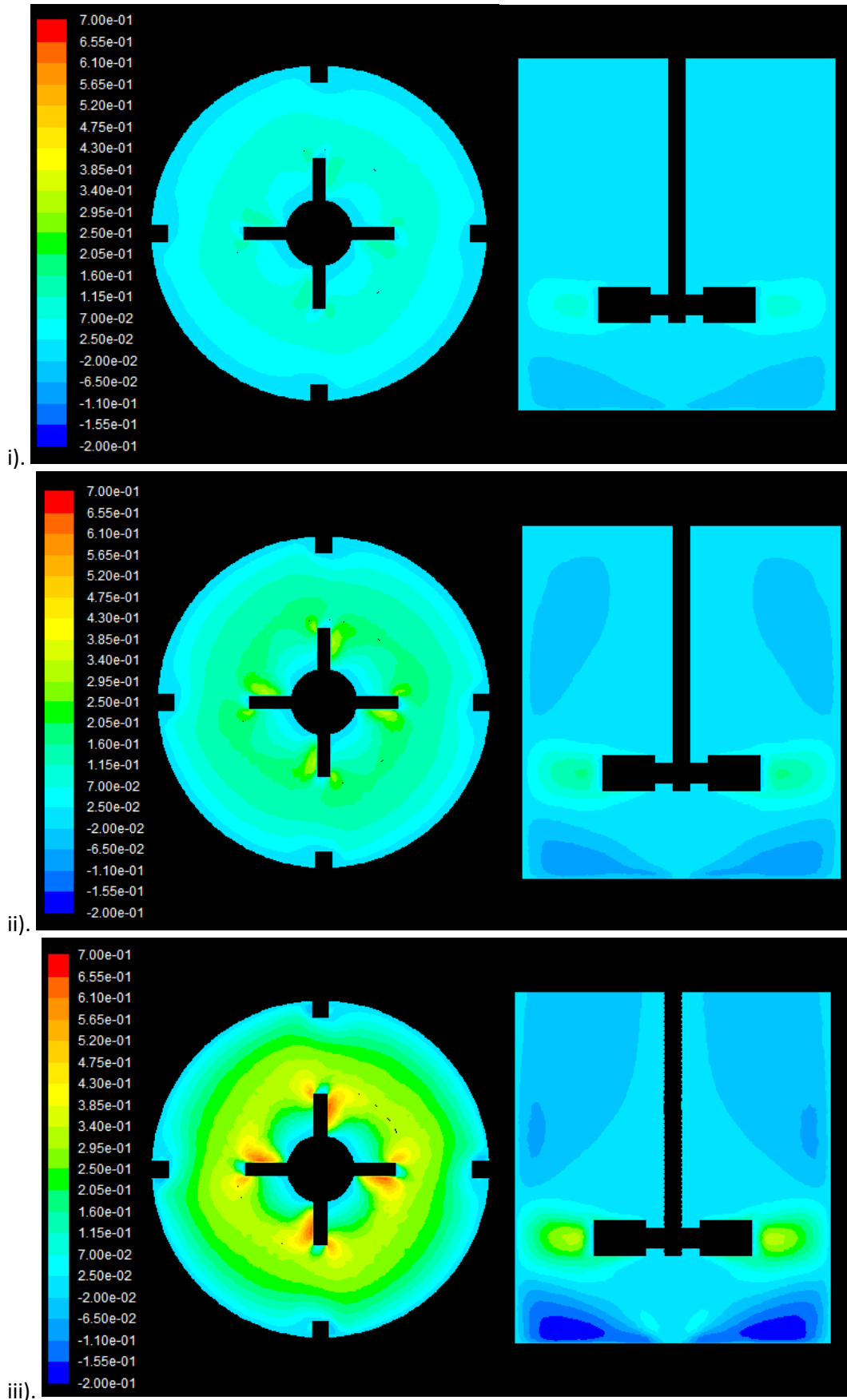


Figure 8.14 – Contour plots of radial velocity for digesters mixed at i). 50 rpm, ii). 100 rpm and iii). 200 rpm

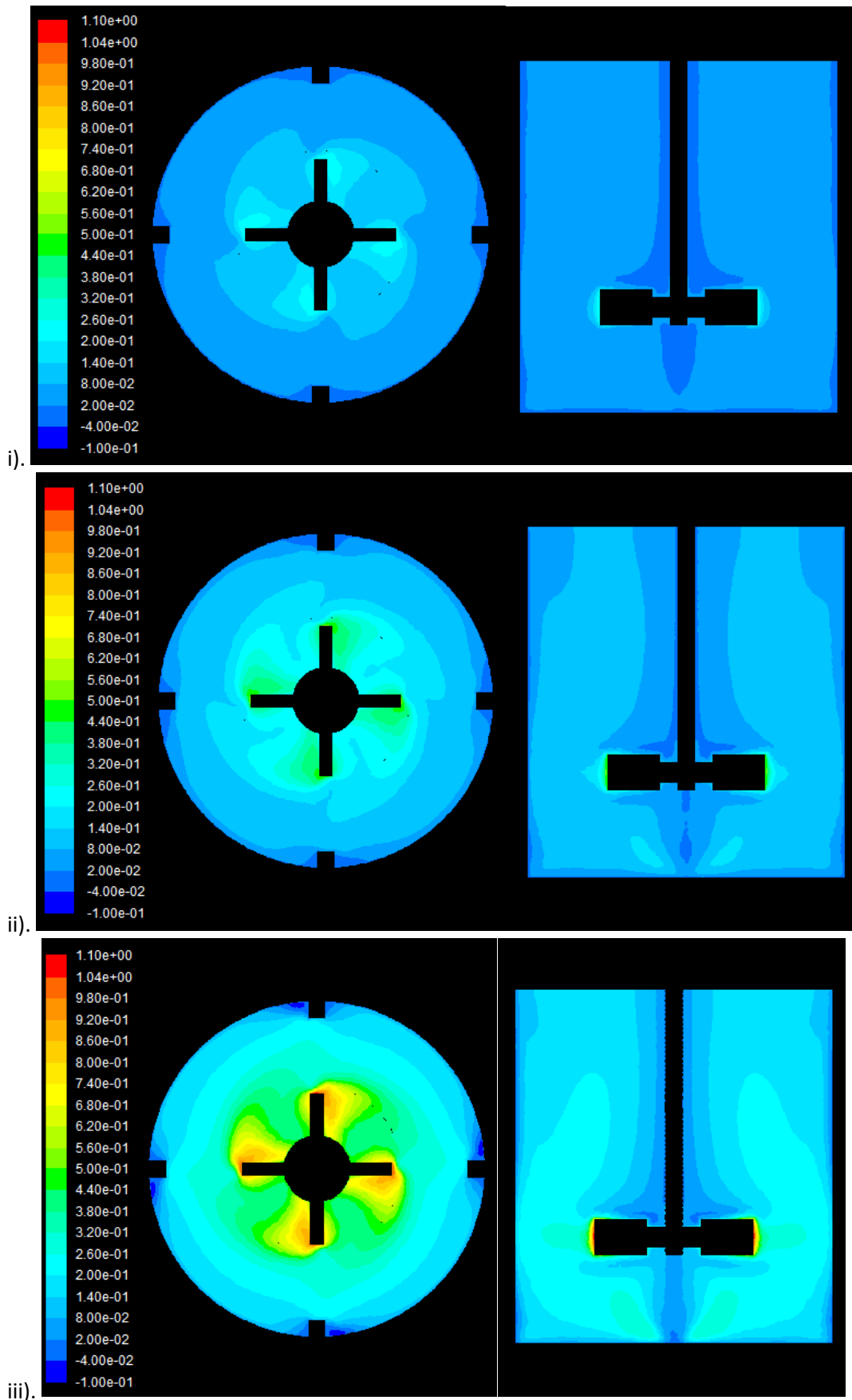


Figure 8.15 – Contour plots of tangential velocity for digesters mixed at i). 50 rpm, ii). 100 rpm and iii). 200 rpm

As with the tangential velocity, the highest radial velocities are experienced in the impeller region, both behind the impeller blades and extending from the leading edge of the impeller tip. The magnitude of the radial velocity falls as the fluid moves further away from the impeller towards the walls of the digester. Similarly, above and below the digester, lower radial velocities are found, and close to the base of the digester and in the top third of the digester, there are significant regions experiencing negative radial velocities, signifying that fluid is moving towards the centre of the digester and away from the walls. This points towards the existence of two circulating loops of fluid, one above and one below the impeller, a flow pattern typical of a radial flow impeller.

The presence of these two circulating loops of fluid is further indicated by the contours of axial velocity. There are clear regions of positive axial velocity close to the walls of the digester above the impellers and close to the centre of the digester below the impellers, where fluid is moving upwards. Conversely, close to the centre of the digester above the impeller and close to the walls of the digester below the impeller, there are regions of negative axial velocity where the fluid flow is towards the base of the digester. Due to the location of the impeller in the digester, the circulatory loop below the impeller is more compact than that above the impeller. Along the centreline of the impeller, the magnitude of the axial velocities is small compared to other areas of the digester. This is due to the fact that the majority of flow in that horizontal plane is in a radial direction as a result of the action of the impeller.

## **8.5 Velocity magnitude analysis**

An analysis of the regions of high, medium and low velocity in the digesters was carried out. Three velocity ranges were assigned based on the velocity magnitudes found across the digester at all modelled mixing speeds. Furthermore, an equivalent floc size was assigned to each of these ranges, defined as the diameter of a floc which would result in a Stokes number of 0.1 according to Equation 7-3. Such a floc would follow the flow of liquid in the digester within a 1 % error margin, as described

in Section 7.2. In order to calculate the equivalent floc size, the density of the floc was assumed to be equal to that of the overall synthetic sludge and flocs were assumed to be spherical. High velocities are considered to be those above 0.1 m/s. At this fluid velocity, a spherical floc with a diameter of approximately 1 cm would be able to accurately follow the flow patterns of the fluid in the digester. Low velocities are considered as those below 0.02 m/s. At this fluid velocity, a floc of approximately 2 cm diameter would be able to accurately follow the flow patterns of the fluid in the digester. Medium velocities cover the intermediate range of 0.02-0.1 m/s, equivalent to a floc with a diameter in the range of 1-2 cm accurately tracing the fluid flow. Figure 8.16 shows the proportion of the digester experiencing each of these velocity groups. It can be seen that as the mixing speed in the digester is increased, there is a corresponding increase in the volumes of the digester experiencing high velocity magnitudes, and hence the size of floc that would accurately trace the flow patterns established in the digester rather than settling out. Conversely, as mixing speed increases, there is a reduction in the volumes experiencing low and medium velocity magnitudes, with low velocity magnitude zones at 200 rpm accounting for less than 5 % of the volume of the digester. This suggests that less particles will settle out at higher mixing speeds. Bridgeman (2012) performed a similar analysis to compare the mixing of sludge with different total dissolved solids (TDS) concentrations. A comparison of these results with that work show similarities between the digester at 100 rpm in this work and those mixing 5.4-7.5 % TDS sludge, which had similar rheological properties, in the work of Bridgeman (2012).

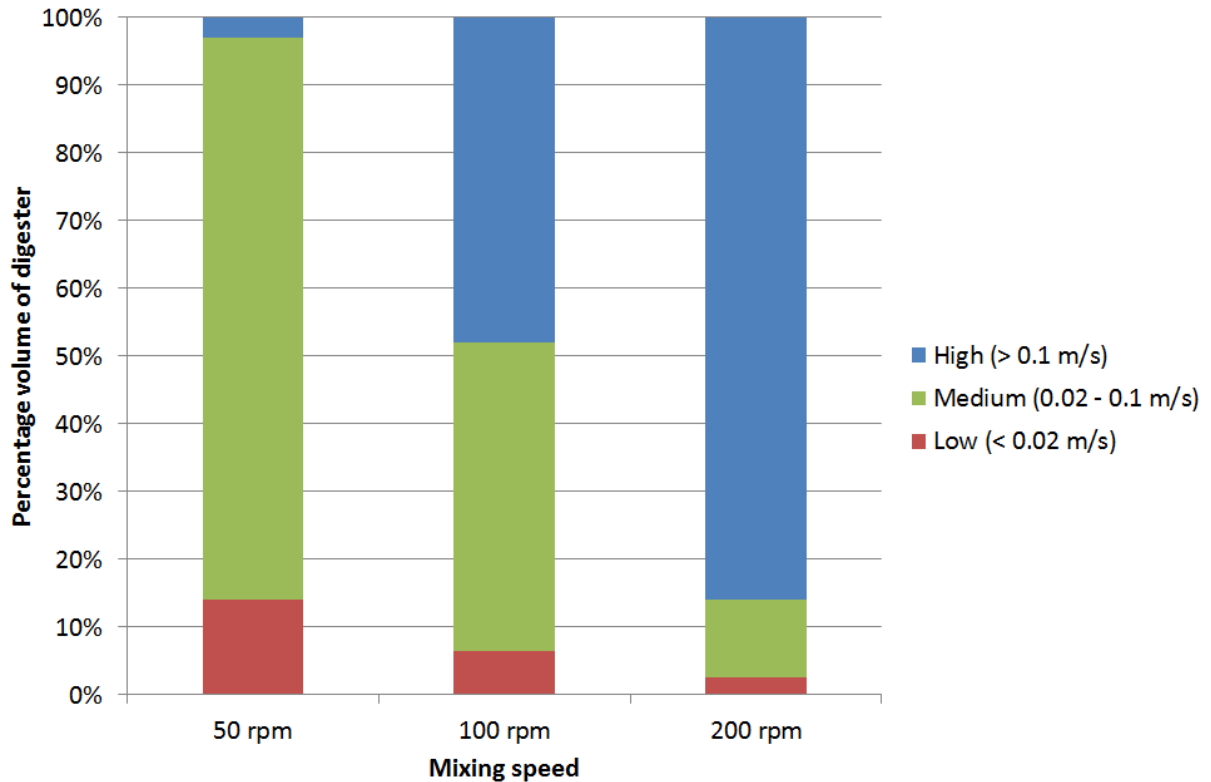


Figure 8.16 – Change in proportion of digester volume experiencing high, medium and low velocity magnitudes with increasing mixing speed

The distribution of velocity magnitude within the digester is demonstrated in Figure 8.17, which shows the mean velocity magnitude in each of the four zones of the CFD model: the impeller region ( $30 < z < 90$  mm), the zones above ( $z > 90$  mm) and below the impeller ( $z < 30$  mm) and the outer region ( $d > 70$  mm) which includes the baffles, alongside the mean velocity magnitude in the overall digester and the overall digester excluding the impeller region, i.e. the bulk region. It can be seen that a similar pattern of velocity magnitudes across the different digester zones is apparent at all mixing speeds. The highest mean velocity magnitude is in the impeller region, where the mean is nearly twice as high as in other zones of the digester. Due to the limited space below the impeller, the mean velocity magnitude in this zone is higher than that in the zone above the impeller or in the outer region of the digester, as more of the volume of the region is close to the impeller.

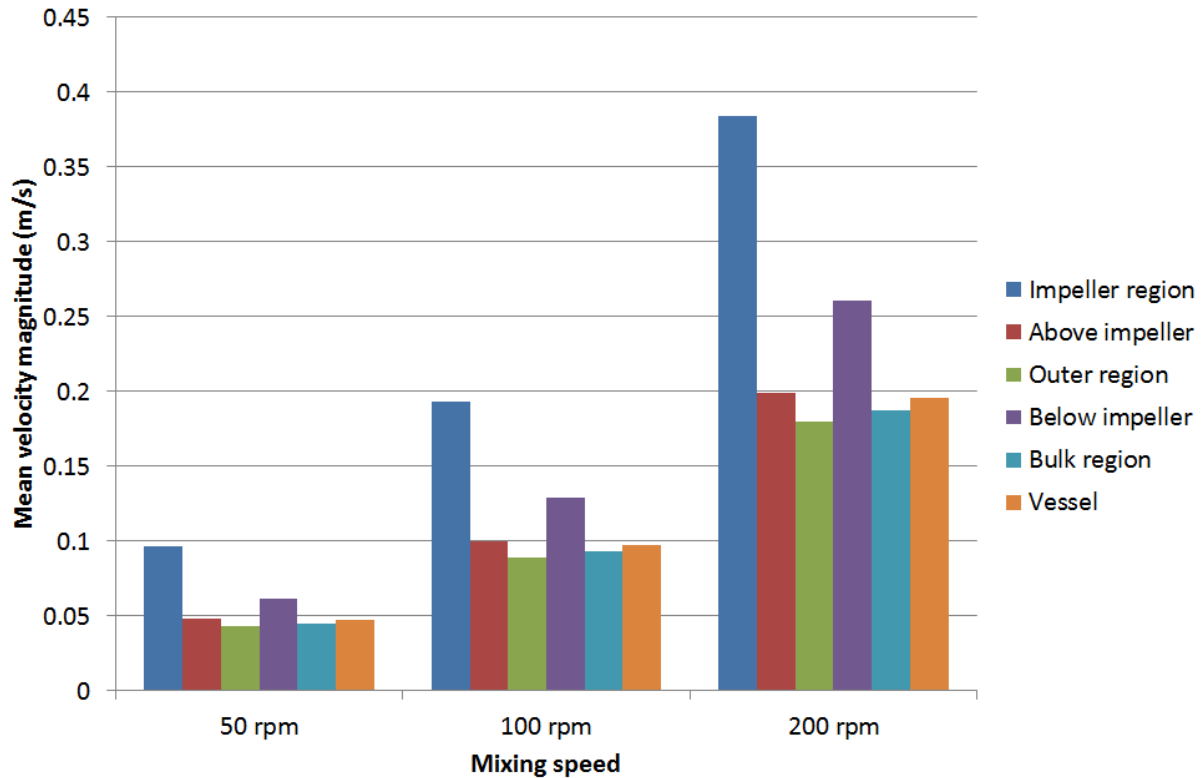


Figure 8.17 – Mean velocity magnitude in different zones and in the digester overall at modelled mixing speeds

For each of these mixing speeds, the volume of dead zone within the digester was calculated. The definition of Vesvikar and Al-Dahhan (2005) was used to determine what constitutes a dead zone. They stated that volumes with a velocity of 5 % or less of the maximum velocity in the digester are considered to be stagnant. Using this definition, dead zone volumes in the digester were calculated as 10 %, 9 % and 8 % in digesters at 50 rpm, 100 rpm and 200 rpm respectively. This suggests that even at 50 rpm, mixing is able to ensure that 90 % of the digester volume is active, i.e. does not act as dead zones and that, with this definition, the presence of dead zones is more likely to be a function of the vessel and impeller geometry and the sludge rheology than the mixing speed. This is less than is suggested by the PEPT data which showed that approximately 30 % of the digester was not covered by the particle in a digester at 50 rpm, though it was shown that sludge rheology played an important role in the volume of particle coverage in the digester mixed at 100 rpm. In the case of the PEPT data, the particle was not observed for any significant period of time in the top third of the digester during the twenty minute observation period and as such, it is not possible to ascertain

whether its velocity is 5 % or less of the maximum velocity in the digester, the condition required by Vesvikar and Al-Dahhan (2005) for the region to be considered stagnant. At low fluid velocity, particles are less well able to accurately trace the flow patterns established by mixing, due to the deposition of particles resulting in a reduced particle coverage in higher areas of the digester. Hence, whilst it is likely that low particle coverage and increased dead zones are linked, further comparison of whether particle coverage corresponds directly to volumes of dead zone in the digester is not feasible with the existing data.

## 8.6 Particle trajectories

Velocity contours alone do not determine the degree of mixing that is taking place in the digester. For example, a packet of fluid that is moving quickly does not experience mixing if all other packets of fluid in the immediate vicinity are moving at the same speed and in the same direction. In order to build a clearer picture of the degree of mixing taking place in the digester, the trajectories of 10 massless, neutrally buoyant particles, injected into the flow along a line halfway between the centre of the digester and the digester wall, are shown in Figure 8.18.

It can be seen that at all three mixing speeds, the movement and mixing of the particles is limited by the movement of the impeller, with the majority of particles remaining either above or below the impeller. Similar results were seen in the work of Bridgeman (2012). The ability for mixing to occur is further limited by the mixing speed of the digester, with the slower impeller speeds leading to less particle motion within the digester. Aspects of these particle trajectories mirror the particle tracks from the PEPT experiments. The trajectories demonstrate that the flow is highly swirling as seen in Figure 7.4. Additionally, the particle trajectories show that there is less coverage of the top third of the digester by the particles than the bottom two thirds of the digester and that the coverage is more densely concentrated around the centreline of the vessel than near to the vessel walls, as seen in Figure 7.2 and Figure 7.4.

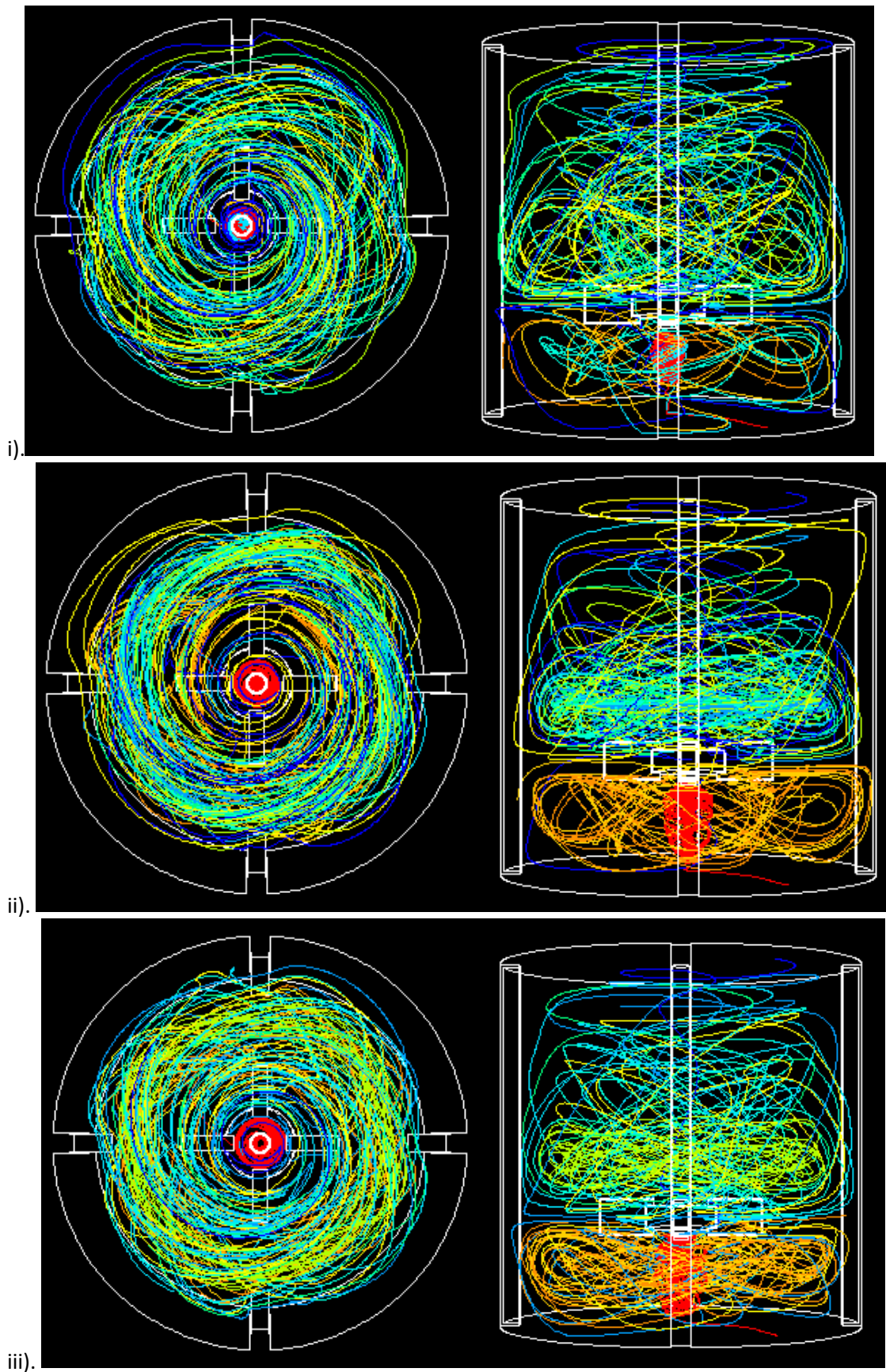


Figure 8.18 – Particle trajectories of ten neutrally buoyant particles for digesters mixed at i). 50 rpm, ii). 100 rpm and iii). 200 rpm

## 8.7 Turbulent kinetic energy and turbulent intensity

TKE is the mean kinetic energy per unit mass. It is the result of fluid shear, friction or buoyancy and therefore may be considered as an indicator of the impact of turbulence on flocs and microbial communities in the digester. As TKE is calculated from the scalar transport equation in Equation 3-22, it is likely that the exact values predicted by the RANS CFD models used here will be inaccurate. The accuracy of these results could be improved by using an LES model, which resolves the turbulence directly. However, the contours and relative magnitudes across the vessel predicted by RANS simulations in this work are still of interest. The  $k$ - $\epsilon$  model used in these simulations models the TKE based on the assumption that turbulence is isotropic. In scenarios where anisotropic turbulence dominates, it is expected that this will lead to the over-prediction of TKE, although this is not the case when comparing the model to the PIV experiments discussed in Section 8.3.2. The effects of this assumption and the resultant inaccuracies are further discussed in Section 10.2.

Figure 8.19 shows the TKE contours in the digester at mixing speeds of 50, 100 and 200 rpm respectively. At a mixing speed of 50 rpm, the predicted TKE across the digester is less than 5 % of the maximum TKE experienced in the impeller region of the digester mixed at 200 rpm. At 100 rpm and 200 rpm, there are differences in the magnitude of the TKE but the contour patterns are similar. Notably, and unsurprisingly, the highest levels of TKE appear in the impeller region, with virtually no TKE predicted in the regions above and below the impeller. The magnitude of TKE at the tips of the impeller blades and in the recirculation regions in the wake of the blades is a magnitude higher than in the bulk of the digester. This clearly demonstrates that it is in the impeller region that the turbulence experienced is at its highest.

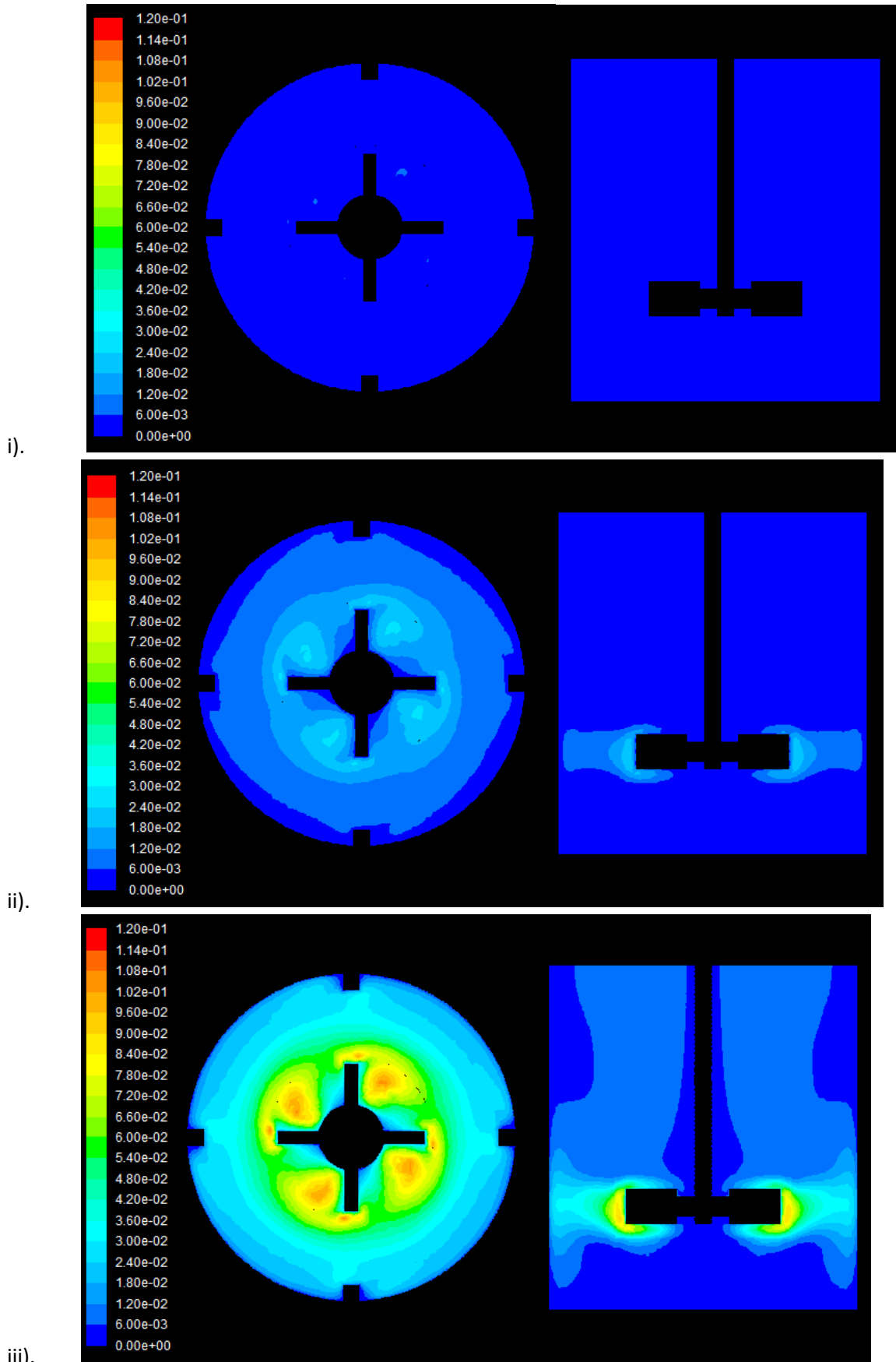


Figure 8.19 – Contour plots of TKE for digesters mixed at i). 50 rpm, ii). 100 rpm and iii). 200 rpm

In order to better assess the TKE in the digesters independently of the scale factor attributed to the mixing speed, the turbulence intensity (TI) is used as a non-dimensional measure of the level of turbulence. It is defined mathematically as:

$$TI = \frac{\sqrt{\frac{2}{3}k}}{u}$$

Equation 8-5

where  $TI$  is turbulence intensity,  $k$  is TKE and  $u$  is the mean velocity.

The mean velocity was selected as the tip speed of the impeller in order to give a global TI. Figure 8.20 shows the TI contours in the digester at mixing speeds of 50, 100 and 200 rpm respectively. It can be seen that, by normalising the TI by dividing by the tip speed, all of the digesters experience similar contours and TI magnitudes. The bulk of the digester experiences very little turbulence, with TI of 10 % or lower. However, in the plane of the impeller, the TI is significantly higher, with intensities of 10-20 % close to the walls and of 20-30 % in the impeller region. Once again, the highest TI are found at the tip of the impeller blades and in the recirculation regions in the wake of the blades. This suggests that the effects of turbulence on the microbiological communities will be most apparent in the high TI regions close to the impeller. In the bulk of the digester, it is likely that the turbulence will have a less detrimental effect on micro-organisms than in the impeller region, though it can be seen in Figure 8.19 that as impeller speed increases, the level of turbulence across the digester increases proportionally. As such, higher mixing speeds are associated with higher turbulence which are likely to have a greater detrimental effect on microbiology and hence gas production.

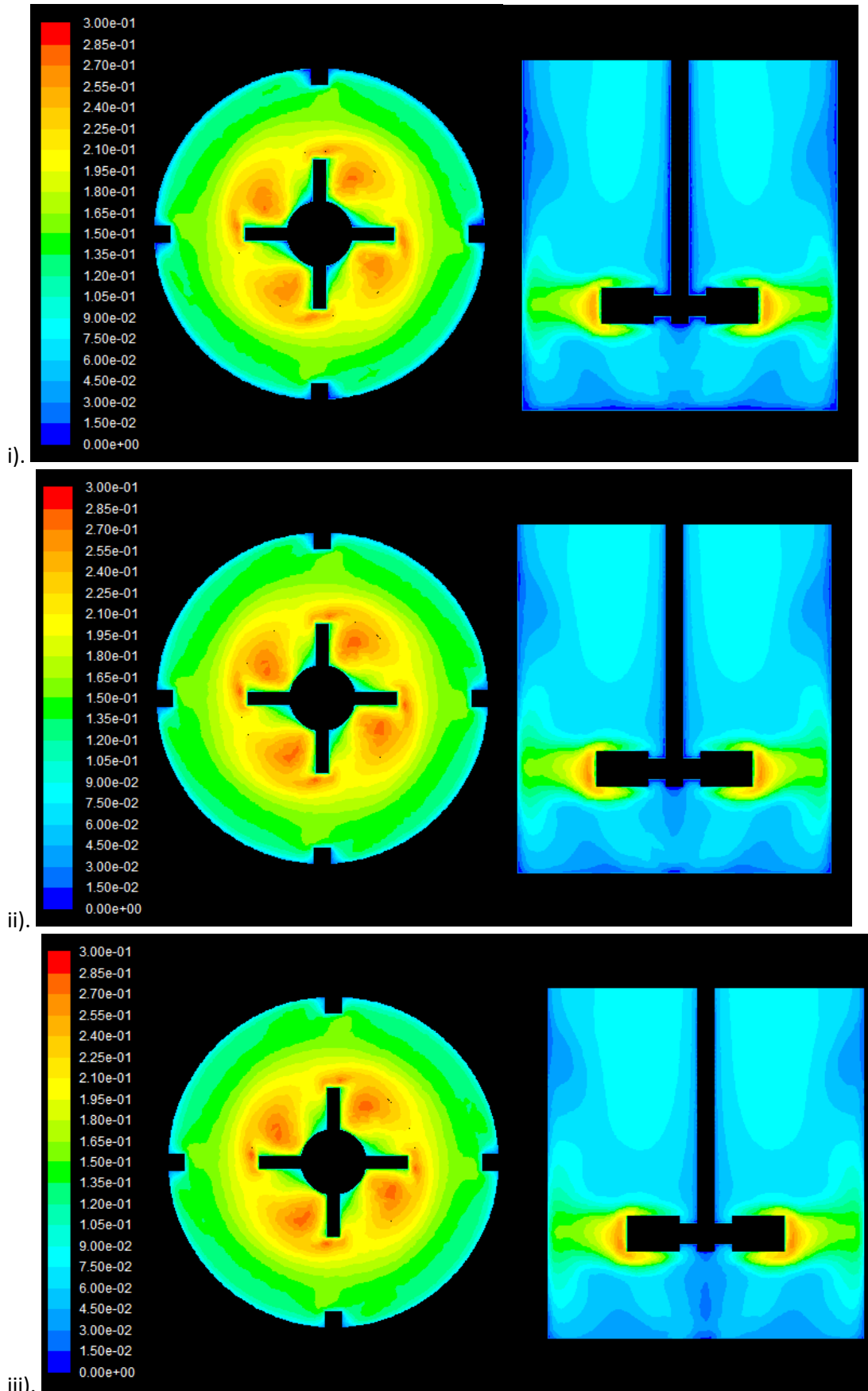


Figure 8.20 – Contour plots of TI for digesters mixed at i). 50 rpm, ii). 100 rpm and iii). 200 rpm

Figure 8.21 shows the mean TI in different zones of the digester as well as the vessel overall. As with the mean velocity magnitude, shown in Figure 8.17, the highest mean TI occurs in the impeller region. Again, the mean in the impeller region is nearly twice as high as in other zones of the digester. However, unlike the mean velocity magnitude, the zone below the impeller experiences the lowest mean TI whilst it experiences the second highest mean velocity magnitude after the impeller region. This demonstrates that, whilst the fluid in this region moves at a higher velocity magnitude than in other regions of the digester, the level of turbulence in this zone is lower than in the rest of the digester.

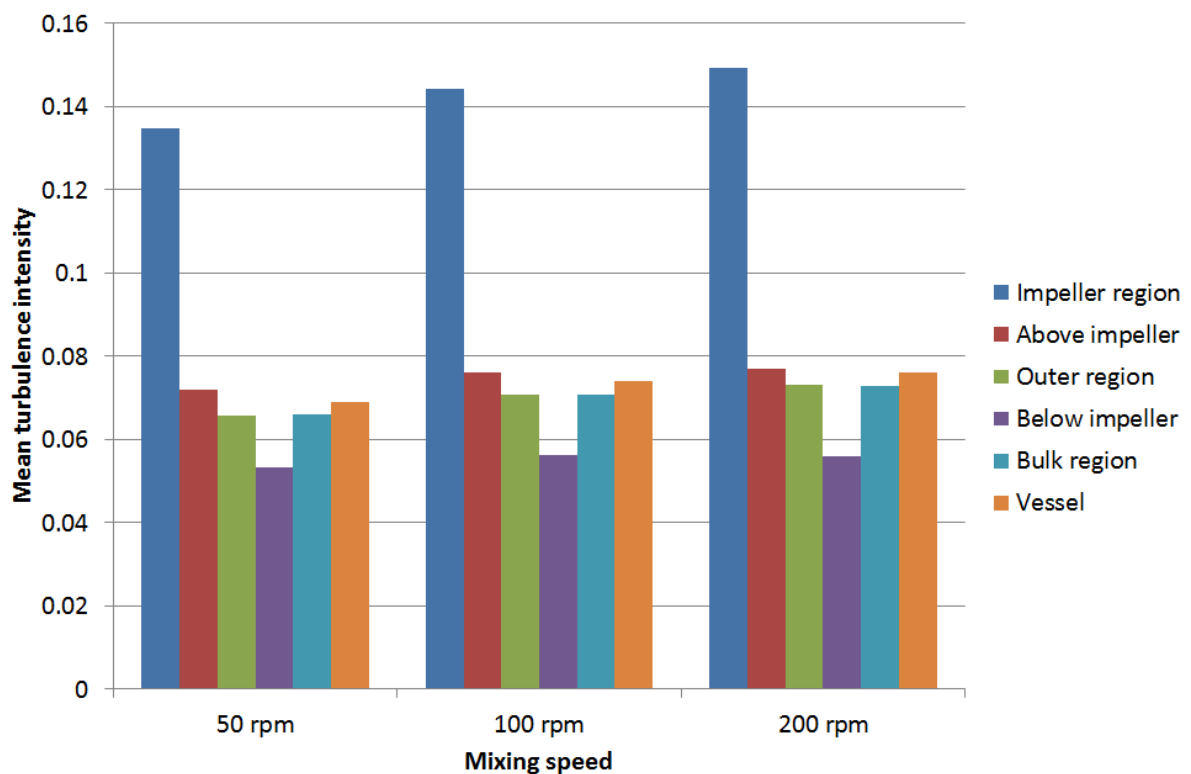


Figure 8.21 – Mean TI in different zones and in the digester overall at modelled mixing speeds

## 8.8 Velocity gradient

The local velocity gradient was calculated from the energy dissipation rate and the kinematic viscosity in each mesh cell according to:

$$G = \sqrt{\frac{\varepsilon}{\nu}}$$

Equation 8-6

Figure 8.22 shows the velocity gradient contours in the digester at mixing speeds of 50, 100 and 200 rpm respectively. As seen before, the patterns of the contours are similar for all mixing speeds, with only the magnitude of the velocity gradients being different. Once again, the bulk of the digester experiences velocity gradients of less than a third of the maximum velocity gradient in the digester. Higher velocity gradients occur in the impeller region, with the maximum occurring at the impeller tips and in the wake of the impeller blades.

Figure 8.23 shows velocity vectors coloured by velocity gradient in the digester at mixing speeds of 50, 100 and 200 rpm respectively. From these, it is clear that at all mixing speeds, fluid that is not in the plane of the impeller experiences virtually no turbulence except for close to the walls and the surfaces of the impeller shaft. The higher velocity gradients close to these surfaces can be explained by the modelling of the boundary layer, in which the gradient represents the velocity difference between the stationary fluid at the wall (the no-slip boundary condition) and the velocity of the bulk fluid beyond the boundary layer. Whilst the difference in velocity between the wall and the bulk fluid describes the physics of the boundary layer, it gives an unrealistic representation of the turbulence present along the surfaces of the digester, magnified by the number of prism layer cells used to capture the boundary layer.

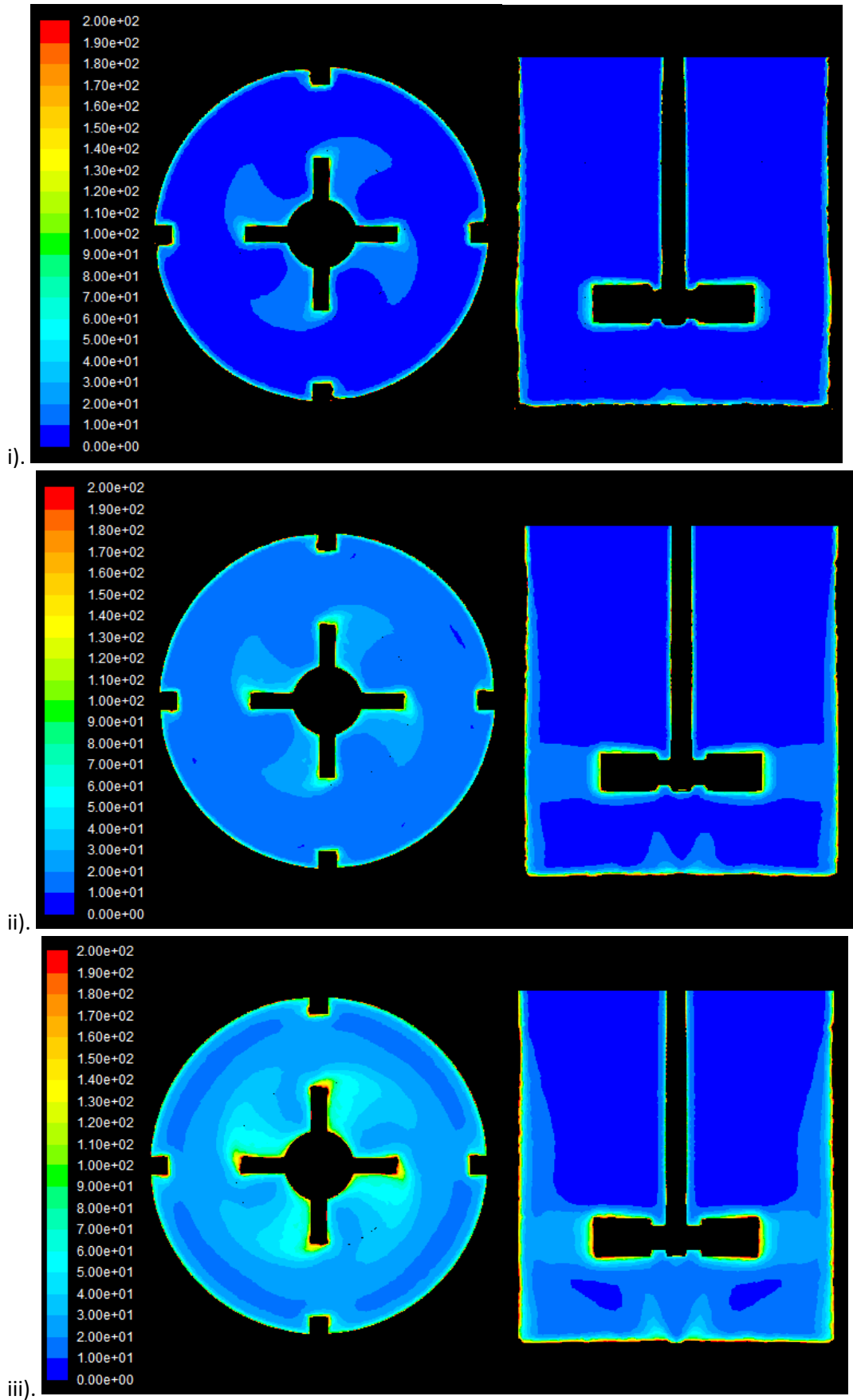


Figure 8.22 – Contour plots of velocity gradient for digesters mixed at i). 50 rpm, ii). 100 rpm and iii). 200 rpm

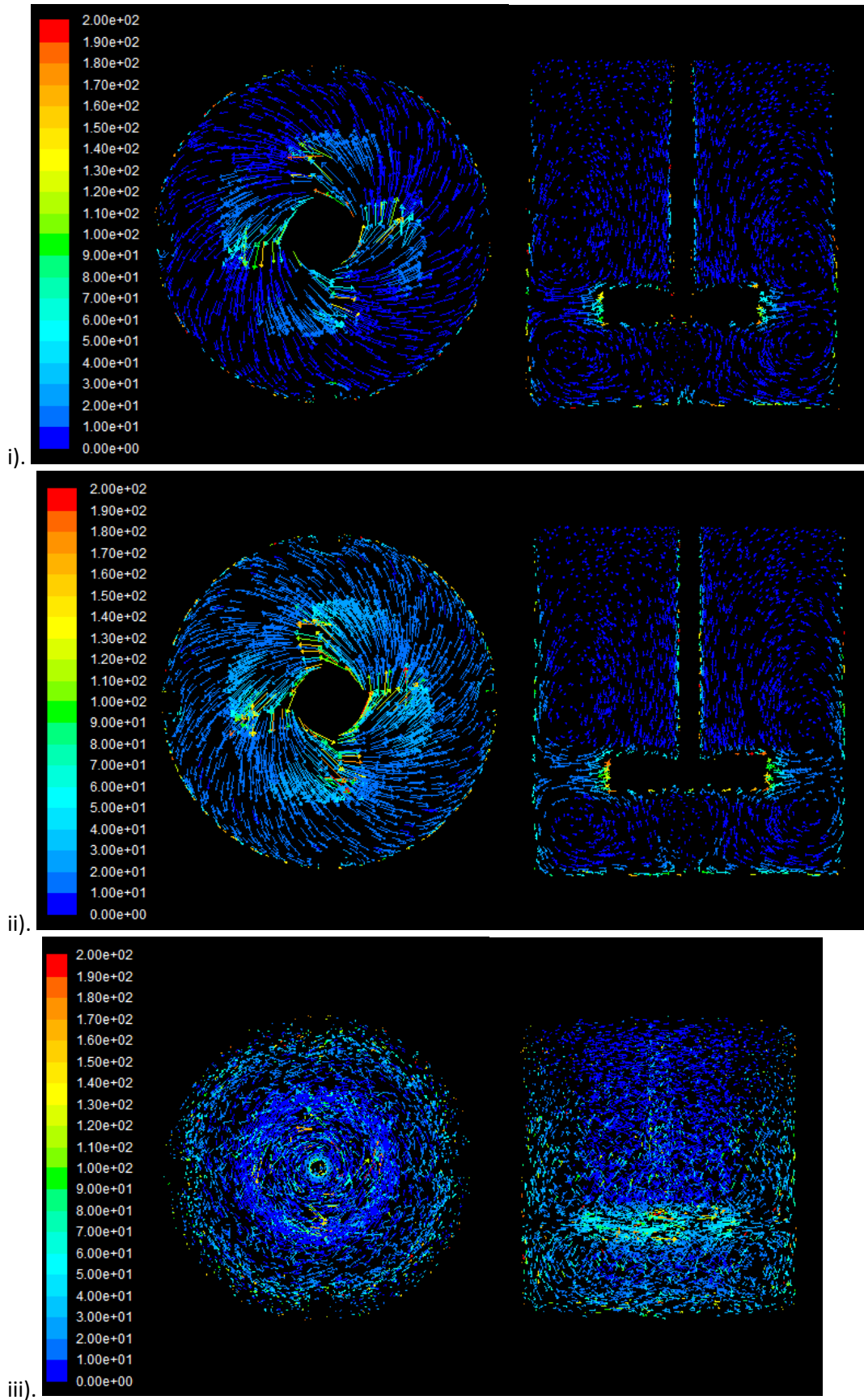


Figure 8.23 – Vector plots of velocity coloured by velocity gradient for digesters mixed at i). 50 rpm, ii). 100 rpm and iii). 200 rpm

Figure 8.24 shows a histogram of the local velocity gradients in the digester, weighted by cell volume, at mixing speeds of 50, 100 and 200 rpm respectively. From this, it can be seen that at the lowest mixing speed, nearly 70 % of the digester experiences velocity gradients of less than  $5 \text{ s}^{-1}$ , which is an order of magnitude below the  $50\text{-}80 \text{ s}^{-1}$  recommended by literature for the design of anaerobic digester mixing systems (Tchobanoglous and Burton, 1991). This falls to just over 40 % at 100 rpm and less than 20 % at 200 rpm. It is not surprising that as the mixing speed increases, the curve of histogram shifts to the right with an increasing percentage of the digester volume experiencing higher velocity gradients. However, it is interesting to note that even at 200 rpm, 80 % of the digester experiences velocity gradients of less than  $20 \text{ s}^{-1}$ , indicating that none of the digesters are operated within the average velocity gradient range recommended by Tchobanoglous and Burton (1991). However, Bridgeman (2012) similarly showed that 5.4-7.5 % TS sludge, mixed at 100 rpm, experienced vessel-wide average velocity gradients of less than  $6 \text{ s}^{-1}$ , with the bulk digester experiencing average velocity gradients of  $3\text{-}5 \text{ s}^{-1}$  and impeller regions experiencing average velocity gradients of  $12\text{-}17 \text{ s}^{-1}$ . Additionally, Wu (2010c) found that for a full-scale digester, the average local velocity gradient was  $3.44 \text{ s}^{-1}$ , with 84.5 % of cells experiencing local velocity gradients of below  $10 \text{ s}^{-1}$ , 7.9 % in the range  $10\text{-}70 \text{ s}^{-1}$  and 7.6 % above  $70 \text{ s}^{-1}$ . This agrees well with the results shown above at all mixing speeds. Although there are significant differences in the dimensions of the digesters (lab-scale compared to full-scale), it is still the case that the majority of both vessels experiences a local velocity gradient of less than  $10 \text{ s}^{-1}$  with smaller volumes of the digester experiencing local velocity gradients nearly an order of magnitude higher.

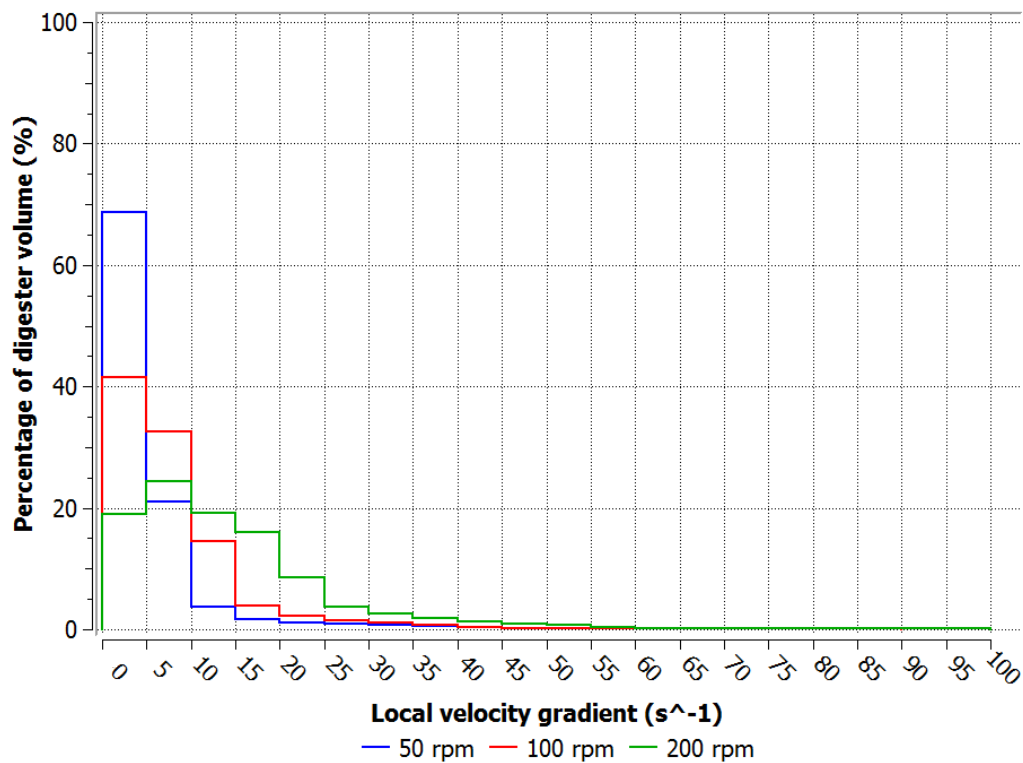


Figure 8.24 - Histogram of local velocity gradient in a lab-scale digester at mixing speeds of 50, 100 and 200 rpm

## 8.9 Summary

This chapter considers the results of CFD models of a lab-scale digester. First, the geometry of the digester, along with the numerical methods and boundary conditions applied to the model, were discussed. The GCI was used to determine mesh independence. The results of simulations making use of the realisable  $k-\epsilon$ , standard  $k-\omega$ , SST  $k-\omega$  and RSM turbulence models were compared to PIV results in order to select the most appropriate model to use. As a result of this analysis, an SM realisable  $k-\epsilon$  model with 1.4 million cells was used for further analysis of the flow profiles. The results of this model were validated against PEPT results and were found to compare favourably.

A study of the velocity distribution within the digester demonstrated that in accordance with published literature, the highest velocities are experienced in the impeller region, with velocities in the recirculation region in the wake of the impeller blades being approximately 17 % higher than the impeller tip speed. Two circulation loops are formed above and below the impeller, a standard pattern for a radial flow impeller such as the one used in this digester. Additionally, it was seen that

tangential velocities were an order of magnitude higher than axial and radial velocities in the impeller region, suggesting a highly swirling motion within the digester caused by the movement of the impeller blades, despite the presence of baffles intended to reduce this effect. It was interesting to note that at all mixing speeds, approximately 10 % of the volume of the digester could be considered as dead zone. A study of particle trajectories in the digester suggested that there is less particle movement in the top third of the digester; this is in agreement with the PEPT analysis. Furthermore, the majority of particles in the digester stay either above or below the impeller, with little mixing occurring between the two circulation loops. Similar results have been published by Bridgeman (2012).

As with velocity magnitude, TKE is highest at the impeller tips and in the recirculation regions in the wake of the impeller blades, with these areas experiencing TKE a magnitude higher than in the bulk of the vessel. TI normalises the turbulence by tip speed and as such, the TI in digesters at all mixing speeds is similar. Contours of TI show that it is less than 10 % in the bulk fluid, 10-20 % close to the digester walls and 20-30 % in the impeller region. Mean TI is lower in the zone below the impeller than in the zone above the impeller, which may suggest that less mixing occurs in this zone.

Velocity gradient in the digester is very low in the bulk of the fluid but is high along the walls of the digester, due to the presence of the boundary layer and the no-slip boundary condition set for all walls. Velocity gradients are also higher around the impeller blades, which are the result of both the boundary layer on the blades and, more importantly, the effects of mixing. A histogram of local velocity gradients shows that as the mixing speed increases, the curve of the histogram shifts to the right with an increasing percentage of the digester volume experiencing higher velocity gradients. However, even at 200 rpm, 80 % of the digester experiences velocity gradients of less than  $20 \text{ s}^{-1}$ . This is significantly lower than the  $50\text{-}80 \text{ s}^{-1}$  recommended in literature for anaerobic digester design

(Tchobanoglous and Burton, 1991) but does agree with the results of Bridgeman (2012) and Wu (2010c).

## **CHAPTER 9      Mixing, digester stability and gas production**

From the PEPT and CFD results discussed in previous chapters, it is clear that mixing and the flow patterns that it establishes in anaerobic digesters have an effect on the location of dead zones, and the distribution of turbulence and velocity gradients. This chapter considers the effects of these differences on the operational stability and biogas production of digesters during lab-scale experiments. A range of key parameters are used to determine the process stability of digesters subjected to different mixing speeds. The biogas production from digesters under these different mixing speeds is compared and the effects on the microbiological communities are considered.

### **9.1 Experimental set-up**

The four mechanically-mixed, lab-scale digesters were run continuously at a constant mixing speed of 100 rpm until they were considered to have been stable for at least one RT, i.e. 24 days. The mixing speeds in three of the digesters were changed to 0 rpm, 50 rpm and 200 rpm, whilst the fourth digester continued to be mixed at 100 rpm. The digesters were operated for a further three RT or until they were considered to be irreversibly soured, whichever happened sooner. Throughout the duration of the experiment, samples were taken from a sidearm on the digesters each weekday. In the second experiment, additional samples were taken from the base of the digesters at 0 rpm and 50 rpm using the feeding tube and a cut-off pipette, in order to gain a more complete picture of the state of the digester under what has been shown by PEPT and CFD results to be poorly-mixed conditions. The samples taken in the second experiment were also used to build up a picture of the microbiological communities present in the digester, through the use of qPCR and scanning electron microscopy (SEM).

## 9.2 Feedstock differences

There were some differences between the feedstocks used in the two experiments. Whilst the second experiment made use of the feedstock described in Chapter 6, the first experiment was carried out whilst this feed was still under development. Thus, in the first experiment, peptone was removed from the feedstock formula described in Chapter 6 and replaced with an equivalent mass of yeast extract. This gave a synthetic sludge with a TS concentration of 30.7 g/l, a VS concentration of 24.8 g/l and a C:N ratio of 35.3 : 5.7 by weight. The results of an ICP-MS semi-quantitative sweep shows the micro-nutrients present in the sludge in Table 9.1. As such, the synthetic sludge used in the first experiment had a similar TS concentration to the feedstock used in the second experiment, a VS concentration 10 % lower, and a C:N ratio 10 % lower but significantly higher concentrations of micro-nutrients.

**Table 9.1 – ICP-MS results of a semi-quantitative metals sweep on synthetic sludge (results are approximate:  $\pm 20$  %). N.B.: Concentrations are listed as dry/dry weight.**

Element	Concentration		Element	Concentration	
	ppb	mL/L		ppb	mL/L
<b>Li</b>	2.1	0.0021	<b>As</b>	49	0.049
<b>B</b>	410	0.41	<b>Se</b>	5.8	0.0058
<b>Na</b>	180000	180	<b>Rb</b>	13	0.013
<b>Mg</b>	4700	4.7	<b>Sr</b>	56	0.056
<b>Al</b>	650	0.65	<b>Y</b>	0.2	0.0002
<b>Si</b>	4500	4.5	<b>Zr</b>	8.8	0.0088
<b>P</b>	23000	23	<b>Mo</b>	12	0.012
<b>K</b>	19000	19	<b>Ag</b>	19	0.019
<b>Ca</b>	10000	10	<b>Cd</b>	2.5	0.0025
<b>Ti</b>	64	0.064	<b>Sn</b>	28	0.028
<b>V</b>	86	0.086	<b>Sb</b>	1.5	0.0015
<b>Cr</b>	35	0.035	<b>Ba</b>	28	0.028
<b>Mn</b>	82	0.082	<b>La</b>	0.4	0.0004
<b>Fe</b>	1000	1	<b>Ce</b>	4.8	0.0048
<b>Co</b>	4.2	0.0042	<b>Nd</b>	0.2	0.0002
<b>Ni</b>	93	0.093	<b>Hf</b>	0.2	0.0002
<b>Cu</b>	99	0.099	<b>W</b>	0.3	0.0003
<b>Zn</b>	200	0.2	<b>Au</b>	4.6	0.0046
<b>Ga</b>	1.4	0.0014	<b>Pb</b>	34	0.034
<b>Ge</b>	1.8	0.0018			

Using this sludge in the first experiment, the digesters were considered stable by Day 65 and it was at that point that mixing was changed. Using the sludge described in Chapter 6 in the second experiment, the digesters were considered stable by Day 59, and so mixing speeds were changed.

### 9.3 Effect of mixing on digester stability

RR was taken to be the primary indicator of stability in a digester. When the RR was below 0.3, the digestion process was taken to be in a stable condition. If the RR rose above 0.8, then the digestion process was considered unstable (Ripley et al., 1986). The higher the RR rose, the more unstable and the closer to irreversible souring the digester was considered to be. The digester was considered to be irreversibly soured if the RR became higher than 3.0, at which point the experiment was terminated. Other indicators of instability included a decline in pH and TA, and an increase in VFA concentration.

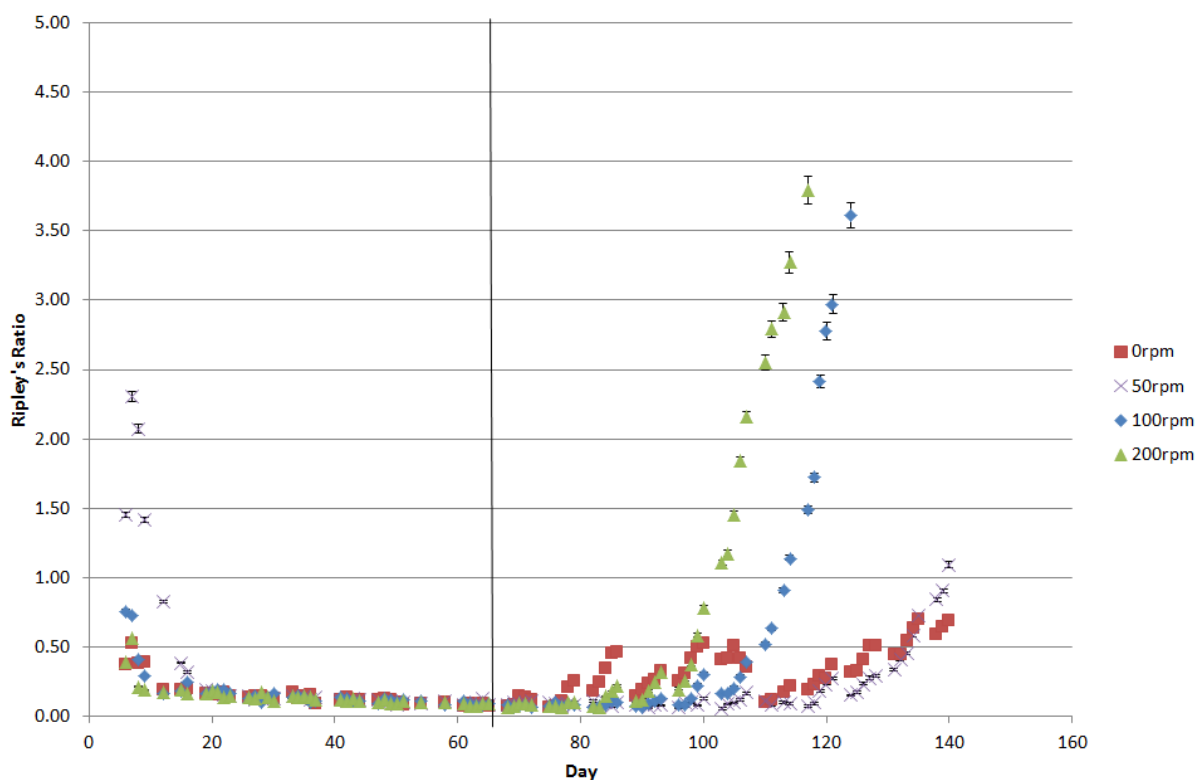


Figure 9.1 – RR of four digesters over the course of the first experiment (mixing changes made on Day 65 indicated by vertical line)

During the first experiment, the stability of the digester mixed at 200 rpm started to deteriorate, with the RR increasing from 0.6 to over 3.0, in less than 1 RT after the change in mixing speed as seen in Figure 9.1. This led to the irreversible souring of the digester 2 RT after the change in mixing speed, indicated by a RR of over 3.0. The digester at 100 rpm started to display similar signs of instability to the digester at 200 rpm at 1.4 RT after the change in mixing speed. This digester was considered to be irreversibly soured within 2.3 RT. Finally, after 3 RT, the digester at 50 rpm started to display instabilities. The unmixed digester did not demonstrate instability in the same way that the other digesters ultimately did, but throughout the experiment was shown to give more variable results in terms of RR and total concentration of VFAs than the other digesters.

It was of interest to note that all three of the mixed digesters demonstrated instabilities during the experiment, and the order in which they did so was that of fastest mixing to slowest mixing.

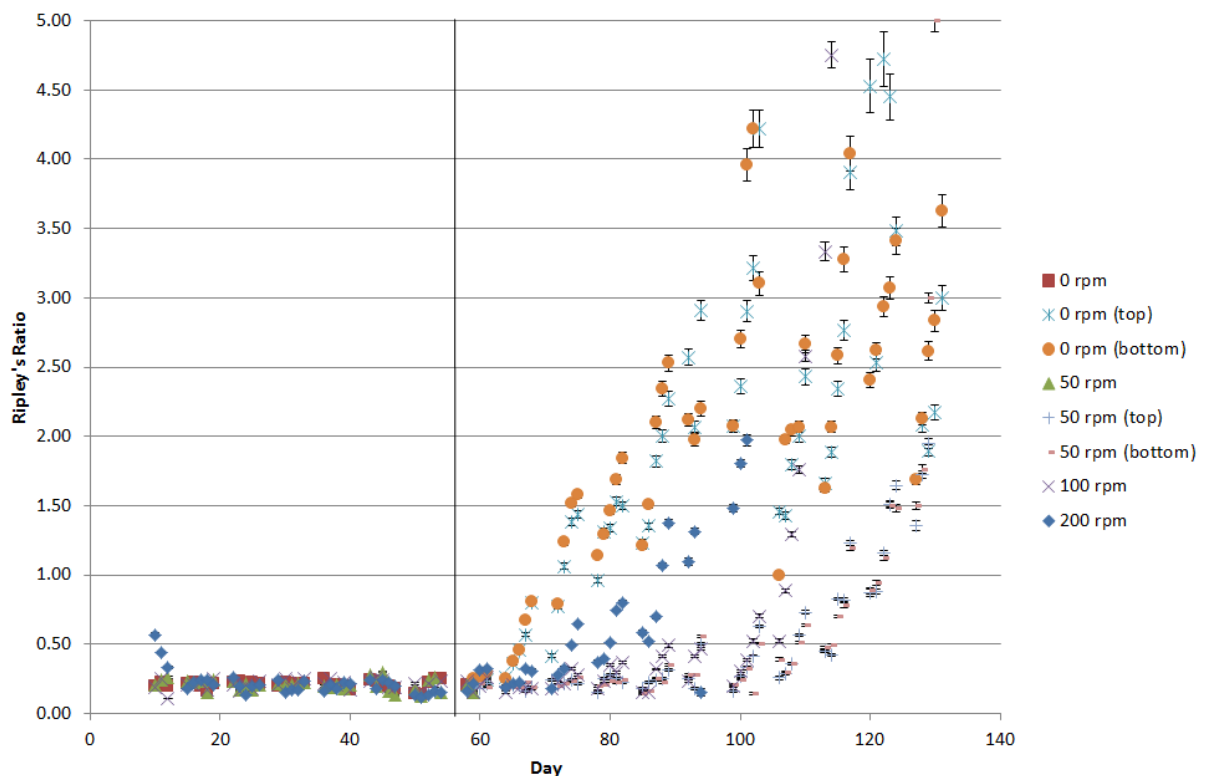


Figure 9.2 – RR of four digesters over the course of the second experiment (mixing changes made on Day 59 indicated by vertical line)

It can be seen in Figure 9.2 that, in the second experiment, within less than 1 RT of the change in mixing speed, RR in the digester under no mixing conditions increased above 0.8, indicating the presence of instabilities within the digester. Similar increases in the RR are seen in the digester at 200 rpm after 1.2 RT. Irreversible souring was considered to have taken place after 1.8 RT for the digesters at 0 rpm and 200 rpm. In the digesters at 50 rpm and 100 rpm, it took longer for instabilities to become evident, with RR remaining under 0.8 for 2 RT and 2.4 RT at 100 rpm and 50 rpm respectively. The digester at 100 rpm was not considered irreversibly soured until 2.3 RT after the change in mixing speed, whilst the digester at 50 rpm was not considered to be irreversibly soured within 3 RT. This was due to the fact that, whilst samples from the bottom of the digester reached 3.0 after 2.9 RT, RR of samples taken from the top of the digester did not exceed 3.0. This indicates that there are differences between the digester environment at the top and bottom of the digester under low mixing conditions.

Instabilities in the digester were recorded earliest in the digesters where mixing was stopped or increased to 200 rpm. However, once these instabilities were present, the digester with no mixing was better able to cope with them than the digester at 200 rpm. This is shown by the fact that the unmixed digester had an RR of between 0.8 and 3.0 for more than 1 RT before irreversible souring occurred, whilst the digester at 200 rpm survived for approximately 0.6 RT. The digesters at 50 rpm and 100 rpm both remained stable for over 2 RT, and the digester at 50 rpm was not considered irreversibly soured within 3 RT.

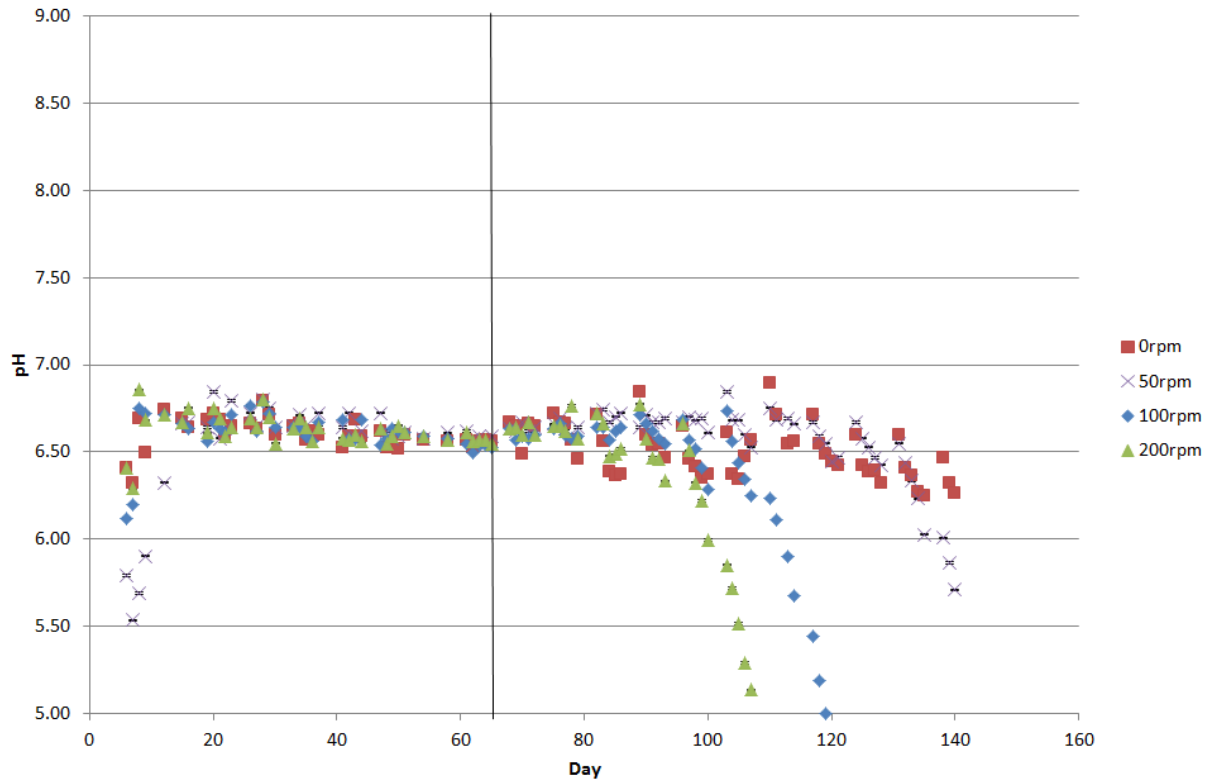


Figure 9.3 – pH of four digesters over the course of the first experiment (mixing changes made on Day 65 indicated by vertical line)

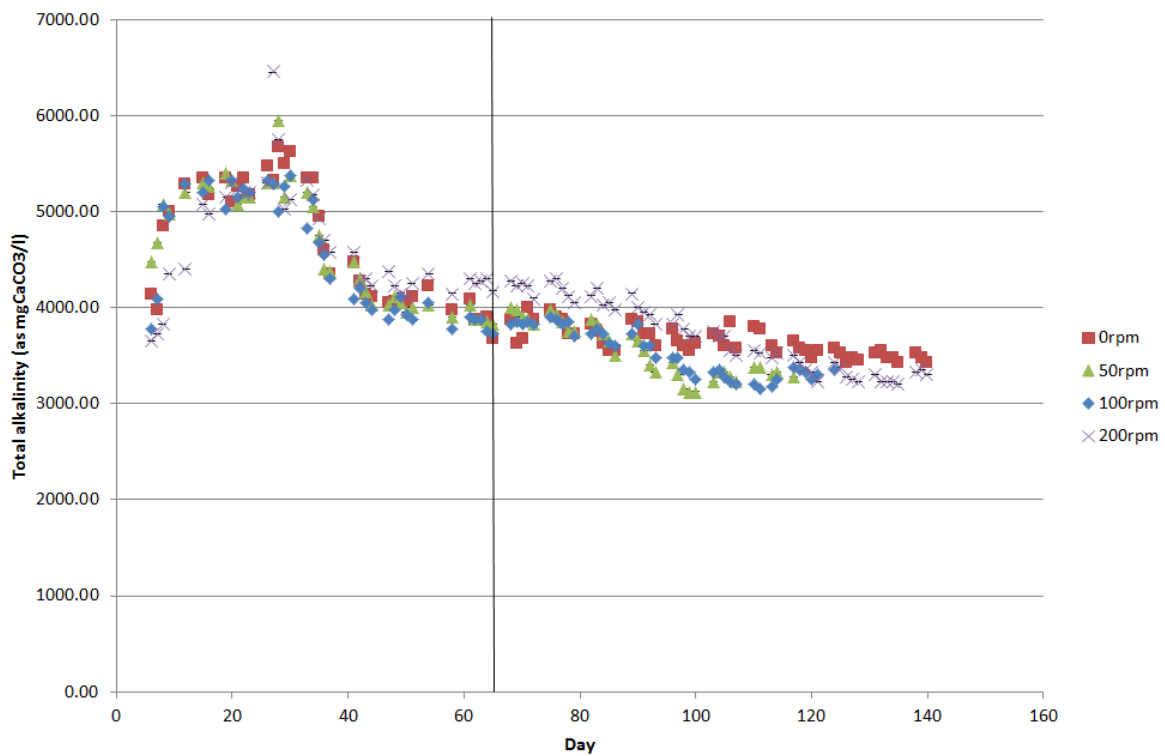


Figure 9.4 – TA of four digesters over the course of the first experiment (mixing changes made on Day 65 indicated by vertical line)

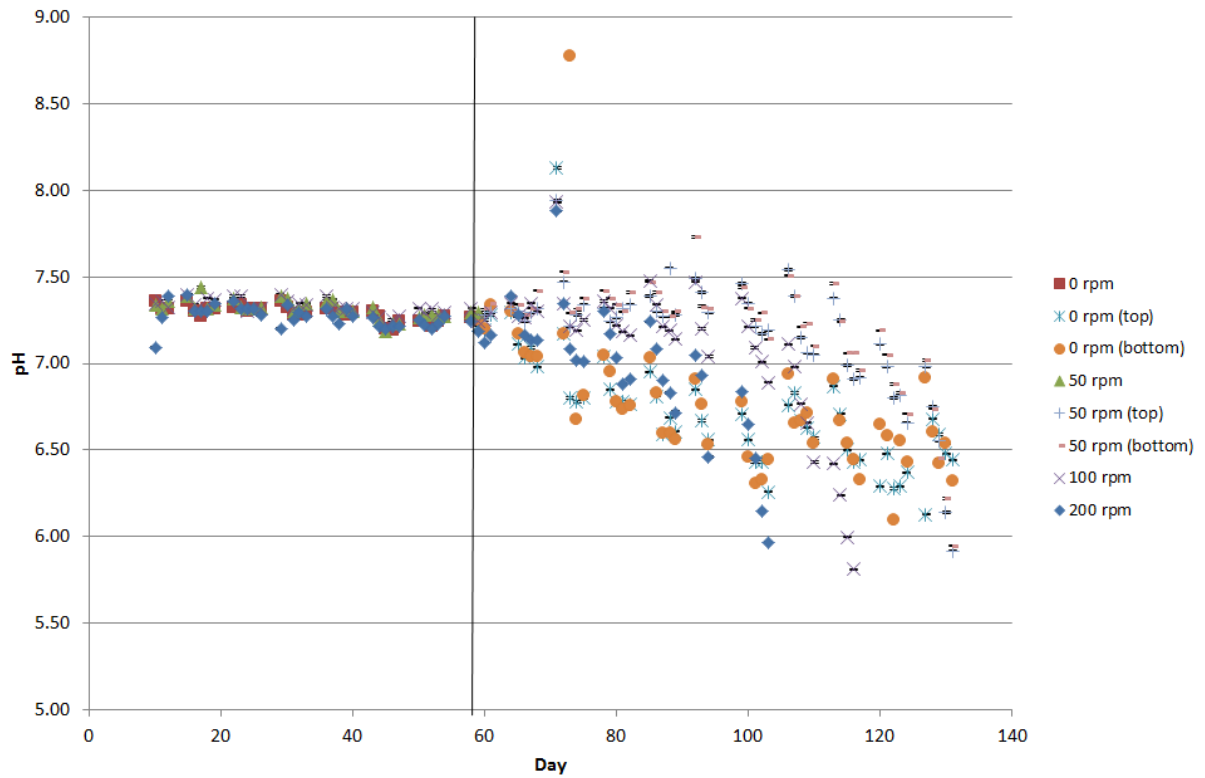


Figure 9.5 - pH of four digesters over the course of the second experiment (mixing changes made on Day 59 indicated by vertical line)

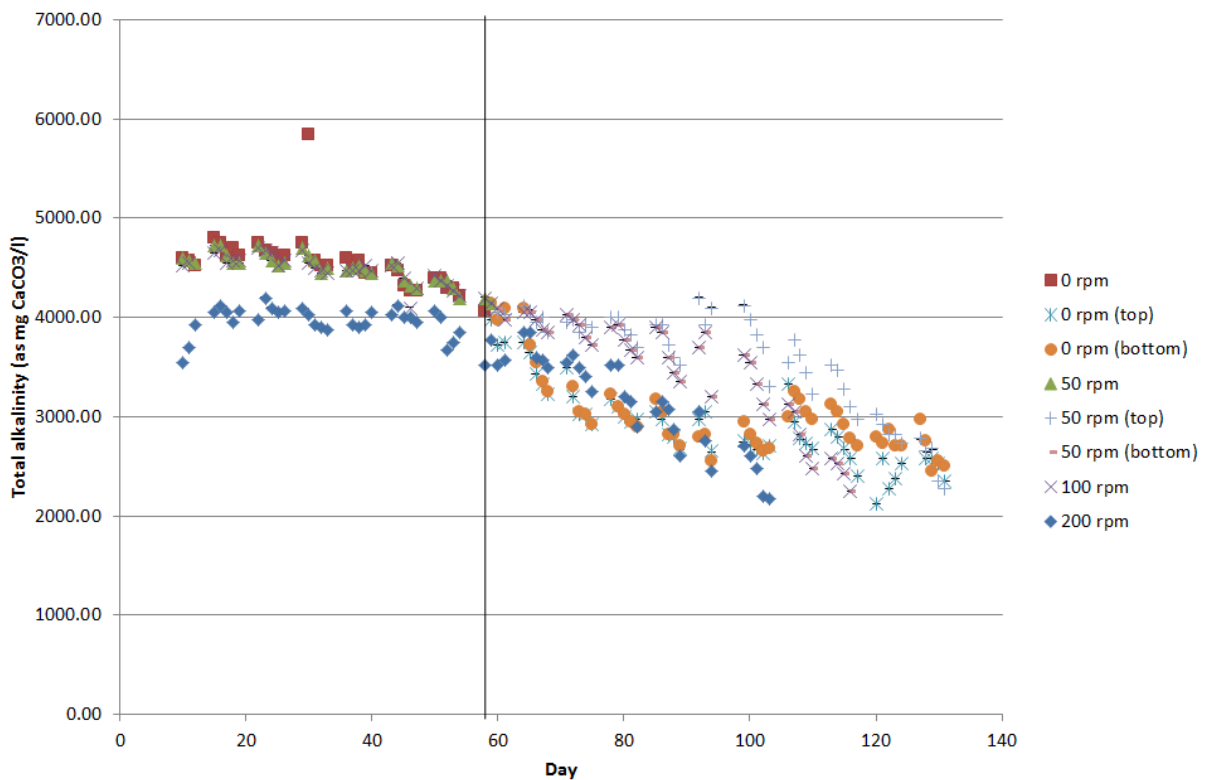


Figure 9.6 - TA of four digesters over the course of the second experiment (mixing changes made on Day 59 indicated by vertical line)

These patterns are replicated in the measurements of pH and TA for both experiments, shown in Figure 9.3 to Figure 9.6, with TA falling below 3500 mg CaCO<sub>3</sub>/l at a similar point to RR increasing above 0.8 and pH dropping below 6.5 at a similar point to RR increasing above 3.0. This happens because TA acts as the buffering capacity of a digester. Therefore, a falling TA acts as an early indication of the accumulation of VFAs, which in turn will lead to increased instability in the digester as indicated by an RR of 0.8 or higher. Similarly, pH drops significantly once the buffering capacity of the digester has been diminished and the concentration of VFAs continue to build up in the digester. At this point, irreversible souring, as indicated by an RR of 3.0 or higher, occurs. There is some difference between the two experiments, with a lower pH throughout the first experiment, which can be accounted for by the difference in the alkalinity of the feedstocks used.

Figure 9.7 and Figure 9.8 show the concentration of VFAs in the digesters over the course of the two experiments. In the first experiment, as the digester at 200 rpm became unstable, the total concentration of VFAs increased from less than 5 mM (0.08 mg/l as acetate) to nearly 100 mM (1.67 mg/l as acetate) before falling to 60 mM (1.02 mg/l as acetate). Prior to this increase in VFA concentration, the total VFA content of the digester had not exceeded 5 mM (0.08 mg/l as acetate). However, in all digesters in the first experiment, the concentration of VFAs is an order of magnitude higher than in the second experiment. While it is not clear what causes this inherent instability in the digesters in the first experiment, it is likely that an intermediary metabolite produced during the digestion of the feedstock causes inhibition of the methanogens present in the digester, reducing their growth rate and thereby causing the eventual washout of the methanogenic population. This may explain the increased build-up of VFAs in the digesters during the first experiment as they are the food source of the methanogens. The source of this metabolite is unclear, though the difference between the two feedstocks and the fact that the effect is not seen to the same extent in the second experiment suggest that it may be a compound in the yeast extract.

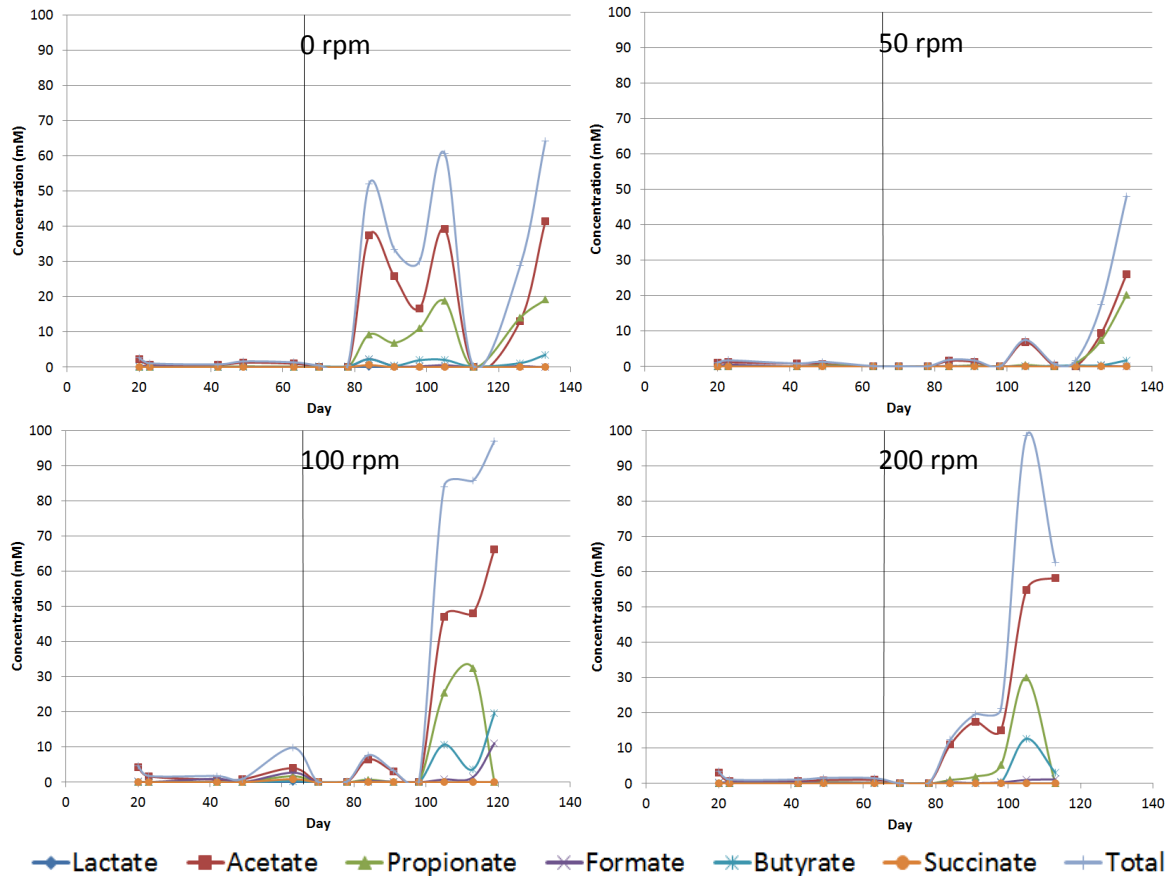


Figure 9.7 – VFA concentrations in four digesters over the course of the first experiment (mixing changes made on Day 65 indicated by vertical line)

In the second experiment, it can be seen that in the digester changed to no mixing, there is an immediate increase in the concentration of VFAs and the variability of the concentration of VFAs over time. This coincides with an increasing RR. The variability is likely to be due to the formation of distinct pockets in the digester under the no mixing conditions, some of which have of high concentration of VFAs. In the other digesters, VFA concentrations start to rise at the same point that instabilities are recorded in the digester by RR increasing above 0.8. A rapid increase in concentrations of VFAs above 5 mM (0.08 mg/l as acetate), with total VFA concentrations in the range of 10-25 mM (0.17-0.42 mg/l as acetate), coincides with the souring of the digester. In all cases, the VFA of highest concentration in the digester was acetate, followed by propionate, and then butyrate. It was only when total VFA concentration rose above 10 mM (0.17 mg/l as acetate),

that the presence of VFAs other than acetate became apparent. The effect of VFA concentration on microbiological communities will be considered in Section 9.6.

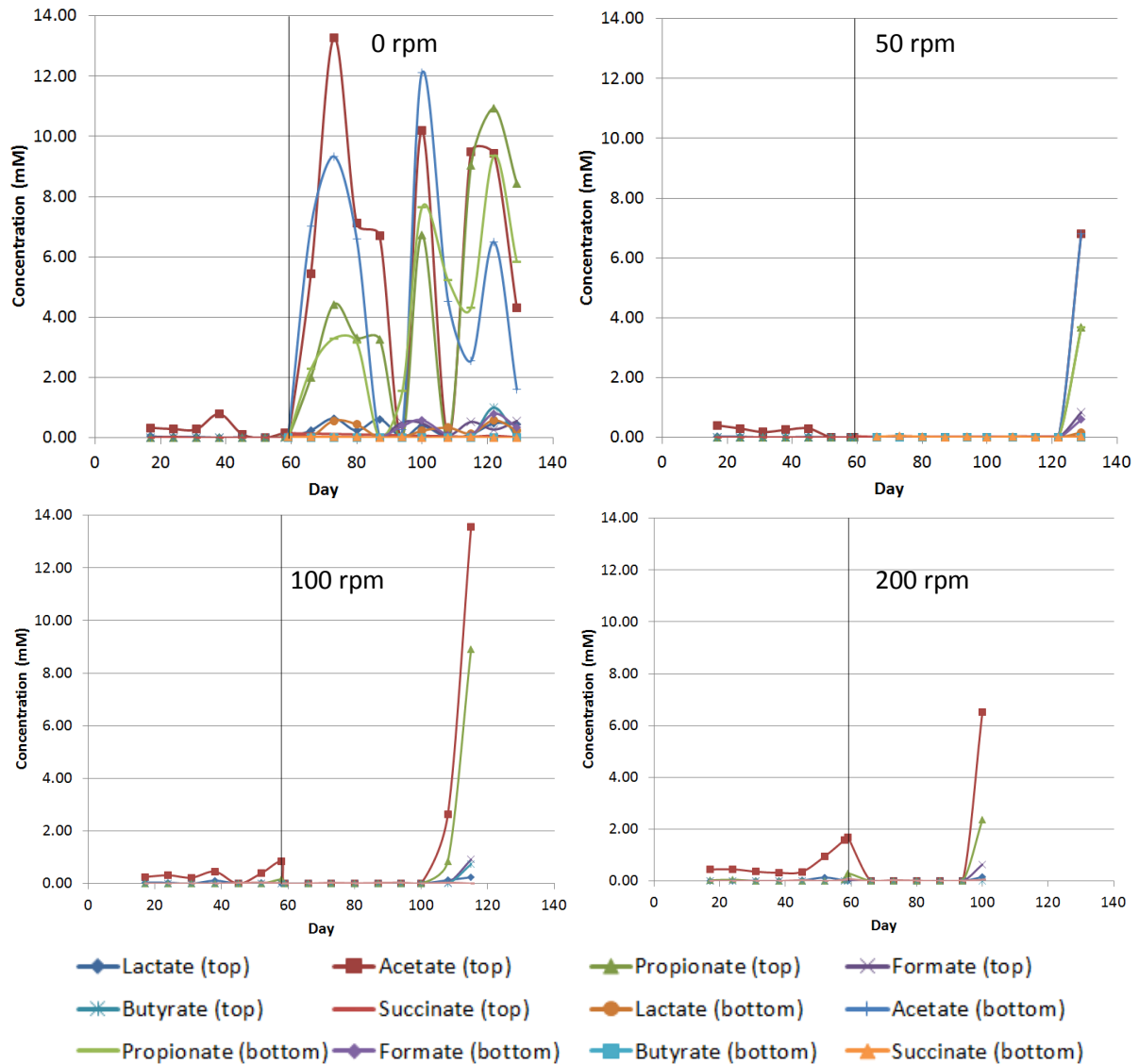


Figure 9.8 - VFA concentrations in four digesters over the course of the second experiment (mixing changes made on Day 59 indicated by vertical line)

These results suggest that whilst digester mixing is beneficial in order to maintain control over the digestion process, a digester is more stable with the minimal possible level of mixing, and an increased level of mixing only increases the instability of the digester. The difference between the stability of the digester with no mixing in the first and second experiments may be accounted for by the increased SRT caused by a combination of stratification and sampling only from the top of the digester in the first experiment. Whilst all of the digesters in the first experiment were adversely

affected by an intermediary metabolite, this increased SRT is likely to have reduced the washout rate of the slow-growing methanogenic population, as compared to sampling from all levels of the digester.

#### **9.4 Effect of mixing on digester performance**

Two important aims of anaerobic digestion highlighted in Chapter 3 are sludge stabilisation and sludge volume reduction. In order to ascertain the digester performance in these areas, TS and VS concentrations were measured in samples taken from the digester. Figure 9.9 to Figure 9.12 show the TS and VS concentrations over the course of each of the two experiments.

It can be seen that TS and VS follow a similar pattern in both of the experiments. During the start-up of the digesters in the first experiment, TS falls from approximately 20 g/l to 12 g/l whilst VS falls from 13 g/l to 7 g/l. This indicates that as the process reaches equilibrium after start-up, the TS reduction in the digesters is approximately 70 % whilst the VS reduction, indicative of sludge stabilisation, is approximately 80 %. The concentrations of TS and VS in the digester at 0 rpm fall to approximately 8 g/l and 4 g/l respectively after the change in mixing speed. In the first experiment, samples were only taken from the top of the digester and this result suggests that stratification of the digester occurred as discussed in Section 9.3, thereby increasing the SRT.

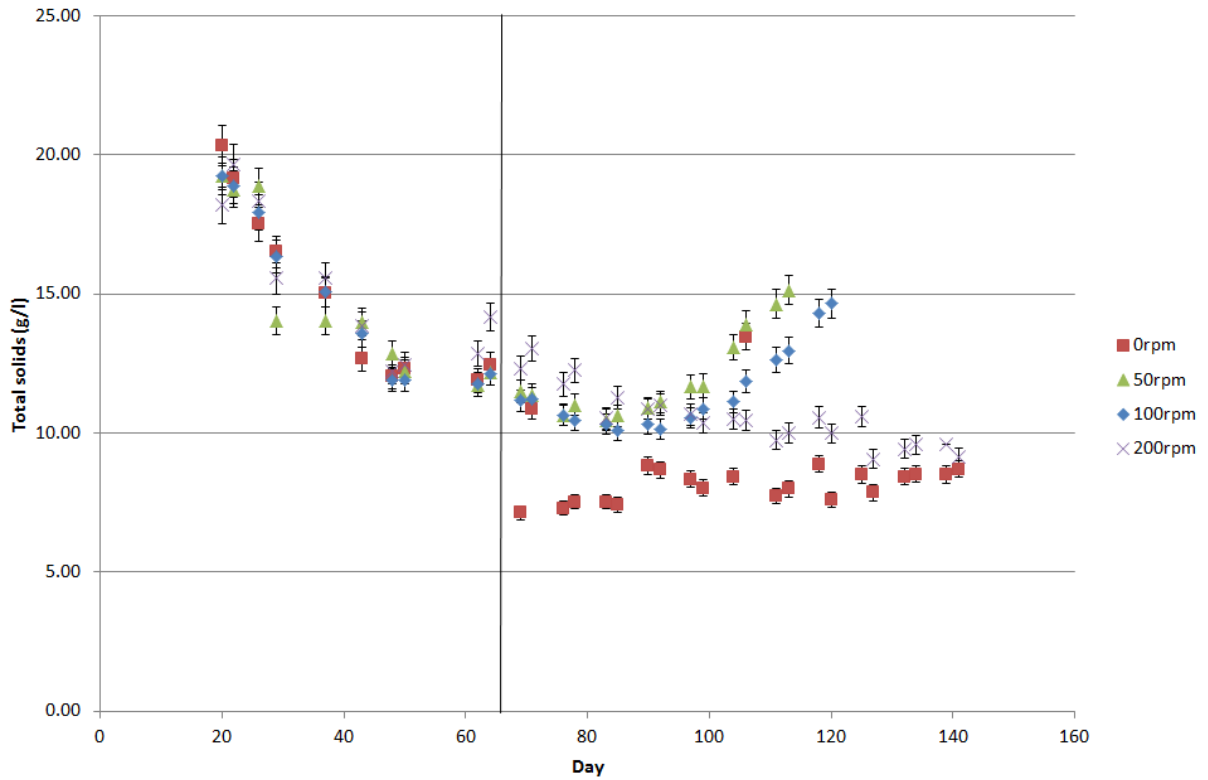


Figure 9.9 – TS concentration of four digesters over the course of the first experiment (mixing changes made on Day 65 indicated by vertical line)

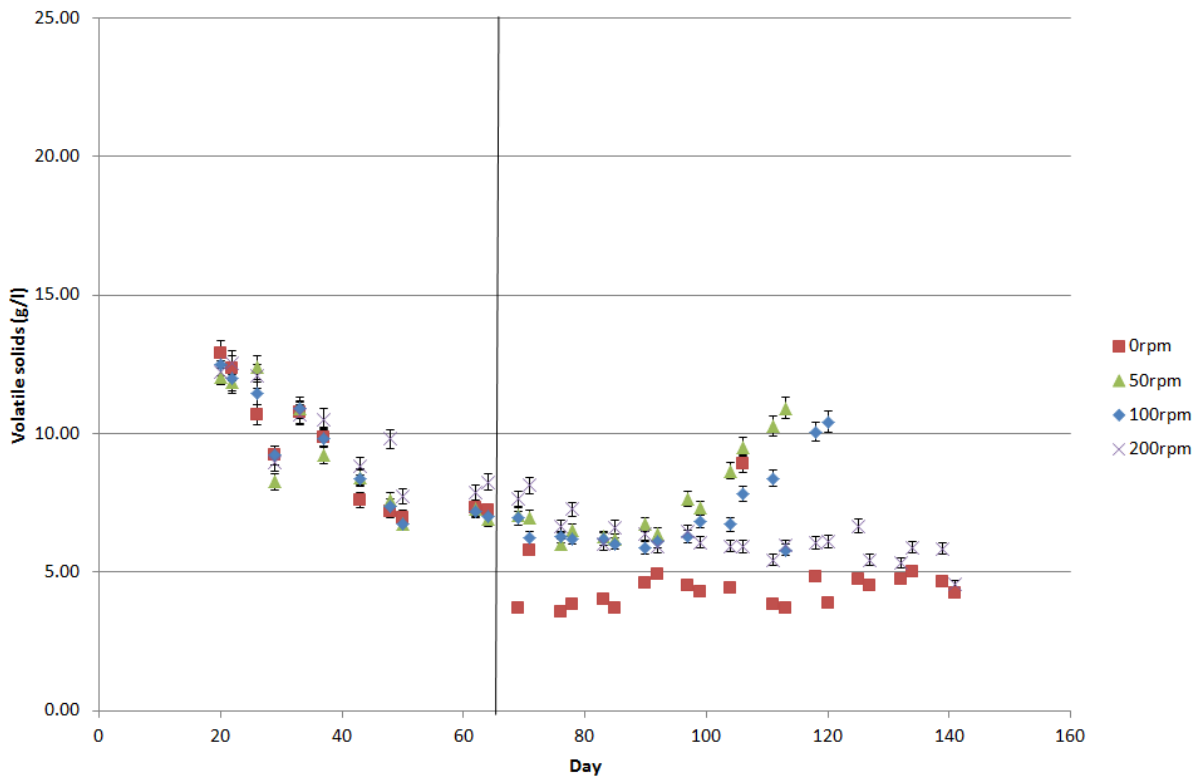


Figure 9.10 – VS concentration of four digesters over the course of the first experiment (mixing changes made on Day 65 indicated by vertical line)

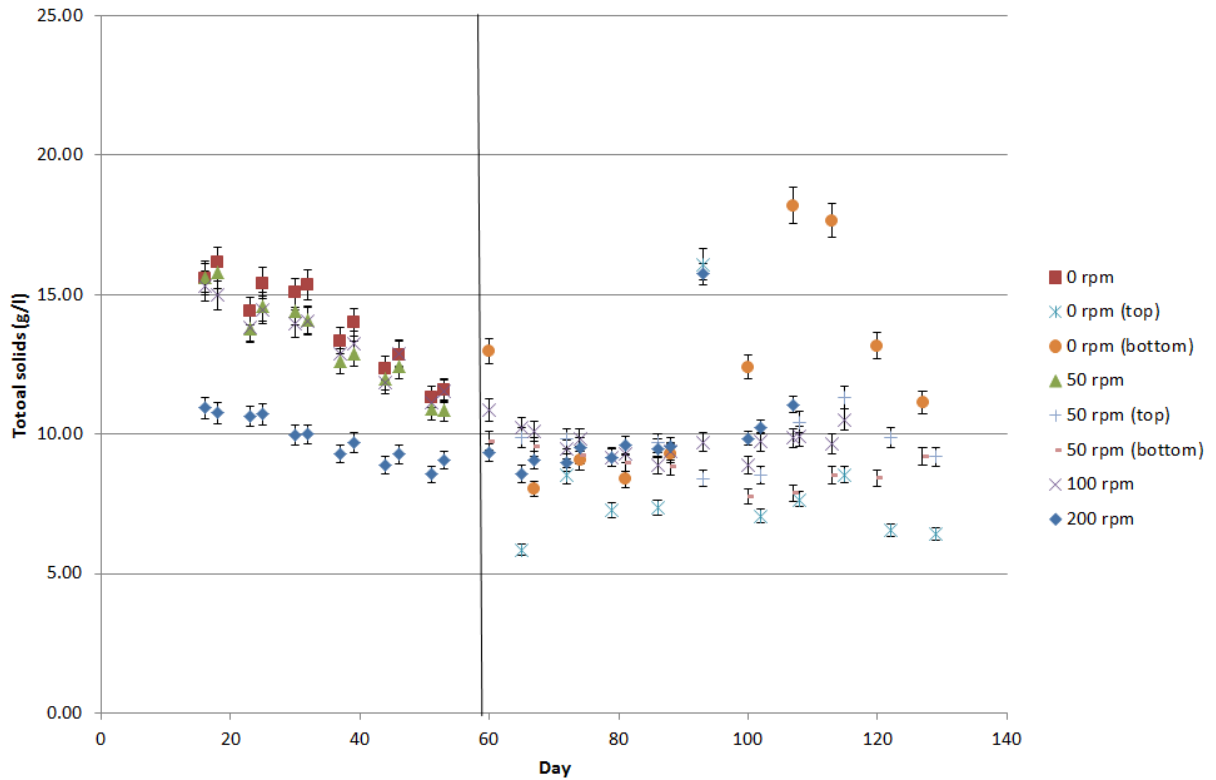


Figure 9.11 – TS concentration of four digesters over the course of the second experiment (mixing changes made on Day 59 indicated by vertical line)

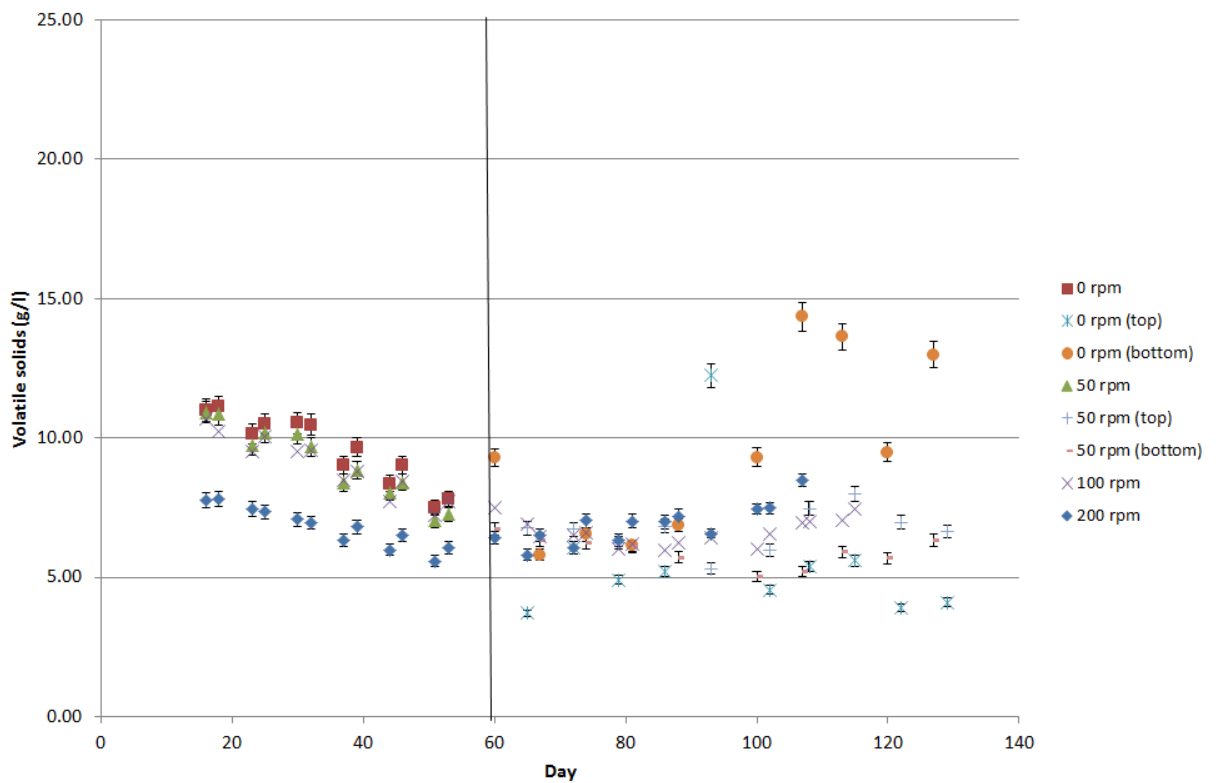


Figure 9.12 – VS concentration of four digesters over the course of the second experiment (mixing changes made on Day 59 indicated by vertical line)

From Day 100, TS and VS concentration in the digesters at 50 rpm and 100 rpm in the first experiment start to increase. It is unclear as to why this increase takes place though it could be caused by floating scum forming at the liquid surface in the digester and being washed out when samples were taken. This could explain the increase in both TS and VS in samples taken from these digesters, as it does not appear to be linked to process instabilities in the digesters. The fact that there was no increase in the TS and VS concentrations in the digester at 200 rpm suggests that the use of a higher mixing speed may have been sufficient to either prevent scum formation or break up the scum layer at the free surface of the digester, a process which is known to require significantly more mixing power than simply achieving mixing (Vera and Lavelle, 2005).

During the start-up of the digesters in the second experiment, TS falls from approximately 15 g/l to 10 g/l whilst VS falls from 10 g/l to 5 g/l. Again, once equilibrium is reached after start-up, the TS reduction in the digesters is approximately 70 % whilst the VS reduction is approximately 80 %. For the most part, the concentration of TS and VS in the digesters after start-up stays between 8 and 10 g/l for TS and between 5 and 8 g/l for VS for the remainder of the experiments. It can be seen that there is an increase in the variability of the concentrations recorded in the digesters at 0 rpm and 50 rpm, where samples are taken from both the top and the bottom of the digester. This indicates that, as expected, in these poorly-mixed digesters, some stratification occurs, with increased solids concentrations found close to the base of the digester compared to the top of the digester.

## **9.5 Effect of mixing on gas production**

Due to problems with the gas flow meter in the first experiment, it was only possible to record the gas volume from Day 43 onwards. The cumulative gas production for the first experiment is shown in Figure 9.13 and the daily gas production is shown in Figure 9.14, whilst the cumulative and daily gas production from the second experiment are shown in Figure 9.15 and Figure 9.16 respectively.

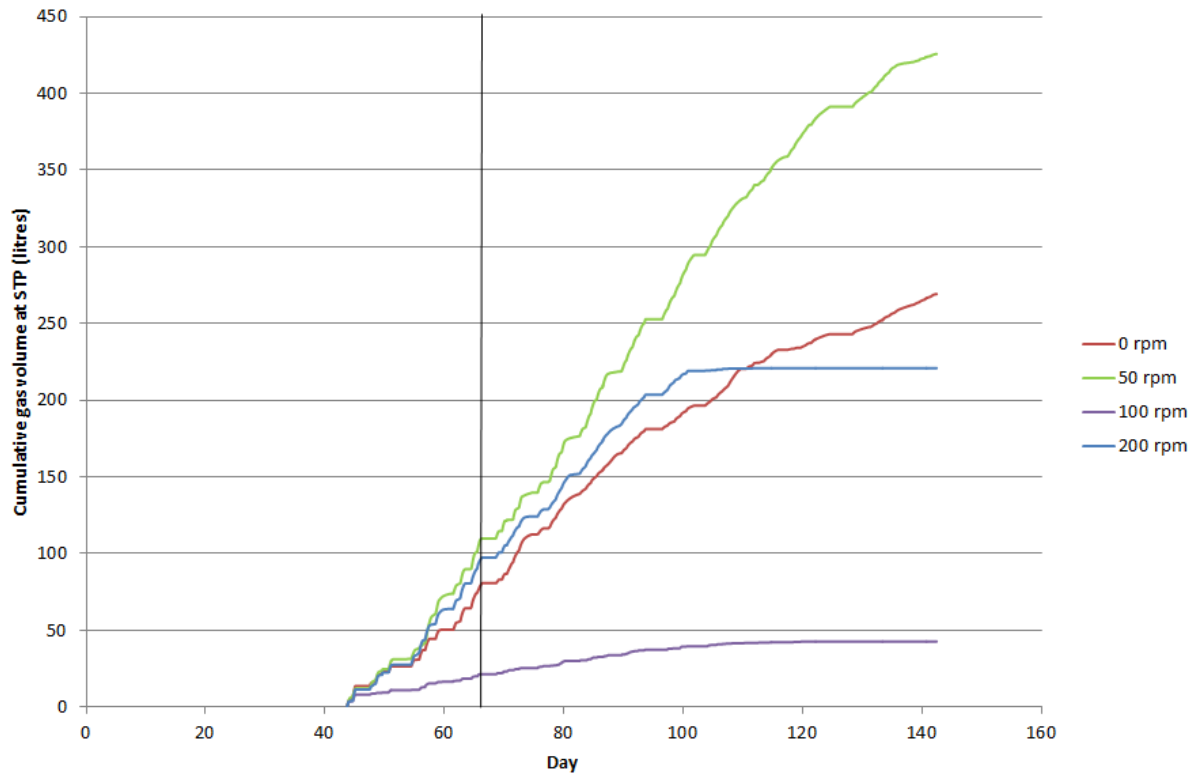


Figure 9.13 - Cumulative biogas production of four digesters over the course of the first experiment (mixing changes made on Day 65 indicated by vertical line)

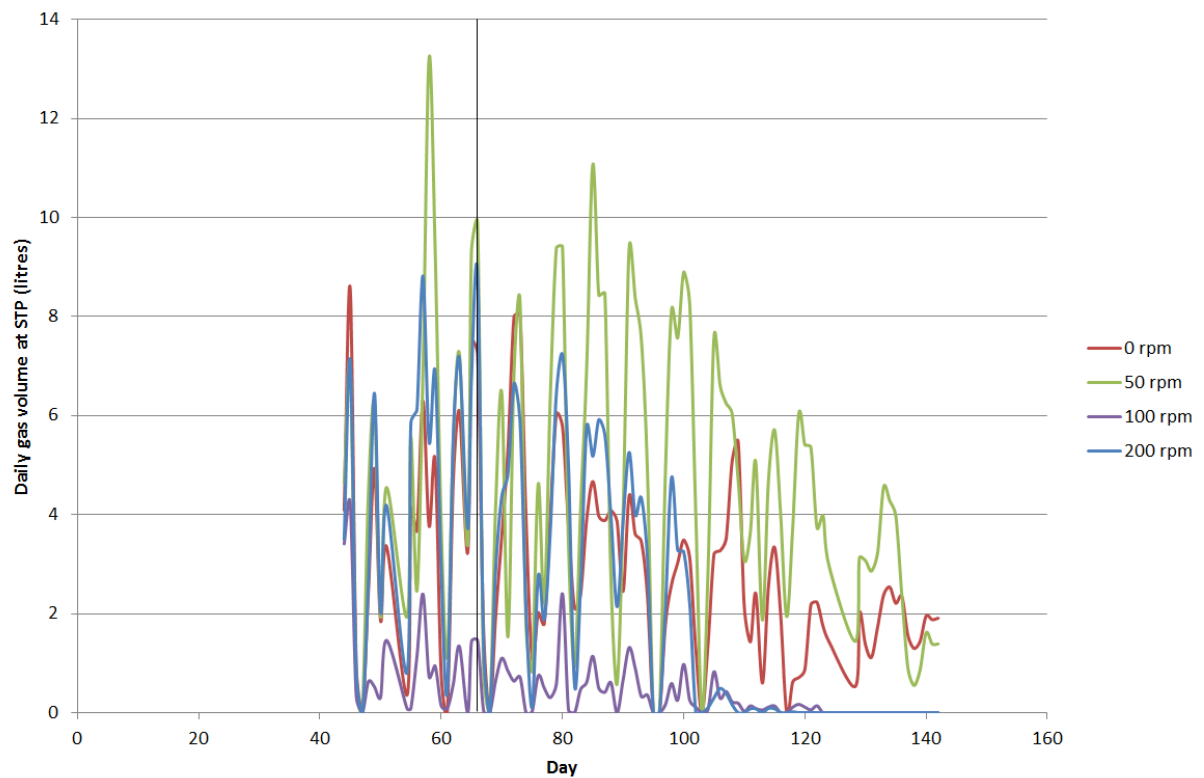


Figure 9.14 - Daily biogas production of four digesters over the course of the first experiment (mixing changes made on Day 65 indicated by vertical line)

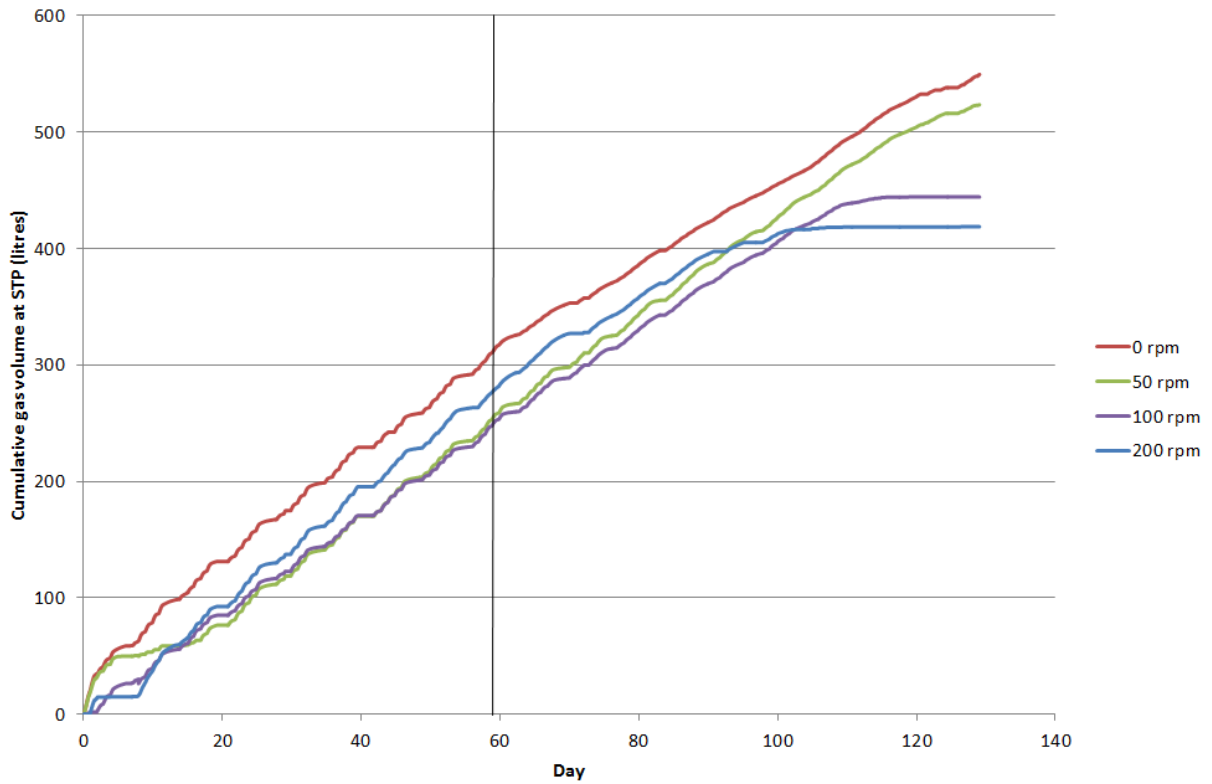


Figure 9.15 - Cumulative biogas production of four digesters over the course of the second experiment (mixing changes made on Day 59 indicated by vertical line)

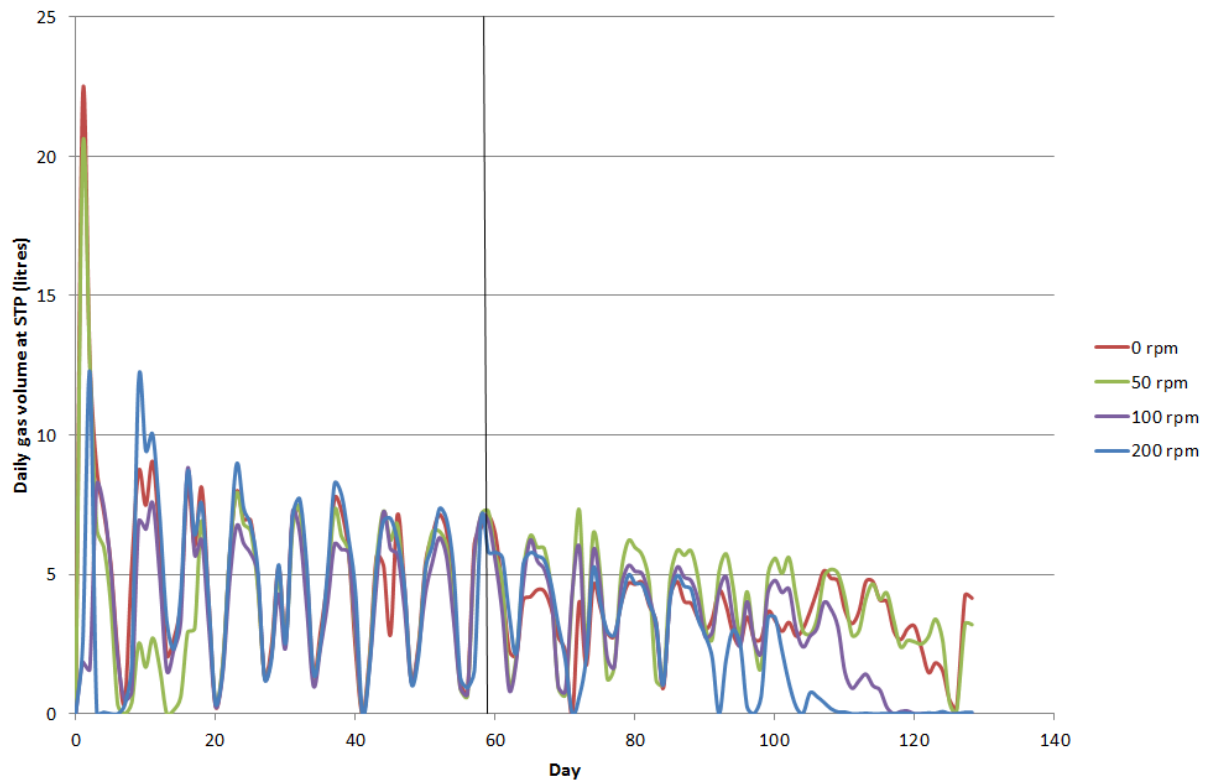


Figure 9.16 - Daily biogas production of four digesters over the course of the second experiment (mixing changes made on Day 59 indicated by vertical line)

The cumulative biogas production curves were split into two sections at the point that the mixing speed was changed, giving pre-change (all digesters at 100 rpm) and post-change (digesters at different mixing speeds) data sets for each experiment. Linear regression was used to fit a straight line to each of these curves and the gradient was calculated. In the cases of digesters that became irreversibly soured before the end of 3 RT, the data for the linear regression was taken from the day that mixing speeds were changed until the point at which irreversible souring was deemed to have occurred. The calculated gradients and R-squared values are shown in Table 9.2 and Table 9.3 for the first and second experiments respectively. It can be seen from the R-squared values that a straight line provided a good fit to the cumulative biogas production curves, with R-squared values greater than 93 % for the first experiment and 98 % for the second experiment. This difference may be accounted for by the greater digester instability in the first experiment as described in Section 9.3. The slowed growth rate and eventual washout of methanogens would result in an impaired digestion process and a reduction in the biogas production rate over time. This would lead to the cumulative biogas production approximating more closely to a curve that plateaus over time, than to a straight line.

**Table 9.2 – Gradients and R-squared values for linear regression performed on biogas production curves in four digesters before and after a change in mixing speed during the first experiment. N.B.: Mixing speeds for each digester are given before and after the change in mixing speeds with the mixing speed in bold relating to the curve whose gradient is calculated**

	<b>Digester mixing speed</b>	<b>Gradient</b>	<b>R-squared</b>
<b>Up to Day 65</b>	<b>100 rpm</b> - 0 rpm	2.75	0.974
	<b>100 rpm</b> - 50 rpm	4.24	0.960
	<b>100 rpm</b> - 100 rpm	0.66	0.946
	<b>100 rpm</b> - 200 rpm	3.77	0.973
<b>After Day 65</b>	100 rpm - <b>0 rpm</b>	2.33	0.955
	100 rpm - <b>50 rpm</b>	4.34	0.974
	100 rpm - <b>100 rpm</b>	0.39	0.950
	100 rpm - <b>200 rpm</b>	2.85	0.932

**Table 9.3 – Gradients and R-squared values for linear regression performed on biogas production curves in four digesters before and after a change in mixing speed during the second experiment. N.B.: Mixing speeds for each digester are given before and after the change in mixing speeds with the mixing speed in bold relating to the curve whose gradient is calculated**

	<b>Digester mixing speed</b>	<b>Gradient</b>	<b>R-squared</b>
<b>Up to Day 59</b>	<b>100 rpm</b> - 0 rpm	4.78	0.995
	<b>100 rpm</b> - 50 rpm	3.93	0.984
	<b>100 rpm</b> - 100 rpm	4.18	0.998
	<b>100 rpm</b> - 200 rpm	4.89	0.996
<b>After Day 59</b>	100 rpm - <b>0 rpm</b>	3.48	0.998
	100 rpm - <b>50 rpm</b>	4.04	0.997
	100 rpm - <b>100 rpm</b>	3.80	0.999
	100 rpm - <b>200 rpm</b>	3.28	0.986

In order to determine whether the rate of gas production demonstrated by the calculated gradients came from the same statistical population, i.e. if the digesters were producing biogas at the same rate, two-sample t-tests assuming equal variance were carried out.

A comparison of the rate of gas production in the four digesters prior to the change of mixing speed in the first experiment showed that at a 95 % confidence interval, only the digesters that would be changed to 50 rpm and 200 rpm were producing biogas at the same rate. The other two digesters (mixed at 0 rpm and 100 rpm after Day 65) were producing biogas at a significantly slower rate. As the sludge feed to each of the digesters was the same and the digesters were treated in the same way during start-up, this suggests that gas was leaking from the digesters, despite all efforts to ensure that they were properly sealed.

As the digesters in the first experiment could not be compared to one another, two-sample t-tests assuming equal variance were carried out to compare the gas production rate in each digester before and after the change in mixing speed. The rate of gas production in the digesters that were changed to 50 rpm and to 0 rpm were found to stay the same as before the change in mixing speed. In the other two digesters, at 100 rpm and 200 rpm, the rate of gas production fell. It should be noted that

these were the two digesters that showed signs of instability within 1.5 RT after the change in mixing speed, indicating that stable digesters are better able to produce a high volume of biogas.

It can be seen in Figure 9.13 that less than 2 RT after the change in mixing speed, the gas production rate from the digester at 200 rpm had fallen to less than 20 ml/l/day. This corresponds with the irreversible souring of the digester. Similarly, in the digester at 100 rpm, the drop in gas production appears to coincide with the digester's irreversible souring, though it is harder to judge exactly when gas production in this digester fails due to its low rate of measured gas production throughout the experiment.

It can be seen from Figure 9.14 that all of the digesters experience a reduction in daily biogas production over the course of the first experiment. This agrees well with the hypothesis that there is a compound in the feed that suppresses the growth rate of some of the micro-organisms present in the digester. This is likely to be the methanogens as they are the most sensitive community to inhibition as seen in Section 2.4.5 and are key to the production of methane-rich biogas. This slowing of the growth rate of the methanogenic population leads to a slow washout of the methanogens, which leads to a reduction in the gas volume produced from the digester, and ultimately digester souring. The rate of gas production is further hampered at high mixing speeds, which result in a more homogenous sludge throughout the digester, so that microbiological community washout is more rapid than under low mixing conditions when communities are more likely to benefit from the increased SRT caused by sedimentation.

The same analysis was undertaken with the results of the second experiment. A comparison of the rate of gas production in the four digesters prior to the change of mixing speed showed that at a 95 % confidence interval, the gradients in the second experiment were all from the same statistical population, i.e. all of the digesters were producing biogas at the same rate. In the same way, two-sample t-tests assuming equal variance were carried out in order to compare the gas production rate

in each digester before and after the change in mixing speed. The rates of gas production in the digester that remained at 100 rpm and the digester that was changed to 50 rpm were found to stay the same after the change in mixing speed. This implies that a cost saving can be achieved by reducing the mixing from 100 rpm to 50 rpm as the same gas volume is produced but less power is required to run the mixer. In the other two digesters, at 0 rpm and 200 rpm, the rate of gas production fell.

It can be seen from the change in gradient that the greatest drop in gas production rate occurs in the digester increased to a mixing speed of 200 rpm. This accompanies the rapid increase in process instability as discussed in Section 9.3. Additionally, 1.8 RT after the change in mixing speed, the gas production rate from the digester had fallen to less than 20 ml/l/day. This corresponds to the irreversible souring of the digester. Similarly, in the digester where mixing was stopped, the drop in gas production coincides with the observation of increasing instabilities in the digester. However, in this case, gas production continued over the remaining RT despite the fact that irreversible souring was deemed to have occurred within 2 RT of the change in mixing speed. This could be a consequence of stratification in the digester. Whilst the increase in the concentration of solids at the base of the digester can help to bring micro-organisms and food sources in the sludge into close proximity and thereby aid the digestion process, the increase in the viscosity of the sludge at the base of the digester can make it more difficult for gas bubbles to escape the digester. As such, gas production recorded after the irreversible souring of the digester could be a result of gas bubbles trapped in the sludge escaping over a prolonged period of time, or of pockets of the digester still functioning well, even after the digester as a whole is deemed irreversibly soured.

It can be seen from Figure 9.16 that all of the digesters experience a reduction in daily biogas production over the course of the experiment. Again, this was attributed to the inhibition of methanogens by an intermediary metabolite produced during the digestion of the synthetic sludge,

reducing the growth rate of the methanogens and resulting in the slow washout of the methanogenic community. Without a detailed analysis of the metabolic pathways involved in the digestion of the synthetic sludge, the source of this intermediary metabolite is not clear.

The percentage of methane measured in the biogas in the two experiments is shown in Figure 9.17 and Figure 9.18. It can be seen in Figure 9.17 that the percentage of methane measured in the biogas in the first experiment is between 40 and 55 % before the change in mixing speed. This is lower than the typical range of 50-75 % methane in digester biogas and is slightly lower than in the second experiment. There is also a greater variability in the percentage methane in this experiment than in the second experiment. This may indicate an inherent instability in the digestion process, caused by the inhibition and washout of methanogens and exacerbated by differences in the synthetic feeds. After the change in mixing speed, the percentage methane from the digester with no mixing becomes yet more varied, between 30 and 60 %. This may be indicative of pockets forming within the digester, leading to an uncontrolled digestion process and hence, more erratic gas production. With the remaining digesters, the percentage of methane starts to fall as instabilities in the digester become apparent, with a methane percentage of less than 10 % coinciding with the irreversible souring of the digesters.

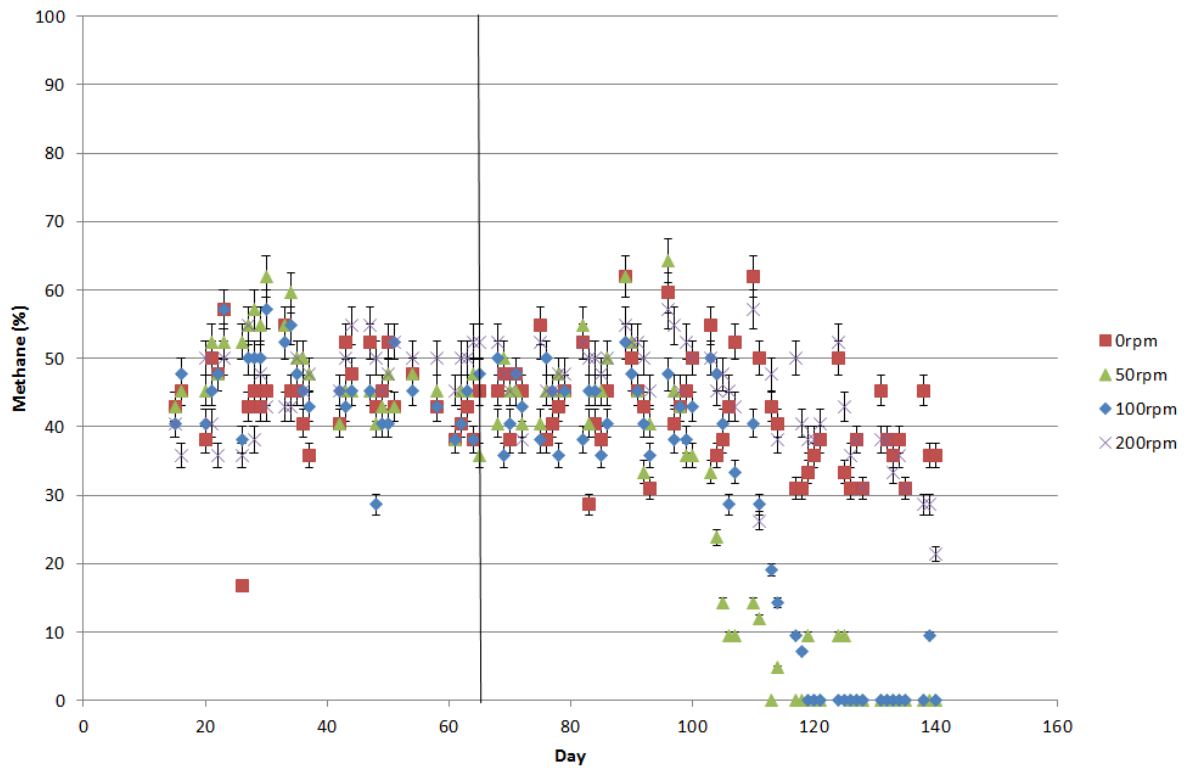


Figure 9.17 – Percentage of methane in biogas produced by each of four digesters over the course of the first experiment (mixing changes made on Day 65 indicated by vertical line)

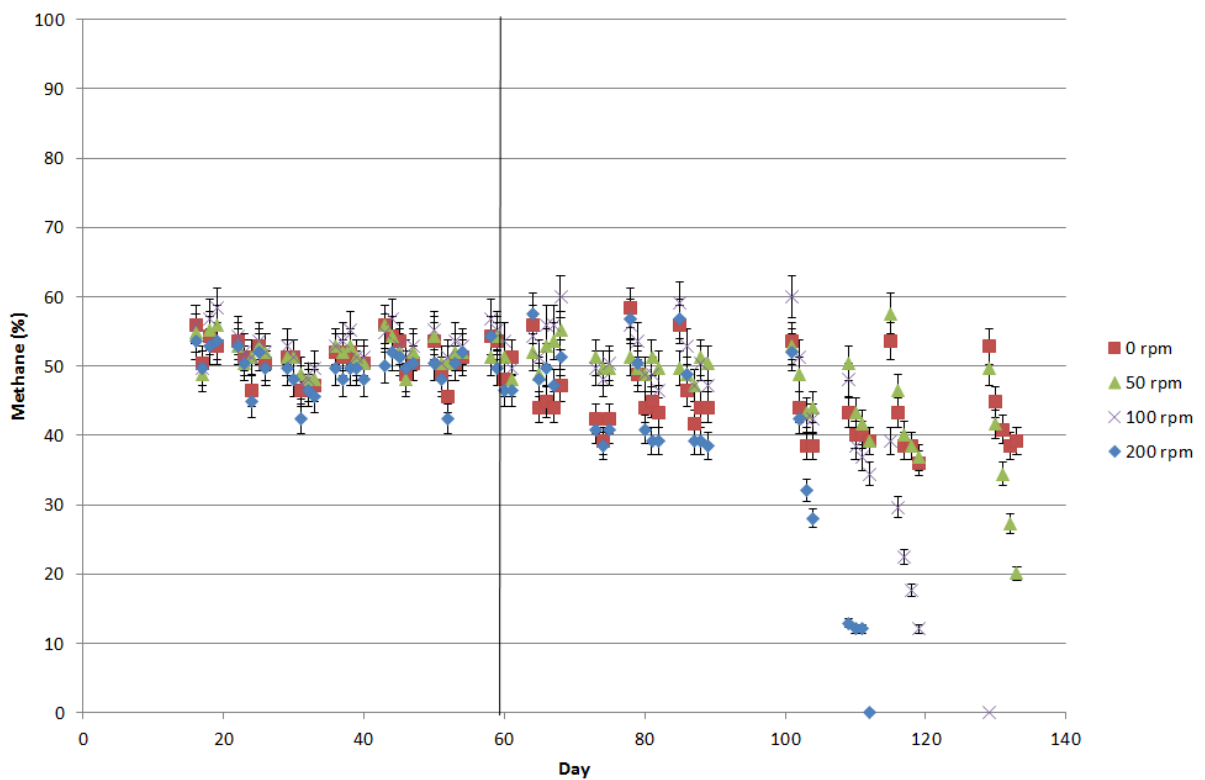


Figure 9.18 – Percentage of methane in biogas produced by each of four digesters over the course of the second experiment (mixing changes made on Day 59 indicated by vertical line)

It can be seen in Figure 9.18 that in the second experiment, the biogas is between 45 and 55 % methane before the change in mixing speed. Whilst this is towards the low end of the typical range of methane in biogas (50-75 %), it does not indicate digester instabilities as the percentage methane remains within the same range until the change in mixing speed. After the change in mixing speed, the percentage methane from the digester with no mixing becomes more varied, between 35 and 55 %. As stated above, this may be indicative of pockets of different environments forming within the digester. The remaining digesters continue to produce similar percentages of methane whilst stable. However, the percentage of methane starts to fall at the point that instabilities in the digester are recorded, with a methane percentage of less than 10 % occurring as irreversible souring occurs. This means that a decreasing percentage of methane in biogas can be used as a simple early indicator of instabilities in a digester, although its accuracy can be affected by the error associated with gas measurement and the variability of gas production. As such, RR acts as a more sensitive indicator of digester stability and should be used in preference to percentage methane if there is any doubt.

It is likely that the effect of a change in mixing speed on the microbiological population structure will take up to one RT to become apparent. As such, Figure 9.19 and Figure 9.20 show the volume of biogas produced by a digester in the two RT after the change in mixing speed, compared to the volume of biogas produced by the same digester in the RT prior to the change in mixing speed, for the first and second experiments respectively. Over each of these three RTs, a mean daily gas volume from each digester was calculated in order to take into account variations in the exact length of the period due to an incomplete gas volume record.

From the results of the first experiment, it was seen that the gas volume produced in the digester at 100 rpm decreased steadily over time. This may have been indicative of its increasing instability due to the inhibition and washout of methanogens, which resulted in its eventual souring. Similarly, the

digester at 200 rpm produced less than half the volume of biogas produced in previous RTs in the final RT prior to its souring.

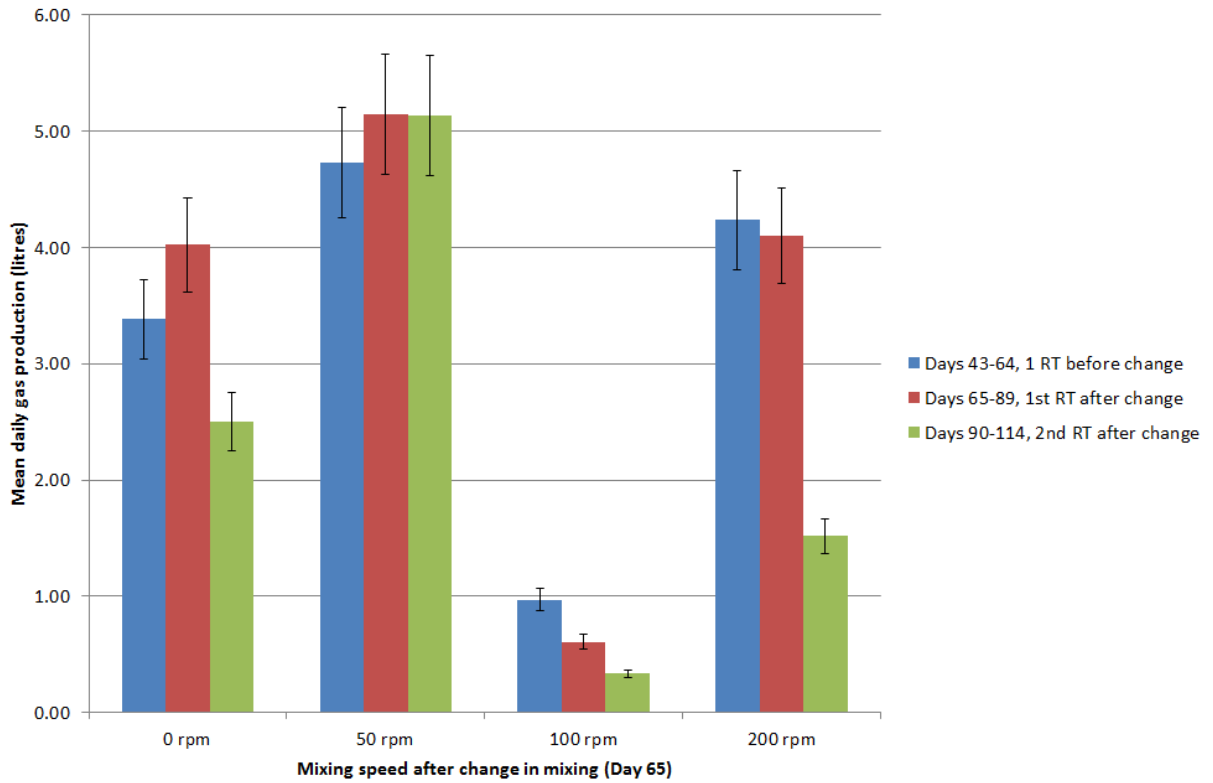
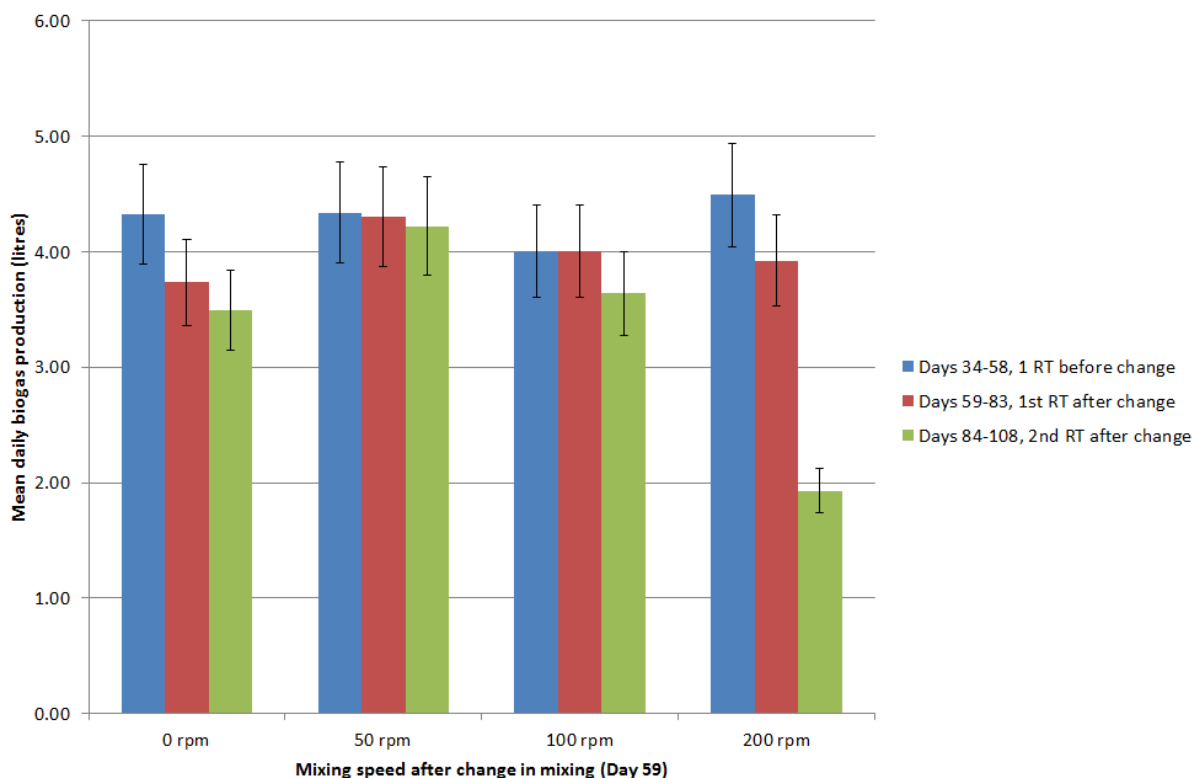


Figure 9.19 – Mean daily gas production over RT either side of the change in mixing speed during the first experiment



**Figure 9.20 – Mean daily gas production over RT either side of the change in mixing speed during the second experiment**

Conversely, the digester that was changed from 100 rpm to 0 rpm experienced a 20 % increase in biogas production in the first RT after the mixing speed was changed. However, this increase could be due to the increased SRT of the digester caused by stratification, as discussed in Section 9.4, and it can be seen that the biogas volume fell to 70 % of its original volume in the second RT after Day 65, which suggests that even though the SRT for the digester was likely to have increased, the inhibition of methanogens still had a detrimental effect on the digestion process. Again, an initial increase in biogas production was experienced in the digester changed from 100 rpm to 50 rpm. In this case, the increase continued in the second RT with a 10 % increase in gas production in each of the two RT after Day 65 as compared to the RT prior to Day 65. These results suggest that a low mixing speed is preferable for maximising biogas production from a digester and has the added advantage of reducing the power required for mixing.

In the second experiment, the digester that remained at 100 rpm after the change in mixing speed shows a small decline in gas production by the second RT after the change. By contrast, the digester

at 200 rpm produced less than half the volume of biogas in the second RT after the change compared to previous RTs. This is likely to be due to the souring of the digester during this period which had a significant negative effect on the gas production rate. The digester changed from 100 rpm to 0 rpm also demonstrated declining gas production, though nowhere near as severely as the digester at 200 rpm, with the mean daily volume by the second RT after change at 80 % of that in the RT prior to the change in mixing speed. As discussed previously, this may be attributed to pockets forming within the digester, leading to uncontrolled digestion and suboptimal use of the digester volume to produce biogas. The only digester in which gas production rate did not appear to suffer was the digester changed to 50 rpm. These results suggest that, whilst mixing is necessary to ensure both process stability and gas production, a low mixing speed is preferable for maximising biogas production from a digester.

## 9.6 Effect of mixing on microbiological communities

During the second experiment, samples were taken for microbial analysis using qPCR at the end of each RT after the change in mixing speed and one RT before the change in mixing speed. Additionally, samples were taken two hours prior to and two hours after the change in mixing speed on Day 59. The samples were tested for abundance of total *eubacteria*, as well as methanogenic orders, *Methanobacteriales* and *Methanomicrobiales*, and two acetoclastic methanogenic families, *Methanosaeta* and *Methanosarcina*, in order to ascertain the effect of mixing on methanogens over the course of the experiment. This is the first time that qPCR has been used to investigate the effects of mixing speed on methanogenic population community in an anaerobic digester.

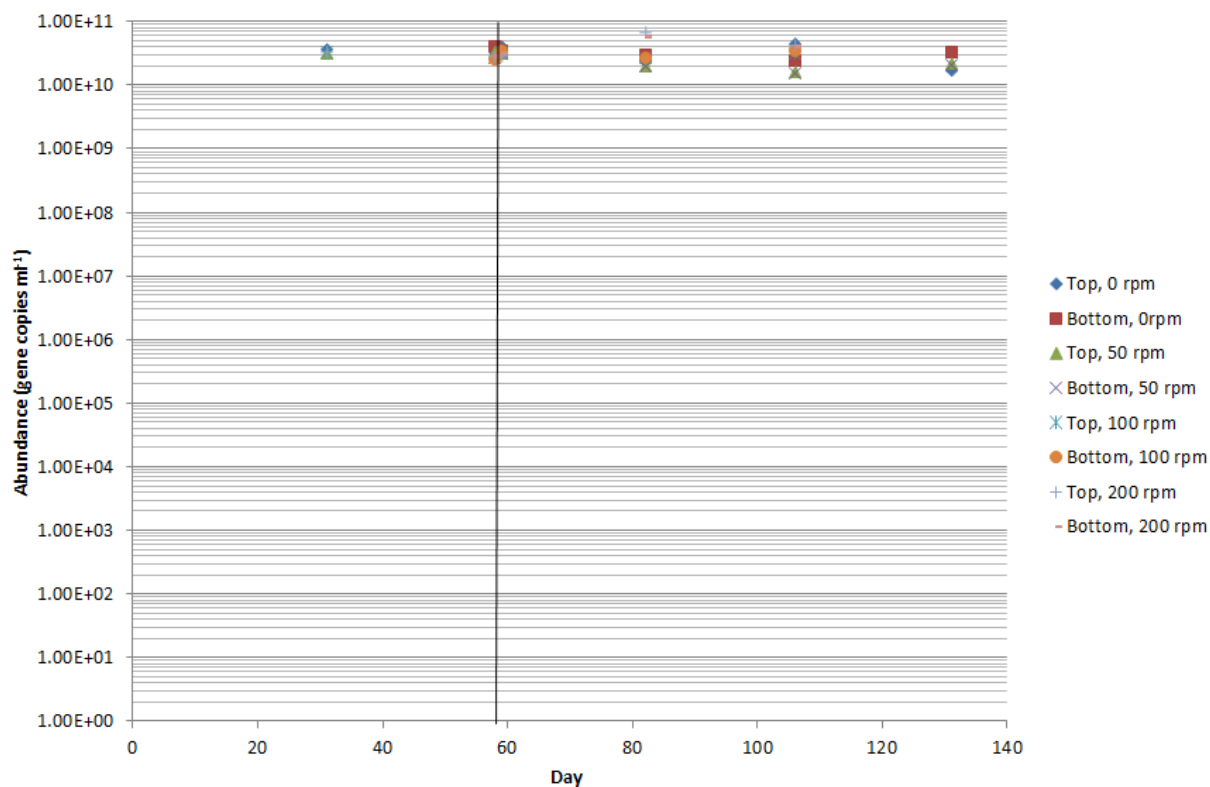


Figure 9.21 – Total eubacteria present in each of four digesters over the course of the second experiment (mixing changes made on Day 59 indicated by vertical line)

Microbial populations in the four digesters were initially composed of the same groups, i.e. those present in the sewage sludge inoculant. It can be seen from Figure 9.21 that the 16S rRNA gene copy number of total *eubacteria* is similar across all digesters throughout the duration of the experiment, with gene copy numbers of  $2\text{-}4 \times 10^{10} \text{ ml}^{-1}$ .

There were, however, variations in the methanogenic population over the course of the experiment. The acetoclastic *Methanosaeta* was the dominant methanogen in all digesters throughout the experiment. In comparison, the acetoclastic *Methanosarcina* was only detected at low levels ( $3.8\text{-}9.9 \times 10^3 \text{ gene copies ml}^{-1}$ ) in the sample taken on Day 131 from the digester with no mixing and the hydrogenotrophic orders, *Methanomicrobiales* and *Methanobacteriales*, were detected at abundances of  $10^4\text{-}10^6 \text{ gene copies ml}^{-1}$ . This suggests that acetoclastic methanogenesis was the main methane production pathway for these digesters. The abundance of *Methanosaeta* is shown in

Figure 9.22 and the abundance of *Methanomicrobiales* and *Methanobacteriales* are shown in Figure 9.23 and Figure 9.24 respectively.

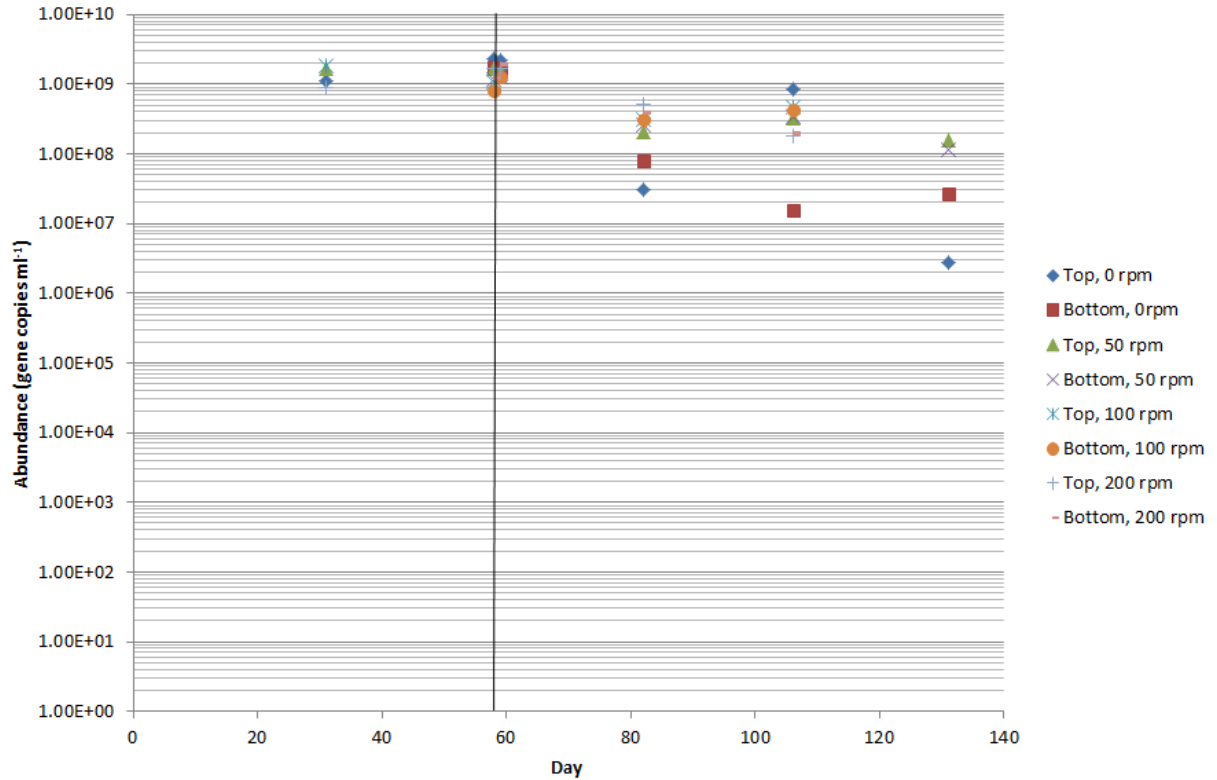


Figure 9.22 – Abundance of *Methanosaeta* present in each of four digesters over the course of the second experiment (mixing changes made on Day 59 indicated by vertical line)

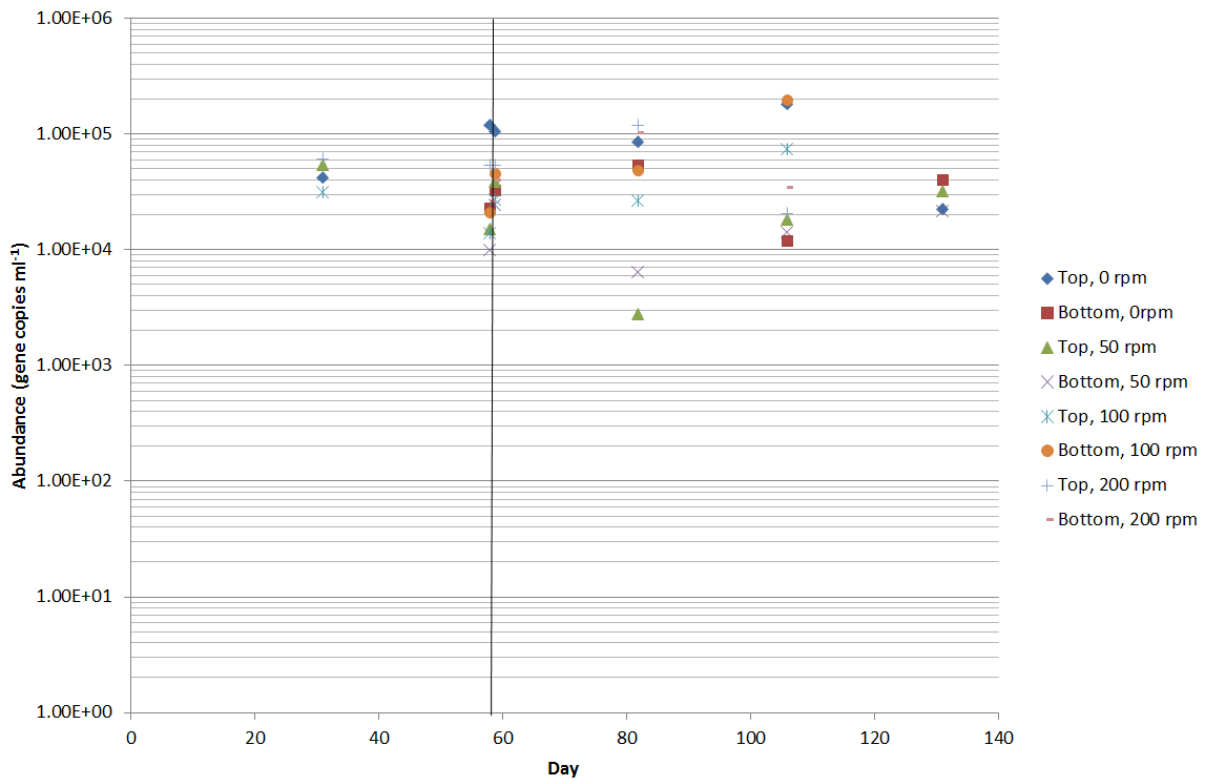


Figure 9.23 – Abundance of *Methanomicrobiales* present in each of four digesters over the course of the second experiment (mixing changes made on Day 59 indicated by vertical line)

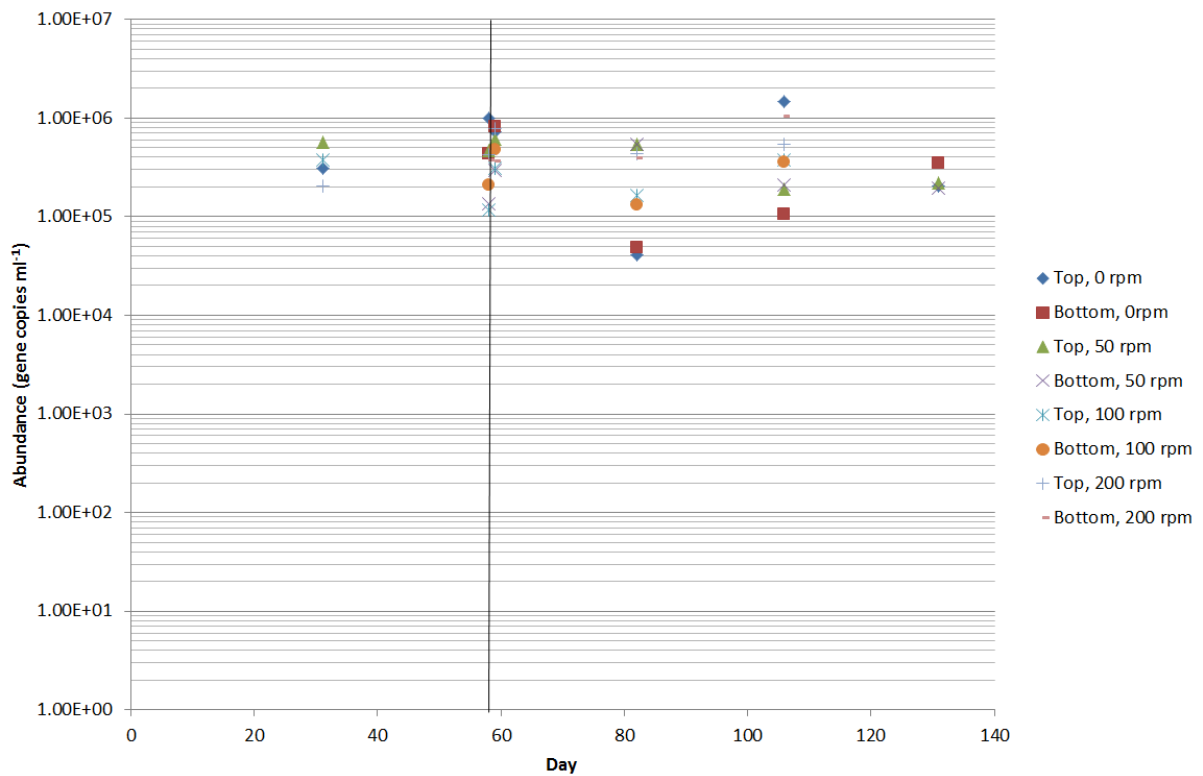


Figure 9.24 – Abundance of *Methanobacteriales* present in each of four digesters over the course of the second experiment (mixing changes made on Day 59 indicated by vertical line)

*Methanosaeta* is expected to dominate digesters, particularly when acetate concentrations are low (Conklin et al., 2006), as is the case for all of the digesters prior to the change in mixing speed and during the first RT after the change in mixing speed.

In the digester at 100 rpm throughout the experiment, the abundance of *Methanosaeta* is similar in samples taken from the top and bottom of the digester, suggesting that sufficient mixing occurred to ensure that the digester has a spatially homogenous methanogenic community. However, over the course of the experiment, there is a downward trend in the abundance of *Methanosaeta*. This is linked to the reduction in daily gas production over the course of the experiment as discussed in Section 9.5. It is hypothesised that this is caused by the slow inhibition of the methanogenic community by an intermediary metabolite produced during the digestion of the synthetic sludge. This would cause the growth rate of methanogens in the digester to slow, leading to greater washout of the methanogenic community and a reduction in biogas production. This is often a problem when running long-term experiments with synthetic sludge (Climenhaga, 2008) and in the long-term, would lead to the failure of the digester as VFAs accumulate, further inhibiting the methanogens and further slowing their growth rate. As seen in Section 2.4.5, it is likely that methanogenic *Archaea* would suffer a greater adverse effect than other micro-organisms involved in the digestion process, due to their increased sensitivity to toxic and inhibitory materials. The reduction in abundance observed with *Methanosaeta* is not apparent amongst the hydrogenotrophic methanogens and it can be seen that towards the end of the experiment, there is an increase in the abundance of *Methanomicrobiales*. This suggests that the hydrogenotrophic methanogens are in competition with the acetoclastic methanogens and hence the hydrogenotrophs benefitted from the inhibition of the acetoclastic methanogens, resulting in a shift of methane production pathway from acetoclastic to hydrogenotrophic.

In the digester at 50 rpm, there is a difference in the abundance of *Methanosaeta* between samples taken from the top and bottom of the digester over the course of the experiment, with a reduction in abundance at the top of the digester that is not seen in the samples taken from the bottom of the digester. This may be indicative of stratification occurring in the digester causing solids to accumulate near the base of the digester. This in turn would increase the abundance of methanogens close to the base of the digester, where the concentration of food sources will be higher. There is a similar reduction in the abundance of *Methanomicrobiales* and *Methanobacteriales* throughout the digester after the change in mixing speed, which may indicate an increase in the dominance of the acetoclastic pathway at low mixing speeds.

In the digester at 200 rpm, the opposite effect is seen. The abundance of *Methanosaeta* is maintained in the sample taken from the top of the digester, whilst there is reduction in the abundance of *Methanosaeta* in samples taken from the bottom of the digester. It is hypothesised that in this case, the higher mixing speed causes sufficient shear stress in the impeller region to have a detrimental effect on the filamentous *Methanosaeta*. This in turn reduces the population of *Methanosaeta* and adversely affects the biogas production from the digester. As the reduction in *Methanosaeta* abundance takes place, there is a small increase in the abundance of *Methanobacteriales*, which suggests that there is competitive interaction between the two groups and that the hydrogenotrophic pathway for methane production becomes more favourable when *Methanosaeta* is inhibited.

In the digester at 0 rpm, the abundance of *Methanosaeta*, *Methanomicrobiales* and *Methanobacteriales* is more variable than in the other digesters. Comparing the concentration of VFAs, and in particular the concentration of acetate, to the peaks and troughs in the abundance of *Methanosaeta*, it can be seen that reductions in the abundance of *Methanosaeta* coincide with increases in acetate concentration, and increases in the abundance of *Methanosaeta* coincide with

reductions in acetate concentration. Acetate is inhibitory to *Methanosaeta* at concentrations above 500 mg/L (Williams et al., 2013) and, as such, *Methanosaeta* abundance is inversely correlated to acetate. This is also the only digester in which *Methanosarcina* was recorded, at low levels ( $3.8\text{--}9.9 \times 10^3$  gene copies  $\text{ml}^{-1}$ ) in the sample taken on Day 131, with three times the number of gene copies in the sample taken from the bottom of the digester as in the sample taken from the top of the digester. By this point in the experiment, there had been multiple acetate peaks recorded in the unmixed digester and *Methanosarcina* is known to dominate acetate-rich digesters (Conklin et al., 2006) so it is not surprising that *Methanosarcina* begins to compete with *Methanosaeta*, particularly at the base of the digester where the increased SRT is likely to produce a higher concentration of intermediary digestion products. Similarly, the peaks and troughs in the abundance of *Methanomicrobiales* and *Methanobacteriales* can be compared to the peaks and troughs in the abundance of *Methanosaeta*. This indicates that at the top of the digester, where food sources are more likely to be in short supply due to sedimentation, the hydrogenotrophic methanogens followed a similar pattern to the acetoclastic methanogens. However, at the base of the digester, where food sources are more readily available, *Methanobacteriales* and *Methanomicrobiales* are better able to take advantage of the reduction in *Methanosaeta* abundance caused by increasing acetate concentration, and increased in abundance as *Methanosaeta* reduced in abundance. The high degree of variability in the concentration of VFAs and methanogens suggests that in the unmixed digester, there are large environmental and microbiological differences between different pockets of the digester. However, without a more detailed dataset describing the spatial and temporal fluctuations in the methanogenic populations across the digester, it is not possible to draw further conclusions.

From this analysis of the microbiological communities present in the digesters over the course of the experiment, it can be seen that slow mixing appears to be most beneficial for the promotion of a stable methanogenic population, and hence for the optimum biogas production from a digester. The

low concentration of acetate in the digesters leads to the acetoclastic methanogenic community being dominated by *Methanosaeta*. If the mixing speed is increased to 200 rpm, the abundance of acetoclastic methanogens in the impeller region is adversely affected; it is hypothesised that this is caused by the high shear stresses in this region pulling apart the filamentous *Methanosaeta*. Under no mixing conditions, the digester is an uncontrolled environment and pockets form which may have high concentrations of acetate, in which case *Methanosaeta* abundance is likely to be low, or low concentrations of acetate, in which case *Methanosaeta* abundance is likely to be higher. Furthermore, the abundance of methanogenic populations in the digesters were shown to decline over the course of the experiment, even when changes to mixing speed were not undertaken. This suggests that there is an intermediary metabolite that is produced during the digestion of the synthetic sludge that is inhibitory to the acetoclastic methanogens present in the digester. This leads to a slower growth rate of methanogens and the slow washout of the methanogenic population. This in turn leads to a reduction in the biogas production rate from the digesters over the course of long-term experiments as seen in Section 9.5.

SEM images were taken of samples collected from the top and bottom of each digester at the end of the experiment. Whilst it is not possible to ascertain the identity of specific methanogens from these images, certain trends can be observed. It can be seen in Figure 9.25 that there was a significantly greater abundance of microbiology in the sample taken from the bottom of the unmixed digester than in the sample taken from the top of the same digester, and a similar result was seen when comparing the samples taken from the top and bottom of the digester at 50 rpm. It can also be seen that the filamentous micro-organisms observed in the sample taken from the bottom of the digester mixed at 200 rpm were generally shorter than those found in the sample taken from the bottom of the digester mixed at 100 rpm, as shown in Figure 9.26. This agrees with the hypothesis that high mixing speeds may damage filamentous methanogens found in the impeller region due to high levels of shear stress.

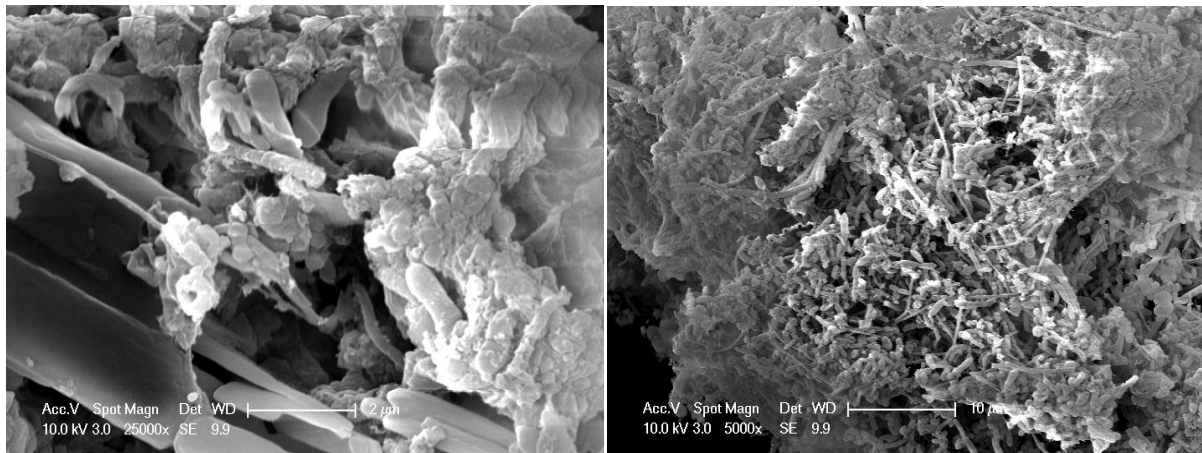


Figure 9.25 - Comparison of samples taken from the top (left) and bottom (right) of the unmixed digester, using SEM

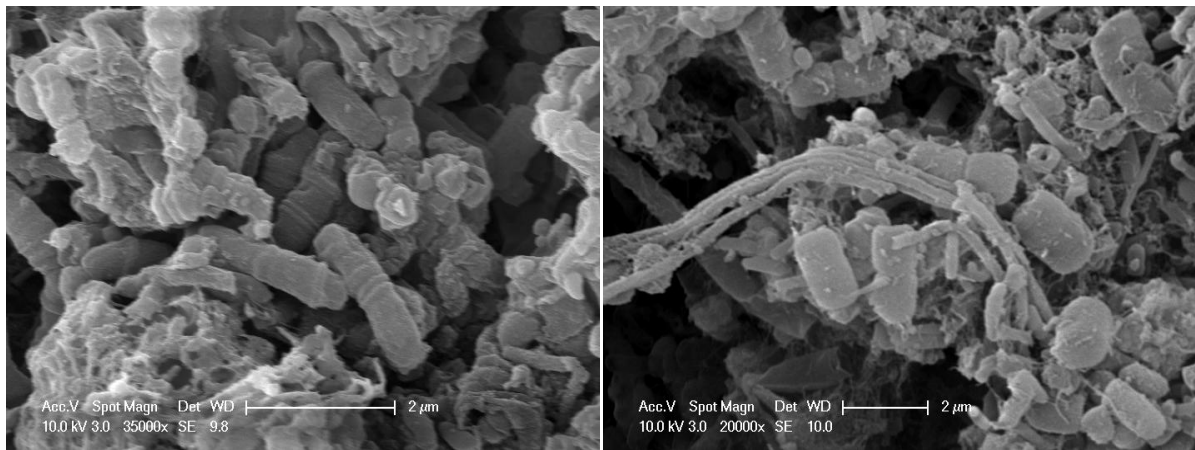


Figure 9.26 - Comparison of samples taken from the bottom of digesters mixed at 200 rpm (left) and 100 rpm (right), using SEM

## 9.7 Summary

This chapter considers the results of long-term lab-scale anaerobic digester experiments. Four mechanically-mixed digesters were run continuously at a constant mixing speed of 100 rpm until they were considered to have been stable for at least 1 RT. The mixing speeds in three of the digesters were then changed to 0 rpm, 50 rpm and 200 rpm whilst the fourth digester remained at 100 rpm. All four digesters were operated for a further 3 RTs or until they were considered to be irreversibly soured.

RR was used as the main indicator of digester stability. In the first experiment, the digester with no mixing was found to be the most stable, with instabilities becoming apparent in the other digesters in the order of fastest mixing to slowest mixing. In the second experiment, instabilities quickly became apparent in the digesters at 0 rpm and 200 rpm, whilst instabilities in the digesters at 50 rpm and 100 rpm were not noted until 2 RT after the change in mixing speed. By this point, both the digester at 0 rpm and 200 rpm were irreversibly soured. The digester at 50 rpm did not irreversibly sour within 3 RT. These patterns were replicated in measurements of pH and TA. The difference between the stability of the unmixed digester in the two experiments was attributed to the increased SRT in the first experiment caused by a combination of digestate stratification and sampling only from the top of the digester. In terms of stability, it appears that whilst mixing is necessary, a lower mixing speed is preferable to a higher mixing speed.

The effects of mixing on sludge stabilisation and sludge volume reduction were considered by studying the total and volatile solids concentrations. TS reduction was approximately 70 % whilst VS reduction was approximately 80 %. This remained constant throughout the experiment although an increase in variability was seen in the digesters at 0 rpm and 50 rpm, due in part to the varying degrees of stratification that occurred.

The rate of gas production in the digesters remained the same after the change in mixing speed for digesters at 0 rpm and 50rpm in the first experiment and at 50 rpm and 100 rpm in the second experiment. This difference between the two experiments was attributed to the difference in sample locations at 0 rpm as explained previously. In the digester at 200 rpm, the rate of gas production fell as the process became unstable, with gas production falling to less than 20 ml/l/day as irreversible souring occurred. A similar result was seen in the digester at 0 rpm in the second experiment. Additionally, percentage methane in the biogas fell as instabilities in the digesters became apparent. All digesters experienced a reduction in daily biogas production over the course

of the experiment. This was attributed to an intermediary metabolite inhibiting the growth of methanogens and causing a slow washout of the methanogenic community from the digester.

For the first time, qPCR has been used to assess the effects of mixing speed on the microbiology of an anaerobic digester. This microbiological community analysis similarly demonstrated that slow mixing appears to be most beneficial for the promotion of a stable methanogenic population, and hence for stable digestion and optimum biogas production. *Methanosaeta* was the dominant methanogen in all of the digesters, indicating that acetoclastic methanogenesis is the main methane production pathway. It is thought that *Methanosaeta* outperformed *Methanosarcina* due to the low acetate concentration in the digesters. However, at 200 rpm, the abundance of filamentous *Methanosaeta* in the lower part of the digester was adversely affected by high shear stresses in the impeller region. Under no mixing conditions, acetate-rich and acetate-poor pockets form in the digester, affecting the abundance of *Methanosaeta*, which is inversely correlated to acetate concentration. Furthermore, it was seen that the acetoclastic methanogenic population in the digesters was detrimentally affected over the course of the experiment even when changes to mixing speed were not undertaken. This supports the theory that an intermediary metabolite was inhibiting the growth of acetoclastic methanogens and causing a slow washout of the methanogenic community from the digester. Hydrogenotrophic methanogens were in competition with acetoclastic methanogens and it was seen that, when the acetoclasts suffered a reduction in abundance due to environmental factors, the abundance of hydrogenotrophs increased.

## CHAPTER 10 Discussion

The principal aim of this research was to identify mixing regimes and associated flow patterns that increase biological activity and hence biogas output, whilst minimising energy input, for lab-scale anaerobic sludge digesters.

For the first time, an experimental investigation into the flow patterns established by mixing was carried out using PEPT. Subsequently, CFD models of these same flows were created to allow a greater understanding of the flow patterns present and, more importantly, of the turbulence characteristics that come about under different operating conditions. The operation of lab-scale anaerobic digesters has shown experimentally the effects of mixing speed upon process stability, microbiological community and gas production.

This chapter considers the development and application of a suitable modelling strategy for characterising flow in a mechanically-mixed digester. Additionally, the efficacy of the experimental method for studying the link between mixing, microbiological community, gas production and process stability is discussed. Subsequently, the practical implications of the main findings of both the numerical and experimental work carried out will be examined. These findings are summarised as follows:

- PEPT is a practical and valuable method for flow visualisation and for the validation of CFD models of anaerobic digesters at lab-scale and in three dimensions, whilst avoiding the complexities of having to recreate sludge properties in a synthetic transparent liquid medium.
- CFD can be used effectively to model flow and characterise turbulence in anaerobic digesters.

- Both process stability and gas production of a digester are negatively affected when operating with no mixing or at high levels of mixing. As such, low levels of mixing are preferable as they improve the energy balance of the digester both by reducing power input and by producing greater gas volumes. The effects of mixing on gas production can be linked to changes in environmental factors and associated changes in the microbiological communities present in the digester.

## 10.1 Flow visualisation

PEPT was used to visualise the flow patterns established by mixing in a lab-scale mechanically-mixed anaerobic digester at a range of mixing speeds. This is the first time that PEPT has been used for flow visualisation in an anaerobic digester and the first time that the flow patterns in a digester have been visualised using real sludge rather than a transparent synthetic sludge.

PEPT offers significant advantages over existing non-invasive flow visualisation techniques such as PIV and laser Doppler anemometry (LDA). PEPT benefits from being able to examine flow phenomena in three dimensions, as it is capable of tracking a particle as it moves around a three-dimensional volume. On the other hand, PIV is limited to recording data within the two-dimensional plane of the laser and LDA is only able to capture data at a single point. This greatly increases the ability of PEPT to construct a more complete picture of the flow patterns generated in a mixing vessel compared to more conventional flow visualisation techniques.

PEPT allows the examination of opaque fluids within opaque apparatus, which represents a significant advantage over traditional optical methods. Due to the inherent opacity of sludge, the visualisation of flow patterns within a digester cannot be carried out using conventional optical methods without the use of a synthetic fluid. This introduces an extra layer of complexity in choosing an appropriate transparent fluid with which to model the rheological properties of sludge (Eshtiaghi et al., 2012). Furthermore, due to the variable nature of sewage sludge, there is little consensus in

the literature as to what rheological properties sludge should possess, beyond it acting as a non-Newtonian fluid (Forster, 2002) and even then, it may be considered as a Newtonian fluid at low solids concentrations as demonstrated in Section 6.3 (Baroutian et al., 2013, Spinosa and Lotito, 2003, Malczewska, 2009). Furthermore, it can be considered to be thixotropic (Tixier et al., 2003) or shear-thinning (Mori et al., 2008). Several standard non-Newtonian fluid models have been used to describe the rheological properties of sewage sludge including simple power law, also known as Ostwald-de Waele, (Moeller and Torres, 1997, Pollice et al., 2007, Hasar et al., 2004), Bingham (Guibaud et al., 2004, Pevere et al., 2007), Herschel-Bulkley (Mori et al., 2008, Yang et al., 2009) and Casson (Yang et al., 2009). As such, it can be seen that there are numerous complications involved in having to approximate sludge to a transparent fluid, making PEPT a desirable technique for flow visualisation in anaerobic digesters.

The comparison of PEPT data to the results of other flow visualisation techniques allows a validation of the process. Due to the challenges involved, little has been done to visualise flow patterns in anaerobic digesters experimentally and the vast majority of work in this field is carried out using numerical modelling, validated against overall performance characteristics such as power consumption or “black-box” validation such as tracer washout concentration. However, the mechanical mixing of other fluids has been visualised using conventional optical techniques (PIV and LDA) and the results compared to PEPT. Pianko-Oprych et al. (2009) compared results from PIV and PEPT of a Newtonian salt solution. Whilst a comparison of these results with existing literature showed that there was limited consistency in the published data, the level of agreement between PIV and PEPT results from their own experiments was at least as good as the agreement between different workers using PIV. As such, their results appear to validate the ability of PEPT to give accurate results, at least for mean velocities. Chiti et al. (2011) compared PEPT results of mixing salt and sugar solutions with a Rushton impeller to LDA results and showed that, whilst generally the PEPT results compared well, they underestimated velocities in the impeller region. This was similarly

noted in the current work and was associated with low data capture due to the high velocity of the particle, and rapid changes in its direction and velocity magnitude.

## **10.2 CFD modelling strategy**

CFD has been used to successfully model the flow of sludge in a mechanically-mixed lab-scale digester at a range of mixing speeds. However, in order for the results to be meaningful, care must be taken when setting up the model.

In modelling mixing vessels, there are a number of key parameters that must be determined which will affect both the computational expense of the model and the accuracy of the results. Best practice guidelines (ERCOFTAC, 2000) indicate that mesh density is one such parameter, with a balance required between the expense of a finer mesh and the possible inaccuracy of a coarser mesh. The level of reporting of mesh densities in the literature varies from non-existent (Wu, 2010b, Wu and Chen, 2008, Wu, 2012a), to an indication of the mesh density used (Wu et al., 2009, Terashima et al., 2009, Meroney and Colorado, 2009, Wu, 2012c), to a full report of mesh density optimisation (Vesvikar and Al-Dahhan, 2005, Wu, 2011, Bridgeman, 2012). In this work, mesh density optimisation is carried out using the GCI method (Roache, 1998) to ensure that the mesh density used is applicable.

There are two common methods for treating rotating flows in simulations, a key aspect of modelling mechanical mixing in an anaerobic digester: MRF or SM. Due to the increased computational expense of running transient SM models, MRF is often selected as the preferred alternative (Wu, 2010b, Wu, 2011, Wu, 2012a), though it is rare that a comparison of the results using both methods is given. Bridgeman (2012) stated that both methods were tested and that, in the case of an unbaffled lab-scale digester, the computational expense of the SM method was too great to be considered practical for use in further simulations. Based on the lack of interaction between the impeller and the rest of the digester geometry (i.e. no rotor-stator interactions), it is understandable

that the MRF and SM solutions for this set-up would yield similar results, and a single rotating frame method may even have been applicable. Wu (2012c) compared RANS models using both MRF and SM. He found that whilst all of the RANS models gave similar results, the SM model was better able to predict impeller power number, although it took approximately 40 times longer to run. In this work, having access to the University of Birmingham's high performance computing facility, BlueBEAR, has meant that an increase in computational expense from a couple of hours to a few days is accepted in exchange for an improved solution, when the extent of effect of interactions between the impeller and the baffles on the flow patterns is initially unclear. However, if computational resources are limited, using MRF instead of SM appears to provide a preferable solution to reducing mesh quality.

To date, the author is only aware of one paper (Wu, 2012c) which considers a higher level approach than RANS (e.g. LES, DNS) to simulate mixing in an anaerobic digester. Wu (2012c) used an LES model, along with three different sub-grid scale models, to simulate mechanical mixing in an unbaffled lab-scale digester. Unfortunately, the lack of a mesh density independence test, the limited mesh density allowed by the computational resources available and a poor validation of the model against experimental data mean that the value of these results is severely restricted. Whilst it is possible that the LES model may produce a more realistic prediction of flow characteristics on a smaller scale, which may have value in evaluating the effect of mixing on microbiological communities, it has not been proven in the existing literature on the mixing on non-Newtonian fluids. This made it an unattractive option for this research when RANS models, closed using two-equation turbulence models of the  $k-\varepsilon$  and  $k-\omega$  forms have been shown to successfully model mechanical mixing of non-Newtonian sludge previously (Bridgeman, 2012, Wu, 2010a).

Once the RANS model has been selected, the choice of an appropriate turbulence model to close the RANS equations is important. In some cases, the assumption of laminar flow is made (Terashima et

al., 2009, Wu, 2012a). Given that laminar flow for mixing requires a Reynolds number of less than 10, it seems unlikely that this is a realistic condition in a digester; the lab-scale digesters used in this work experienced Reynolds numbers of between  $2.6 \times 10^4$  and  $2.6 \times 10^5$ , depending on mixing speed. In order to achieve laminar flow in the lab-scale digesters used in this work, the impeller would have to be slowed to 1.2 revolutions per hour. More commonly, the standard  $k-\varepsilon$  model (Meroney and Colorado, 2009, Vesvikar et al., 2005, Wu and Chen, 2008) or realisable  $k-\varepsilon$  model (Wu, 2010b) is applied. Wu (2011) carried out a comparison of six turbulence models (standard  $k-\varepsilon$ , realisable  $k-\varepsilon$ , RNG  $k-\varepsilon$ , standard  $k-\omega$ , SST  $k-\omega$  and RSM) for simulating mechanical mixing in anaerobic digesters and found that realisable  $k-\varepsilon$  and standard  $k-\omega$  models were best able to model mixing of a wide range of sludge viscosities in a reasonable timeframe. In this work, a comparison of turbulence models to experimental data showed that the realisable  $k-\varepsilon$  model was most appropriate, in agreement with Wu (2011).

It can be seen that, with tangential velocities in the impeller region being a level of magnitude higher than the axial and radial velocities, swirl plays an important role in the flow patterns in this region of the digester. The realisable  $k-\varepsilon$  model is mathematically considered to be unsuitable for highly swirling flows (ANSYS-Fluent, 2012) so it is surprising that it has been shown to produce creditable results in a number of cases (Wu, 2010b, Wu, 2011), including in this research. As stated in Section 8.7, the two-equation models considered in this work model the TKE based on the assumption that turbulence is isotropic. In scenarios where anisotropic turbulence dominates, such as in highly swirling flow where turbulence is generally greater in the tangential and axial directions than in the radial direction, two-equation models would be expected to over-predict TKE. As such, it would be expected that the RSM would be better suited to modelling flows in the digester. However, this was shown not to be the case when comparing various turbulence models to the PIV results. It has been shown using PIV that turbulence, when mixing water in a stirred vessel of a similar size to the digesters used in this research, is isotropic outside of the trailing vortices (Khan, 2005). This may

account for the success of the realisable  $k-\varepsilon$  model, as the high viscosity of the CMC used in the PIV experiments, and of the sludge used in the experimental work, limits the volume of the digester affected by the trailing vortices to that close to the impeller. It would be expected that the correlation between the two sets of results would be less favourable in parts of the digester which come into close contact with these vortices, i.e. within the impeller region.

The results of the PEPT experiments carried out within this work demonstrated that even small differences in the rheological properties of sludge can have a significant effect on the flow patterns established by mixing within a digester. Similarly, existing literature in which flow within digesters is simulated using CFD recognises the importance of accurately modelling sludge rheology (Terashima et al., 2009, Meroney and Colorado, 2009, Bridgeman, 2012). In the case of this work, the sludge was assumed to follow a non-Newtonian power law, with the rheological properties determined experimentally using a Couette viscometer (Fann Model 35). Within the literature, the non-Newtonian power law is found to be a simple yet robust method of modelling sludge and as such, has been used in a number of simulations (Wu and Chen, 2008, Terashima et al., 2009, Wu, 2012c). Sludge is still modelled as a Newtonian fluid in some cases (Meroney and Colorado, 2009, Vesvikar et al., 2005), which appears to be a gross oversimplification with the clear capacity to introduce errors into the modelled results. A further assumption made during this work and frequently made within the existing literature is that of constant sludge rheology over time, when in fact the digestion process causes a reduction in sludge viscosity over time (Dieude-Fauvel et al., 2014, Craig et al., 2013). This is in agreement with the results of the batch digestions conducted in Chapter 6. However, if the digester is run as a continuous or semi-continuous process and is well-mixed, the effects of feeding and removing sludge should allow a state of equilibrium to be reached, as demonstrated by the solids concentrations in samples taken from the digesters in Section 9.4. In this situation, constant sludge viscosity becomes a realistic simplifying assumption and sludge viscosity can be ascertained from the sludge removed from the digester, which in a well-mixed vessel is

representative of the sludge throughout the digester. In this case, the tested samples were taken from the digester over the duration of the experiment and the results were averaged in order to select a single appropriate model to represent sludge in all of the digesters over the course of the experiment. Whilst two of the four digesters in this study were well-mixed, it was shown during the experimental work that the digesters with the lowest levels of mixing experienced varying degrees of stratification. As such, an assumption of constant rheology in these digesters will have an impact on the accuracy of the predicted flow patterns. However, flow patterns are not predicted in the unmixed digesters where the degree of stratification is predicted to be greatest. In the digester mixed at 50 rpm, the predicted flow patterns may incur a higher level of error although, with the difficulties in validating the CFD against PEPT at low mixing speeds, the degree of error is unclear. Without running a complex and computationally expensive multiphase model, it would be challenging to improve the accuracy of this model. In order to compensate for this simplifying assumption of consistent sludge rheology throughout the digester, an average viscosity was assumed based on mixed samples taken from both the top and bottom of the digester.

Validation is a vital aspect of any CFD simulation and without it the results have questionable value. As discussed in Section 10.1, it is often difficult to achieve good quality flow visualisation for mixing in an anaerobic digester. As such, validation techniques include overall performance characteristics such as power consumption (Bridgeman, 2012), power number and flow number (Wu, 2010b, Wu, 2012a) or tracer response curves (Terashima et al., 2009). Alternatively, a comparison is made between CFD results and experimental flow visualisation data in the existing literature (Vesvikar and Al-Dahhan, 2005, Wu and Chen, 2008, Wu, 2010c, Wu, 2012c). Whilst this is likely to be the most complete form of validation, it is limited by the quality of the data in the existing literature, as laid out in Section 10.1, and is often hampered by differences between the CFD model set-up and the experimental set-up. In this work, it has been possible to validate CFD results against both PIV and

PEPT results. This allows a considerable level of confidence in the modelled results and represents an improvement in validation techniques in the existing literature.

### **10.3 Experimental method**

Lab-scale mechanically-mixed digesters were operated for several months to ascertain the effects of mixing on gas production and process stability. In order for these results to have value, it is important to consider the sources of error and limitations of the experiments conducted.

For the purpose of these experiments, synthetic sludge was used as a feedstock. This has significant advantages over real sludge in terms of ease of storage and providing a consistent feedstock throughout the experiments. However, there are limitations to its use. Due to the nature of the feedstock, solids tended to settle out, causing variability in both the rheology and the solids content. Whilst variability would also be seen in real sludge, it should be avoided if possible to ensure that the experiments are run under controlled conditions with a minimum of variables. To avoid sludge variability impacting on the digesters, the feedstock was well shaken before digester feeding.

It was seen that over the course of the experiments, the rate of biogas production reduced in all digesters regardless of mixing speed. This was attributed to the use of synthetic sludge, which, it was hypothesised, led to the production of an intermediary metabolite which caused the growth rate of the methanogens to slow thereby increasing the rate at which they were washed out of the digester. Whilst it is not clear what this metabolite was, it is analogous to the inhibition of methanogens by trace elements. It has been shown that the accumulation of certain trace elements over extended periods of digestion, including calcium, sodium, magnesium, potassium and sulphur, can lead to failure of the anaerobic digestion process (Climenhaga, 2008) and in particular the methanogenic stage, as methanogens are more sensitive to the digestion environment than many of the other micro-organisms involved (Lin, 1993). Whilst the use of a synthetic sludge clearly had a negative impact on the digestion process over the course of these long-term experiments, the change in

production rate with time falls within the confidence interval used during the statistical analysis of the gas data in the second experiment. This is evidenced by the biogas production rate in the digester that remained at 100 rpm being constant throughout the experiment.

In the first experiment, the biogas production rate at 100 rpm did not remain constant throughout the experiment, indicating a more severe reduction in the gas production over time and a more negative impact on the digestion process over time. This was attributed to small differences between the two feedstocks which may have exacerbated the inhibition of methanogenesis in the digester. Without a detailed analysis of the metabolic pathways involved in the digestion of the synthetic sludge, which is beyond the scope of this work, it is impossible to pinpoint which constituent components of the sludge cause this difference. However, it seems likely that a more rapid accumulation of this metabolite in the first experiment is the underlying cause of the difference in gas production rates in the two experiments.

Gas volume was measured using a semi-continuous tipping bucket mechanism and percentage methane was measured daily using a hand-held methane leak detector. The tipping-bucket mechanism was calibrated with a small aeration pump and so does not take into account the loss of water vapour, carbon dioxide or methane to the barrier solution. However, acidified 75 % saturated sodium chloride solution was used as a barrier solution and, in accordance with the findings of Walker et al. (2009), this reduces losses of carbon dioxide to 8 % and losses of methane to 1 % after approximately 15 days of operation. As the gas flow meter was operated from start-up even when data recording was not possible, it is highly likely that by the time the rate of gas production was being compared in the 24 days prior to the change in mixing speed and after the change, the barrier solution would be saturated with carbon dioxide and methane and as such, the effect on gas flow results would be negligible. For the purposes of calculating relative gas volumes in the produced biogas, the biogas mixture was assumed to consist only of methane and carbon dioxide. This allows

the losses of water vapour in the mixture to be neglected and as such, the loss of water vapour to the barrier solution is inconsequential. Using the gas flow meter in this way, (Walker et al., 2009) suggest that gas volumes can be reported well within a 5 % tolerance band, provided results are corrected to standard temperature and pressure.

The gas was assumed to be at the same temperature as that of the digester and at atmospheric pressure when it reached the gas flow meter. The assumption of equal temperature is justified by the short length of tubing between the digester and the gas flow meter (less than 50 cm). Atmospheric pressure was taken from hourly records at Birmingham International Airport, approximately 12 km from the Civil Engineering Labs at University of Birmingham where the experiments took place. Whilst there are likely to be some discrepancies between the hourly recorded atmospheric pressure at the data recording site and the atmospheric pressure actually experienced by the gas, this was the only complete record of air pressure available in the vicinity. A difference of 20 mbar between the two sites, which is highly unlikely except under localised storm conditions, would cause an error of less than 5 % and so it is considered that the use of this record introduces negligible error.

The hand-held methane leak detector was calibrated against syringes of gas of known methane concentration. However, as this was “dry” gas, i.e. minimal water vapour present, there is a possible source of error in the calibration when compared to “wet” biogas samples from the digesters. In order to determine the size of this error, a second calibration was carried out alternating samples with known methane concentration and samples from the digester to simulate the effect of water vapour on the probe. This showed that the “wet” gas samples of known concentration consistently gave a gas reading indicating a percentage of methane 3 % lower than “dry” gas samples. This is within an acceptable margin of error and may go some way to explaining the lower than expected percentage methane recorded in the biogas.

Several authors have considered the effects of mixing on gas production from anaerobic digestion. The experimental work presented in this thesis demonstrates that low levels of mixing are preferable as they improve the energy balance of the digester both by reducing power input and by producing greater gas volumes.

This appears to be in strong agreement with the findings of Kaparaju et al. (2008) who determined that, at lab-scale, greater gas production was achieved when mixing on a shaker table was gentle (35 times per minute) rather than vigorous (110 times per minute), although these experiments were carried out at a thermophilic temperature of 55 °C. These results were recreated at pilot-scale as continuous or intermittent mixing using two impellers. This showed that intermittent mixing was preferable to continuous mixing for gas production. Furthermore, Vavilin and Angelidaki (2005) established that when organic loading of a mixture of manure and municipal and household solid waste was high, intensive mixing caused acidification of the digester and process failure, as seen with the digester at 200 rpm in the experimental work carried out for this thesis, whilst low mixing intensity aided successful digestion. At low organic loading, mixing intensity had no significant effect.

Karim et al. (2005b) demonstrated that mixed digesters treating 10 % TS sludge showed an increase in biogas production of 15-29 % compared to an unmixed digester, with slurry recirculation resulting in the highest increase in biogas production (29 %), followed by impeller mixing (22 %) and biogas recirculation resulting in the lowest increase in biogas production (15 %). This agrees with the 20 % difference in gas production from the digester prior to a change in mixing speed and after a change to no mixing. They also found that mixing had little effect when dealing with sludge with 5 % TS. Whilst a number of mixing methods were considered in the work of Karim et al. (2005a), there was no attempt made to characterise the mixing methods in terms of a comparable parameter such as velocity gradient or turbulence intensity. As such, it is difficult to compare the results to that of the current work in any great detail.

The lack of a comparable parameter is a common theme within the existing literature and, although there is a body of literature that recommends low mixing intensity instead of high mixing intensity, there is no comparable measure used to describe what entails low or high mixing intensity. This is discussed further in Section 10.5 and is the subject of Sindall et al. (2013). Sindall et al. (2013) considers the velocity gradient as an indicator of the level of mixing in lab-scale mechanically-mixed digesters and links this to a digester's gas production. This allows the identification of a threshold, between  $7.2$  and  $14.3 \text{ s}^{-1}$  above which increased mixing is no longer beneficial for increasing gas production.

The only literature which the author can find that attempts to assess the effect of mixing speed using a comparable parameter is that of Hoffman et al. (2008), in which shear stress was quantified using CARPT in conjunction with CFD and compared to gas production from lab-scale digesters fed cattle manure. The four unbaffled 4.5 litre digesters were mixed using a 62 mm diameter axial flow impeller at mixing speeds of 50 rpm, 250 rpm, 500 rpm and 1500 rpm. CFD models of the digesters at 250 rpm and 500 rpm were used to calculate the localised shear stress and the maximum shear stress in the digesters was used as a method of comparing the mixing intensity in the four digesters. However, in both cases, the maximum shear stress was found in the impeller region and was an order of magnitude higher than the maximum shear stress recorded in the bulk of the digester. As such, maximum local shear stress does not give a fair comparison of the overall mixing characteristics in the digester.

The overall velocity gradient in each of the digesters was calculated experimentally by measuring the torque on the stirrer and was found to be  $17 \text{ s}^{-1}$ ,  $210 \text{ s}^{-1}$ ,  $630 \text{ s}^{-1}$  and  $3500 \text{ s}^{-1}$  for the digesters at 50 rpm, 250 rpm, 500 rpm and 1500 rpm respectively. These velocity gradients are significantly higher than those calculated in the present work and this is attributed to the difference in the methods used to calculate the velocity gradient. In the case of this work, the velocity gradient is

calculated in each cell of the CFD model and then spatially averaged across the digester, whilst Hoffman et al. (2008) calculate the velocity gradient from an experimentally determined torque. This biases the calculated average velocity gradient towards the higher velocity gradients experienced in the impeller region. Additionally, the lack of baffles in the digester of Hoffman et al. (2008) promotes high shear due to the high tangential velocities and this too will impact on the velocity gradients experienced in the digester, particularly in the impeller region.

A comparison of the maximum shear stress with the gas production of the digesters during the experiments of Hoffman et al. (2008) showed that the differences in shear stress at the mechanical mixing speeds considered had little effect on the gas production and this is discussed further in Section 10.5.

#### **10.4 Microbiological community analysis**

Whilst qPCR has been used on a number of occasions to analyse the microbiological communities present in anaerobic digesters, as seen in Section 2.8, this is the first instance of this analysis technique being used to consider the impact of mixing intensity on digester microbiology.

Hoffman et al. (2008) is the only paper available to date which considers the effects of mixing intensity on microbiological community structure in anaerobic digesters. Samples were collected from 4.5 litre digesters fed with cow manure and mixed at 50 rpm, 250 rpm, 500 rpm and 1500 rpm and the microbiological community was analysed using membrane hybridisation and FISH. This demonstrated that whilst mixing intensity did not appear to have an effect on bacterial abundance in the digesters, there were differences in the levels of *Methanosaeta concilii* and *Methanosarcina* spp over the course of the experiment. This was also true of the digesters operated in Chapter 9. Whilst this work showed that *Methanosaeta* was the dominant methanogen in all of the digesters, Hoffman et al. (2008) showed that *Methanosarcina* was more abundant in the digesters at 500 rpm and 1500 rpm and that *Methanosaeta* was the dominant methanogen in the digesters at 50 rpm and 100 rpm.

Given that the highest mixing speed used in this work was 200 rpm, these results agree well and suggest that higher mixing speeds than those used in this work would be required before *Methanosarcina* was able to gain a competitive advantage from changes in mixing speed. The threshold above which *Methanosarcina* becomes more abundant may not be much greater than the highest mixing intensity tested in Chapter 9 as it is seen that at 200 rpm, *Methanosaeta* is adversely affected in the lower part of the digester, close to the impeller region. This was attributed to the filamentous structure of *Methanosaeta*, which it is hypothesised would be more adversely affected than the coccoidal *Methanosarcina* under high shear stress conditions. Hoffman et al. (2008) further suggest that the effects of mixing on digester microbiology may not be solely influenced by the direct effects of induced shear stresses on the methanogens but that changes to the environmental conditions, such as VFA concentration, can indirectly link mixing to changes in the methanogenic community. This is seen not only in the results in Chapter 9 but also in other literature which compares the microbiology of digesters to environmental conditions, such as Williams et al. (2013). Williams et al. (2013) demonstrated a clear link between the effects of VFA concentration in an industrial food waste digester and changes to the acetoclastic methanogenic community. To some extent, this link was observed in this work but samples were not taken on a sufficiently regular basis to clearly link VFA concentration to methanogenic community structure.

As samples were only taken from the top and bottom of each digester at the end of each RT, there are limitations on the conclusions that can be drawn from this dataset regarding the link between mixing and microbiological community structure. However, it demonstrates that qPCR can be a useful tool to link mixing speed to microbiological community. A more comprehensive sampling regime could provide further insight into how this link affects microbiological communities on a local scale.

## 10.5 Coupling of CFD and experimental findings

By considering the local velocity gradients in a digester calculated from CFD models, as discussed in Section 8.8, a novel comparison of the mixing in digesters can be made, not only between digesters at different mixing speeds but also between digesters with different mixing mechanisms and at different scales. By combining the local velocity gradient with the daily gas production at different mixing speeds from the second experimental run, Figure 10.1 shows the link between average velocity gradient ( $\bar{G}$ ) and average daily gas production for the first time. Gas production results were taken from the second retention time after the change in mixing speed, from the second, more complete set of experimental data. It can be seen from this that whilst there is an increase in gas production as velocity gradient increases from zero (i.e. no mixing), there is a point above which increasing velocity gradient is no longer an advantage and gas production begins to drop. This cut-off appears at approximately  $6 \text{ s}^{-1}$ . It is likely that close to and above this threshold, damage to the microbiological community of the digester takes place. This threshold is far lower than the typical design parameter of  $\bar{G}=50\text{-}80 \text{ s}^{-1}$  stated previously in the literature (Tchobanoglous and Burton, 1991), although it is noted that Tchobanoglous and Burton provide no justification for their stated range. However, the context of the stated range suggests that it has been calculated to prevent solids deposition and the creation of extensive dead zones in the digester, rather than to optimise gas production. The results of linking the computer modelling and the experimental work undertaken for this thesis suggest that  $\bar{G}$  values a degree of magnitude lower than that stated by Tchobanoglous and Burton (1991) are more suitable to promote biogas production. It is seen in Section 8.8 that Bridgeman (2012) similarly showed that vessel-wide average velocity gradients in a lab-scale digester were less than  $6 \text{ s}^{-1}$  with the bulk digester experiencing average velocity gradients of  $3\text{-}5 \text{ s}^{-1}$  and impeller regions experiencing average velocity gradients of  $12\text{-}17 \text{ s}^{-1}$ . Furthermore, Wu (2010c) found that even for a full-scale digester, the majority of the digester experienced local velocity gradients of less than  $10 \text{ s}^{-1}$ .

As mentioned in Section 10.3, Hoffman et al. (2008) linked mixing and gas production using shear rate and showed no difference in gas production at different shear rates. It should be noted that their lab-scale digesters were operated at average velocity gradients of between  $17 \text{ s}^{-1}$  and  $3500 \text{ s}^{-1}$ , significantly higher than the digesters in this work and above the threshold beyond which additional mixing is no longer beneficial. This may suggest that above this threshold there is not a gradual decrease in gas production but a steep drop-off and then a consistently lower gas production. Alternatively, it may be possible for the microbiological community to adapt to higher velocity gradients when subjected to them from start-up. This may partially explain the differences in microbiological communities seen in their work at different mixing speeds.

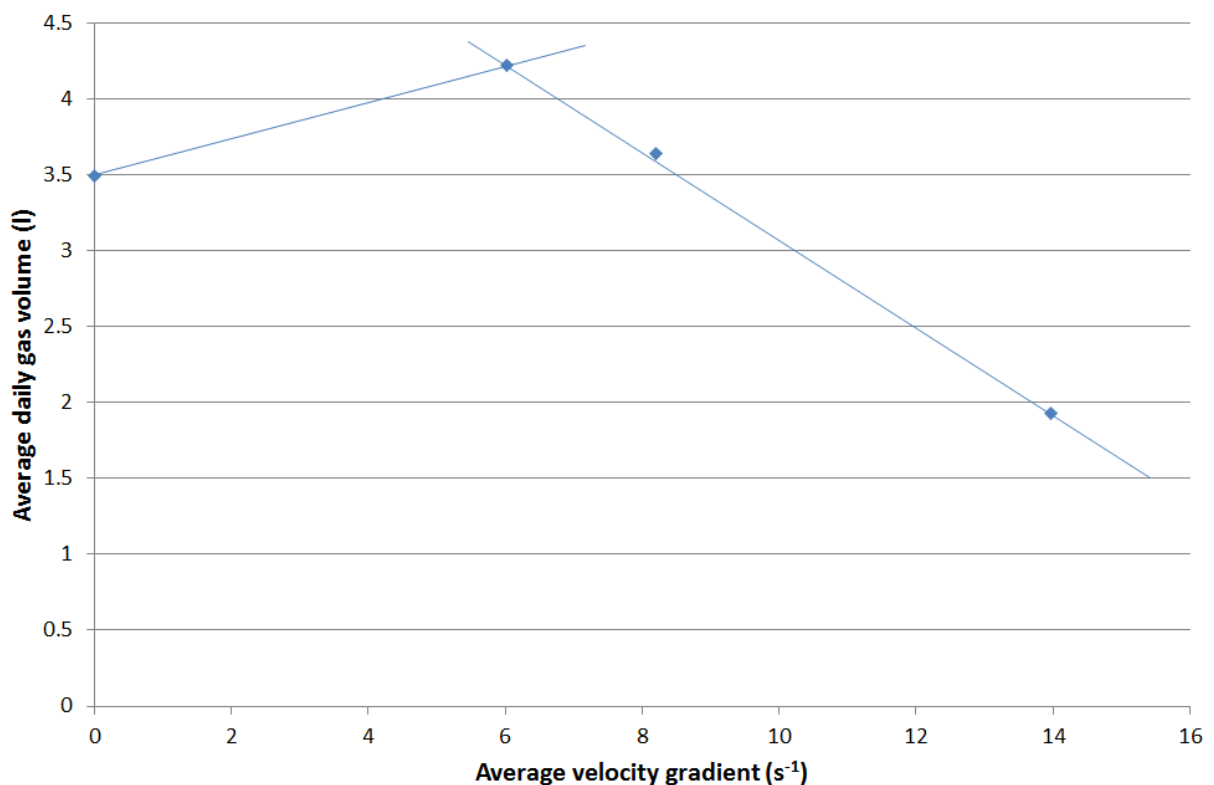


**Figure 10.1 - Average daily gas volume produced in the second retention time after a change in mixing speed, measured during experiments, against average velocity gradient, calculated from CFD models of the digester**

The novel process of linking mixing to gas production via velocity gradient was repeated with the results of the first experimental run. However, due to the differences in gas production before the change in mixing speed in these digesters, the daily gas volume was not considered to be a viable

measure of the effect of mixing speed. As such, the percentage change in gas volume between the second RT after mixing and the RT prior to a change in mixing was plotted against velocity gradient, as shown in Figure 10.2, alongside the equivalent results from the second experiment. From this it can be seen that as hypothesised above, in this experiment, in which greater instability was apparent throughout, there is a steep drop-off and then a consistently lower gas production as average velocity gradient in the digester increases. However, in both cases, the threshold occurs in the same shaded region, between 6 and 8  $s^{-1}$ , below which increased mixing is beneficial and above which increased mixing no longer stimulates increased biogas production.

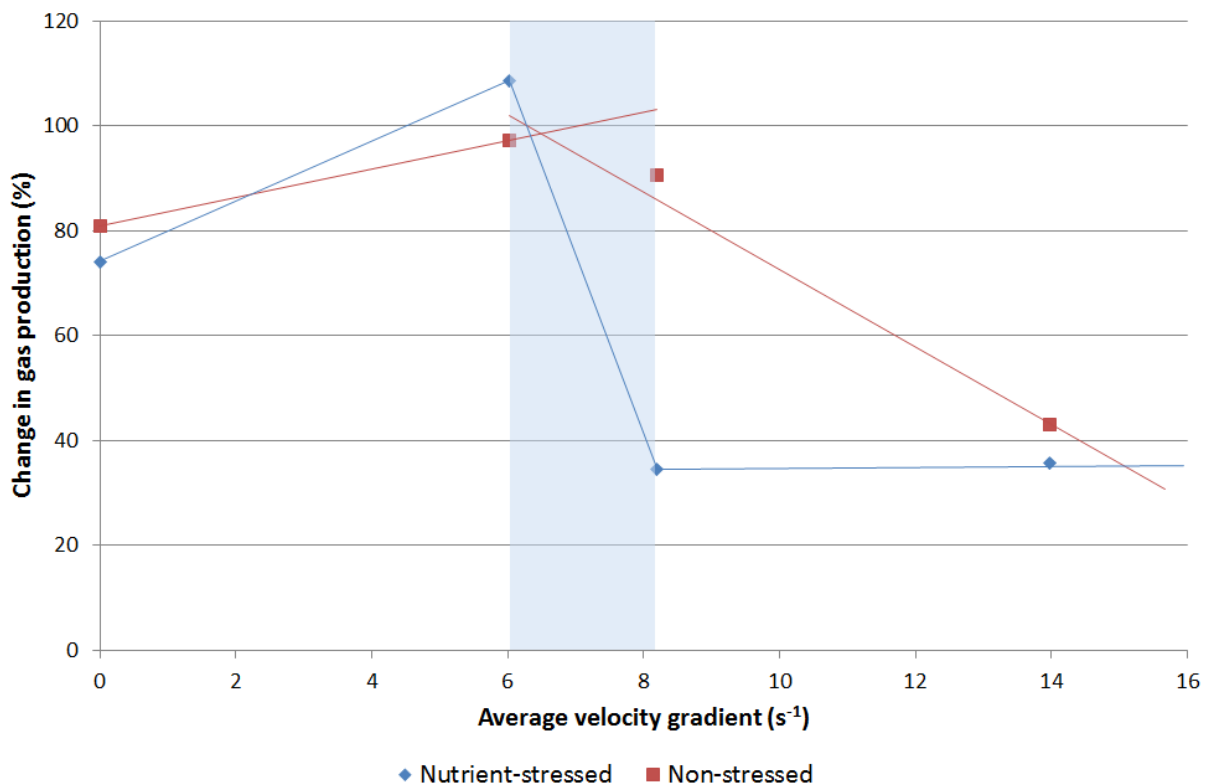


**Figure 10.2 - Percentage change in gas production volume produced in the second retention time after a change in mixing speed, measured during experiments, against average velocity gradient, calculated from CFD models of the digester, for lab-scale, mechanically-mixed digesters fed with nutrient-stressed and non-stressed feedstock**

Whilst plotting the average velocity gradient against gas production is practical, it has been argued, as seen in Section 3.1.6, that the concept of average velocity gradient is an approximation that does not fully represent a complex flow field. This is partially rectified by calculating the local velocity gradient in each cell of the CFD model and then spatially averaging the results. This is an

improvement on calculating the average velocity gradient from a single number representing power input to the digester as a whole. However, in order to fully represent the flow field, the full distribution of local velocity gradients would need to be considered across the digester, as it is these that are likely to have an impact on microbiological communities. As such, in order to fully understand the intermediary links between mixing, micro-organisms and biogas production, it would be beneficial to study in greater detail the microbiological communities present in areas that represent different levels of local velocity gradient. This could lead to a greater understanding of a local velocity gradient threshold above which micro-organisms or microbiological communities are damaged. The proof of this concept has been demonstrated through the analysis of the microbiological community in the regions above and below the impeller carried out in this work, as discussed in Sections 9.6 and 10.4.

## **10.6 Implications for full-scale anaerobic digestion**

The work undertaken in this research has related digester stability, microbiological community structure and gas production to the differences in the mixing regime of mechanically-mixed lab-scale digesters. Taking this research as proof of concept, it seems likely that, with further work, these results could be used to optimise digester mixing within the wastewater industry. In order for this to be the case, digesters would need to be considered on a case-by-case basis, and CFD models of each digester would need to be created and suitably validated. This would require a full understanding of the rheology of the sludge in the digester, the appropriate modelling of the applied mixing method and accurate drawings of the digester. Whilst the computing power for a full-scale digester simulation is currently accessible in academia and to some specialist consultancy companies, it is unlikely that this level of high performance computing is within easy reach of most wastewater treatment companies. As such, it is likely that such an optimisation of anaerobic digester mixing at full-scale would require collaboration between industry and academia in the first instance.

Due to the expense involved in adopting this methodology in order to optimise gas production from digesters on a case-by-case basis, it is unlikely to be widely adopted by wastewater treatment companies. However, as the drive for sustainability continues, the potential rewards of optimising anaerobic digesters will grow, both as a method to reduce energy usage and to increase sustainable energy recovery from sludge. It is likely that whilst the methodology may be used to optimise individual digesters which are considered to be of commercial importance, the more likely approach will be the optimisation of an “average” digester and the subsequent general application of these results. This allows wastewater treatment companies to improve, though not necessarily optimise, the mixing and the energy balance in a large number of digesters without the need to undertake a costly analysis of each digester.

## **10.7 Summary**

This chapter has considered the methods used in this research and their limitations as well as the implications of the research findings.

It is seen that PEPT offers significant advantages over existing non-invasive flow visualisation techniques, including its ability to visualise flow patterns in three dimensions and to operate within opaque fluids. PEPT is successfully used in this work as both a flow visualisation technique and to validate CFD models. The implications of the CFD modelling strategy, including mesh density, treatment of the rotating flow, and selection of turbulence and rheological models, on the results of the simulation were considered, and were found to compare well with best practice as ascertained from existing literature. Furthermore, simulated results were found to compare well with PEPT results during validation.

The experimental method is evaluated in the same manner. This suggests that the use of the synthetic feedstock is likely to have had an effect on the stability of the process and the gas production of the digesters, though it offered significant advantages in limiting the variability of the

feedstock. Although there were limitations in the gas measurement methods used, they were in line with best practice and are unlikely to have introduced significant error into the results. The results from this experimental work agree well with parts of the existing literature, but the high number of variables that can affect gas production during anaerobic digestion mean that it is somewhat challenging to compare results from different experiments.

For the first time, qPCR has been used to analyse the effects of mixing on microbiological communities in anaerobic digesters. It was shown that *Methanosaeta* was the dominant methanogen in all of the digesters run during the experimental work and that lower mixing speeds were beneficial for methanogenic communities dominated by *Methanosaeta*. This is in agreement with the results of Hoffman et al. (2008). It is hypothesised that methanogenic communities are not only directly affected by the level of shear stress that they experience in the digester but are also indirectly affected by changes in the digester environment, such as VFA concentration. Whilst a larger dataset would be required to fully analyse whether it is direct or indirect effects that have a greater impact on the link between mixing and methanogenic community structure, which in turn affects the methane production, this work proves that qPCR can act as a useful tool for such analysis.

The velocity gradient can act as a scale-independent transferable parameter for the comparison of different digester mixing methods and regimes. In this work, by coupling the results of the CFD and experimental work, it is clear that there is an average velocity gradient threshold, between 6 and 8 s<sup>-1</sup>, above which increasing mixing speed is no longer beneficial to increasing gas production. The effects of exceeding this threshold appear to have greater detrimental effect when dealing with digesters that are already suffering from instability.

This research provides proof of concept for linking mixing to biogas production via flow pattern visualisation and the velocity gradient. In order to replicate this work in the water industry, it would

be beneficial to recreate the links determined here at pilot-scale or at full-scale and with other mixing methods, in particular gas mixing. However, as the velocity gradient is a scale-independent transferable parameter, unlike measures such as rotational mixing speed, following the same steps undertaken in this research, digester mixing could be optimised on a case-by-case basis. Due to the computing power required for this, it is likely that, in the first instance, this would require collaboration between industry and academia.

## CHAPTER 11 Conclusions and recommendations

Within this chapter, conclusions which relate to the aims and objectives of the research are presented. These are followed by a number of recommendations for further work in this area.

### 11.1 Conclusions

- PEPT offers significant advantages over existing non-invasive flow visualisation techniques for lab-scale anaerobic digesters; in particular, PEPT is capable of examining flow phenomena in three dimensions and can be used to visualise flow in opaque fluids or within opaque apparatus. This reduces the error involved in selecting an appropriate transparent fluid with which to model the rheological properties of sludge and makes it a valuable tool for the validation of CFD models. PEPT is limited by an underestimation of velocities in the impeller region, where low data capture arises from the high velocity of the particle and its rapid change in direction and velocity magnitude.
- Flow visualisation of lab-scale digesters at a range of mixing speeds reveal flow patterns characteristic of a radial flow impeller. At 50 rpm and 100 rpm mixing sewage sludge and at 50 rpm mixing synthetic sludge, the top third of the digester experiences low levels of mixing and is poorly covered by the particle, with further small areas of poor particle coverage existing in corners around baffles and close to the base of the digester at all mixing speeds. As mixing speed increases, the low level of particle coverage in the higher viscosity sewage sludge is more persistent than in the lower viscosity synthetic sludge, demonstrating that the level of achieved mixing is affected by fluid viscosity as well as by mixing speed.
- Flow patterns generated using CFD models of flow in a lab-scale mechanically-mixed anaerobic digester compare well to PEPT results. The SM method is used to model the

rotating impeller and the realisable  $k-\varepsilon$  model is deemed to be the most appropriate turbulence model for recreating flow patterns established using PIV.

- CFD models of the lab-scale digester indicate that, at all mixing speeds, approximately 10 % of the digester volume can be considered as dead zone. These dead zones are predominantly situated above the impeller. Particle trajectories indicate that particle movement tends to be limited to volumes either above or below the impeller and therefore experience different turbulent characteristics.
- TKE increases within the digester as mixing speed increases. The highest levels of turbulence are found in the impeller region, and in particular at the impeller tips and in recirculation zones behind the blades, where velocity magnitude is 17 % higher than tip speed. TI in the impeller region is approximately double that of the TI in other areas of the digester.
- Calculating local velocity gradients in the digester demonstrates that velocity gradients of  $10 \text{ s}^{-1}$  or lower account for the majority of the digester volume. As mixing speed increases, the volume of the digester which experiences higher velocity gradients increases, but even at 200 rpm, 80 % of the digester volume experiences velocity gradients of  $20 \text{ s}^{-1}$  or less.
- Digester stability is adversely affected in lab-scale mechanically-mixed digesters with no mixing and at high mixing speeds (200 rpm) when compared to digesters at low mixing speeds (50 rpm). In digesters that are already displaying signs of instability, mixing has a greater effect on digester stability, though in the case of the digester with no mixing, the digester demonstrated greater stability. This was attributed to the increased SRT associated with stratification of digesters with little or no mixing, and a sampling location at the top of the digester.
- Gas production, measured as percentage methane and biogas volume, is also adversely affected in digesters with no mixing and at high mixing speeds (200 rpm) when compared to digesters at low mixing speeds (50 rpm). Again, mixing has a greater detrimental effect on

gas production in digesters that are already displaying signs of instability. Gas production is linked to digester stability, with percentage methane starting to fall as instabilities become apparent whilst biogas volume starts to fall much later, as digester souring occurs.

- Gas production in all digesters fell over the course of the experiments. This was attributed to the slow inhibition of methanogens by an intermediary metabolite produced during the digestion of the synthetic sludge used as feedstock. The accumulation of this metabolite in the digesters over time led to the slowing of the growth rate of methanogens and an increased rate of methanogenic wash-out and hence a reduction in the digester gas production.
- qPCR can be successfully used to link microbiological community structure to mixing.
- *Methanosaeta* was the dominant methanogen in all of the digesters, though low levels of mixing were more beneficial than high levels of mixing for establishing strong methanogenic populations in the digester. Relative levels of methanogens fell in the lower part of the digester, near to the impeller, at mixing speeds of 200 rpm and this was attributed to the higher shear stresses in this region detrimentally affecting the filamentous *Methanosaeta*.
- Mixing also has indirect effects on the methanogenic population structure through changes in environmental conditions in the digester, such as VFA concentrations. The relative importance of these direct and indirect effects are not certain.
- Coupling CFD and experimental results allows the velocity gradient to be used as a link between turbulence caused by mixing and biogas production. This allows the comparison between mixing in digesters of different sizes and digesters that make use of different mixing methods. In the case of the lab-scale mechanically-mixed digesters operated in this research, gas production increased as average velocity gradient increased from zero, i.e. no mixing. However, there was a threshold at  $6\text{-}8\text{ s}^{-1}$ , above which increasing the velocity

gradient was no longer beneficial and gas production fell. This is significantly lower than the average velocity gradient of 50-80 s<sup>-1</sup> recommended for mixing in existing literature.

- This research acts of proof of concept for linking turbulence caused by mixing and biogas production from an anaerobic digester via the velocity gradient.

## **11.2 Recommendations for further work**

In order for this research to be applicable at full-scale, further work should focus on carrying out tests at both pilot-scale and full-scale to ensure the reproducibility of the results demonstrated at lab-scale, which link mixing to gas production via velocity gradient.

Of greater importance, it should be determined whether digesters operating with other mixing methods, in particular gas mixing, which is widely used in the wastewater treatment industry, produce similar results. This would require not only a comparison of gas production under different mixing methods, e.g. impeller mixing and gas mixing, but also of key design parameters which affect the efficacy of the gas mixing, including confined and unconfined gas mixing, and the aspect ratio of the digester. Similarly, the effects of changing key design parameters, in relation to impeller mixing, would be valuable in order to ascertain how different impeller types and digester aspect ratios affect the gas production, and whether these effects can similarly be quantified by the use of the velocity gradient as a comparable parameter.

Of less practical importance, but of value in reinforcing the knowledge of the science underpinning the link between mixing and biogas production, the effects of local velocity gradients on microbiological communities could be further studied. The application of CFD models that make use of higher level turbulence modelling, such as LES, may provide an improved localised visualisation of the flow patterns and associated turbulence brought about by mixing in a digester. This could be paired with a more detailed analysis of the microbiological communities present in specific areas of a digester in order to gain a deeper comprehension of the link between mixing and microbiology.

If future research is to make use of synthetic sludge to minimise the effects of sludge variability, as is the case in this research, the synthetic sludge recipe requires further development. Specifically, the inhibitory component of the synthetic sludge needs to be identified and removed or replaced to ensure that long-term experiments can be undertaken without methanogenic inhibition.

In addition, there may be scope for the novel methods of assessing the level of mixing used in this research to be linked to existing assessments of the level of mixing, such as residence time distribution, to better validate the results gained from these techniques. Furthermore, the effects of rheology on the efficacy of digester mixing should not be overlooked, and any improvement in the understanding of the link between rheology, mixing and gas production using these novel methods would be of value.

## References

- AGLER, M. T., AYDINKAYA, Z., CUMMINGS, T. A., BEERS, A. R. & ANGENENT, L. T. 2010. Anaerobic digestion of brewery primary sludge to enhance bioenergy generation: A comparison between low- and high-rate solids treatment and different temperatures. *Bioresource Technology*, 101, 5842-5851.
- AMANN, R. I., LUDWIG, W. & SCHLEIFER, K. 1995. Phylogenetic identification and in situ detection of individual microbial cells without cultivation. *Microbiology and Molecular Biology Review*, 59, 143-169.
- AMANULLAH, A., BUCKLAND, B. C. & NIENOW, A. W. 2004. Mixing in the Fermentation and Cell Culture Industries. In: PAUL, E. L., ATIEMO-OBENG, V. A. & KRESTA, S. M. (eds.) *Handbook of Industrial Mixing: Science and Practice*. Hoboken, New Jersey: John Wiley & Sons, Inc.
- ANGELIDAKI, I. & AHRING, B. K. 1993. Thermophilic anaerobic digestion of livestock waste: the effect of ammonia. *Applied Microbiology and Biotechnology*, 38, 560-564.
- ANGELIDAKI, I., ELLEGAARD, L. & AHRING, B. K. 1993. A mathematical model for dynamic simulation of anaerobic digestion of complex substrates: Focusing on ammonia inhibition. *Biotechnology and Bioengineering*, 42, 159-166.
- ANGENENT, L. T., KARIM, K., AL-DAHMAN, M. H., WRENN, B. A. & DOMINGUEZ-ESPINOSA, R. 2004. Production of bioenergy and biochemicals from industrial and agricultural wastewater. *Trends in Biotechnology*, 22, 477-485.
- ANSYS-FLUENT 2010a. Fluent 13.0. Lebanon, NH.
- ANSYS-FLUENT 2010b. Workbench 13.0. Lebanon, NH.
- ANSYS-FLUENT 2012. *ANSYS Fluent Theory Guide*, Canonsburg, PA, ANSYS-Fluent.
- APPELS, L., BAEYENS, J., DEGREVE, J. & DEWIL, R. 2008. Principles and potential of the anaerobic digestion of waste-activated sludge. *Progress in Energy and Combustion Science*, 34, 755-781.
- AUTY, D. & MARQUET, R. 2009. Digester Mixing - Industry Overview.
- BAROUTIAN, S., ESHTIAGHI, N. & GAPES, D. J. 2013. Rheology of a primary and secondary sewage sludge mixture: Dependency on temperature and solid concentration. *Bioresource Technology*, 140, 227-233.
- BAUDEZ, J. C., AYOL, A. & COUSSOT, P. 2004. Practical determination of the rheological behaviour of pasty biosolids. *Journal of Environmental Management*, 72, 181-188.
- BENBELKACEM, H., GARCIA-BERNET, D., BOLLON, J., LOISEL, D., BAYARD, R., STEYER, J.-P., GOURDON, R., BUFFIERE, P. & ESCUDIE, R. 2013. Liquid mixing and solid segregation in high-solid anaerobic digesters. *Bioresource Technology*, 147, 387-394.
- BORJA, R., MARTIN, A., SANCHEZ, E., RINCON, B. & RAPOSO, F. 2005. Kinetic modelling of the hydrolysis, acidogenic, and methanogenic steps in the anaerobic digestion of two-phase olive pomace (TPOP). *Process Biochemistry*, 40, 1841-1847.
- BORJA, R., SANCHEZ, E., WEILAND, P., TRAVIESO, L. & MARTIN, A. 1994. Kinetic of anaerobic digestion of cow manure with biomass immobilised on zeolite. *Chemical Engineering Journal*, 54, B9-B14.
- BOUSSINESQ, J. 1877. Essai sur la théorie des eaux courantes. *Mémoires présentés par divers savants à l'Académie des Sciences*, 23, 1-680.
- BRADY, C. E. & NOONE, G. P. 1981. Anaerobic sludge digestion - need it be expensive? Making more of existing resource. *Water Pollution Control*, 80, 70-94.
- BRIDGEMAN, J. 2012. Computational fluid dynamics modelling of sewage sludge mixing in an anaerobic digester. *Advances in Engineering Software*, 44.
- BUGAY, S., ESCUDIE, R. & LINE, A. 2002. Experimental analysis of hydrodynamics in axially agitated tank. *American Institute of Chemical Engineers Journal*, 48, 463-475.

- CARDINALI-REZENDE, J., COLTURATO, L. F. D. B., COLTURATO, T. D. B., CHARTONE-SOUZA, E., NASCIMENTO, A. M. A. & SANZ, J. L. 2012. Prokaryotic diversity and dynamics in a full-scale municipal solid waste anaerobic reactor from start-up to steady-state conditions. *Bioresource Technology*, 119, 373-383.
- CARLIELL-MARQUET, C. 2000. *The effect of phosphorus enrichment on fractionation of metals and phosphorus in anaerobically digested sludge*. PhD, University of Loughborough.
- CAVE, M. 2009. Independent Review of Competition and Innovation in Water Markets: Final Report. London: Department for Environment, Food and Rural Affairs.
- CHAE, K. J., JANG, A., YIM, S. K. & KIM, I. S. 2008. The effects of digestion temperature and temperature shock on the biogas yields from the mesophilic anaerobic digestion of swine manure. *Bioresource Technology*, 99, 1-6.
- CHEN, Y., CHENG, J. J. & CREAMER, K. S. 2008. Inhibition of anaerobic digestion process: A review. *Bioresource Technology*, 99, 4044-4064.
- CHITI, F., BAKALIS, S., BUJALSKI, W., BARIGOU, M., EAGLESHAM, A. & NIENOW, A. W. 2011. Using positron emission particle tracking (PEPT) to study the turbulent flow in a baffled vessel agitated by a Rushton turbine: Improving data treatment and validation. *Chemical Engineering Research and Design*, 89, 1947-1960.
- CHOLETTE, A. & CLOUTIER, L. 1959. Mixing efficiency determinations for continuous flow systems. *The Canadian Journal of Chemical Engineering*, 37, 105-112.
- CLIMENHAGA, M. A. 2008. *Anaerobic digestion of catering wastes*. PhD, University of Southampton.
- CONKLIN, A., STENSEL, H. D. & FERGUSON, J. 2006. Growth kinetics and competition between *Methanosarcina* and *Methanosaeta* in mesophilic anaerobic digestion. *Water and Environmental Research*, 78, 486-495.
- COONEY, M., MAYNARD, N., CANNIZZARO, C. & BENEMANN, J. 2007. Two-phase anaerobic digestion for production of hydrogen-methane mixtures. *Bioresource Technology*, 98, 2641-2651.
- CRAIG, K. J., NIEUWOUDT, M. N. & NIEMAND, L. J. 2013. CFD simulation of anaerobic digester with variable sludge rheology. *Water Research*, 47, 4485-4497.
- DAVIDSON, P. A. 2004. *Turbulence: An introduction for scientists and engineers*, Oxford, Oxford University Press.
- DAWSON, M. & OZGENCIL, H. 2009. *Digester and Sludge Tank Mixing Design Guide*. Cranfield: BHR Group.
- DEFRA & DECC 2011. A commitment to increasing energy from waste through anaerobic digestion. In: DEPARTMENT FOR ENVIRONMENT, FOOD AND RURAL AFFAIRS, F. A. R. A. & CHANGE, D. O. E. A. C. (eds.). London: Department for Environment, Food and Rural Affairs.
- DIEUDE-FAUVEL, E., HERITIER, P., CHANET, M., GIRAULT, R., PASTORELLI, D., GUIBELIN, E. & BAUDEZ, J. C. 2014. Modelling the rheological properties of sludge during anaerobic digestion in a batch reactor by using electrical measurements. *Water Research*, 51, 104-112.
- DOUGLAS, J. F., GASIOREK, J. M., SWAFFIELD, J. A. & JACK, L. B. 2005. *Fluid Mechanics*, Harlow, UK, Pearson Education Ltd.
- EATON, A. D., CLESCERI, L. S., RICE, E. W. & GREENBURG, A. E. (eds.) 2005. *Standard Methods for the Examination of Water and Wastewater*, Washington D.C.: APHA-AWWA-WEF.
- EDGINGTON, R. 2001. What are we achieving with digester mixing? In: *Sludge Digester Mixing and Heating Systems Seminar*, 22 May 2001, Cranfield. 63-70.
- ERCOFTAC 2000. *ERCOFTAC Special Interest Group on "Quality and Trust in Industrial CFD": Best Practice Guidelines*, Winterthur, Switzerland, Sulzer Innotec.
- ESHTIAGHI, N., YAP, S. D., MARKIS, F., BAUDEZ, J. C. & SLATTER, P. 2012. Clear model fluids to emulate the rheological properties of thickened digested sludge. *Water Research*, 46, 3014-3022.

- FAJNER, D., PINELLI, D., GHADGE, R. S., MONTANTE, G., PAGLIANTI, A. & MAGELLI, F. 2008. Solids distribution and rising velocity of buoyant solid particles in a vessel stirred with multiple impellers. *Chemical Engineering Science*, 63, 5876-5882.
- FANGARY, Y. S., BARIGOU, M., SEVILLE, J. P. K. & PARKER, D. J. 2000. Fluid trajectories in a stirred vessel of non-Newtonian liquid using positron emission particle tracking. *Chemical Engineering Science*, 55.
- FAO 1997. Methane Production. In: MIYAMOTO, K. (ed.) *Renewable biological systems for alternative sustainable energy production*. FAO - Food and Agricultural Organization of the United Nations.
- FORSTER, C. F. 2002. The rheological and physico-chemical characteristics of sewage sludge. *Enzyme and Microbial Technology*, 30, 340-345.
- FREI, W. 2013. *Which turbulence model should I choose for my CFD application?* [Online]. <http://www.comsol.com/blogs/which-turbulence-model-should-choose-cfd-application/>: COMSOL Inc. [Accessed 12 December 2013].
- GANIDI, N., TYRREL, S. & CARTMELL, E. 2009. Anaerobic digestion foaming causes - A review. *Bioresource Technology*, 100, 5546-5554.
- GARCIA-OCHOA, F., SANTOS, V. E., NAVAL, L., GUARDIOLA, E. & LOPEZ, B. 1999. Kinetic model for anaerobic digestion of livestock manure. *Enzyme and Microbial Technology*, 25, 55-60.
- GERARDI, M. H. 2003. *The microbiology of anaerobic digesters*, Hoboken, New Jersey, John Wiley & Sons Inc.
- GHANIMEH, S. A., EL-FADEL, M. & SAIKALY, P. E. 2012. Mixing effect on thermophilic anaerobic digestion of source-sorted organic fraction of municipal solid waste. *Bioresource Technology*, 117, 63-71.
- GILBRAD, K. A., LEE, D. Y. & BEAUDETTE, L. A. 2006. Molecular techniques in wastewater: understanding microbial communities, detecting pathogens, and real-time process control. *Journal of Microbiological Methods*, 66, 1-20.
- GOMEZ, X., CUETOS, M. J., CARA, J., MORAN, A. & GARCIA, A. I. 2006. Anaerobic co-digestion of primary sludge and the fruit and vegetable fraction of the municipal solid wastes. Conditions for mixing and evaluation of the organic loading rate. *Renewable Energy*, 31, 2017-2024.
- GRIFFIN, M. E., MCMAHON, K. D., MACKIE, R. I. & RASKIN, L. 1998. Methanogenic population dynamics during start-up of anaerobic digesters treating municipal solid waste and biosolids. *Biotechnology and Bioengineering*, 57, 342-355.
- GRIFFIN, P. 11 March 2009. *RE: How much energy is used in digester mixing*. Type to CARLIELL-MARQUET, C. M.
- GUIBAUD, G., DOLLET, P., TIXIER, N., DAGOT, C. & BAUDU, M. 2004. Characterisation of the evolution of activated sludges using rheological measurements. *Process Biochemistry*, 39, 1803-1810.
- HARVIE, S. 2007. Review of 'The Impact of Digester Mixing on Gas Production'. Coventry: Severn Trent Water.
- HASAR, H., KINACI, C., UNLU, A., TOGRUL, H. & IPEK, U. 2004. Rheological properties of activated sludge in a sMBR. *Biochemical Engineering Journal*, 20, 1-6.
- HEMRAJANI, R. R. & TATTERSON, G. B. 2004. Mechanically Stirred Vessels. In: PAUL, E. L., ATIEMO-OBENG, V. A. & KRESTA, S. M. (eds.) *Handbook of Industrial Mixing: Science and Practice*. Hoboken, New Jersey: John Wiley and Sons, Inc.
- HOFFMAN, R., GARCIA, M. L., VESVIKAR, M., KARIM, K., AL-DAHMAN, M. H. & ANGENENT, L. T. 2008. Effect of shear on performance and microbial ecology of continuously stirred anaerobic digesters treating animal manure. *Biotechnology and Bioengineering*, 100, 38-48.
- HOWE, A. 2009. Evidence: Renewable energy potential for the water industry. Report: SC070010/R5. Bristol: Environment Agency.

- ISODA, H., INAGAWA, S., TAKEDA, H., ISOGAI, S., TAKEHARA, Y. & SAKAHARA, H. 2003. Preliminary study of tagged MR image velocimetry in a replica of an intracranial aneurysm. *American Journal of Neuroradiology*, 24, 604-607.
- JANSSEN, P. H. 2003. Selective enrichment and purification of cultures of *Methanosaeta* spp. *Journal of Microbiological Methods*, 52, 239-244.
- JENKINS, S., MORGAN, J. & SAWYER, C. 1983. Measuring anaerobic sludge digestion and growth by a simple alkalimetric titration. *Journal of the Water Pollution Control Federation*, 55, 448-453.
- JOSHI, J. B., ELIAS, C. B. & PATOLE, M. S. 1996. Role of hydrodynamic shear in the cultivation of animal, plant and microbial cells. *The Chemical Engineering Journal*, 62, 121-141.
- KAPARAJU, P., BUENDIA, I., ELLEGAARD, L. & ANGELIDAKI, I. 2008. Effects of mixing on methane production during thermophilic anaerobic digestion of manure: Lab-scale and pilot-scale studies. *Bioresource Technology*, 99, 4919-4928.
- KARIM, K., HOFFMAN, R., KLASSON, K. T. & AL-DAHMAN, M. H. 2005a. Anaerobic digestion of animal waste: Effect of mode of mixing. *Water Research*, 39, 3597-3606.
- KARIM, K., HOFFMAN, R., KLASSON, K. T. & AL-DAHMAN, M. H. 2005b. Anaerobic digestion of animal waste: Waste strength versus impact of mixing. *Bioresource Technology*, 96, 1771-1781.
- KARIM, K., KLASSON, K. T., HOFFMAN, R., DRESCHER, S. R., DEPAOLI, D. W. & AL-DAHMAN, M. H. 2005c. Anaerobic digestion of animal waste: Effect of mixing. *Bioresource Technology*, 96, 1607-1612.
- KARIM, K., VARMA, R., VESVIKAR, M. & AL-DAHMAN, M. H. 2004. Flow pattern visualization of a simulated digester. *Water Research*, 38, 3659-3670.
- KAWASE, M. & MOO-YOUNG, M. 1990. Mathematical models for design of bioreactors: Applications of Kolmogoroff's theory of isotropic turbulence. *The Chemical Engineering Journal*, 43.
- KESHTKAR, A., GHAFORIAN, H., ABOLHAMD, G. & MEYSSAMI, B. 2001. Dynamic simulation of cyclic batch anaerobic digestion of cattle manure. *Bioresource Technology*, 80, 9-17.
- KESHTKAR, A., MEYSSAMI, B., ABOLHAMD, G., GHAFORIAN, H. & KHALAGI ASADI, M. 2003. Mathematical modeling of non-ideal mixing continuous flow reactors for anaerobic digestion of cattle manure. *Bioresource Technology*, 87, 113-124.
- KHAN, F. R. 2005. *Investigation of turbulent flows and instabilities in a stirred vessel using particle image velocimetry*. PhD, Loughborough University.
- KILANDER, J. & RASMUSON, A. 2005. Energy dissipation and macro instabilities in a stirred square tank investigated using an LE PIV approach and LDA measurements. *Chemical Engineering Science*, 60, 6844-6856.
- KIM, J., LIM, J. & LEE, C. 2013. Quantitative real-time PCR approaches for microbial community studies in wastewater treatment systems: Applications and considerations. *Biotechnology Advances*.
- KOSTER, I. W. & LETTINGA, G. 1988. Anaerobic digestion at extreme ammonia concentrations. *Biological Wastes*, 25, 51-59.
- KOWALCZYK, A., HARNISCH, E., SCHWEDE, S., GERBER, M. & SPAN, R. 2013. Different mixing modes for biogas plants using energy crops. *Applied Energy*, 112, 465-472.
- LAUNDER, B. E. & SPALDING, D. B. 1972. *Lectures in Mathematical Models of Turbulence*, London, Academic Press.
- LEE, C., CHO, N. K. & MAENG, W. J. 1995. Using the pressure of biogas created during anaerobic digestion as the source of mixing power. *Journal of Fermentation and Bioengineering*, 80, 415-417.
- LEE, C., KIM, J., HWANG, K., O'FLAHERTY, V. & HWANG, S. 2009. Quantitative analysis of methanogenic community dynamics in three anaerobic batch digesters treating different wastewaters. *Water Research*, 43, 157-165.
- LEHWALD, A., JANIGA, G., THEVENIN, D. & ZHRINGER, K. 2012. Simultaneous investigation of macro- and micro-mixing in a static mixer. *Chemical Engineering Science*, 79, 8-18.

- LIN, C. Y. 1993. Effects of heavy metals on acidogenesis in anaerobic digestion. *Water Research*, 27, 147-152.
- LIN, H., ZHANG, M., WANG, F., MENG, F., LIAO, B.-Q., HONG, H., CHEN, J. & GAO, W. 2014. A critical review of extracellular polymeric substances (EPS) in membrane bioreactors: Characteristics, roles in membrane fouling and control strategies. *Journal of Membrane Science*, 460, 110-125.
- LIU, J., OLSSON, G. & MATTIASSON, B. 2004. On-line monitoring of a two-stage anaerobic digestion process using a BOD analyser. *Journal of Biotechnology*, 109, 263-275.
- LUBKEN, M., WICHERN, M., SCHLATTMANN, M., GRONAUER, A. & HORN, H. 2007. Modelling the energy balance of an anaerobic digester fed with cattle manure and renewable energy crops. *Water Research*, 41, 4085-4096.
- MACKIE, R. I. & BRYANT, M. P. 1995. Anaerobic digestion of cattle waste at mesophilic and thermophilic temperatures. *Applied and Environmental Microbiology*, 43, 346-350.
- MALCZEWSKA, B. 2009. Variability of rheological parameters in function of gravimetric concentration of sludge. *Electronic Journal of Polish Agricultural Universities*, 12.
- MARSHALL, E. M. & BAKKER, A. 2004. Computational Fluid Mixing. In: PAUL, E. L., ATIEMO-OBENG, V. A. & KRESTA, S. M. (eds.) *Handbook of industrial mixing: science and practice*. Hoboken, New Jersey: John Wiley and Sons.
- MCCMAHON, K. D., STROOT, P. G., MACKIE, R. I. & RASKIN, L. 2001. Anaerobic codigestion of municipal solid waste and biosolids under various mixing conditions - II. Microbial population dynamics. *Water Research*, 35, 1817-1827.
- MENTER, F. R. 1994. Two-equation eddy-viscosity turbulence models for engineering applications. *AIAA Journal*, 32, 1598-1605.
- MERONEY, R. N. & COLORADO, P. E. 2009. CFD simulation of mechanical draft tube mixing in anaerobic digester tanks. *Water Research*, 43, 1040-1050.
- MOELLER, G. & TORRES, L. G. 1997. Rheological characterisation of primary and secondary sludges treated by both aerobic and anaerobic digestion. *Bioresource Technology*, 61, 207-211.
- MONTEIRO, P. S. 1997. The influence of the anaerobic digestion process on the sewage sludges rheological behaviour. *Water Science and Technology*, 36, 61-67.
- MONTERO, B., GARCIA-MORALES, J. L., SALES, D. & SOLERA, R. 2007. Evolution of microorganisms in thermophilic-dry anaerobic digestion. *Bioresource Technology*, 99, 3233-3243.
- MORI, M., ISAAC, J., SEYSSIECQ, I. & ROCHE, N. 2008. Effect of measuring geometries and of exocellular polymeric substances on the rheologica behaviour of sewage sludge. *Chemical Engineering Research and Design*, 86, 554-559.
- MYINT, M., NIRMALAKHANDAN, N. & SPEECE, R. 2007. Anaerobic fermentation of cattle manure: Modelling of hydrolysis and acidogenesis. *Water Research*, 41, 323-332.
- NI, S., WOESE, C. R., ALDRICH, H. C. & BOONE, D. R. 1994. Transfer of *Methanobrevibacter smithii* to the genus *Methanosarcina*, naming it *Methanosarcina smithii*, and emedation of the genus *Methanosarcina*. *International Journal of Systematic Bacteriology*, 44, 357-359.
- NIENOW, A. W., SCOTT, W. H., HEWITT, C. J., THOMAS, C. R., LEWIS, G., AMANULLAH, A., KISS, R. & MEIER, S. J. 2013. Scale-down studies for assessing the impact of different stress parameters on growth and product quality during animal cell culture. *Chemical Engineering Research and Design*, 91, 2265-2274.
- ONG, H. K., GREENFIELD, P. F. & PULLAMMAMAPPALLIL, P. C. 2002. Effect of mixing on biomethanation of cattle-manure slurry. *Environmental Technology*, 23, 1081-1090.
- OWEN, W. F. 1982. Anaerobic Treatment Processes. *Energy in Wastewater Treatment*. Englewood Cliffs, N.J.: Prentice-Hill, Inc.
- PARK, C., LEE, C., KIM, S., CHEN, Y. & CHASE, H. A. 2005. Upgrading of anaerobic digestion by incorporating two different hydrolysis processes. *Journal of Bioscience and Bioengineering*, 100, 164-167.

- PATANKER, S. V. & SPALDING, D. B. 1972. A calculation procedure for heat, mass and momentum transfer in three-dimensional parabolic flows. *International Journal of Heat and Mass Transfer*, 15, 1787-1806.
- PAUL, E. L., ATIEMO-OBENG, V. A. & KRESTA, S. M. 2004. Introduction. In: PAUL, E. L., ATIEMO-OBENG, V. A. & KRESTA, S. M. (eds.) *Handbook of Industrial Mixing: Science and Practice*. Hoboken, NJ: Wiley and Sons Inc.
- PEVERE, A., GUIBAUD, G., GOIN, E., VAN HULLEBUSCH, E. & LENS, P. 2009. Effects of physico-chemical factors on the viscosity evolution of anaerobic granular sludge. *Biochemical Engineering Journal*, 43, 231-238.
- PEVERE, A., GUIBAUD, G., VAN HULLEBUSCH, E. & LENS, P. 2007. Identification of rheological parameters describing the physico-chemical properties of anaerobic sulphidogenic sludge suspensions. *Enzyme and Microbial Technology*, 40, 547-554.
- PEVERE, A., GUIBAUD, G., VAN HULLEBUSCH, E., LENS, P. & BAUDU, M. 2006. Viscosity evolution of anaerobic granular sludge. *Biochemical Engineering Journal*, 27, 315-322.
- PIANKO-OPRYCH, P., NIENOW, A. W. & BARIGOU, M. 2009. Positron emission particle tracking (PEPT) compared to particle image velocimetry (PIV) for studying the flow generated by a pitched-blade turbine in single phase and multi-phase systems. *Chemical Engineering Science*, 64, 4955-4968.
- PINELLI, D., MONTANTE, G. & MAGELLI, F. 2004. Dispersion coefficients and settling velocities of solids in slurry vessels stirred with different types of multiple impellers. *Chemical Engineering Science*, 59, 3081-3089.
- PINHO, F. T. & WHITELAW, J. H. 1990. Flow of non-Newtonian fluids in a pipe. *Journal of non-Newtonian fluid mechanics*, 34, 129-144.
- PIOMELLI, U. 2008. Wall-layer models for large-eddy simulations. *Progress in Aerospace Sciences*, 44, 437-446.
- POLLICE, A., GIORDANO, C., LAERA, G., SATURNO, D. & MININNI, G. 2007. Physical characteristics of the sludge in a complete retention membrane bioreactor. *Water Research*, 41, 1832-1840.
- POPE, S. B. 2000. *Turbulent Flows*, Cambridge, Cambridge University Press.
- PRAJAPATI, P. & EIN-MOZAFFARI, F. 2009. CFD investigation of mixing of yield-pseudoplastic fluids with anchor impellers. *Chemical Engineering Technology*, 32, 1211-1218.
- RAJESHWARI, K. V., BALAKRISHNAN, A., K., LATA, K. & KISHORE, V. V. N. 2000. State-of-the-art of anaerobic digestion technology for industrial wastewater treatment. *Renewable and Sustainable Energy Reviews*, 4, 135-156.
- RAMMOHAN, A. R., KEMOUN, A., AL-DAHMAN, M. H. & DUDUKOVIC, M. P. 2001. Characterisation of single phase flows in stirred tanks via computer automated radioactive particle tracking (CARPT). *Chemical Engineering Research and Design*, 79, 831-844.
- REYNOLDS, O. 1883. An experimental investigation of the circumstances which determine whether the motion of water shall be direct or sinuous, and of the law of resistance in parallel channels. *Philosophical Transactions of the Royal Society of London. A*, 174, 935-982.
- REYNOLDS, O. 1895. On the dynamical theory of incompressible viscous fluids and the determination of the criterion. *Philosophical Transactions of the Royal Society of London. A*, 186, 123-164.
- RINCON, B., BORJA, R., MARTIN, M. A. & MARTIN, A. 2010. Kinetic study of the methanogenic step of a two-stage anaerobic digestion process treating olive mill solid residue. *Chemical Engineering Journal*, 160, 215-219.
- RIPLEY, L., BOYLE, W. & CONVERSE, J. 1986. Improved alkalimetric monitoring for anaerobic digestion of high-strength wastes. *Journal of the Water Pollution Control Federation*, 58, 406-411.
- ROACHE, P. J. 1998. Verification of Codes and Calculations. *American Institute of Aeronautics and Astronautics Journal*, 36, 696-702.
- SCHLICHTING, H. & GERSTEN, K. 2000. *Boundary-Layer Theory*, Springer-Verlag.

- SCHMIDT, J. E. & AHRING, B. K. 1999. Immobilization patterns and dynamics of acetate-utilizing methanogens immobilized in sterile granular sludge in upflow anaerobic sludge blanket reactors. *Applied and Environmental Microbiology*, 65, 1050-1054.
- SHIH, T. H., LIOU, W. W., SHABBIR, A., YANG, Z. & ZHU, J. 1995. A new k- $\epsilon$  eddy viscosity model for high reynolds number turbulent flows - model development and validation. *Computers Fluids*, 24, 227-238.
- SILES, J. A., MARTIN, M. A., CHICA, A. & BORJA, R. 2008. Kinetic modelling of the anaerobic digestion of wastewater derived from the pressing of orange rind produced in orange juice manufacturing. *Chemical Engineering Journal*, 140, 145-156.
- SINDALL, R., BRIDGEMAN, J. & CARLIELL-MARQUET, C. 2013. Velocity gradient as a tool to characterise the link between mixing and biogas production in anaerobic waste digesters. *Water Science and Technology*, 67, 2800-2806.
- SPEECE, R. 1988. A survey of municipal anaerobic sludge digesters and diagnostic activity assays. *Water Research*, 22, 365-372.
- SPINOSA, L. & LOTITO, V. 2003. A simple method for evaluating sludge yield stress. *Advances in Environmental Research*, 7, 655-659.
- STAFFORD, D. A. 1982. The effects of mixing and volatile fatty acid concentrations on anaerobic digester performance. *Biomass*, 2, 43-55.
- STANLEY, S. J. & SMITH, D. W. 1995. Measurement of Turbulent Flow in Standard Jar Apparatus. *Journal of Environmental Engineering*, 121, 902-910.
- STROOT, P. G., MCMAHON, K. D., MACKIE, R. I. & RASKIN, L. 2001. Anaerobic codigestion of municipal solid waste and biosolids under various mixing conditions - I. digester performance. *Water Research*, 35, 1804-1816.
- SUZUKI, M. T., TAYLOR, L. T. & DELONG, E. F. 2000. Quantitative analysis of small-subunit rRNA genes in mixed microbial populations via 5'-nuclease assays. *Applied and Environmental Microbiology*, 66, 4605-4614.
- TCHOBANOGLIOUS, G. & BURTON, F. L. 1991. Design of facilities for the treatment and disposal of sludge. In: METCALF & EDDY, I. (eds.) *Wastewater Engineering: Treatment, Disposal, Reuse*. New York, New York: McGraw-Hill Inc.
- TENNEKES, H. & LUMLEY, J. L. 1982. *A first course in turbulence*, Cambridge, MA, USA, The MIT Press.
- TERASHIMA, M., GOEL, R., KOMATSU, K., YASUI, H., TAKAHASHI, H., LI, Y. Y. & NOIKE, T. 2009. CFD simulation of mixing in anaerobic digesters. *Bioresource Technology*, 100, 2228-2233.
- TIAN, Z., CHAULIAC, D. & PULLAMMANAPPALLIL, P. 2013. Comparison of non-agitated and agitated batch, thermophilic anaerobic digestion of sugarbeet tailings. *Bioresource Technology*, 129, 411-420.
- TIEHM, A., NICKEL, K., ZELHORN, M. & NEIS, U. 2001. Ultrasonic waste activated sludge disintegration for improving anaerobic stabilisation. *Water Research*, 35, 2003-2009.
- TIXIER, N., GUIBAUD, G. & BAUDU, M. 2003. Determination of some rheological parameters for the characterisation of activated sludge. *Bioresource Technology*, 90, 215-220.
- TRIVERSI, D., VILLA, S., LORENZI, E., DEGAN, R. & GILLI, G. 2012. Application of a real-time qPCR method to measure the methanogen concentration during anaerobic digestion as an indicator of biogas production capacity. *Journal of Environmental Management*, 111, 173-177.
- UK METEOROLOGICAL OFFICE 2012. Met Office Integrated Data Archive System (MIDAS) Land and Marine Surface Stations Data (1853-current). Internet: NCAS British Atmospheric Data Centre.
- USEPA 1976. Anaerobic Sludge Digestion Operations Manual.
- VAN HAANDEL, A. & VAN DER LUBBE, J. 2007. *Handbook of Biological Waste Water Treatment: Design and optimisation of activated sludge systems*, Leidschendam, The Netherlands, Quist Publishing.

- VAVILIN, V. A. & ANGELIDAKI, I. 2005. Anaerobic degradation of solid material: Importance of initiation centres for methanogenesis, mixing intensity, and 2D distributed model. *Biotechnology and Bioengineering*, 89, 113-122.
- VAVILIN, V. A., RYTOV, S. A. & LOKSHINA, L. Y. 1996. A description of hydrolysis kinetics in anaerobic degradation of particulate organic matter. *Bioresource Technology*, 56, 229-237.
- VERA, M. A. & LAVELLE, P. 2005. Digester mixing for scum and grit deposition control. *10th European Biosolids and Biowaste Conference*. UK.
- VERSTEEG, H. K. & MALALASEKERA, W. 2007. *An introduction to computational fluid dynamics: the finite volume method*, Harlow, UK, Pearson Education Ltd.
- VESVIKAR, M. & AL-DAHMAN, M. H. 2005. Flow pattern visualization in a mimic anaerobic digester using CFD. *Biotechnology and Bioengineering*, 89, 719-732.
- VESVIKAR, M., VARMA, R., KARIM, K. & AL-DAHMAN, M. H. 2005. Flow pattern visualization in a mimic anaerobic digester: Experimental and computational studies. *Water Science and Technology*, 52, 537-543.
- VILLERMAUX, J. 1996. Trajectory length distribution (TLD), a novel concept to characterize mixing in flow systems. *Chemical Engineering Science*, 51, 1939-1946.
- WAGNER, A. O., LINS, P., MALIN, C., REITSCHULER, C. & ILLMER, P. 2013. Impact of protein-, lipid-, and cellulose-containing complex substrates on biogas production and microbial communities in batch experiments. *Science of the Total Environment*, 458-460, 256-266.
- WALKER, M., ZHANG, Y., HEAVEN, S. & BANKS, C. 2009. Potential errors in the quantitative evaluation of biogas production in anaerobic digestion processes. *Bioresource Technology*, 100, 6339-6346.
- WARD, A. J., HOBBS, P. J., HOLLIMAN, P. J. & JONES, D. L. 2008. Optimisation of the anaerobic digestion of agricultural resources. *Bioresource Technology*, 99, 7928-7940.
- WATER UK. 2009. *Water industry at the hub of anaerobic digestion - Water UK* [Online]. Water UK. Available: <http://water.org.uk/home/news/press-releases/ad-vision?s1=anaerobic&s2=digestion> [Accessed 05/05/2011 2011].
- WATER UK 2009. Sustainability Indicators 2008/09. London: UK Water.
- WATER UK 2012. Sustainability Indicators 2010/11. London: UK Water.
- WILCOX, D. C. 1998. *Turbulence modeling for CFD*, La Canada, California, DCW Industries, Inc.
- WILLIAMS, J., H., W., DINSDALE, R., GUWY, A. & ESTEVES, S. 2013. Monitoring methanogenic population dynamics in a full-scale anaerobic digester to facilitate operational management. *Bioresource Technology*, 140, 234-242.
- WRC 1975. Equipment for measurement of gas production at low rates of flow. *Technical Memorandum*. Water Research Centre.
- WU, B. 2010a. CFD simulation of gas and non-Newtonian fluid two-phase flow in an anaerobic digester. *Water Research*, 44, 3861-3874.
- WU, B. 2010b. CFD simulation of mixing in egg-shaped anaerobic digesters. *Water Research*, 44, 1507-1519.
- WU, B. 2010c. Computational Fluid Dynamics investigation of turbulence models for non-Newtonian fluid flow in anaerobic digesters. *Environmental Science and Technology*, 44, 8989-8995.
- WU, B. 2011. CFD investigation of turbulence models for mechanical agitation of non-Newtonian fluids in anaerobic digesters. *Water Research*, 45, 2082-2094.
- WU, B. 2012a. CFD simulation of mixing for high-solids anaerobic digestion. *Biotechnology and Bioengineering*, 109, 2116-2126.
- WU, B. 2012b. Integration of mixing, heat transfer, and biochemical reaction kinetics in anaerobic methane formation. *Biotechnology and Bioengineering*, 109, 2864-2874.
- WU, B. 2012c. Large eddy simulation of mechanical mixing in anaerobic digesters. *Biotechnology and Bioengineering*, 109.

- WU, B., BIBEAU, E. L. & GEBREMEDHIM, K. G. 2009. Three-dimensional simulation model of biogas production for anaerobic digesters. *Canadian Biosystems Engineering*, 51, 8.1-8.7.
- WU, B. & CHEN, S. 2008. CFD simulation of non-Newtonian fluid flow in anaerobic digesters. *Biotechnology and Bioengineering*, 99, 700-711.
- YANG, F., BICK, A., SHANDALOV, S., BRENNER, A. & ORON, G. 2009. Yield stress and rheological characteristics of activated sludge in an airlift membrane bioreactor. *Journal of Membrane Science*, 334, 83-90.
- YU, L., MA, J. & CHEN, S. 2011. Numerical simulation of mechanical mixing in high solid anaerobic digester. *Bioresource Technology*, 102, 1012-1018.
- YU, Y., LEE, C., KIM, J. & HWANG, S. 2005. Group-specific primer and probe sets to detect methanogenic communities using quantitative real-time polymerase chain reaction. *Biotechnology and Bioengineering*, 89, 670-679.
- ZHANG, T. & FANG, H. H. P. 2006. Applications of real-time polymerase chain reaction for quantification of micro-organisms in environmental samples. *Applied Microbiology and Biotechnology*, 70, 281-289.